1-1-2011

Seismic Response of Ground Cylindrical and Elevated Conical Reinforced Concrete Tanks

Mehdi Moslemi
Ryerson Univ

SEISMIC RESPONSE OF GROUND CYLINDRICAL AND ELEVATED CONICAL REINFORCED CONCRETE TANKS

by

Mehdi Moslemi
Master of Applied Science,
Science & Research Institute,
Tehran, Iran, 2005

A dissertation

presented to Ryerson University

in partial fulfillment of the

requirements for the degree of

Doctor of Philosophy

in the Program of

Civil Engineering

Toronto, Ontario, Canada, 2011

© Mehdi Moslemi 2011

AUTHOR'S DECLARATION

I hereby declare that I am the sole author of this thesis.

I authorize Ryerson University to lend this thesis to other institution or individuals for the purpose of scholarly research.

Mehdi Moslemi

I further authorize Ryerson University to reproduce this thesis by photocopying or by other means, in total or in part, at the request of other institution or individuals for the purpose of scholarly research.

Mehdi Moslemi

SEISMIC RESPONSE OF GROUND CYLINDRICAL AND ELEVATED CONICAL REINFORCED CONCRETE TANKS

Doctor of Philosophy, 2011

Mehdi Moslemi

Department of Civil Engineering

Ryerson University

ABSTRACT

In this study, the seismic performance of concrete ground-supported cylindrical as well as liquid-filled elevated water tanks supported on concrete shaft is evaluated using the finite element method. The effects of a wide spectrum of parameters such as liquid sloshing, tank wall flexibility, vertical ground acceleration, tank aspect ratio, base fixity, and earthquake frequency content on dynamic behaviour of such structures are examined. Furthermore, the adequacy of current practice in seismic analysis and design of liquid containing structures is investigated. A comprehensive parametric study covering a wide range of tank capacities and aspect ratios found in practice today is also carried out on elevated tanks. Two different innovative strategies to reduce the seismic response of elevated tanks are examined, in the first strategy the inclined cone angle of the lower portion of the vessel is increased while in the second strategy the supporting shaft structure is isolated either from the ground or the vessel mounted on top.

The results of this study show the capability of the proposed finite element technique. Using this method, the major aspects in fluid-structure interaction problems including wall flexibility,

sloshing motion, damping properties of fluid domain, and the individual effects of impulsive and convective terms can be considered. The effects of tank wall flexibility, vertical ground acceleration, base fixity, and earthquake frequency content are found to be significant on the dynamic behaviour of liquid tanks. The parametric study indicates that the results can be utilized with high level of accuracy in seismic design applications for conical elevated tanks. This study further shows that increasing the cone angle of the vessel can result in a significant reduction in seismically induced forces of the tank, leading to an economical design of the shaft structure and the foundation system. It is also concluded that the application of passive control devices to conical elevated tanks offers a substantial benefit for the earthquake-resistant design of such structures.

ACKNOWLEDGEMENTS

TABLE OF CONTENTS

LIST OF TABLES

LIST OF FIGURES

xiii

LIST OF APPENDICES

LIST OF SYMBOLS

A_c	Cross-sectional area of concrete pedestal
A_f	Area of the face of the element
AI	Arias intensity
a_n	Acceleration component on the boundary along the direction outward normal n
b	Half of the width of liquid tank
$[C]$	Damping matrix
C_c	Seismic response coefficient for convective term
$[C_e^p]$	Fluid damping matrix
C_i	Seismic response coefficient for impulsive term
C_I	Coefficient for determining the fundamental frequency of the tank-liquid system
C_n	Equivalent damping of dashpots in simplified mechanical model
C_{vx}	Seismic distribution factor
C_w	Coefficient for determining the fundamental frequency of the tank-liquid system
d	Vertical displacement of the liquid free surface
D	Tank diameter in cylindrical containers
d_k	Rubber material constants
d_w	Mean diameter of concrete pedestal
d_1	Material incompressibility parameter
E	Modulus of elasticity
$E(D)$	Total energy input during time D
f	Natural frequency of vibration
F	Net horizontal force acting on the tank in simplified mechanical model
F_a	Short-period site coefficient (at 0.2 second period)
$\{F^a\}$	Applied load vector
$\{F_D\}$	Damping force vector
F_{Dj}	Damping forces in a typical MDOF system
$\{F_e^{pr}\}$	Fluid pressure load vector at fluid-structure interface
$\{F_I\}$	Inertia force vector

F_{Ij}	Inertia forces in a typical MDOF system
F_j	External forces in a typical MDOF system
f_p	Predominant frequency of earthquake record
$\{F_S\}$	Stiffness force vector
F_{Sj}	Stiffness forces in a typical MDOF system
F_v	Long-period site coefficient (at 1.0 second period)
Fx	Base horizontal reaction
Fz	Base vertical reaction
g	Acceleration due to gravity
h_c	Equivalent height of convective mass
h_i	Equivalent height of impulsive mass
$\overline{H}_i$	Equivalent height of the equivalent single degree of freedom oscillator
H_l	Liquid height in tank model
h_n	Equivalent height of convective mass in simplified mechanical model
h_r	Pedestal wall thickness
hshaft	Height of the supporting shaft
htop	Freeboard (distance between the water free surface and the roof)
H_w	Height of the tank wall
h_0	Equivalent height of impulsive mass in simplified mechanical model
h3	Height of water in the cylindrical portion of the elevated tank
I	Importance factor
$I_1(y)$	Modified Bessel function of the first kind of order one with the argument y
$I_1'(y)$	Derivative of $I_1(y)$ with respect to y
J	Ratio of the deformed elastic volume over the undeformed volume of material
$J_1(y)$	Bessel function of the first kind of order one with the argument y
$J_1'(y)$	Derivative of $J_1(y)$ with respect to y
K	Bulk modulus
$[K]$	Stiffness matrix
k_c	Elevated tank lateral stiffness

Ke	Elastic horizontal stiffness of bearing
$\left[K_e^p\right]$	Fluid stiffness matrix
K_n	Equivalent stiffness of spring in simplified mechanical model
Kp	Plastic horizontal stiffness of bearing
Ks	Stiffness of concrete shaft
Kv	Vertical stiffness of bearing
l	Half of the length of liquid tank
L_g	Distance from base to centroid of the stored water in elevated tanks
M	Total mass of fluid
$[M]$	Mass matrix
M_c	Equivalent mass of convective fluid
M_{dr}	Mass of the tank's floor
$\left[M_e^p\right]$	Fluid mass matrix
$\overline{m}_i$	Equivalent mass of the equivalent single degree of freedom oscillator
M_i	Equivalent mass of impulsive fluid
m_n	Equivalent mass of each sloshing mode in simplified mechanical model
M_s	Mass of the shaft and interior platforms
M_{tw}	Impulsive mass of water and the walls of the vessel
M_y	Base moment reaction
m_0	Equivalent fluid mass rigidly attached to the tank in simplified mechanical model
n	Number of degrees of freedom in a typical MDOF system
$\{n\}$	Unit normal to the fluid interface
N	Order of the Ogden Potential function
$\{N\}$	Shape function for fluid pressure
$\{N'\}$	Shape functions used to discretize the structural displacement components
p	Hydrodynamic pressure
P	Impulsive force
P_a	Power index
P_c	Hydrodynamic convective force

$\{p_e\}$	Nodal pressure vector
P_i	Hydrodynamic impulsive force
P_r	Inertia force exerted on the roof
P_w	Inertia force exerted on the wall
p_1	Impulsive pressure
p_2	Convective pressure
$p3$	Liquid pressure due to the wall deformation relative to the base
Qy	Yield strength of bearing
R	Tank radius in cylindrical containers
R_c	Response modification factor corresponding to convective term
$[R_e]$	Coupling matrix
R_i	Response modification factor corresponding to impulsive term
Rroot	Radius of the supporting shaft structure
rt	Radius of the cylindrical steel shell in elevated tanks
r - ϕ - z	Cylindrical coordinate system
Sac	Spectral acceleration corresponding to the convective mode
Sai	Spectral acceleration corresponding to the impulsive mode
S_{DS}	Design spectral response acceleration at short periods
S_{D1}	Design spectral response acceleration at 1-second period
S_S	Mapped MCE (Maximum Considered Earthquake) spectral response acceleration at short periods
S_1	Mapped MCE spectral response acceleration at 1-second period
t	Time
T	Natural period of vibration
T_c	Natural period of convective mode
tcon	Average thickness of the conical portion of the elevated tank
tcyl	Average thickness of the cylindrical portion of the elevated tank
teta	Cone angle in elevated tanks
T_f	Fundamental period of the tank/pedestal system
tfloor	Thickness of the elevated tank's floor

T_i	Natural period of impulsive mode
$T_i(C_j)$	Engineering stress values
T_i^E	Experimental stress values
t_r	Total duration of the ground motion
tshaft	Thickness of the concrete shaft wall
t_w	Thickness of the tank wall
t_0	Time at the beginning of the strong shaking phase
$\{u\}$	Displacement vector
$\{\dot{u}\}$	Velocity vector
$\{\ddot{u}\}$	Acceleration vector
$\{u_e\}$	Nodal displacement component vector
$\ddot{u}_i^t$	Total acceleration of the equivalent simple oscillator
$\dot{u}_0$	Ground velocity
$\ddot{u}_0$	Ground acceleration
$\dot{u}, \dot{v}, \dot{w}$	Fluid velocity components in x, y, and z directions
$\ddot{u}, \ddot{v}, \ddot{w}$	Fluid acceleration components in x, y, and z directions
V	Seismic base shear
V_r	Wall velocity relative to the ground
W	Strain energy potential
W_c	Effective weight of the stored liquid corresponding to convective component
W_e	Total effective weight of the system
W_i	Effective weight of the stored liquid corresponding to impulsive component
WL	Weight of the contained liquid
W_r	Weight of the tank roof
W_w	Weight of the tank wall
x	Displacement of the container in simplified mechanical model
x_n	Displacement of the equivalent masses relative to the tank wall in simplified mechanical model
X_0	Excitation amplitude for the case of harmonic pure lateral excitation of the tank

x-y-z	Cartesian coordinate system
α	Rayleigh damping constant
α_i	Rubber material constants
β	Rayleigh damping constant
γ	Shear strain
ε	Effective mass coefficient
ε_{bulk}	Bulk strain
ε_i	Principal value of the engineering strain tensor in the ith direction
η	Viscosity
θ	Angle of oscillation in fluid domain
θ_H	Angle of oscillation at liquid free surface
θ_{Hm}	Maximum angular amplitude of fluid motion at the free surface
λ_i	Principal stretch ratio
$\overline{\lambda}_i$	Modified principal stretch ratio
μ	Initial shear modulus of the material
μ_i	Rubber material constants
ζ	Damping ratio
ρ_l	Liquid density
σ	Stress
τ	Shear stress
ϕ	Circumferential coordinate in cylindrical tanks
$\widetilde{\Phi}$	Velocity potential function
Φ_1	Potential function due to ground acceleration only
Φ_2	Potential function due to the sloshing only
Φ_3	Potential function due to the relative wall velocity
Ω	Excitation frequency for the case of harmonic pure lateral excitation of the tank
ω	Natural circular frequency

CHAPTER 1

INTRODUCTION

1.1 Background

There are a large number of storage tanks around the world most of which are used as water and oil storage facilities. Different configurations of liquid storage tanks have been constructed. However, ground supported, circular cylindrical tanks are more numerous than any other type because of their simplicity in design and construction, and also their efficiency in resisting hydrostatic and hydrodynamic applied loads. These structures play an important role in municipal water supply and fire fighting systems. Cylindrical tanks may be made of either concrete or steel. They can be easily constructed in different sizes to fulfill the capacity requirements.

Many storage tanks are considered as essential facilities and are expected to be functional after severe earthquakes. This is partly due to the need for water to extinguish fires that usually occur during such earthquakes. Furthermore, damaged tanks containing petroleum or other hazardous chemicals could cause irreparable environmental pollution. In such situations, fire and fluid spillover are of main concerns.

In order to provide the head of water required for water supply process, cylindrical tanks are usually installed on a supporting tower, thereby instead of requiring heavy pumping facilities, the necessary pressure can be obtained by gravity. The supporting structure could be an axisymmetrical concrete shaft or a framed assembly (both steel braced frame and reinforced concrete). Elevated tanks normally consist of a thin-walled steel vessel welded at its base to a circular steel plate which in turn is anchored to the underlying concrete slab. The steel vessel is

1

normally constructed from curved panels, but welded together along circumferential and longitudinal edges. In practice, there are three common configurations for elevated composite steel-concrete tanks: dome floor, slab floor, and suspended steel floor. The elevated composite tanks with dome floor system which are investigated in this study are generally preferred to other types (see Figure 1.1).
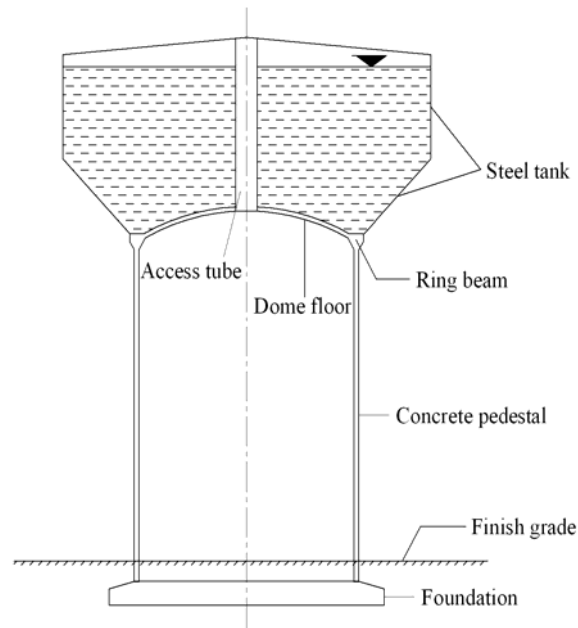
Figure 1.1 Configuration of elevated composite tanks used in this study

The structural design criteria of liquid containing structures against earthquake are different from those of general building structures. Reinforced concrete tanks require serviceability limit states such as leakage, deflection, and durability limit, due to the nature of their use.

Only few guidelines are presently available in North America for earthquake-resistant design of liquid storage tanks. In addition, parts of these guidelines are not in full consistency with the rest. Currently, ACI 350.3-06 (2006) standard in conjunction with ASCE 7-05 (2006) and ACI 371R-08 (2008) are used for seismic design of elevated tanks. Most of the current codes

and standards have adapted Housner's method (Housner 1957; 1963) for seismic analysis and design of LCS. There are some debates that the corresponding available guidelines are inaccurate in terms of the seismic induced loads on the tank wall which can consequently affect the required section properties of the earthquake-resistant structural system.

Most of the current codes including ACI 350.3-06 assume rigid wall boundary condition in estimating the hydrodynamic forces acting on the tank wall. However, tank wall flexibility could increase the hydrodynamic pressure significantly as compared to the rigid wall assumption. As a result, more investigation regarding the effect of wall flexibility on seismic behavior of cylindrical liquid-filled tanks seems essential.

The poor seismic performance of both steel and concrete ground-supported water tanks under earthquake ground motions has been observed in major past earthquakes. In regions with high seismic intensity many tanks have been severely damaged and some have collapsed with disastrous outcomes. For example, severe damages suffered during the 1933 Long Beach, 1952 Kern County, 1964 Alaska, 1964 Niigata, 1966 Parkfield, 1971 San Fernando,1978 Miyagi prefecture, 1979 Imperial County, 1983 Coalinga, 1994 Northridge and 1999 Kocaeli earthquakes which revealed a complex behavior of ground-supported liquid storage tanks during seismic motions (Rinne (1967), Shibata (1974), Kono (1980), and Sezen and Whittaker (2006)). This weakness in seismic performance was also observed among elevated water tanks. As for example, one can refer to the poor performance of some elevated water tanks having reinforced concrete shaft-type supports during the 2001 Bhuj (Rai (2002)) and the 1997 Jabalpur (Rai et al. (1997)) earthquakes in India. In the Bhuj earthquake, three elevated water tanks collapsed completely, and many more were damaged severely. Similar damage was also observed in the

3

Jabalpur earthquake. Reviewing the available literature, one can say that little effort has been done to better identify the dynamic behavior of elevated tanks.

The reported damage due to previous seismic events could have happened due to the following three reasons:

1) Coupled motion of the tank shell and stored liquid due to the short-period component of the seismic wave. This behavior is referred to as bulging. Under such vibration, a large part of the stored liquid acts as inertial mass with a period much shorter than the sloshing natural period. Tank walls are expected to be subjected to considerable inertial force and dynamic fluid pressure as a result of this type of vibration.

2) Liquid sloshing due to the long-period component of the seismic wave. Sloshing response in tanks may have long natural period of several seconds to a few tens of seconds. This phenomenon may result in highly localized pressure on the body of the tank, substantial uplifting pressure at the tank roof or may cause spillover of stored liquid in open top tanks. Sloshing response in tanks particularly depends on the tank geometry/dimensions and dynamic characteristics of the ground motion.

3) Loss of soil bearing capacity as a result of liquefaction which in turn could result in nonuniform settlement of the tank foundation.

The conventional method for earthquake-resistant design of elevated water tanks is to increase the strength of the structure so that it can tolerate the design earthquake safely. As a result of this strengthening, higher seismic forces will be applied to the structure. Contrarily, the effect of seismic input can be significantly reduced using *menshin* (earthquake reduction) method (Kumieda (1976), MITI (1980), and Aoyagi and Shiomi (1985)). Menshin method is a technique for reducing the amplitude of seismic vibrations being exerted on the structure. Considering the

large number and size of liquid storage tanks, any safe reduction in structural material results in economical benefit. In menshin technique, safety of the structure is ensured through adjusting the dynamic properties of the structure properly. This could be implemented by either one or combination of following methods:

1) *"Natural period adjustment method"* in which the seismic response of the structure is reduced by increasing its natural period far beyond the predominant periods of the input earthquake. This may be accomplished by either mounting the structure on certain flexible mounts such as elastomeric bearings or by making alterations in structural configuration/geometry leading to a more flexible structural design.

2) *"Energy dissipation method"* in which the input seismic energy is absorbed by means of energy absorbing devices attached to the structure. Devices such as lead-rubber bearings, viscous dampers, or friction dampers may be used for this purpose.

3) *"Isolation method"* in which the structure is decoupled from the ground by means of isolators. The structure may be free to slide easily if mounted on low friction pads. Isolation could be implemented using fluids (floating type), sliding plates, or different types of bearings. In this study, the base isolation of elevated water tanks using lead-rubber and elastomeric bearings is discussed in detail. Further details on the above-mentioned methods will be provided in Chapter 8.

In menshin technique application, appropriate evaluation of the dynamic characteristics of ground motion, menshin device, and structure is essential. It is also necessary to employ a highly accurate method of dynamic analysis. In this study a rigorous finite element model (FEM) to simulate the precise three-dimensional behavior of the isolated elevated tanks involving nonlinear behavior of isolation devices is used. Using this FEM, one can therefore estimate the

seismic response of isolated elevated tanks taking into account the properties of isolation devices in detail.

The main challenge in predicting the seismic behavior of liquid-filled structures is the identification of the vibration response of the tank taking into account the fluid-structure interaction (FSI). A dynamic study of such tanks must allow for the motion of the water relative to the tank as well as the motion of the tank relative to the ground. In this study, different numerical techniques are employed for dynamic analysis of fluid domain.

For tanks which are closed and fully filled with water or are completely empty, the behavior of the tank may be well estimated as a one-mass system. However, usually the tanks are partially filled with water. In this case, the tank has a free water surface and thus, there will be the sloshing of the water free surface during a seismic motion, which makes the behavior of the tank-liquid system a complicated coupled problem. In this case, the dynamic behavior of the tank may be quite different. For certain proportions of the tank-liquid system, the response of the system is dominated by the sloshing of the water, on the other hand, there are other proportions that the sloshing may have minor contributions in response. Therefore, an understanding of the seismic behavior of liquid-filled tanks requires an understanding of the hydrodynamic pressures and forces associated with the oscillating water. These pressures and forces depend on the characteristics of the ground motion, the properties of the contained liquid, and the geometrical and physical properties of the tank itself.

In this study, the finite element (FE) technique is used to investigate the seismic response of ground-supported as well as elevated water tanks. The results of this research will provide some useful information regarding the actual behavior of LCS under seismic motions. This study will

also lead to some recommendations for more accurate seismic analysis and design of elevated water tanks.

1.2 Objectives and scope

The main focus of the current study is to evaluate the performance of ground-supported cylindrical as well as liquid-filled elevated water tanks supported on concrete shaft under seismic loading. Different types of analysis including modal, spectral and time history analysis (using both modal superposition and direct integration methods) are performed using the general-purpose finite element analysis program ANSYS®. Using the proposed FE technique, impulsive and convective response components are obtained separately. Furthermore, the effects of wide range of parameters including tank wall flexibility, sloshing of the water free surface, vertical component of earthquake, base fixity, and higher impulsive and convective modes on dynamic response of these tanks are addressed.

In order to investigate the effect of earthquake frequency content on dynamic behavior of such structures, four different ground motions having different frequency contents ranging from low to high are used.

In addition, to investigate the accuracy of code provisions in seismic analysis and design of liquid containing structures, a comparison between the calculated FE results and those proposed by current practice is made.

Through this research, a detailed parametric study is also carried out on elevated water tanks. The tank geometry parameters used for the study covers a broad range of tank capacities and aspect ratios found in practice today. Based on the results of parametric study, graphs

7

corresponding to both impulsive and convective hydrodynamic pressure distribution are produced which can be easily employed in design applications for elevated water tanks.

Furthermore, two different techniques to reduce the seismic response of elevated water tanks are investigated; the first is to increase the inclined cone angle of the lower portion of the combined vessel, and the second is to isolate the tank using different types of isolation devices such as elastomeric and lead-rubber bearings.

In summary, the main objectives of this research are as follows:

1) Perform a comprehensive study on the dynamic behavior of cylindrical ground-supported and elevated water tanks and determine the deciding factors based on the obtained results.

2) Understand the effect of a broad range of parameters on dynamic behavior of liquid containing structures such as: tank aspect ratio, vertical component of earthquake, sloshing of the liquid free surface, wall flexibility, damping characteristics of the liquid components, rocking motion of the vessel in elevated tanks, base fixity, and higher impulsive and convective modes.

3) Investigate the effect of ground motion frequency content on dynamic response of elevated water tanks.

4) Simulate fluid-structure interaction problems in tanks with complex geometries such as conical tanks.

5) Verify the proposed FE models by comparing the calculated results with those obtained through exact analytical solution and/or other experimental studies reported in the literature.

6) Investigate the validity of the current practice in estimating the seismic response of cylindrical ground-supported and elevated water tanks.

7) Develop a parametric model capable of creating any FE model of a 3D liquid-filled tank either elevated or ground-supported with varying parameters such as shaft radius, shell thickness, tank radius, shaft height, tank height, and liquid depth.

8) Carry out an extensive parametric study on the dynamic response of elevated water tanks and provide hydrodynamic pressure distribution graphs to be used in seismic design of elevated water tanks.

9) Examine two innovative techniques for seismic response reduction in elevated water tanks. The proposed techniques are: a) increase the inclined cone angle of the vessel, and b) isolate the supporting shaft structure.

The scope of this study is summarized as follows:

1) The tanks are assumed to be rigidly anchored to the rigid ground such that no sliding or uplift may occur. As a result, the effect of soil-structure interaction is not considered.

2) The tank walls are considered to be of constant thickness.

3) Only open top cylindrical ground-supported and conical elevated tanks supported on concrete shaft are considered through this study. However, one can use the proposed FE technique with some modifications to estimate the dynamic response of tanks having other configurations.

4) In dynamic analysis of elevated water tanks, only the effect of horizontal ground motion is considered. However, in seismic analysis of ground-supported tanks effect of vertical vibration is also taken into account.

5) The fluid is assumed incompressible and inviscid.

6) Study of the convective response of the contained liquid is based on the linear theory of sloshing.

7) In FE modeling of the tanks, all structural materials except for the isolators' materials are assumed to behave as linear elastic.

1.3 Research significance

The FE method used in this study has several advantages over previous studies carried out on liquid containing structures. One of the main advantages of the current method is in assigning desired damping amounts to different liquid components (impulsive or convective) as well as different structural segments. Using this technique, the response of both components can be obtained separately.

In this research, study of liquid sloshing effects in tanks with complex geometries such as conical shaped tanks is made possible. The results of this study show that the proposed finite element technique is capable of accounting for the fluid-structure interaction in liquid containing structures. The suggested FE model is verified by comparing the obtained results with well-proved analytical and experimental results available in the literature.

One of the important factors regarding the dynamic behavior of circular containers, not taken into consideration precisely in previous investigations, is the effect of vertical ground acceleration. This effect was generally neglected in the dynamic analysis. However, studying the near-field earthquake records and the associated damages observed, revealed the importance of considering such effects in the seismic design of such structures. In most of the current codes, the vertical excitation effect is accounted for by assuming the two thirds of the horizontal response

spectrum as the vertical acceleration. However, this approximation could be unreasonable since recent studies have shown that the vertical response spectrum values could differ significantly depending on the distance of the site to the seismic source. The values are higher in the near-field regions and in the high-frequency range of the response spectrum. As a result, the values recommended by current practice could be extremely unconservative at high frequencies in the near-field regions and therefore the applicability of such provisions is questionable.

The other parameter which is ignored in the current practice is the effect of base fixity. The natural period of vibration of the tank-liquid system and as a result the hydrodynamic forces could be affected by different conditions at the base. This is an important factor not studied adequately in the literature and therefore needs more investigation.

Regarding the seismic analysis and design of elevated water tanks the need for such study is even more. In FE analysis of conical elevated tanks, due to the inclination of the walls, the boundary conditions affecting the hydrodynamic pressure developed are different from those acting on cylindrical tanks. In elevated tank design, usually for simplicity the conical portion of the vessel is ignored in modeling and the entire vessel is modeled as an equivalent cylinder. However, using the rigorous technique introduced in this research, studying the effect of fluid-structure interaction in tanks with complex geometries such as conical tanks has been made possible and practical guidelines to overcome these modeling difficulties are addressed.

The other deciding factor which has not been addressed in design codes and standards is the role of rocking mode of vibration of the supporting tower. Haroun (1985) studied this effect by including both lateral translational and rotational degrees of freedom at the top of the supporting shaft. It was concluded that the effect of rocking motion could be significant especially when the

11

coupling between wall flexibility and tank rotation is considered. However, some important effects were not included in Haroun's study such as;

1) the liquid was not modeled as a continuous medium and its effect was only accounted for by an equivalent mechanical model consisting of lumped masses located at a specific height from the tank floor.

2) liquid sloshing component was neglected in the model proposed for flexible elevated tanks.

3) emphasis was placed only on the seismic behavior of the supporting structure, no effort was made to study the dynamic behavior of the vessel.

4) the vessel was assumed to be rigidly connected to the supporting tower that is no relative rotation could occur between the vessel base and the tip of the tower.

5) vessels in elevated water tanks usually consist of a conical lower section having inclined side walls. This inclination could have a significant effect on dynamic behavior of the vessel as well as the supporting shaft. The method proposed in Haroun's study is not capable of considering this effect.

6) only horizontal excitation can be investigated using Haroun's model.

Considering above-mentioned deficiencies, evaluating the accuracy of current practice by comparing the code results with those obtained from a rigorous analysis seems necessary. Throughout this research, effort has been made to address this important objective. The results of this research provide some useful insights in terms of the dynamic behavior of these types of structures.

Concerning the dynamic response of ground-supported and elevated water tanks there are areas in the literature that need to be further investigated. Kianoush and Chen (2006) studied the

combined effect of horizontal and vertical ground accelerations in rectangular liquid storage tanks, however no study has been carried out to consider such effect for cylindrical ones.

The effect of earthquake frequency contents on the dynamic behavior of liquid-filled tanks need to be investigated by selecting input ground motions having low, intermediate and high frequency contents and performing a series of rigorous time-history analyses.

In addition, very few studies can be found in the literature regarding the seismic behavior of liquid-filled conical elevated tanks. The need for proposing a thorough method capable of considering all deciding parameters and assessing the relative importance of such effects on the overall seismic response of elevated tanks seems essential. This can be achieved through performing an extensive parametric analysis encompassing the range of conical elevated tanks typically found in use today.

Recent investigations show that seismic isolation is an effective alternative for reducing the vibration amplitude of the structures under seismic waves. However, there are very few studies in the literature regarding the application of this technique to elevated water tanks. In all of these studies, the entire system including the isolation system, shaft structure, and contained fluid is modeled as a discrete three or four-degree-of-freedom model. During this study, effort has been made to develop a detailed three-dimensional FE model in order to eliminate the inaccuracies associated with such simplifications in dynamic analysis of isolated elevated tanks. The proposed model is also capable of accounting for the nonlinear hysteretic behavior of the isolators.

1.4 Thesis layout

The outline of this thesis involves nine chapters defined according to the objectives and scope of the research. The first chapter includes the introduction, the scope, objectives and significance of the research and the outline of the thesis.

The second chapter presents a summary of the previous research studies carried out on dynamic response of liquid containing structures, both ground-supported and elevated tanks. An overview on existing codes, standards, and guides used in design of liquid storage tanks is also provided in this chapter.

Chapter 3 addresses analytical formulations regarding the calculation of fluid dynamic response in cylindrical liquid containers. Lamina fluid theory and velocity potential theory commonly used for obtaining the hydrodynamic pressures and sloshing response of the tanks under seismic excitations are explained in this chapter.

Chapter 4 deals with the finite element formulation of three-dimensional liquid containing structures. A discussion on how to consider the fluid-structure coupling effect in finite element modeling of liquid containing structures is made. In addition, the corresponding equations of motion of liquid domain accounting for both the impulsive and sloshing components of response are addressed.

The dynamic behavior of cylindrical ground-supported water tanks is discussed in Chapter 5. Effects of important parameters including sloshing of liquid free surface, tank wall flexibility, vertical ground acceleration, tank aspect ratio, and base fixity are addressed in this chapter. The validity of current practice in seismic analysis of liquid-filled cylindrical containers is also investigated.

In Chapter 6, the dynamic behavior of conical elevated tanks in a three-dimensional space is investigated using the proposed FE technique. Furthermore, the accuracy of current practice in predicting the dynamic behavior of elevated water tanks is studied. In the second part of the chapter, the effect of earthquake frequency content on the seismic behavior of liquid-filled conical elevated tanks is studied.

Chapter 7 discusses the results of a comprehensive parametric study carried out on liquid-filled conical elevated tanks using the finite element technique. A wide spectrum of tank capacities and geometries typically found in practice today is covered in this parametric study. Based on the results of this parametric study, pressure distribution graphs corresponding to impulsive and convective components are created by carrying out spectral analyses on a large number of conical elevated tanks with different capacities and geometrical properties. It is shown that the proposed pressure graphs can be utilized conveniently with high level of accuracy in design applications for liquid-filled conical elevated tanks.

In Chapter 8, the application of *menshin* techniques to liquid-filled conical elevated tanks is examined using a rigorous finite element method in a three-dimensional space. The effectiveness of two different menshin techniques in elevated water tanks is investigated. In the first part of the chapter, the first menshin technique called *"Natural period adjustment method"* is applied to elevated water tanks. To this end, it is recommended to increase the inclined cone angle of the lower portion of the vessel. The efficiency of the proposed method is studied by carrying out FE time-history analyses on different elevated tank models with different cone angles and comparing the obtained results. The second part of the chapter deals with the application of seismic isolation using elastomeric and lead-rubber bearings to liquid-filled conical elevated tanks.

In Chapter 9, conclusions and some suggestions for future work are presented. The thesis ends with a list of references and three appendices. In the first appendix, details of the lamina fluid theory discussed in Chapter 3 are presented. The second appendix provides the input text command files for the tank's parametric model and the post-processors used in Chapter 7. The pressure distribution graphs obtained through the parametric study explained in Chapter 7 are given in the third appendix.

CHAPTER 2

LITERATURE REVIEW

2.1 Introduction

In this chapter an extensive literature review on dynamic response of liquid containing structures is presented. In Section 2.2 seismic performance of liquid storage tanks and associated damage types suffered during actual seismic events is discussed. Section 2.3 reviews and summarizes the available literature on seismic response of liquid storage tanks. Both ground-supported and elevated tanks are addressed. The significant contributions made by previous researchers are also explained. An overview on existing codes, standards, and guides used in design of liquid storage tanks along with a literature review on application of seismic isolation to liquid storage tanks are provided in Section 2.4.

2.2 Earthquake damage to liquid storage tanks

There are frequent reports regarding the damage to liquid storage tanks due to previous earthquakes in the literature. For instance, there were heavy damages to both concrete and steel storage tanks during the strong seismic events such as 1933 Long Beach, 1952 Kern County, 1964 Alaska, 1964 Niigata, 1966 Parkfield, 1971 San Fernando, 1978 Miyagi prefecture, 1979 Imperial County, 1983 Coalinga, 1994 Northridge, and 1999 Kocaeli earthquakes (Rinne (1967), Shibata (1974), Kono (1980), Manos and Clough (1985), and Sezen and Whittaker (2006)).

Severe damage levels were also observed in elevated water tanks during the 1960 Chilean as well as the 1997 Jabalpur (Rai et al. (1997)) and 2001 Bhuj (Rai (2002) and Dutta et al. (2009)) earthquakes in India. During the Bhuj earthquake many elevated tanks suffered severe damages

17

in terms of flexural cracks in the circumferential direction in their supporting shafts near the base. Three elevated water tanks located in the highest intensity shaking zones also collapsed. Anshel (1999) has also reported heavy damages to cylindrical buried concrete tanks due to the 1995 Kobe earthquake. An underground concrete tank was also damaged severely in the from of the collapse of the wall during the 1971 San Fernando earthquake (Jennings (1971)).

Failure mechanism of liquid storage tanks depends on different parameters such as construction material, tank configuration, tank type, and supporting mechanism. Reported damage to liquid containing structures (LCS) during past earthquakes fall into one or more of the following categories:

1) Buckling of the shell caused by excessive axial compression of the shell structure due to exerted overturning moment (elephant-foot buckling)

2) Deformation, cracks and leakage in side shell

3) Damage to the roof or the upper shell of the tank, due to sloshing of the upper portion of the contained liquid in tanks with insufficient free board provided between the liquid free surface and the roof

4) Spillover of the stored liquid

5) Failure of piping and other accessories connected to the tank because of the relative movement of the flexible shell

6) Damage to the supporting structure in elevated water tanks

7) Damage to the anchor bolts and the foundation system

8) Failure of supporting soil due to over-stressing

In the 1964 Niigata earthquake, several damage modes including damage modes 3 and 4 due to excessive sloshing, mode 8 due to liquefaction of the supporting soil as well as damage modes 7 and 5 became prominent.

In the 1964 Alaska and 1971 San Fernando earthquakes, the lower part of the side shell bulged all along the perimeter as a result of mode 1 (elephant-foot buckling). This buckling type damage generally happens due to the excessive overturning moment generated during the seismic event.

In cases where the tank contains hazardous materials, liquid spillover (damage mode 4) and fire subsequent to a major earthquake may result in even more severe damage than the earthquake itself. The extensive uncontrolled fire eruption during the Niigata earthquake at Showa Petroleum blazed for about 15 days, resulting in main destruction of the plant and residential apartments (Niigata Nippo Co. (1964)). The Niigata and Alaska earthquakes of 1964 resulted in considerable loss in the petroleum storage tanks. This significant loss attracted many practicing engineers and researchers to further investigate the seismic behavior of liquid storage tanks especially when the stored liquid is a hazardous material such as petroleum.

As an example of damage mode 4, one can mention oil spillover into the harbor that happened in the Sendai Refinery of Tohoku Petroleum Company during the 1978 Miyagi earthquake (Hazardous Material Technology Standards Committee: Fire Defense Agency (1979)).

During the Northridge earthquake main lifeline facilities of the Los Angeles area experienced severe damage. Five steel tanks were also damaged in the San Fernando Valley area. Buckling was the prominent form of damage in all of the damaged tanks. Several other tanks also suffered roof collapse due to the excessive sloshing of the stored liquid (Lund (1996)).

It is important to note that the damage mode in concrete tanks is different from that of steel tanks. Elephant-foot buckling, anchorage system failure, and sloshing damage to the roof and upper shell of the tank are the most common damages in steel tanks (see Figure 2.1).

In tanks found in practice, full base anchorage is not always a possible or economical alternative. Therefore, many tanks are either unanchored or partially anchored at their base. If the tank is not rigidly anchored to the ground, the generated overturning moment due to earthquake may be large enough to result in lift-off of the tank base. As the tank base falls back down after lift-off, high compressive stresses are generated in the wall near the base leading to elephant-foot wall buckling. This mode of damage is more common in steel tanks since they are generally more flexible than concrete tanks.

Some studies show that base lift-off in tanks having flexible soil foundations does not cause high axial compressive stresses in the tank wall. As a result, unanchored tanks flexibly supported at their base are less susceptible to elephant-foot buckling mode, but are more susceptible to uneven settlement of the foundation (Malhotra (1995) and Malhotra (1997A)).

On the other hand, damage mode 2 is the most common type of damage in concrete tanks. Stresses caused by large hydrodynamic pressures together with the additional stresses resulted from the large inertial mass of concrete could cause cracking, leakage and ultimately failure of the tank. That is why the design criteria for concrete tanks are based on crack control.

It is worth noting that elevated water tanks are very susceptible to seismic excitations because of the concentrated large mass located at top of the shaft structure. As a result, strong lateral seismic motions may result in large tensile stresses on one side of the concrete shaft section which may eventually lead to severe cracking or even collapse of the concrete pedestal.

As mentioned before, many elevated tanks collapsed during the 1960 Chilean, 1997 Jabalpur and 2001 Bhuj earthquakes since insufficient reinforcement was provided in the shaft section.
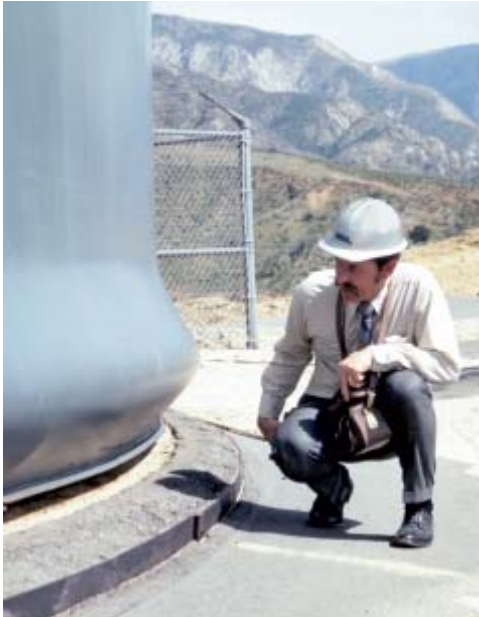
(a)

(b)

(c)

Figure 2.1 Common damage modes: (a) Elephant-foot buckling, (b) Inelastic stretching of

an anchor bolt at the tank base (c) Sloshing damage to the upper shell of the tank

(adapted from Malhotra et al. (2000) and Malhotra (2000))

The significance of preventing such damages has led to a great deal of research to be carried out on dynamic behavior of such structures. These research studies could result in a better comprehension of the complicated behavior of liquid containing structures under seismic excitations.

2.3 Previous research

2.3.1 Response of ground-supported tanks

A comprehensive research work on dynamic behavior of liquid-filled tanks has been carried out both theoretically and experimentally. Initial studies involved analytical investigation of dynamic response of liquid containing structures having rigid wall and supported on rigid foundations. Extensive study on the dynamic behavior of liquid containing structures started in the late 1940's. Jacobsen (1949) and Jacobsen and Ayre (1951) studied the dynamic response of cylindrical tanks subjected to horizontal ground motions. They estimated the effective hydrodynamic masses and mass moments for the accelerated contained liquid.

In the early 1960s, Housner (1963) proposed a useful idealization for obtaining liquid response of rigid rectangular and cylindrical water tanks fully anchored to the rigid foundation and subjected to horizontal ground motion. Liquid was assumed to be incompressible and inviscid. This method is probably one of the most well-known procedures available in the literature. However, attention should be drawn to the effect of tank wall flexibility which is not considered in this simplified technique. Housner separated the tank hydrodynamic response into "impulsive" motion, in which the liquid is assumed to be rigidly attached to the tank and moves in unison with the tank shell, and "convective" motion, which is characterized by long-period oscillations and involves vertical displacement of the fluid free surface. Under seismic motions,

impulsive water undergoes the same acceleration as the ground. This component is believed to have a significant contribution to the base shear and base moment. In this study, Housner developed simple equations to approximate the hydrodynamic pressures in the tanks using lumped mass approach.

Many current standards and guides such as ACI 350.3-06 and ACI 371R-08 have adapted Housner's method with some modifications which were the results of subsequent studies by other researchers for seismic design of liquid storage tanks. As mentioned before Housner's method is not capable of accounting for the effect of tank wall flexibility. Therefore, as an approximate method ACI 350.3-06 accounts for wall flexibility by determining the oscillating water mass components from the rigid tank solution and only using the amplified pseudoacceleration corresponding to the fundamental natural frequency of the system instead of the ground acceleration. This approximation may be unduly inaccurate for values of H/R (liquid depth/tank radius) greater than 1 (Veletsos (1984)).

Edwards (1969) for the first time suggested a finite element method to be employed for estimating the seismic response of deformable liquid storage tanks. A cylindrical liquid storage tank with the height to diameter ratio of less than one was analyzed using the finite element technique. The proposed FEM was capable of accounting for the coupled interaction between the stored liquid and the elastic tank shell.

Using Housner's model, Epstein (1976) produced design curves for calculating the overturning moment due to hydrodynamic pressures in both rectangular and cylindrical storage tanks.

Veletsos (1974) and Yang (1976) showed that the flexibility of the tank shell could have a significant effect on dynamic forces induced by horizontal ground motion in liquid-filled

cylindrical containers. It was concluded that the flexibility of the walls of such tanks has a substantial effect on the impulsive component of the response. Veletsos and Yang (1977) modified this method by using Flugge's shell theory (Flugge, 1960) in combination with the Rayleigh-Ritz procedure to calculate the natural frequencies of the liquid-shell system. Both shell analysis and the simpler beam-type analysis were carried out.

The dynamic behavior of horizontally accelerated liquid storage tanks containing inviscid liquid was further investigated by Hunt and Priestley (1978). Both rectangular and cylindrical configurations were examined. The results of the study led to derivation of mathematical equations regarding the contained fluid motion under dynamic excitations. The displacement of liquid free-surface was measured experimentally for a cylindrical water tank tested on a shaking table and subjected to both sinusoidal and seismic excitations. The predicted theoretical results were in close agreement with those obtained through experiment.

Clough and Clough (1977) and Clough et al. (1979) for the first time performed a series of experimental tests on large-scale thin-walled liquid storage tanks. The obtained hydrodynamic pressures were much larger than those proposed by Housner's analytical method. The difference in pressures was believed to be due to the tank wall flexibility effect. Several other numerical and analytical studies taking into account the interaction between flexible shell and the containing liquid were conducted among which significant contributions were made by Haroun (1980) and Barton and Parker (1987).

Haroun and Housner (1981A) studied the behavior of deformable liquid storage tanks using modal superposition analysis. In this study, the tank shell was modeled by finite elements and the fluid domain was treated mathematically using boundary solution technique.

Haroun and Housner (1981B) developed a mechanical model capable of including the effect of wall deformability. The proposed three-degree-of-freedom (DOF) mechanical model involved three equivalent lumped masses corresponding to the convective component contributed by the sloshing of the liquid, the impulsive component which varies in unison with the horizontal ground acceleration, and the short period component contributed by the deformable wall vibrations. The latter component is only present in flexible liquid containers. In a tank with rigid wall boundary condition, only the first two components need to be considered. The study also showed that the tank wall deformability may result in the hydrodynamic pressures several times larger than those experienced in rigid wall tanks. Based on this study, design charts for estimating the equivalent lumped masses of the proposed mechanical model were derived. It was assumed that the liquid contained in the tank was incompressible and had irrotational flow.

Balendra et al. (1982) presented a finite element analysis of an annular cylindrical tank with an axisymmetric elastic dome, using a FE code. The fluid inside the tank was considered as inviscid and incompressible. However, sloshing of the fluid was neglected.

Minowa (1980 and 1984) further studied the tank wall flexibility effect and the corresponding hydrodynamic pressure exerted on the tank shell. He also performed experimental studies on the dynamic behavior of rectangular liquid-filled tanks.

Haroun (1983) also performed a series of experimental investigations including forced and ambient vibration tests on flexible ground-supported cylindrical tanks. In order to determine the mode shapes of vibrations and corresponding natural frequencies, three full scale water storage tanks were tested. This study led to a better understanding of dynamic behavior of liquid storage tanks.

Haroun (1984) evaluated the dynamic response of rectangular concrete liquid storage tanks using the classical potential flow approach assuming a rigid wall boundary condition. The fluid was assumed to be homogeneous, incompressible and inviscid. The tank was assumed to be subjected to the simultaneous action of horizontal and vertical components of earthquake. Bending moments developed in the walls of rectangular liquid-filled tanks due to seismic excitation at their base were calculated. As a result of this study, theoretical equations to evaluate the internal moments in the tank wall were derived and numerical values of moment coefficients to be used in seismic design of rectangular tanks were tabulated.

Veletsos and Kumar (1984) developed a simplified approach for estimating the effect of vertical ground motion on cylindrical liquid storage tanks.

Haroun and Tayel (1985) employed the finite element technique for investigating the dynamic behavior of cylindrical liquid storage tanks having elastic wall and subjected to vertical seismic excitations. The proposed method was based on the superposition analysis technique using the axisymmetrical free vibration modes of the tank-liquid system. The axial and radial components of the wall displacement together with the resulting stresses were calculated. In obtaining the dynamic response of the tanks, effect of liquid sloshing was ignored.

Veletsos and Tang (1990) studied the dynamic behavior of liquid containing tanks resting on flexible foundations through rigid base mats. The results of the study indicated that the translational and rocking vibrations of the tank base resulted in extended impulsive period and also larger effective damping. They had previously concluded that soil-structure interaction reduces the hydrodynamic effects in tanks subjected to vertical excitations (Veletsos and Tang (1986)).

Park et al. (1992) used a coupled boundary element-finite element method (BEM-FEM) to study the dynamic behavior of concrete rectangular tanks. The dynamic response of the tanks was obtained using the time-history analysis method. Both impulsive and convective components were included.

Coupled free vibration dynamics of cylindrical liquid storage tanks was studied by Gupta (1995). The vibration study of the container was made possible using Flugge's exact equations of motion. The hydrodynamic pressure associated with the contained liquid was obtained using the velocity potential approach. The obtained results compared well with those calculated by Haroun and Housner method.

Kim et al. (1996) used Rayleigh-Ritz method to study the dynamic response of a flexible rectangular liquid storage tank. In this study, the effect of sloshing component of the contained liquid was neglected.

The dynamic response characteristics of rectangular fluid containers was further studied by Dogangun et al. (1997 and 2004). He used analytical methods as well as finite element method using the modified structural analysis program SAPIV to evaluate the dynamic response. The fluid domain was modeled by displacement-based fluid elements. Effect of tank wall flexibility on dynamic behavior of tanks was also investigated. The proposed model was capable of including the effects of fluid compressibility and free-surface sloshing motion. The obtained FE results were compared with those obtained through boundary-finite element method (BEM-FEM) and requirements of Eurocode-8.

Koh et al. (1998) proposed a coupled BEM-FEM technique including free-surface sloshing vibration, to investigate the dynamic behavior of three dimensional rectangular water storage tanks under horizontal ground motions. In their study, finite element method was employed to

model the solid wall while the indirect boundary element method was used to model the fluid domain.

In a study by Chen and Kianoush (2005) a new procedure called sequential method for estimating the hydrodynamic pressures in rectangular tanks was introduced. In this method, fluid and structure domains are coupled through applying the results from the first analysis as loads or boundary conditions for the second analysis. The study was performed in a two-dimensional space and the effect of tank wall flexibility was also included. However, the effect of fluid sloshing was not taken into account.

Virella (2006) investigated the natural periods, mode shapes, and dynamic response to horizontal ground excitations of cylindrical tanks partially filled with a liquid. The finite element package ABAQUS was used to perform the computations. The contained fluid was modeled using two different techniques: the added mass formulation and acoustic fluid elements based on linear wave theory. The considered tanks had the height to diameter ratios from 0.40 to 0.95. No sloshing waves were considered in the study. It was concluded that the response of a tank-liquid system under horizontal excitation can be precisely estimated by considering just the fundamental mode. Furthermore, it was verified that the tanks with height to diameter ratios larger than 0.63 have the fundamental modes similar to the first mode of a cantilever beam. For the shortest tank considered in the study (H/D = 0.4), the fundamental mode was a bending mode.

The dynamic behavior of rectangular containers under vertical seismic excitations was also investigated in a later study by Kianoush and Chen (2006) in a two-dimensional space. It was concluded that the vertical ground excitation could cause significant seismic response in rectangular concrete tanks and therefore such effect should be considered in design.

A new approach for seismic analysis of rectangular liquid storage tanks in time domain taking into account the effects of both impulsive and convective components was introduced by Kianoush et al. (2006). The method was able to solve the coupled liquid-filled tank problem in three-dimensional space.

Ghaemmaghami et al. (2010) investigated the seismic behavior of both concrete rectangular and cylindrical liquid storage tanks in three-dimensional space. The containers were assumed to be fixed to the rigid ground. Both impulsive and sloshing components of response were considered. The tank models were analyzed in time domain under the horizontal and vertical components of a real earthquake record. Fluid-structure interaction effects were taken into account incorporating wall flexibility. The study indicated that the effect of vertical excitation on the seismic response of the liquid tanks could be significant when considered individually, however it was of less significance when the horizontal and vertical earthquake components were applied together. This was valid for both rectangular and cylindrical tanks.

As opposed to ground-supported liquid storage tanks, limited number of literature is available regarding the dynamic response characteristics of elevated water tanks. Several attempts have been made over the past few decades to investigate the fluid-structure interaction effects in elevated water tanks.

2.3.2 Response of elevated tanks

The well-known Housner method enabled practicing engineers to carry out the seismic response analysis of elevated tanks using a two-mass idealization (Housner 1963). This simplified model allowed for the motion of water relative to the tank as well as the motion of the tank relative to the ground. Further application of such simple model in seismic analysis of

29

elevated tanks was reported by Sonobe (1969). In this study, both free vibration and stationary vibration tests were performed on two scale models of elevated water tanks. The first model was a cylindrical tank model supported by a frame which had several levels of rigidity. The ratio of the model to the prototype was 1/10 – 1/20. The second model was a spherical tank of the same size. Furthermore, a forced vibration test under the input of pseudo El-Centro NS 1940 record was carried out on the cylindrical elevated tank model. From the test, the dynamic response of the tank including maximum displacement and acceleration of the frame and maximum sloshing height of the stored water was measured. Experimental results were in good agreement with those obtained from the analytical solution using a simplified two-DOF system. In creating this equivalent model, the weight of the frame plus dead water was assumed to be rigidly fastened to the tank, while the weight of free water was assumed to be attached to the tank by means of springs.

Some researchers such as Chandrasekaran and Krishna (1965) and Tamiah and Gupta (1966) proposed that a satisfactory estimation of dynamic response of elevated water tanks may be obtained using a single-DOF model.

Shepherd (1972) also used a two-mass idealization model to represent the dynamic behavior of elevated water tanks. The validity of the model was verified by comparing the analytical values with those of a simple dynamic test conducted on a prestressed concrete elevated water tank. The examined tank was a prestressed concrete tubular tower supporting a cylindrical reinforced concrete tank. The equivalent water masses, the moment arms, and the effective spring stiffness were calculated using Housner's formulation. The predicted natural frequencies of the two modes of vibration obtained through analytical solution were compared with those measured through a simple pull-back test. The sloshing frequency of the water inside the tank

was determined by hand shaking tests. The percentage equivalent viscous critical damping was determined from the decay of the free vibration test results as 1.3%. The results of the study indicated that the use of a two mass equivalent model will provide satisfactory estimations of the natural frequencies of the elevated water tanks.

Ifrim and Bratu (1969) and Garcia (1969) also used a two-DOF representation to investigate the seismic response of elevated tanks.

Haroun and Ellaithy (1985) presented an equivalent mechanical model for evaluating the dynamic response of elevated water tanks. A cross braced frame as well as a concrete pedestal tower were analyzed. The effect of tank wall flexibility and both rocking and translational motions of vessel were included in the study. Analyses indicated that the rocking component of vessel could have a significant effect on maximum shear and moment exerted at the top of the tower. However, in their study the vessel was assumed to be rigidly connected to the supporting tower that is no relative rotation could occur between the vessel base and the tip of the tower.

Following the collapse of a conical tank in Belgium during the 1970s, an experimental research work was carried out on the stability of conical tanks under hydrostatic loading by Vandepitte et al. (1982). A similar problem was further addressed by El Damatty et al. (1997A) using an extensive numerical study. In this study, a finite element model capable of including both geometric and material non-linearities for stability analysis of liquid-filled conical tanks under hydrostatic loading was proposed. The effect of geometric imperfections on the stability of such structures was examined. The effect of such imperfections was modeled by introducing initial strains into the finite element model of the tank before applying the loads.

Joshi (2000) presented an equivalent mechanical model for seismic analysis of rigid intze type tanks under horizontal acceleration. Model parameters were evaluated for a wide spectrum

31

of tank shapes and compared with those of the equivalent cylindrical tanks. Fluid pressure was calculated using linearized potential flow theory. The fluid was assumed inviscid and incompressible and the sloshing height was assumed to be small. Furthermore, in developing the mechanical model only first sloshing mode was taken into account. It was concluded that the associated errors due to the use of equivalent cylindrical tank model instead of the original intze tanks were negligible. As a result, for design applications, the intze tank models may be replaced by the equivalent cylindrical models without loss of accuracy.

Seismic behavior of elevated conical steel tanks was studied by El Damatty et al. (1997B; 1997C). In the study, a numerical model was developed in which the tank wall was modeled by shell elements and the fluid effect was considered using the coupled boundary-shell element technique. Only the impulsive component of the hydrodynamic pressure was considered. Several tank models classified as tall or broad according to their aspect ratio (the ratio of the tank radius to its height) were taken into consideration. The supporting structure was accounted for by adding linear springs to the vessel base and the vessel was also prevented from rocking. The effects of both material and geometric nonlinearities were included in the model. Both free vibration and non-linear time history analyses were carried out. It was concluded that elevated conical tanks, especially the tall tanks, are very sensitive to seismic excitations and their design must be based on large static load factors in order to be safe during strong seismic events. It was also indicated that the vertical ground motion contributes significantly to the dynamic instability of conical elevated tanks and as a result its effect must be included properly in seismic analysis of such structures.

Later, El Damatty et al. (2000) proposed an analytical model for estimating the free surface sloshing response of conical tanks under dynamic motions. The model was applicable to both

purely conical and combined conical-cylindrical vessels. It was assumed that the sloshing response could be estimated while considering the rigid wall boundary condition. The shell vibration was determined assuming zero hydrodynamic pressure at the liquid free-surface. The validity of this analytical model was verified in a later experimental study carried out by Sweedan and El Damatty (2002) on a small-scale purely conical tank.

The dynamic characteristics of liquid-filled combined vessels in which vessels consisted of a conical steel section with superimposed top cylindrical shell were identified experimentally in later studies by El Damatty (2005). This study was the first experimental study carried out on a small-scale liquid-filled conical vessel. The fundamental frequencies as well as the frequencies of $\cos(\theta)$-modes of vibration were determined using shake table test. The experimental values were compared with those obtained from the analytical and numerical methods and in general an excellent agreement was observed. It was found that the $\cos(\theta)$-modes which lead to base shear and overturning moment in tanks subjected to seismic motions, show themselves as higher modes of vibration.

Sweedan and El Damatty (2005) investigated the dynamic response of purely conical tanks under vertical acceleration. It was shown that vertical excitation of such tanks could cause significant increase in the compressive meridional stresses generated in the tank walls.

To further simplify the seismic analysis of elevated tanks, Sweedan (2009) proposed an equivalent mechanical model to duplicate forces induced in combined elevated tanks subjected to vertical ground acceleration. The proposed model was able to consider the flexibility of the tank wall. The stored liquid was modeled as flexible and rigid components. The flexible component was associated with the vibration of the tank walls, while the rigid component vibrated in synchronism with the base excitation. Parametric analyses were performed to evaluate the

natural frequencies of the axisymmetrical modes of vibration. The contribution of the stored liquid mass to the impulsive response was also determined by performing modal analyses.

Moslemi et al. (2011) evaluated the performance of conical elevated tanks under seismic motions. The FE technique was employed to estimate the seismic response. Both time history and free vibration analyses were carried out. The effects of liquid sloshing and tank wall flexibility were considered in the proposed FEM. The obtained results were also compared with those recommended by current practice (ACI 350.3-06 in conjunction with ASCE 7-05). In this study, the difficulties associated with modeling of the tanks having complex geometries such as conical shaped vessels were addressed. The accuracy of the method was verified by comparing the obtained results with experimental and numerical values available in the literature. Modal FE analyses resulted in natural frequencies and effective water mass ratios very close to those obtained from Housner's formulations. The results of the study also showed that the current practice could predict the dynamic response of elevated water tanks with reasonable accuracy. Further details on this study will be presented in this thesis.

2.4 Other related studies

2.4.1 Application of seismic isolation to liquid storage tanks

The application of base isolation technique to buildings and bridges has been extensively developed in the past. However, a few studies regarding such application to liquid storage tanks can be found in literature. Base isolators both deflect and absorb the seismic input energy transmitted to the structure. Seismic isolation is normally suggested for the rehabilitation of structures expecting to have unsatisfactory performance under seismic events. There are examples of such application to liquid storage tanks in practice. For instance, in Seattle several

elevated water tanks were proposed to be rehabilitated using this technique (Bleiman and Kim (1993)). The tanks under consideration were very large capacity storage tanks. After performing detailed analyses on seismic isolation and other conventional rehabilitation alternatives, the project engineers came to the conclusion that seismic isolation technique was the most effective and cost-efficient rehabilitation option.

As a result, seismic isolation may be considered as an easy and economical technique for such structures, especially in moderate to high seismic intensity zones in which the design of the structure is governed by seismic loads.

Chalhoub and Kelly (1990) carried out shake table tests on fixed base as well as base isolated ground-supported tanks. A substantial reduction in total hydrodynamic pressure and base reaction values was reported. However, a slight increase in the free-surface sloshing height of the isolated tank relative to the fixed base tank was observed.

Bo and Jia-xiang (1994) modeled an isolated ground-supported tank using FE method. Only a single earthquake record was considered. The results showed reduction in hydrodynamic pressures, shell amplitudes, and liquid sloshing height as a result of isolation.

Kim and Lee (1995) conducted an experimental study on isolated liquid containers. They performed a series of pseudodynamic tests incorporating a substructuring technique on the isolated liquid storage tanks subjected to uni-directional acceleration. Two types of tanks namely tall and broad were tested to predict the hydrodynamic forces. In the testing algorithm, the base isolators were tested as the tested part, while the tank was simulated in a computer with a proper modeling technique as the computed part. The liquid storage tank was modeled as a discrete mechanical model. The effect of stored liquid was accounted for using three equivalent lumped masses. The tanks were isolated by laminated rubber bearings. Free vibration tests as well as

seismic tests using real earthquake records were carried out. The seismic isolation was found to be quite effective in reducing the dynamic response.

The seismic performance of ground-supported tanks having various isolation and energy dissipation mechanisms was further investigated by Malhotra (1997B, 1997C, and 1998).

Several rehabilitation solutions including vertical isolation, lateral isolation, and passive energy dissipation devices as hold-down anchors were investigated. In all cases, significant improvement in the seismic behavior of the tanks under consideration was reported. However, a slight increase in the free surface sloshing height in the laterally isolated tank was observed. In these studies, a new method for seismic isolation of ground-supported cylindrical tanks was proposed. In this method, the tank wall was disconnected from the base plate and was supported on a ring of isolation bearings. The base plate was resting directly on the ground. A flexible membrane was used between the wall and the base plate in order to prevent the liquid leakage from the tank and also to allow the free movement of the wall. It was shown that this isolation scheme could reduce substantially the dynamic base shears, overturning moments, and axial compressive stresses in the wall of the tank. However, since the weight applied on the bearings was small compared to the total weight of the stored fluid, a net tensile force was observed in the bearings of the tall tanks subjected to strong seismic excitations.

Shenton III and Hampton (1999) studied the seismic response of isolated elevated water tanks using a discrete three-DOF model. The natural frequencies and mode shapes of the isolated structure were determined and response spectral analyses were carried out. Only a linear elastic isolation system was considered. Furthermore, the tank walls were assumed to be rigid and the effect of rocking of the tower on dynamic response was ignored. Isolation bearings were assumed to be effectively rigid in the vertical direction. Results of the isolated tank models were

compared with those of the corresponding non-isolated tank models and it was concluded that the base isolation was effective in reducing the seismic response of the liquid-filled elevated tanks. It was also shown that isolation was most effective for the smallest capacity tank.

Shirmali and Jangid (2003) investigated the seismic behavior of isolated elevated tanks under real earthquake excitations using a four-DOF model. The isolation system considered was lead-rubber bearings. The fluid domain was modeled as lumped masses. Isolators were assumed to be effectively rigid in the vertical direction. As a result, the effects of uplift and rocking were not considered. It was observed that the seismic response of the isolated tanks was reduced significantly. In addition, a simplified decoupled analysis was proposed in which the motion of tower structure was assumed to be rigid under seismic excitation. This assumption led to a two-DOF model and two single-DOF models. It was concluded that this simplified method could accurately estimate the peak seismic response of the isolated elevated tanks with less computational efforts.

Later, Jadhav and Jangid (2004) investigated the dynamic behavior of liquid storage tanks isolated by elastomeric bearings and sliding mechanism under real earthquake records. The fluid domain was modeled as sloshing, impulsive, and rigid lumped masses. The same model was employed to study the seismic behavior of liquid storage tanks subjected to near-fault ground excitations (Jadhav and Jangid (2006)).

Shekari et al. (2009) further investigated the seismic behavior of isolated cylindrical liquid storage tanks under horizontal ground motions in a three-dimensional space. The structure was modeled by finite shell elements while the fluid domain was simulated using the internal boundary elements. The base isolation system was modeled by bilinear hysteretic elements. It was indicated that the dynamic response of isolated tanks could be dramatically reduced

compared to the fixed base tanks. However, it was observed that the liquid free surface displacement was increased due to base isolation. It was also concluded that the base-isolation system was more effective when the stiffness of base isolators was smaller. However, the isolators should be stiff enough to assure the tank stability.

2.4.2 Codes and standards

In this section a brief review on various codes and standards available for seismic design of liquid containing structures is presented. The main focus is on the codes and standards used in North America. International Building Code, IBC (2011) is one of the most comprehensive and preferred codes currently used in the United States. In the last revision of this code, the ASCE 7-10 (2010) standard is referred to for seismic design of common liquid storage tanks. In ASCE 7-10, the input ground motion is defined as a response spectrum corresponding to the Maximum Considered Earthquake (MCE) which represents an earthquake with a 2% probability of exceedance in a 50-year period (equivalent to a recurrence interval of approximately 2500 years).

Currently, there are no direct guidelines for structural design of environmental structures in Canadian design standards. However, useful guidelines may be found in a variety of other codes and standards such as ACI 350.3-06 (2006), New Zealand Standard NZS 3106 (2010), European Eurocode-8 (2006), and British Standard BS 8007 (1987), among which ACI 350.3-06 is the most comprehensive and widely adopted one.

ACI 350.3-06 standard reported by the American Concrete Institute, Committee 350 is presently used as an obligatory document for seismic design of reinforced concrete liquid storage tanks in North America. Supplementary guidelines regarding the analysis and design of elevated concrete and composite steel-concrete water storage tanks may be found in ACI 371R-08 (2008).

The Committee 350 was formed by the American Concrete Institute (ACI) in 1964 as a technical board responsible for providing guidelines for the design of environmental engineering structures. In 2001, ACI published the first standard for design of environmental engineering concrete structures in North America (ACI 350-01 and ACI 350.3-350.3R-01). In that standard, two different methods of design (working stress method and modified ultimate strength method) were proposed. The design methods were calibrated in such a way to provide comparable but not necessarily identical designs.

Current revision of the Code (ACI 350.3-06) is based on the ultimate strength design method. In this standard, an equivalent mechanical model based on the Housner's method (Housner (1963)) has been incorporated by which the resultant seismic forces acting on the walls of rigid containers can be estimated.

Two different standards intended for the design of prestressed concrete liquid storage tanks were published by the American Water Work Association (AWWA); AWWA D110 (1995), and AWWA D115 (1995). The guidelines regarding the design of welded steel liquid storage containers were provided in AWWA D100 (2005).

The American Petroleum Institute (API) published two standards; API 650 (1998), and API 620 (1998) for the design of tanks used in the petroleum industry.

American Society of Civil Engineers (ASCE) provided two publications including useful guidelines regarding the seismic design of storage tanks used in the nuclear industry; ASCE 4-98 (1998), and ASCE 58 (1980). Tanks used in the nuclear industry should meet more stringent design requirements compared to those used in other industries because of the potential hazard of radioactive materials to public safety.

Most of the standards including ACI 350.3-06, AWWA D100, AWWA D110, and API 650 have employed the Housner's mechanical model (Housner (1963)) with some modifications for determining the seismic forces associated with the accelerated contained liquid. In NZS 3106 (2010), the mechanical model proposed by Veletsos and Yang (1977) is used for seismic analysis of rigid tanks while the model developed by Haroun and Housner (1981B) is used for deformable liquid storage tanks.

In Eurocode-8 (2006) the dynamic analysis of rigid circular tanks is performed using Veletsos and Yang's model (1977). Models developed by Veletsos (1984) and Haroun and Housner (1981B) together with the approach proposed by Malhotra et al. (2000) are used for dynamic analysis of flexible circular tanks. Housner's method (1963) is recommended for seismic evaluation of rigid rectangular tanks, while no practical approach is assigned for flexible rectangular containers.

In seismic design, the seismic response values corresponding to the impulsive and convective parts are combined using an appropriate combination method. All codes and standards except the Eurocode-8, recommend SRSS (Square Root of Sum of Squares) rule to be used for combining the impulsive and convective seismic effects. Eurocode-8 suggests absolute summation combination rule.

Different standards specify different damping values to be considered for impulsive component. However, all codes and standards agree on the damping ratio of 0.5% to be used for convective component. ACI 350.3-06, ASCE 7-05, AWWA D100, AWWA D110, AWWA D115, and API 650 recommend a damping ratio of 5% for impulsive component for all tank types. In Eurocode-8, a damping ratio of 5% is proposed for the impulsive component of concrete tanks while 2% damping is specified for steel tanks. As a result of different damping

ratios associated with impulsive and convective liquid components, different response spectra corresponding to these components are provided in LCS design codes and standards.

In NZS 3106 (2010), the appropriate damping ratio for the impulsive component is determined based on the tank geometry, tank aspect ratio, tank material, and shear wave velocity in foundation soil.

CHAPTER 3

THEORETICAL ANALYSIS

3.1 Introduction

Fluid dynamic response using analytical formulations is addressed in this chapter. Two important theories namely lamina fluid theory and velocity potential theory capable of predicting the hydrodynamic pressure applied by the fluid on the tank wall and maximum sloshing heights due to seismic motions are described. For design purposes, the resulting hydrodynamic forces can be obtained by integrating the hydrodynamic pressures over the wetted area. All derived formulations are based on the basic theory of linear sloshing.

This chapter deals with the fluid response to pure lateral excitations for typical upright cylindrical containers. Also, the development of equivalent models as approximate mechanical systems used in dynamic analysis of partially filled liquid containers is briefly discussed. These equivalent mechanical models are realistic representatives of the fluid dynamics inside closed containers and are extensively used in current design codes and standards. By developing such mechanical models, the problem of dynamic system behavior can be formulated more easily.

Finally, a brief discussion on current design guidelines such as ACI 350.3-06 (2006) is presented. Discussion on how to estimate different dynamic effects in cylindrical liquid tanks, including inertia effects and impulsive and convective hydrodynamic effects is given.

3.2 Theories for dynamic analysis of liquid containers

Generally, there are two different theories for analysis of the dynamic behavior of liquid storage tanks:

1- Lamina fluid theory (Housner's method)

2- Theory of velocity potential

Vibration analysis of liquid-filled tanks using lamina fluid theory having rigid body was initiated by Housner (1957; 1963). Housner's method models the vibration of contained fluid in terms of an equivalent lumped mass mechanical system having two degrees of freedom. This method is simple to use but neglects the effect of higher order sloshing modes and further can not be readily used for coupled vibration analysis of elastic containers.

In the theory of velocity potential it is assumed that stored fluid can be regarded as potential flow. In this theory, the fluid motion is represented in terms of continuity conditions of contained fluid and boundary conditions of the contact interface between fluid and tank body as well as free surface of the fluid. Various methods are available for dynamic analysis of tanks using this theory. However, the most common method is based on the derivation of equation of motion for vibration of the tank, the fluid, and their interaction using the velocity potential theory for stored liquid and the shell theory for the tank body. Then a variety of numerical analysis methods such as finite element method, boundary element method or boundary integral equation may be employed for solving the obtained equations. Lamina fluid theory is explained in detail in Appendix A. The application of velocity potential theory in cylindrical containers is presented here.

3.2.1 Theory of velocity potential

The calculation of hydrodynamic pressures and sloshing wave height can also be achieved using velocity potential method. In this section the basic analytical formula of liquid behavior under horizontal excitation are presented. All equations are derived based on the theory of linear

sloshing. The generalized linear theory is discussed in details by Fox and Kuttler (1983). Furthermore, the fluid is assumed to be incompressible, irrotational and inviscid.

3.2.1.1 Dynamic response under horizontal random excitation

Figure 3.1 shows a typical upright cylindrical tank in a cylindrical coordinate system (r, ϕ, z). The tank is assumed to have a flexible wall and is subjected to the base acceleration $\ddot{u}_o(t)$. Therefore, the coupling effect between the sloshing response of fluid and the deformations of the flexible wall is included in deriving the equations. The analytical approach presented in this section can be employed to study explicitly the effect of wall deformations on the hydrodynamic pressures as well as the free surface sloshing height of the contained liquid. As suggested in numerous research studies, the fluid pressure can be split into three parts:

"Impulsive pressure" (p_1), which is the liquid pressure due to the ground acceleration, considering the tank wall to be rigid.

"Convective pressure" (p_2), which is the liquid pressure due to liquid free surface sloshing.

$p3$, which is the liquid pressure due to the wall deformation relative to the base in deformable containers.

As obvious, in regimes p_1 and $p3$ a distribution of the fluid surface displacement will also be produced, resulting in a coupling between the pressure components p_1, $p3$ and the pressure component p_2. This coupling effect is considered in the theoretical procedure given in this section. It is important to note that here not only the wall deformation due to sloshing, but also that due to the impulsive motion of the tank is considered.

$$\frac{\partial^2 \widetilde{\Phi}}{\partial t^2} + g\frac{\partial \widetilde{\Phi}}{\partial z} = 0$$

$$\frac{\partial \widetilde{\Phi}}{\partial t} = 0$$

$$\nabla^2 \widetilde{\Phi} = 0$$

$$-\frac{\partial \widetilde{\Phi}}{\partial r} = \dot{u}_0(t) + V_r(z,t)$$

$$\frac{\partial \widetilde{\Phi}}{\partial z} = 0$$
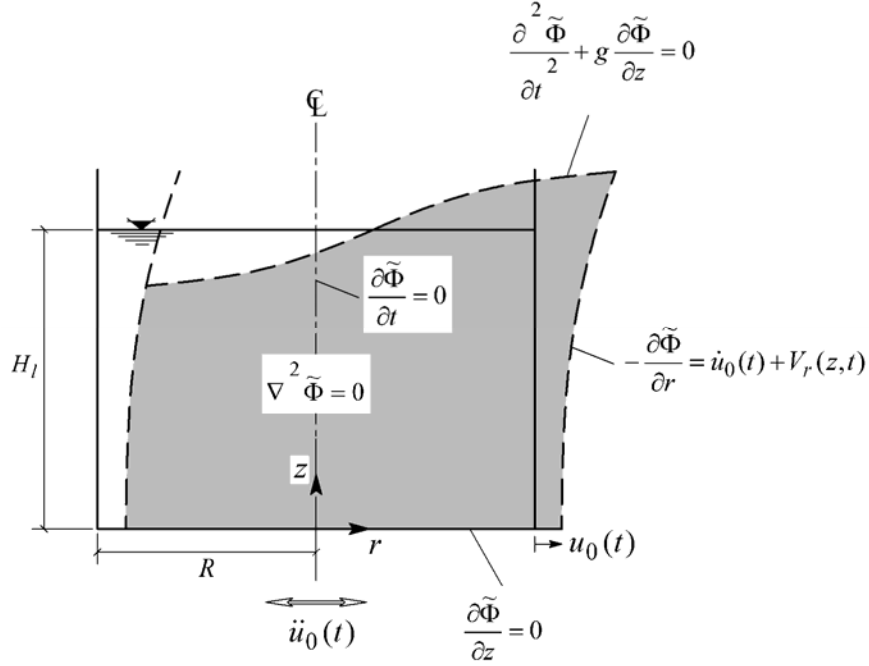
Figure 3.1 Cylindrical tank model and assigned boundary conditions

A series expansion can be used in solving the pressure wave equation for different sets of boundary conditions. To be able to obtain a closed form analytical solution, various types of the relative wall deformation pattern can be assumed based on the practical observations and numerical investigations. Generally tall tanks with aspect ratio $\frac{H_l}{R} > 1$ deform in a more or less linear pattern over the tank's height. Broad tanks having aspect ratio $\frac{H_l}{R} < 1$ normally show concave or convex wall deformation patterns which can be approximately defined as a "sin" or "$(1-\cos)$" functions, respectively.

The radial displacement of the tank relative to the ground is assumed to be defined as $q(t)\psi(z)\cos\phi$, where $q(t)$ is a time (t) history function, which is the same for all points located along one generator. Function $\psi(z)$ defines the "type" of the wall deformation which is

45

considered as input information. Function $\cos\phi$ represents a cosine deformation pattern for the tank around the circumference. This assumption means that under horizontal base excitation, only basic radial modes with wave number 1 are assumed to be activated.

The hydrodynamic pressure distribution assuming an ideal fluid (incompressible and irrotational) can be described using the classical potential fluid theory:

$$\nabla^2\widetilde{\Phi} = \frac{\partial^2\widetilde{\Phi}}{\partial r^2} + \frac{1}{r}\frac{\partial\widetilde{\Phi}}{\partial r} + \frac{1}{r^2}\frac{\partial^2\widetilde{\Phi}}{\partial\widetilde{\Phi}^2} + \frac{\partial^2\widetilde{\Phi}}{\partial z^2} = 0 \tag{3-1}$$

In which, $\widetilde{\Phi}$ is the velocity potential. The fluid velocity components are computed from the spatial derivative of the potential as

$$V^T = (-\frac{\partial\widetilde{\Phi}}{\partial r}, -\frac{1}{r}\frac{\partial\widetilde{\Phi}}{\partial\phi}, -\frac{\partial\widetilde{\Phi}}{\partial z}) \tag{3-2}$$

Considering linearized Bernoulli equation for pressure, we have:

$$p = \rho_l\frac{\partial\widetilde{\Phi}}{\partial t} \tag{3-3}$$

where ρ_l is the liquid mass density. For the irrotational flow, the velocity potential function, $\widetilde{\Phi}(r,\phi,z,t)$ can be expressed as

$$\widetilde{\Phi}(r,\phi,z,t) = \Phi(r,z,t)\cos\phi \tag{3-4}$$

As can be observed from this equation, only the first mode of the Fourier expansion of $\widetilde{\Phi}$ and p with respect to the circumferential coordinate ϕ is considered. This is because of the fact that only this component will cause a resultant external force or moment. For the typical tank shown in Figure 3.1, the following boundary conditions may be considered:

$$\text{at } r=0, \ \frac{\partial\Phi}{\partial t} = 0 \tag{3-5}$$

since the pressure distribution is antisymmetric.

at $r = R$, $-\dfrac{\partial \Phi}{\partial r} = \dot{u}_0(t) + V_r(z,t)$ (3-6)

since the fluid velocity must be equal to the wall velocity, which is the sum of the ground

velocity $\dot{u}_0(t)$ and the wall velocity relative to the ground $V_r(z,t)$.

at $z = 0$, $\dfrac{\partial \Phi}{\partial z} = 0$ (3-7)

since the fluid velocity along z-direction is 0 at the base $z = 0$.

at $z = H_l$, $\dfrac{\partial^2 \Phi}{\partial t^2} + g\dfrac{\partial \Phi}{\partial z} = 0$ (3-8)

since the sloshing of liquid free surface yields the condition that $p(r, H_l, t) = \rho_l g d(r, H_l, t)$,

where g is the acceleration due to gravity and d is the vertical displacement of the liquid free

surface.

The following kinematic condition relates the liquid free surface displacement d to the

vertical component of the liquid velocity at the free surface. In a linearized form, the condition is

as follows:

at $z = H_l$, $\dot{d} = \dfrac{\partial d}{\partial t} = -\dfrac{\partial \widetilde{\Phi}}{\partial z}$ (3-9)

As explained before, the function Φ can be split into three parts:

$\Phi = \Phi_1 + \Phi_2 + \Phi_3$ (3-10)

where,

Φ_1 is the potential function due to ground acceleration $\ddot{u}_o(t)$ only (impulsive component).

Φ_2 is the potential function due to the sloshing only (convective component).

Φ_3 is the potential function due to the relative wall velocity $V_r(z,t)$.

Following sets of boundary conditions are available for potential functions Φ_1, Φ_2, and Φ_3:

47

For Φ_1: at $r=0$: $\dfrac{\partial \Phi_1}{\partial t}=0$, at $r=R$: $-\dfrac{\partial \Phi_1}{\partial r}=\dot{u}_0(t)$, at $z=0$: $\dfrac{\partial \Phi_1}{\partial z}=0$,

at $z=H_l$: $\dfrac{\partial \Phi_1}{\partial t}=0$ $\hspace{4cm}$ (3-11)

For Φ_2: at $r=0$: $\dfrac{\partial \Phi_2}{\partial t}=0$, at $r=R$: $\dfrac{\partial \Phi_2}{\partial r}=0$, at $z=0$: $\dfrac{\partial \Phi_2}{\partial z}=0$,

at $z=H_l$: $\dfrac{\partial^2 \Phi_2}{\partial t^2}+g\dfrac{\partial \Phi_2}{\partial z}=-g(\dfrac{\partial \Phi_1}{\partial z}+\dfrac{\partial \Phi_3}{\partial z})$ $\hspace{2.5cm}$ (3-12)

For Φ_3: at $r=0$: $\dfrac{\partial \Phi_3}{\partial t}=0$, at $r=R$: $-\dfrac{\partial \Phi_3}{\partial r}=V_r(z,t)$, at $z=0$: $\dfrac{\partial \Phi_3}{\partial z}=0$,

at $z=H_l$: $\dfrac{\partial \Phi_3}{\partial t}=0$ $\hspace{4cm}$ (3-13)

Hydrodynamic pressure solutions corresponding to the three response components considered can be evaluated from the expression of the velocity potential function that satisfies the Laplace equation, as well as the appropriate boundary conditions as defined in Eqs. (3-11) to (3-13).

The solution for problem (3-11) can be found in the literature (Haroun and Housner (1981A), Tokuda et al. (1995)). At $\phi=0$ the impulsive solution for hydrodynamic pressure is as follows:

$$p_{1,0}=\rho_l\frac{\partial \Phi_1}{\partial t}=-\ddot{u}_0(t)\rho_l H_l\sum_{i=1}^{\infty}8\frac{(-1)^{i+1}}{[(2i-1)\pi]^2}\times\frac{I_1[(2i-1)\frac{\pi}{2}\frac{r}{H_l}]}{I_1'[(2i-1)\frac{\pi}{2}\frac{r}{H_l}]}\cos[(2i-1)\frac{\pi}{2}\frac{z}{H_l}]$$ (3-14)

in which $I_1(y)$ is the modified Bessel function of the first kind of order one with the argument y and $I_1'(y)$ is its derivative defined as:

$$I_1'(y) = \frac{dI_1(y)}{dy} \tag{3-15}$$

In Chapter 5 the hydrodynamic impulsive pressure in a rigid ground-supported tank subjected to a horizontal random excitation will be evaluated using Eq. (3-14) and the obtained results will be compared with those calculated from FE in order to verify the proposed FEM. The analytical solution for problem (3-13) can be found in several research studies (Yang (1976), Fischer (1979), Haroun and Housner (1981A)). For a given relative wall velocity $V_r(z,t) = \dot{q}(t)\psi(z)$, the solution for hydrodynamic pressure p_3 at $\phi = 0$ is as follows:

$$p_{3,0} = \rho_l \frac{\partial \Phi_3}{\partial t} = -\ddot{q}(t)\rho_l H_l \sum_{i=1}^{\infty} 4\frac{\beta_i}{(2i-1)\pi} \times \frac{I_1[(2i-1)\frac{\pi}{2}\frac{r}{H_l}]}{I_1'[(2i-1)\frac{\pi}{2}\frac{r}{H_l}]} \cos[(2i-1)\frac{\pi}{2}\frac{z}{H_l}] \tag{3-16}$$

and

$$\beta_i = \frac{1}{H_l}\int_0^{H_l} \psi(z)\cos[(2i-1)\frac{\pi}{2}\frac{z}{H_l}]dz = \int_0^1 \psi(\zeta)\cos[(2i-1)\frac{\pi}{2}\zeta]d\zeta \tag{3-17}$$

Clearly the deformation of the tank wall must be first determined to evaluate the hydrodynamic pressure p_3.

To obtain the hydrodynamic pressure solution due to sloshing (p_2), the following homogeneous solution for Φ_2 is considered:

$$\Phi_{2,i} = C_i J_1(\lambda_i \frac{r}{R})\cosh(\lambda_i \frac{z}{R})f_i(t), \quad \text{and} \quad \Phi_2 = \sum_{i=1}^{\infty} \Phi_{2,i} \tag{3-18}$$

in which, $J_1(y)$ is the Bessel function of the first kind of order one with the argument y and its derivative $J_1'(y)$ is defined as $J_1'(y) = \frac{dJ_1(y)}{dy}$. In addition, C_i's are constants, and $f_i(t)$'s are

time dependant functions. λ_i's are the zeros of $J_1'(y)$ which are determined from $J_1'(\lambda_i) = 0$ leading to solution $\lambda_1 = 1.8412$, $\lambda_2 = 5.3314$, and so on (Abromowitz and Stegun (1972)).

Considering the boundary condition at liquid free surface ($z = H_l$) given in Eq. (3-12), the following relation can be derived:

$$\sum_{i=1}^{\infty} C_i J_1(\lambda_i \frac{r}{R})[\ddot{f}_i(t)\cosh(\frac{\lambda_i H_l}{R}) + g\frac{\lambda_i}{R}\sinh(\frac{\lambda_i H_l}{R})f_i(t)] =$$

$$-g\sum_{i=1}^{\infty}[\frac{4}{(2i-1)\pi}\ddot{u}_0 + 2\beta_i(-1)^{i-1}\dot{q}] \times \frac{I_1[(2i-1)\frac{\pi}{2}\frac{r}{H_l}]}{I_1[(2i-1)\frac{\pi}{2}\frac{R}{H_l}]} \qquad (3\text{-}19)$$

As can be observed from this expression, the second term within the brackets on the right hand side of the above equation represents the coupling with the flexible wall deformation. If the right hand side of the above equation is zero (i.e. free vibration solution), the circular sloshing frequencies ω_i's (considering $f_i(t) = \exp(i\omega_i t)$) are determined as:

$$\omega_i^2 = \frac{\lambda_i g}{R}\tanh(\frac{\lambda_i H_l}{R}) \qquad (3\text{-}20)$$

After some algebraic manipulations, the pressure distribution due to sloshing (p_2) at $\phi = 0$ can be determined as:

$$p_{2,0} = \rho_l \frac{\partial \Phi_2}{\partial t} =$$

$$-2\rho_l R\sum_{n=1}^{\infty}\frac{\omega_n}{(\lambda_n^2-1)}\frac{J_1(\lambda_n \frac{r}{R})}{J_1(\lambda_n)} \times \frac{\cosh(\lambda_n \frac{z}{R})}{\cosh(\lambda_n \frac{H_l}{R})}\int_o^t \sin(\omega_n(t-\tau))[\ddot{u}_0(\tau) + k_n\ddot{q}(\tau)]d\tau \qquad (3\text{-}21)$$

where, the coefficient k_n is calculated as

$$k_n = 2\frac{\lambda_n\frac{H_l}{R}}{\tanh(\lambda_n\frac{H_l}{R})}\sum_{i=1}^{\infty}\frac{(-1)^{i+1}(2i-1)\frac{\pi}{2}\beta_i}{(\lambda_n\frac{H_l}{R})^2 + [(2i-1)\frac{\pi}{2}]^2} \qquad (3\text{-}22)$$

k_n can be computed numerically for the integer variable n and different wall deformation patterns $\psi(\zeta)$. It can be observed from Eq. (3-21) that the obtained expression for hydrodynamic pressure due to sloshing (p_2) can take into account the effect of the flexible wall displacement by the term $k_n \ddot{q}(\tau)$. For simplicity, one can define a parameter γ_i as:

$$\gamma_i = \frac{1}{(2i-1)\dfrac{\pi}{2}\dfrac{R}{H_l}} \frac{I_1[(2i-1)\dfrac{\pi}{2}\dfrac{R}{H_l}]}{I_1'[(2i-1)\dfrac{\pi}{2}\dfrac{R}{H_l}]} \qquad (3\text{-}23)$$

Finally, using Eqs. (3-14), (3-16), and (3-21), the total hydrodynamic pressure on the tank wall ($r = R$) at $\phi = 0$ can be evaluated as:

$$p_0(z,t) = p_{1,0} + p_{2,0} + p_{3,0}\big|_{r=R} =$$

$$-2\rho_l R \left\{ \begin{array}{l} \ddot{u}_0(t)\displaystyle\sum_{i=1}^{\infty}\frac{2(-1)^{i+1}}{(2i-1)\pi}\gamma_i\cos[(2i-1)\frac{\pi}{2}\frac{z}{H_l}]+ \\[4mm] \ddot{q}(t)\displaystyle\sum_{i=1}^{\infty}\beta_i\gamma_i\cos[(2i-1)\frac{\pi}{2}\frac{z}{H_l}]+\sum_{i=1}^{\infty}\frac{\omega_i}{\lambda_i^2-1}\times\frac{\cosh(\lambda_i\frac{z}{R})}{\cosh(\lambda_i\frac{H_l}{R})}\int_0^t\sin\omega_i(t-\tau)[\ddot{u}_0(\tau)+k_i\ddot{q}(\tau)]d\tau \end{array} \right\}$$

$$(3\text{-}24)$$

3.2.1.2 Equivalent mechanical model

As mentioned before, generally the fluid hydrodynamic pressure in rigid tanks can be divided into two distinct parts. One is directly proportional to the ground acceleration and is caused as a result of fluid motion in unison with the tank. The second is convective pressure which is due to sloshing at the liquid free surface. As a result, the liquid dynamic behavior inside closed tanks can be approximated by an equivalent model capable of taking into account the effects of both liquid components. This equivalence criterion is met by equating the resulting

forcers and moments acting on the tank wall between the actual model and its mechanically equivalent model.

Assuming linear planar liquid motion, an equivalent mechanical model in the form of a series of mass-spring systems is presented in this section. To develop an equivalent mechanical model under lateral excitations, the following conditions should be met:

1. The equivalent masses must be maintained.

2. In the case of small oscillations, the center of gravity must remain the same.

3. Models must have the same oscillation modes and must produce the same damping forces.

4. The resulting forces and moments must be equivalent to those developed in the actual model.

Figure 3.2 illustrates a schematic diagram of the considered equivalent model. The model consists of a mass m_0 rigidly attached to the tank and moving in unison with the walls, and a series of masses m_n representing the equivalent mass of each sloshing mode. Each mass m_n is fastened to the tank wall by means of a spring K_n and a dashpot C_n. In the derivation of equations, for the sake of simplicity, damping is neglected and also only pure translational excitation is considered here. Furthermore, the tank wall is assumed to be rigid.

As mentioned before, the equivalent model should satisfy the equivalent mass condition as follows:

$$M = m_0 + \sum_{n=1}^{\infty} m_n \qquad (3\text{-}25)$$

where, M is the total mass of fluid.
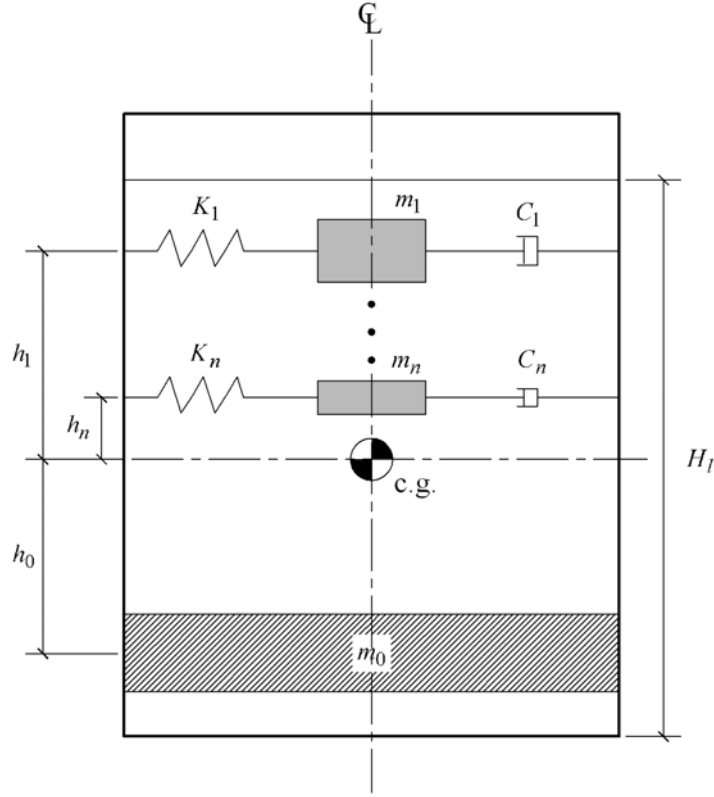
Figure 3.2 Mass-spring-dashpot equivalent mechanical model

In addition, the center of mass must be preserved, therefore:

$$m_0 h_0 - \sum_{n=1}^{\infty} m_n h_n = 0 \qquad (3\text{-}26)$$

The spring constants K_n for each sloshing mass can be obtained from the equation of circular sloshing frequencies ω_n's. From Eq. (3-20) we have:

$$\omega_n^2 = \frac{K_n}{m_n} = \frac{\lambda_n g}{R} \tanh(\frac{\lambda_n H_l}{R}) \qquad (3\text{-}27)$$

Let the displacement of the equivalent masses relative to the tank wall be denoted by x_n, and x be the displacement of the container. The net force acting on the container in the horizontal direction is determined by adding the reversed inertia forces of the accelerated masses as:

$$m_0\ddot{x} + \sum_{n=1}^{\infty} m_n(\ddot{x} + \ddot{x}_n) = -F \tag{3-28}$$

Likewise, the slosh equation of the nth mode corresponding to the nth equivalent sloshing mass can be found as:

$$m_n(\ddot{x} + \ddot{x}_n) + K_n x_n + 2m_n \omega_n \zeta_n \dot{x}_n = 0 \tag{3-29}$$

where, the term $2m_n \omega_n \zeta_n \dot{x}_n$ represents the damping force. ζ_n is the damping factor of the equivalent dashpot. The net moment acting on the tank can be determined as:

$$m_0 h_0 \ddot{x} - g\sum_{n=1}^{\infty} m_n x_n + \sum_{n=1}^{\infty} m_n h_n(\ddot{x} + \ddot{x}_n) = M_y \tag{3-30}$$

As an example, the special case of harmonic pure lateral excitation of the tank defined as $x(t) = X_0 \sin \Omega t$ is considered here and the corresponding equations are extracted. X_0 and Ω are the excitation amplitude and frequency. It is assumed no damping is present in the system. As a result, the slosh equation, Eq. (3-29) takes the form:

$$m_n \ddot{x}_n + K_n x_n = m_n X_0 \Omega^2 \sin \Omega t \tag{3-31}$$

The steady state solution for this equation is as follows:

$$x_n = \frac{\Omega^2}{\omega_n^2 - \Omega^2} X_0 \sin \Omega t \tag{3-32}$$

The force equation, Eq. (3-28) becomes:

$$F = -m_0 \ddot{x} - \sum_{n=1}^{\infty} m_n(\ddot{x} + \ddot{x}_n) = X_0 \Omega^2 \sin \Omega t \left\{ m_0 + \sum_{n=1}^{\infty} m_n \left[\frac{\Omega^2}{\omega_n^2 - \Omega^2} + 1 \right] \right\} =$$

$$MX_0 \Omega^2 \sin \Omega t \left\{ 1 + \sum_{n=1}^{\infty} \frac{m_n}{M} \left(\frac{\Omega^2}{\omega_n^2 - \Omega^2} \right) \right\} \tag{3-33}$$

The moment equation, Eq. (3-30) becomes:

$$M_y = m_0 h_0 \ddot{x} - g\sum_{n=1}^{\infty} m_n x_n + \sum_{n=1}^{\infty} m_n h_n (\ddot{x} + \ddot{x}_n) =$$

$$- X_0 \Omega^2 \sin\Omega t \left\{ m_0 h_0 + \sum_{n=1}^{\infty} \frac{g m_n}{(\omega_n^2 - \Omega^2)} + \sum_{n=1}^{\infty} m_n h_n \left(\frac{\omega_n^2}{\omega_n^2 - \Omega^2}\right) \right\} = \tag{3-34}$$

$$- X_0 \Omega^2 \sin\Omega t \left\{ m_0 h_0 + \sum_{n=1}^{\infty} m_n \left(h_n + \frac{g}{\omega_n^2}\right) + \sum_{n=1}^{\infty} m_n \left(h_n + \frac{g}{\omega_n^2}\right)\left(\frac{\Omega^2}{\omega_n^2 - \Omega^2}\right) \right\}$$

This equation gives the moment taken about the center of mass of the solidified liquid. Now the values of the equivalent mechanical model parameters can be evaluated by comparing the values of the undamped model with those of the ideal liquid discussed before. For the special case of sinusoidal lateral excitation ($x(t) = X_0 \sin\Omega t$), the hydrodynamic force acting on the walls of a rigid cylindrical tank can be evaluated using the theory of velocity potential as (Ibrahim (2005)):

$$F = \int_{\phi=0}^{2\pi} \int_{z=0}^{H_l} p \cos\phi R d\phi dz =$$

$$MX_0 \Omega^2 \sin\Omega t \left\{ 1 + \sum_{n=1}^{\infty} \frac{2R\Omega^2 \tanh(\frac{\lambda_n H_l}{R})}{\lambda_n H_l (\lambda_n^2 - 1)(\omega_n^2 - \Omega^2)} \right\} \tag{3-35}$$

The hydrodynamic moment due to liquid forces for a cylindrical tank under sinusoidal lateral excitation ($x(t) = X_0 \sin\Omega t$) can also be obtained using the theory of velocity potential as (Ibrahim (2005)):

$$M_y = MX_0 \Omega^2 \sin\Omega t \times \sum_{n=1}^{\infty} \frac{2R\tanh(\frac{\lambda_n H_l}{R})}{\lambda_n H_l (\lambda_n^2 - 1)} \left\{ \frac{g + (\frac{H_l\Omega^2}{2})\left[1 - (\frac{4R}{\lambda_n H_l})\tanh(\frac{\lambda_n H_l}{R})\right]}{(\omega_n^2 - \Omega^2)} \right\}$$

$$\tag{3-36}$$

Comparing the above two equations with those obtained for the equivalent model, one can determine the following equivalent parameters:

$$\frac{m_n}{M} = \frac{2R}{\lambda_n H_l (\lambda_n^2 - 1)} \tanh(\frac{\lambda_n H_l}{R})$$

(3-37)

$$\frac{m_0}{M} = 1 - \sum_{n=1}^{\infty} \frac{m_n}{M} = 1 - \sum_{n=1}^{\infty} \frac{2R}{\lambda_n H_l (\lambda_n^2 - 1)} \tanh(\frac{\lambda_n H_l}{R})$$

(3-38)

$$\frac{h_n}{H_l} = \frac{1}{2} \left[1 - \frac{4R \tanh(\frac{\lambda_n H_l}{R})}{\lambda_n H_l} \right]$$

(3-39)

Figure 3.3 indicates the variations of the nonsloshing mass ratio $\frac{m_0}{M}$ as well as modal sloshing mass ratios $\frac{m_n}{M}$ versus aspect ratio $\frac{H_l}{R}$ for the first three sloshing modes. It can be observed from the Figure that the amount of sloshing mass decreases rapidly for all modes as the ratio $\frac{H_l}{R}$ increases, while a reverse trend is observed for the rigid mass m_0.

Using Eq. (3-26) together with Eqs. (3-37) to (3-39), the following expression can be obtained:

$$\frac{h_0}{H_l} = \frac{1}{1 - \sum_{n=1}^{\infty} (\frac{2R}{\lambda_n H_l (\lambda_n^2 - 1)}) \tanh(\frac{\lambda_n H_l}{R})} \times$$

(3-40)

$$\left[\frac{1}{2(\frac{H_l}{R})^2} - \sum_{n=1}^{\infty} \frac{\lambda_n \tanh(\frac{\lambda_n H_l}{R}) + 4(\frac{R}{(H_l \cosh(\frac{\lambda_n H_l}{R})})}{\lambda_n^2 (\lambda_n^2 - 1) H_l}{R} \right]$$
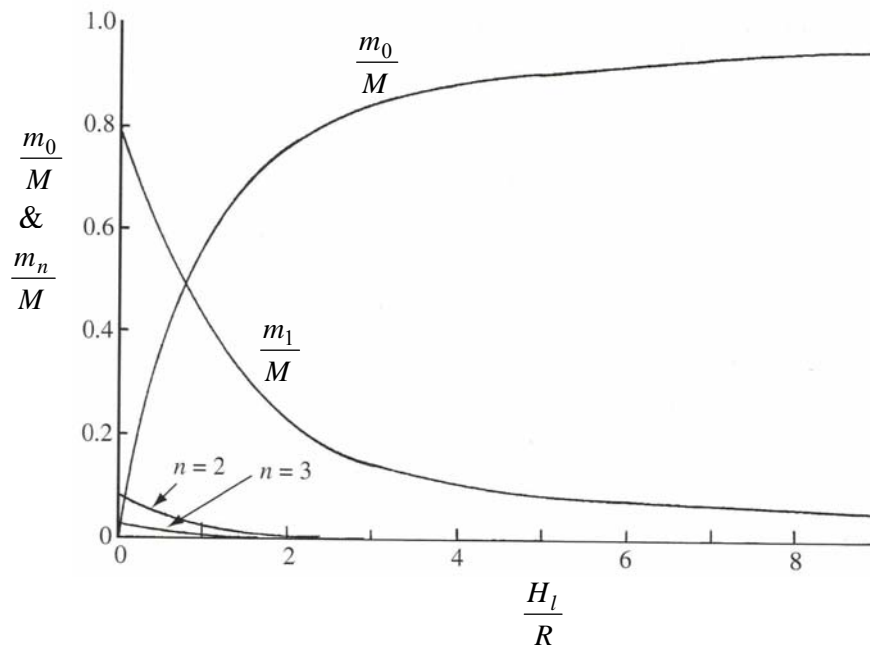
Figure 3.3 Mechanical model equivalent masses in a circular cylindrical tank

3.3 ACI guidelines for LCS

Based on ACI 350.3-06 (2006), the walls of LCS should be designed for static as well as dynamic forces. The following dynamic effects should be considered in the design of such structures:

1. Inertia forces exerted on the wall (P_w) and the roof (P_r).

2. Hydrodynamic impulsive force (P_i) due to accelerated contained liquid.

3. Hydrodynamic convective force (P_c) due to accelerated contained liquid.

4. Dynamic earth pressure from the supporting soil acting against the buried portion of the wall.

5. Vertical excitation effects.

These dynamic forces are calculated using the following equations:

$$P_w = C_i I \left[\frac{\varepsilon W_w}{R_i} \right] \tag{3-41}$$

$$P_r = C_i I \left[\frac{W_r}{R_i} \right] \tag{3-42}$$

$$P_i = C_i I \left[\frac{W_i}{R_i} \right] \tag{3-43}$$

$$P_c = C_c I \left[\frac{W_c}{R_c} \right] \tag{3-44}$$

where, C_i and C_c are the period-dependant seismic response coefficients for impulsive and convective terms, respectively; I is the importance factor as listed in Table 3.1; ε is effective mass coefficient defined as the ratio of equivalent dynamic mass of the tank wall to its actual total mass; W_w and W_r are the weights of the tank wall and tank roof, respectively; W_i and W_c are the effective weights of the stored liquid corresponding to impulsive and convective components, respectively which are adapted from Housner's method (Housner (1957; 1963)); R_i and R_c are the response modification factors corresponding to impulsive and convective terms, respectively (see Table 3.2). Since the impulsive and convective terms of response are not in phase with each other, their effects can be combined using the square-root sum-of-the-squares (SRSS) method as per ACI 350.3-06.

After hydrodynamic forces P_i and P_c are determined, they are vertically distributed over the wall height of the tank in a linear pattern using approximate distribution functions. These hydrodynamic pressures are distributed horizontally across the tank diameter in a cosine pattern. One-half the hydrodynamic forces P_i and P_c are applied symmetrically about $\phi = 0$ acting outward on one-half of the tank's circumference. The other half is applied symmetrically about

$\phi = 180$ acting inward on the opposite half of the tank's circumference. The wall's inertia force should be distributed uniformly around the entire tank's circumference. Other dynamic effects if present should be superimposed on these lateral forces in a proper manner.

Table 3.1 Importance factor I (ACI 350.3-06)

	Tank use	Factor I
III	Tanks containing hazardous materials	1.5
II	Tanks that are intended to remain usable for emergency purposes after an earthquake, or tanks that are part of lifeline systems	1.25
I	Tanks not listed in Categories II or III	1.0

Table 3.2 Response modification factors R (ACI 350.3-06)

Type of structure	R_i		R_c
	On or above grade	Buried	
Anchored, flexible-base tanks	3.25	3.25	1.0
Fixed or hinged-base tanks	2.0	3.0	1.0
Unanchored, contained, or uncontained tanks	1.5	2.0	1.0
Pedestal-mounted tanks	2.0	-----	1.0

The schematic vertical and horizontal distribution of these dynamic forces acting on the walls of a cylindrical tank is shown in Figure 3.4. The impulsive and convective equivalent

weights of stored liquid (W_i and W_c) and their equivalent heights above the base (h_i and h_c) are determined according to Housner's formulations given in Appendix A.

(a)

(b)
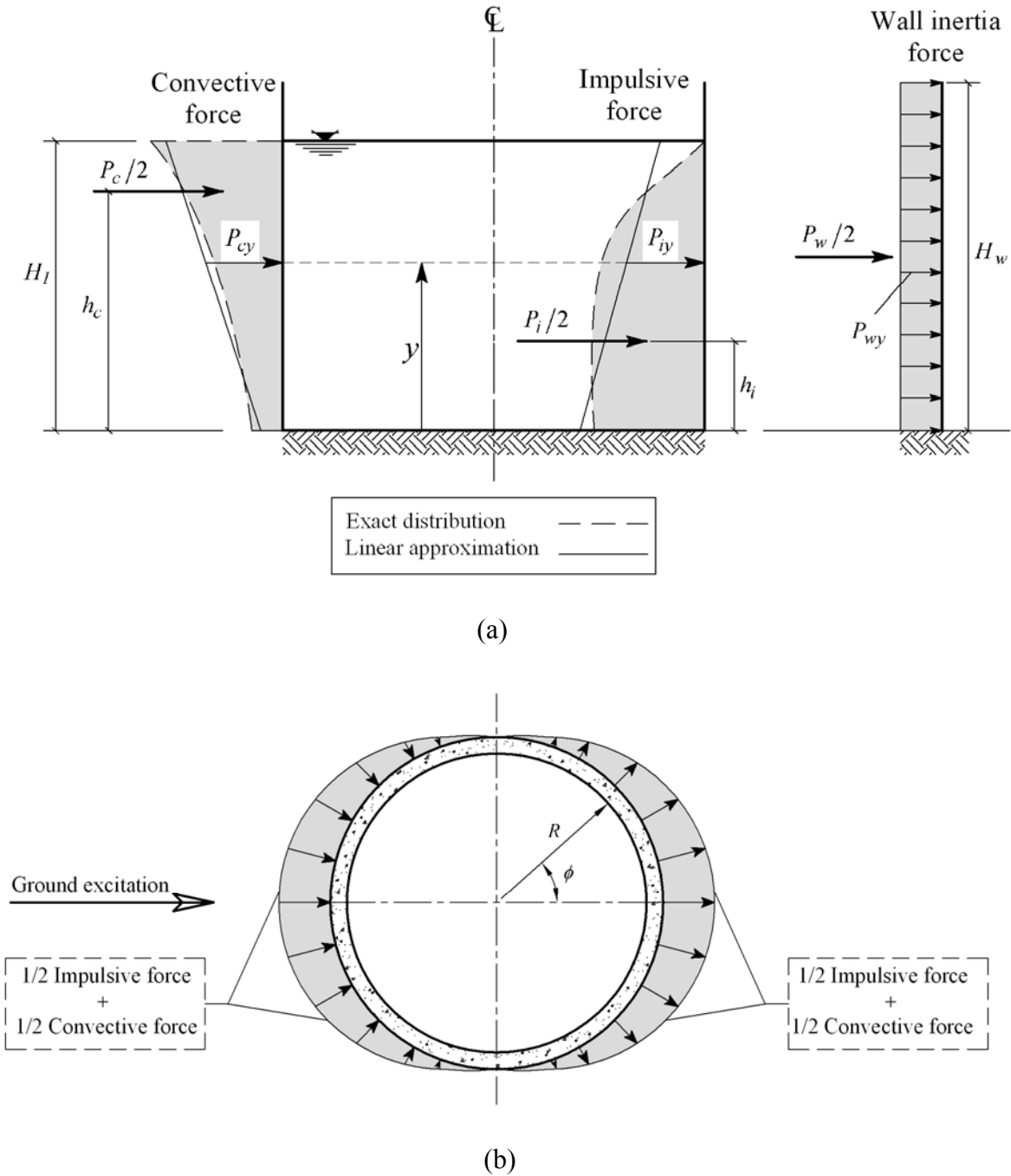
Figure 3.4 Dynamic force distribution in tank walls; (a) Vertical distribution,

(b) Horizontal distribution

The impulsive seismic response coefficient C_i is determined as follows:

$$\text{For } T_i \leq T_s, \ C_i = S_{DS} \tag{3-45}$$

$$\text{For } T_i > T_s, \ C_i = \frac{S_{D1}}{T_i} \leq S_{DS} \tag{3-46}$$

The convective seismic response coefficient C_c is determined as follows as per ACI 350.3-06:

$$\text{For } T_c \leq {}^{1.6}\!\!/\!_{T_s}, \ C_c = \frac{1.5 S_{D1}}{T_c} \leq 1.5 S_{DS} \tag{3-47}$$

$$\text{For } T_c > {}^{1.6}\!\!/\!_{T_s}, \ C_c = 6\frac{0.4 S_{DS}}{T_c^2} = \frac{2.4 S_{DS}}{T_c^2} \tag{3-48}$$

where,

$S_{DS} = \dfrac{2}{3} F_a S_s =$ Design spectral response acceleration at short periods

$S_{D1} = \dfrac{2}{3} F_v S_1 =$ Design spectral response acceleration at 1-second period

$T_s = \dfrac{S_{D1}}{S_{DS}}$

T_i, $T_c =$ Natural period of impulsive mode and convective mode, respectively

$S_S =$ Mapped MCE (Maximum Considered Earthquake) spectral response acceleration at short periods

$S_1 =$ Mapped MCE spectral response acceleration at 1-second period

$F_a =$ Short-period site coefficient (at 0.2 second period)

$F_v =$ Long-period site coefficient (at 1.0 second period)

The coefficients S_S, S_1, F_a, and F_v are determined in accordance with ASCE 7-05. Figure 3.5 which is adapted from ACI 350.3-06 shows the design response spectrum used in determining the impulsive seismic response coefficient C_i.
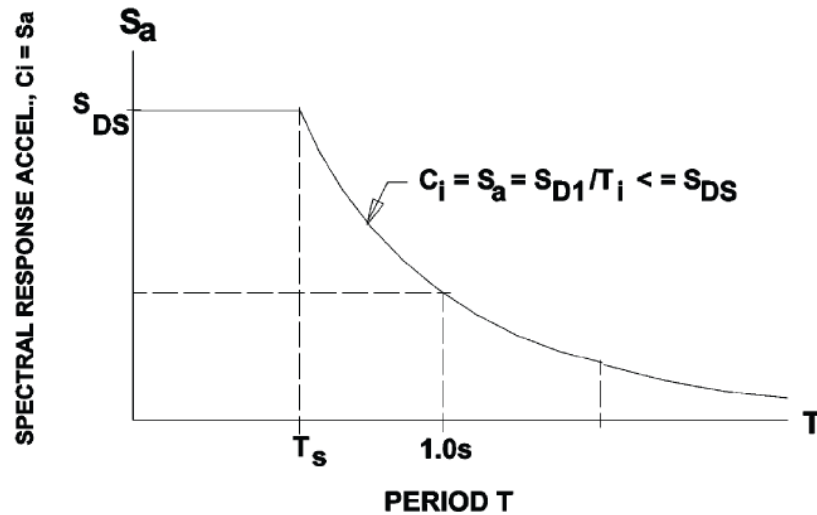
Figure 3.5 Design response spectrum (adapted from ACI 350.3-06)

Regarding the dynamic analysis of elevated tanks, additional guidelines are provided in ACI 371R-08. This guide suggests that only the impulsive seismic response coefficient needs to be considered in determining the seismic induced forces. Therefore, no provisions regarding the convective component of response are specified in this guide. The design response spectrum is the same as that provided by ACI 350.3.

3.4 Summary

This chapter addresses the dynamic response of cylindrical liquid storage tanks. It introduces two different theories commonly used for studying fluid dynamics in liquid containers. It also explains how velocity potential and as a result hydrodynamic pressures can be determined for a

deformable cylindrical tank under a random ground excitation. Using this theory, the analytical distribution of hydrodynamic pressure on the walls of a cylindrical tank can be computed under an actual seismic record. This analytical solution will be used later in this thesis to verify the FE method proposed in this study.

The velocity potential method introduced here enables one to obtain the fluid dynamic response components due to impulsive action, free surface liquid sloshing, and flexible wall deformation, separately. The total dynamic effect can therefore be determined by adding up these three components.

This chapter also summarizes a general procedure for developing the equivalent mechanical models used in dynamic analysis of liquid tanks. It is worth noting that the mechanical models introduced here are only applicable to rigid containers supported on rigid foundations. Using these models, various dynamic responses such as sloshing modes natural frequencies, sloshing displacement, resultant dynamic shear and overturning moment due to both impulsive and convective liquid components can be calculated much more simply. These equivalent models are the basis for most of the current codes and standards dealing with the seismic design of LCS including ACI 350.3-06. The ACI provisions given in this chapter will be used later in this thesis to verify the validity of current practice in estimating the seismic response of cylindrical liquid tanks.

CHAPTER 4

FINITE ELEMENT MODELING

4.1 Introduction

In this chapter the fluid-structure interaction problem is formulated using the finite element (FE) technique. In the previous chapter, basic equations of motion in fluid dynamics were formulated. The remaining task to be addressed in this chapter is to solve these equations using an appropriate method capable of accurately simulating the actual behavior of liquid containers under dynamic loadings. Here, first the general equations of motion are derived for MDOF structures discretized as systems with a finite number of degrees of freedom. Then, an overview of how the fluid-structure coupling effect is accounted for in the proposed FE technique along with the corresponding equations of motion of fluid domain is presented.

In order to obtain the seismic response history of liquid tanks, the discretized structural equations and the fluid domain equations of motion have to be considered simultaneously as coupled sets of equations. The main objective of this chapter is to address this issue using FE method.

This chapter also provides a brief discussion on the problems associated with fluid damping, and boundary conditions at fluid/structure interface and free surface of the fluid. Moreover, the element types and meshing patterns used for FE modeling of the tank models are explained. The general purpose FE analysis software ANSYS® is used for dynamic analysis of liquid tank models.

4.2 Derivation of structural equations of motion

In this section a general formulation is derived for a typical MDOF system subjected to external forces $F_j(t)$, $j = 1$ to n. Consider a classic MDOF system with n degrees of freedom as shown in Figure 4.1. This classic idealization is very convenient for indicating how the equations of motion are developed for a typical MDOF system. The forces acting on each accelerated mass is shown in Figure 4.1 (b). These include the external force $F_j(t)$, the stiffness force F_{Sj}, the damping force F_{Dj}, and the inertia force F_{Ij} ($j = 1$ to n).

(a)

(b)
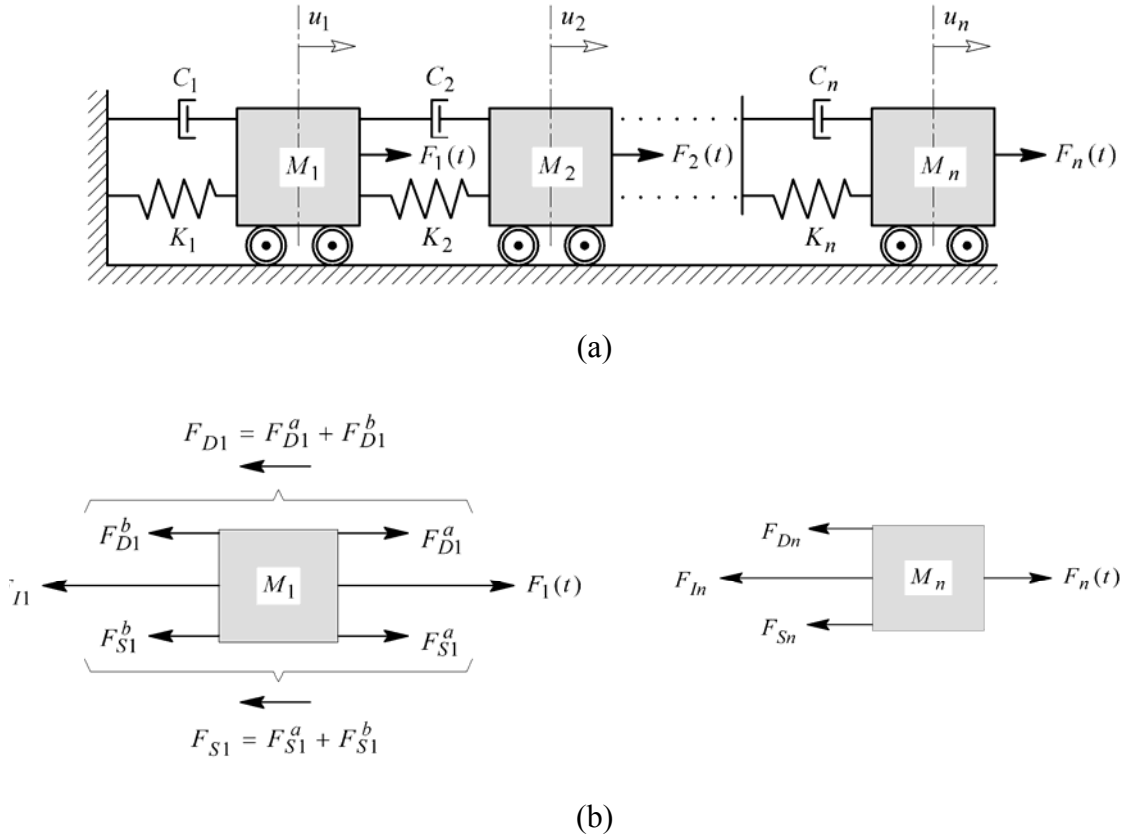
Figure 4.1 (a) Classic MDOF system; (b) Free-body diagrams

As shown in the figure, the stiffness and damping forces act in the opposite direction of the external forces because they are internal forces that resist the exerted motion. Inertial force is equal to the product of the mass times its acceleration which acts in the opposite direction of acceleration. From the free-body diagrams and based on the condition of dynamic equilibrium, for each mass we have:

$$F_{Ij} + F_{Dj} + F_{Sj} = F_j(t) \tag{4-1}$$

The above equation contains n equations for $j = 1$ to n and therefore can be written in matrix form as:

$$\{F_I\} + \{F_D\} + \{F_S\} = \{F^a\} \tag{4-2}$$

where, $\{F^a\}$ denotes the applied load vector.

The inertia force vector $\{F_I\}$ and the acceleration vector $\{\ddot{u}\}$ are related through the mass matrix $[M]$ as:

$$\{F_I\} = [M]\{\ddot{u}\} \qquad \text{or} \tag{4-3}$$

$$
\begin{Bmatrix}
F_{I1} \\
F_{I2} \\
. \\
. \\
. \\
F_{In}
\end{Bmatrix}
=
\begin{bmatrix}
M_{11} & M_{12} & . & . & . & M_{1j} & . & . & . & M_{1n} \\
M_{21} & M_{22} & . & . & . & M_{2j} & . & . & . & M_{2n} \\
. & . & & & & . & & & & . \\
. & . & & & & . & & & & . \\
. & . & . & & & . & & & & . \\
M_{n1} & M_{n2} & . & . & . & M_{nj} & . & . & . & M_{nn}
\end{bmatrix}
\begin{Bmatrix}
\ddot{u}_1 \\
\ddot{u}_2 \\
. \\
. \\
. \\
\ddot{u}_n
\end{Bmatrix}
$$

In general, for a lumped mass idealization, the mass matrix is diagonal:

$$M_{ij} = 0 \quad \text{for} \quad i \neq j \qquad \text{and} \qquad M_{jj} = M_j \text{ or } 0 \tag{4-4}$$

The damping force vector $\{F_D\}$ and the velocity vector $\{\dot{u}\}$ are related through the damping matrix $[C]$ as:

$$\{F_D\} = [C]\{\dot{u}\} \qquad \text{or} \qquad\qquad\qquad\qquad (4\text{-}5)$$

$$\begin{Bmatrix} F_{D1} \\ F_{D2} \\ \cdot \\ \cdot \\ \cdot \\ F_{Dn} \end{Bmatrix} = \begin{bmatrix} C_{11} & C_{12} & \cdot & \cdot & \cdot & C_{1j} & \cdot & \cdot & \cdot & C_{1n} \\ C_{21} & C_{22} & \cdot & \cdot & \cdot & C_{2j} & \cdot & \cdot & \cdot & C_{2n} \\ \cdot & \cdot & & & & \cdot & & & & \cdot \\ \cdot & \cdot & & & & \cdot & & & & \cdot \\ \cdot & \cdot & & & & \cdot & & & & \cdot \\ C_{n1} & C_{n2} & \cdot & \cdot & \cdot & C_{nj} & \cdot & \cdot & \cdot & C_{nn} \end{bmatrix} \begin{Bmatrix} \dot{u}_1 \\ \dot{u}_2 \\ \cdot \\ \cdot \\ \cdot \\ \dot{u}_n \end{Bmatrix}$$

The stiffness force vector $\{F_S\}$ and the displacement vector $\{u\}$ are related through the stiffness matrix $[K]$ as:

$$\{F_S\} = [K]\{u\} \qquad \text{or} \qquad\qquad\qquad\qquad (4\text{-}6)$$

$$\begin{Bmatrix} F_{S1} \\ F_{S2} \\ \cdot \\ \cdot \\ \cdot \\ F_{Sn} \end{Bmatrix} = \begin{bmatrix} K_{11} & K_{12} & \cdot & \cdot & \cdot & K_{1j} & \cdot & \cdot & \cdot & K_{1n} \\ K_{21} & K_{22} & \cdot & \cdot & \cdot & K_{2j} & \cdot & \cdot & \cdot & K_{2n} \\ \cdot & \cdot & & & & \cdot & & & & \cdot \\ \cdot & \cdot & & & & \cdot & & & & \cdot \\ \cdot & \cdot & & & & \cdot & & & & \cdot \\ K_{n1} & K_{n2} & \cdot & \cdot & \cdot & K_{nj} & \cdot & \cdot & \cdot & K_{nn} \end{bmatrix} \begin{Bmatrix} u_1 \\ u_2 \\ \cdot \\ \cdot \\ \cdot \\ u_n \end{Bmatrix}$$

We can now write the equations of motion for a MDOF system subjected to external dynamic forces $F_j(t)$ ($j = 1$ to n) by substituting Eqs. (4-3) to (4-6) into Eq. (4-2):

$$[M]\{\ddot{u}\} + [C]\{\dot{u}\} + [K]\{u\} = \{F^a\} \qquad\qquad (4\text{-}7)$$

This matrix equation represents n differential equations governing the motion of a MDOF system subjected to external dynamic forces. The equations are coupled and must be solved simultaneously.

4.3 Fluid-structure coupling

A fluid-structure interaction problem involves modeling the fluid domain and the surrounding structure. The interaction of the contained fluid and the structure at an interface

causes the hydrodynamic pressure to apply a force exerted on the structure and the structural motions produce an effective fluid load.

In order to derive the fluid-structure coupling formulations, $\{F^a\}$ in Eq. (4-7) is separated into the fluid pressure load acting at the interface $\{F_e^{pr}\}$ and resultant of all other forces $\{F_e\}$. Thus, the elemental structural equation can be rewritten as:

$$[M_e]\{\ddot{u}_e\} + [C_e]\{\dot{u}_e\} + [K_e]\{u_e\} = \{F_e\} + \{F_e^{pr}\} \tag{4-8}$$

The fluid pressure load vector $\{F_e^{pr}\}$ at fluid-structure interface S can be determined by integrating the pressure over the interface surface area as:

$$\{F_e^{pr}\} = \int_S \{N'\}p\{n\}d(S) \tag{4-9}$$

in which,

$\{N'\}$ is the shape functions used to discretize the structural displacement components (obtained from the structural element).

p is the fluid pressure.

$\{n\}$ is the normal at the fluid boundary.

Using the finite element approximating shape functions for the spatial variation of the fluid pressure, one can write:

$$p = \{N\}^T \{p_e\} \tag{4-10}$$

where,

$\{N\}$ is the shape function for fluid pressure.

$\{p_e\}$ is the nodal pressure vector.

Substituting Eq. (4-10) into Eq. (4-9) gives:

$$\{F_e^{pr}\} = \int_S \{N'\}\{N\}^T \{n\} d(S)\{p_e\} \tag{4-11}$$

By definition, the coupling matrix $[R_e]$ relates the pressure of the fluid and the forces on the fluid-structure interface. Therefore one can write:

$$\{F_e^{pr}\} = [R_e]\{p_e\} \tag{4-12}$$

By comparing the Eqs. (4-11) and (4-12), the coupling matrix is found to be:

$$[R_e]^T = \int_S \{N'\}\{N\}^T \{n\} d(S) \tag{4-13}$$

Finally, the dynamic elemental equation of the structure is obtained by substituting Eq. (4-12) into Eq. (4-8) as:

$$[M_e]\{\ddot{u}_e\} + [C_e]\{\dot{u}_e\} + [K_e]\{u_e\} - [R_e]\{p_e\} = \{F_e\} \tag{4-14}$$

4.4 Derivation of fluid finite element formulations

The hydrodynamic pressure distribution throughout the fluid domain is governed by the pressure wave equation explained in the previous chapter. The following assumptions are made in deriving the equations:

(1) The fluid is incompressible (density does not change due to pressure variations)

(2) The fluid is inviscid

(3) There is no mean flow of the fluid

(4) The fluid undergoes small-amplitude irrotational motion

Therefore, the wave equation of the fluid system can be written in general three-dimensional space (x, y, z) as:

$$\nabla^2 p(x, y, z, t) = 0 \tag{4-15}$$

in which, $p = p(x, y, z, t)$ is the hydrodynamic pressure. Since the fluid viscosity is neglected, the above equation is referred to as the lossless wave equation. In order to accurately simulate the fluid-structure interaction problem, the discretized structural equation, Eq. (4-7) and the wave equation, Eq. (4-15) have to be considered simultaneously in finite element implementation. To discretize the wave equation within fluid domain, first the following matrix operators (gradient and divergence) are introduced:

$$\nabla.(\ ) = \{L\}^T = \left| \frac{\partial}{\partial x} \frac{\partial}{\partial y} \frac{\partial}{\partial z} \right| \tag{4-16}$$

$$\nabla(\ ) = \{L\} \tag{4-17}$$

Therefore, Eq. (4-15) can be rewritten as:

$$\nabla.\nabla p = 0 \tag{4-18}$$

or in matrix notation as:

$$\{L\}^T (\{L\}p) = 0 \tag{4-19}$$

The hydrodynamic pressure p in this equation could be due to horizontal and vertical dynamic excitations of the tank walls and floor. Dynamic motions at these boundaries are related to the hydrodynamic pressure in fluid domain by defining appropriate boundary conditions along fluid-structure interfaces as follows:

$$\frac{\partial p(x, y, z, t)}{\partial n} = -\rho_l a_n(x, y, z, t) \tag{4-20}$$

or in matrix notation as:

$$\{n\}.\{\nabla p\} = -\rho_l \{n\}.\frac{\partial^2 \{u\}}{\partial t^2} \qquad \text{or} \tag{4-21}$$

70

$$\{n\}^T \left(\{L\}p\right) = -\rho_l \{n\}^T \left[\frac{\partial^2}{\partial t^2}\{u\}\right] \tag{4-22}$$

where,

ρ_l is the liquid density.

a_n is the acceleration component on the boundary along the direction outward normal n.

$\{n\}$ is the unit normal to the interface S.

$\{u\}$ is the displacement vector of the structure at the interface.

t is time.

In deformable containers a_n is the sum of the ground acceleration and the wall acceleration relative to the ground. While, in rigid containers it is obviously equal to the ground acceleration. Based on the small-amplitude wave assumption on the fluid free surface, one can write the following boundary condition accounting for the sloshing effects:

$$\frac{1}{g}\frac{\partial^2 p}{\partial t^2} + \frac{\partial p}{\partial z} = 0 \tag{4-23}$$

where, g is the acceleration due to gravity and z represents the vertical direction. This equation is the same as Eq. (3-8) but it is written in terms of fluid pressure rather than velocity potential function. By applying this boundary condition, one can obtain the convective pressure distribution within the fluid domain.

If only the impulsive component of the fluid response is to be considered, the above-mentioned boundary condition at fluid free surface should be replaced with the following boundary condition which imposes zero impulsive pressure at the free surface:

at $z = H_l$, $p(x, y, z, t) = 0$ \hfill (4-24)

in which, H_l is the height of the stored liquid.

Employing the finite element shape functions for the spatial variation of the fluid pressure p and displacement components u, the following equations can be written:

$$p = \{N\}^T \{p_e\} \quad \text{and}$$

$$u = \{N'\}^T \{u_e\} \tag{4-25}$$

where,

$\{u_e\}$ is the nodal displacement component vectors.

$\{N\}, \{p_e\}$, and $\{N'\}$ are as defined previously in section 4.3.

Here for simplicity in deriving the equations, the following notation is introduced:

$$[B] = \{L\}\{N\}^T \tag{4-26}$$

Finally, using finite element discretization and imposing the previously mentioned boundary conditions, the discretized wave equation in matrix notation can be found to be:

$$\left[M_e^p\right]\{\ddot{p}_e\} + \left[K_e^p\right]\{p_e\} + \rho_l[R_e]^T\{\ddot{u}_e\} = \{0\} \tag{4-27}$$

where,

$$\left[M_e^p\right] = \frac{1}{g}\int_{Ae}\{N\}\{N\}^T dA = \text{fluid mass matrix}$$

$$\left[K_e^p\right] = \int_{Vol}[B]^T[B]d(Vol) = \text{fluid stiffness matrix}$$

$$[R_e] = \int_S\{N\}\{n\}^T\{N'\}^T d(S) = \text{coupling matrix}$$

In these equations, *Ae* and *Vol* represent free surface and volume of the fluid element, respectively. As mentioned before, *S* denotes fluid-structure interface.

Dissipation of energy due to fluid damping can be accounted for by adding a dissipation term to the above equation to get:

$$\left[M_e^p\right]\{\ddot{p}_e\} + \left[C_e^p\right]\{\dot{p}_e\} + \left[K_e^p\right]\{p_e\} + \rho_l\left[R_e\right]^T\{\ddot{u}_e\} = \{0\} \tag{4-28}$$

where, $\left[C_e^p\right]$ is the matrix representing the damping in fluid which depends on several factors such as fluid viscosity, and pressure wave absorption in fluid domain as well as at the boundaries. This will be further discussed later in this chapter.

Eq. (4-28) together with Eq. (4-14) describe the complete finite element discretized equations for the fluid-structure interaction problem. These equations can be rewritten in assembled form as:

$$\begin{bmatrix}\left[M_e\right] & \left[0\right] \\ \left[M^{fs}\right] & \left[M_e^p\right]\end{bmatrix}\begin{Bmatrix}\{\ddot{u}_e\} \\ \{\ddot{p}_e\}\end{Bmatrix} + \begin{bmatrix}\left[C_e\right] & \left[0\right] \\ \left[0\right] & \left[C_e^p\right]\end{bmatrix}\begin{Bmatrix}\{\dot{u}_e\} \\ \{\dot{p}_e\}\end{Bmatrix} +$$

$$\begin{bmatrix}\left[K_e\right] & \left[K^{fs}\right] \\ \left[0\right] & \left[K_e^p\right]\end{bmatrix}\begin{Bmatrix}\{u_e\} \\ \{p_e\}\end{Bmatrix} = \begin{Bmatrix}\{F_e\} \\ \{0\}\end{Bmatrix} \tag{4-29}$$

in which:

$$\left[M^{fs}\right] = \rho_l\left[R_e\right]^T$$

$$\left[K^{fs}\right] = -\left[R_e\right]$$

It can be observed from Eq. (4-29) that the coupling matrix $\left[R_e\right]$ transfers the structural acceleration to the fluid domain as well as the fluid pressure to the structure.

In a fluid-structure interaction problem all the submatrices with superscript p in addition to the coupling submatrices ($\left[M^{fs}\right]$ and $\left[K^{fs}\right]$) are generated by the fluid elements. While all other submatrices without a superscript are generated by the compatible structural elements used in the finite element model.

The direct integration as well as the modal superposition methods are used to determine the time history response of the fluid-tank system. Using the direct integration scheme, the displacement and hydrodynamic pressure values at time increment $i+1$ can be calculated given the displacement and hydrodynamic pressure at time increment i. In this technique, the step by step integration is used directly to obtain the solution for the original equations of motion of the system. During each time step, the structural characteristics are assumed to be constant. However, these structural properties could differ from one step to another in nonlinear systems or remain the same during all steps in systems having linear behavior. The modal superposition method uses the natural frequencies and mode shapes of a linear structure to determine the response to transient forcing functions.

The accuracy of the time history dynamic solution depends on the integration time step defined for the solution algorithm. It should be noted that a time step that is too large may cause errors in the overall response of the system. On the other hand, a time step that is too small results in time and computer resource wastes. In this study, an integration time step of 0.005 second is used to be small enough to characterize the fluid-structure response in systems with linear elastic behavior. This was also suggested in various research studies conducted on liquid containers (Barton and Parker (1987), Mirzabozorg et al. (2003), and Kianoush et al. (2006)). It is worth noting that the time step of 0.005 second considered for time history dynamic analyses is smaller than those of recorded ground accelerations used in this study. Moreover, the results of dynamic analysis using a smaller time step shows that using 0.005 sec as an integration time step is adequate to provide accurate results.

In the case of nonlinear and/or inelastic systems (seismic isolators in Chapter 8), automatic time stepping option of ANSYS® program is employed. This option which is also known as time

step optimization, automatically adjusts the integration time step during solution according to the response frequency and the nonlinearity effects. As a result, the program decides when to increase or decrease the time step during the solution. For systems having nonlinear and/or inelastic behavior, this feature gives the added advantage of incrementing the loads appropriately and retreating to the previous converged solution if convergence is not obtained.

4.5 Damping within the fluid domain

Damping is present in most systems including liquid containers and therefore should be accounted for properly in a dynamic analysis. In fact, damping in liquid tanks depends on several factors and as a result an accurate evaluation of damping properties of a liquid filled tank is a difficult task which needs more considerations. However, an appropriate estimation of damping in such systems can be attained using the classical damping scheme known as Rayleigh damping (Alpha and Beta damping). Alpha damping and Beta damping are used to define Rayleigh damping constants α and β. The damping matrix within the fluid domain $\left[C_e^p \right]$ includes two components which are due to impulsive and convective parts of the stored fluid:

$$\left[C_e^p \right] = \alpha \left[M_e^p \right] + \beta \left[K_e^p \right] \tag{4-30}$$

where, $\left[M_e^p \right]$ and $\left[K_e^p \right]$ are the mass and stiffness matrices of the fluid element, respectively. α is determined based on the natural frequency of the fundamental sloshing mode and accounts for the damping due to sloshing on the liquid free surface. β is determined based on the fundamental frequency of the tank and simulates the damping due to the impulsive component.

Eq. (4-30) can be rewritten in the following form:

$$\zeta_i = \frac{\alpha}{2\omega_i} + \frac{\beta \omega_i}{2} \tag{4-31}$$

where,

ζ_i is the ratio of actual damping to critical damping for a particular mode of vibration, i.

ω_i is the natural circular frequency of mode i.

The natural frequencies corresponding to the fundamental convective and impulsive modes are obtained through finite element analysis and are used to determine the damping constants α and β.

Figure 4.2 shows the schematic variation of Rayleigh damping with respect to damping ratio ζ and natural circular frequency ω.
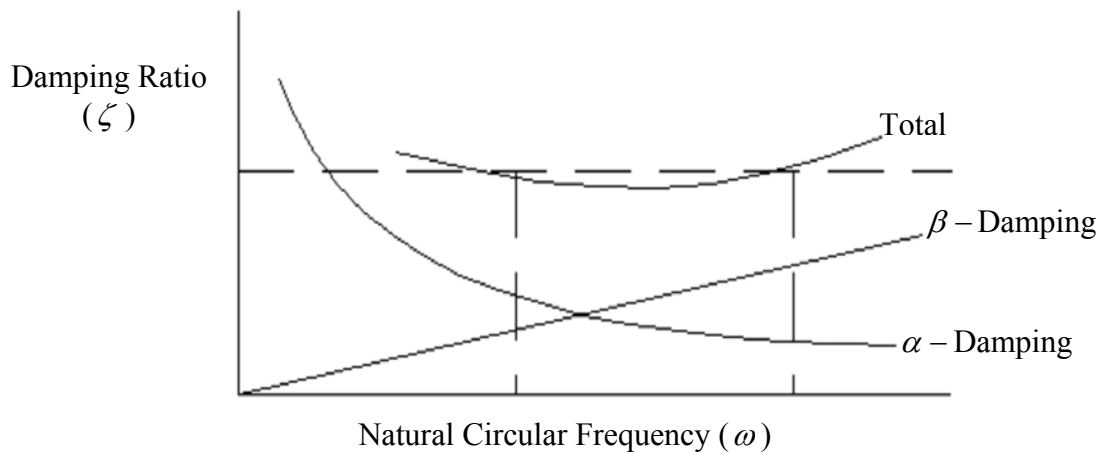
Figure 4.2 Rayleigh damping

As suggested by ACI 350.3-06, the damping ratios of 0.5 and 5 percent are assigned for the convective and impulsive components, respectively. Furthermore, the stiffness proportional damping equivalent to 5 and 2 percent of critical damping is assumed as structural damping for concrete and steel parts of the tank model, respectively.

4.6 Finite element models

In this study, two cylindrical ground-supported tanks having different aspect ratios, namely "Shallow" and "Tall" are modeled using the proposed finite element technique. The tanks are assumed to be rigidly anchored to the rigid ground. As a result, no sliding or uplift may occur. The diameters of the tanks are adjusted such that the volume of contained water in both tanks remains the same. The dimensions and other properties of the tanks are fully explained in the corresponding chapter of this thesis. The finite element idealizations along with the simplified geometries of the tanks are shown in Figure 4.3.

The "Shallow" tank is modeled using 2940 fluid elements and 336 shell elements whereas, 4752 fluid elements along with 576 shell elements are employed in FE modeling of the "Tall" tank. In general, as the mesh size is reduced, that is, as the number of elements is increased, the accuracy of the solution increases. However, the goal here is to refine the mesh to achieve the required accuracy by using only as many degrees of freedom as necessary. To illustrate this point, a study on the FE solution convergence is conducted for rigid "Shallow" and "Tall" tank models and the resulting FE error is estimated considering different numbers of fluid elements. The discretization error can be defined as:

$$E(\%) = \frac{(p_{EX}) - (p_{FE})}{(p_{EX})} \times 100 \tag{4-32}$$

Here, the exact analytical solution (p_{EX}) based on the Eq. (3-14) explained in Chapter 3 is used as a baseline solution for error estimation and to provide guidance for mesh revision. The mesh refinement is continued until the difference between the results obtained from one mesh and the previously refined mesh becomes negligible.
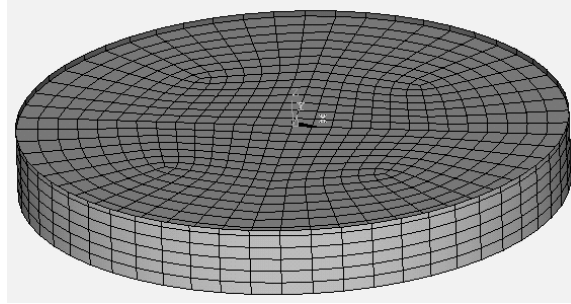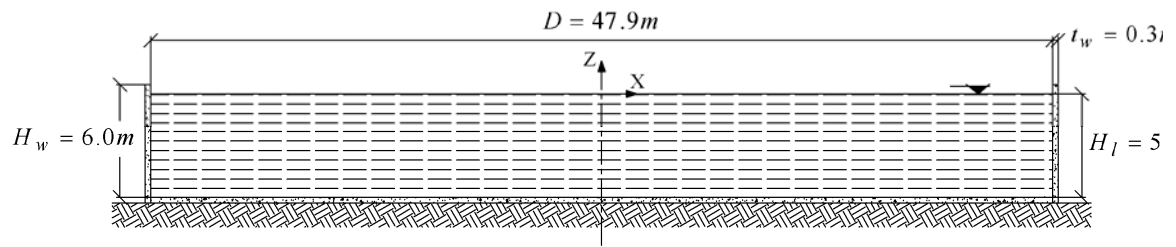
(a)
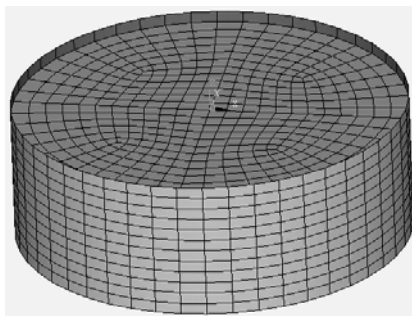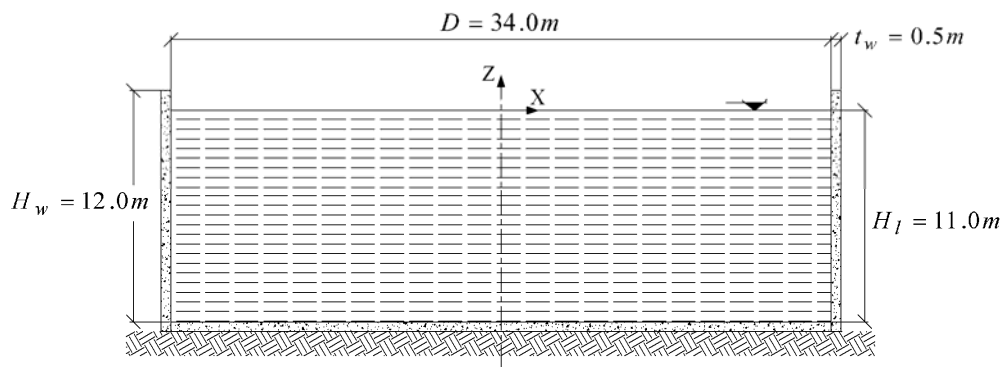
(b)

Figure 4.3 Ground-supported tank models; (a) "Shallow" tank, (b) "Tall" tank

Figure 4.4 is a plot of the resulting error in the impulsive pressure at the bottom of both rigid "Shallow" and "Tall" tank models versus the number of fluid elements. As obvious from the Figure, error percentages of around 1.63% and 1.9% are found for "Shallow" and "Tall" models, respectively assuming the number of elements mentioned above. The time history variation of impulsive pressure is obtained for the considered tank models under the horizontal component of 1940 El-Centro record scaled to the peak ground acceleration of 0.4g. The obtained discretization errors are within the acceptable range typically observed in numerical simulations. Further details on the comparison of analytical and FE results will be provided later in Chapter 5.

(a)   (b)
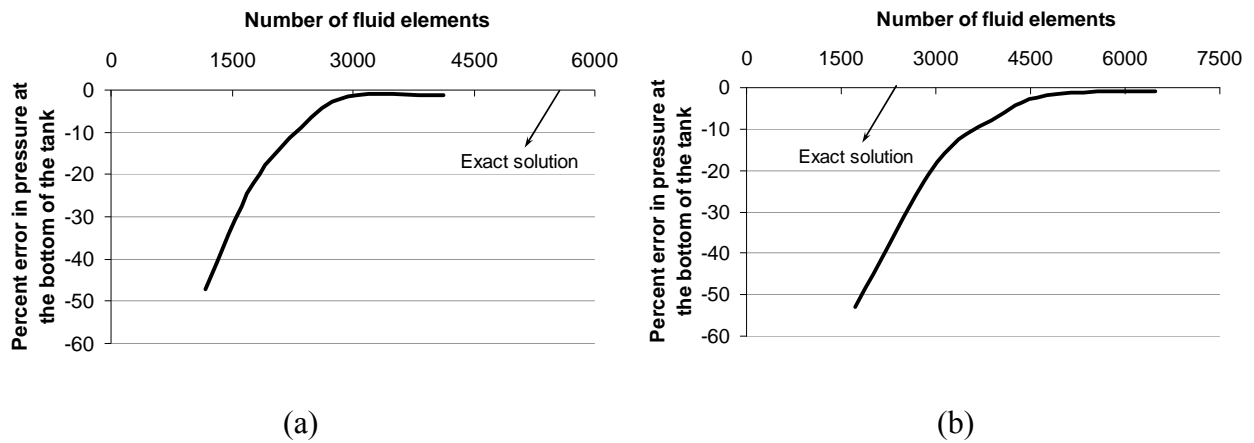
Figure 4.4 Inaccuracy of FE solution as a function of the number of fluid elements;

(a) Shallow tank, (b) Tall tank

A typical finite element idealization of an elevated tank model investigated in this study is indicated in Figure 4.5. Shown in the figure is also the simplified geometry of the tank. The total number of elements used for finite element modeling of the tank varies depending on the tank geometric properties. Full details regarding the finite element modeling of each specific elevated tank under consideration is provided in the corresponding sections of the thesis.
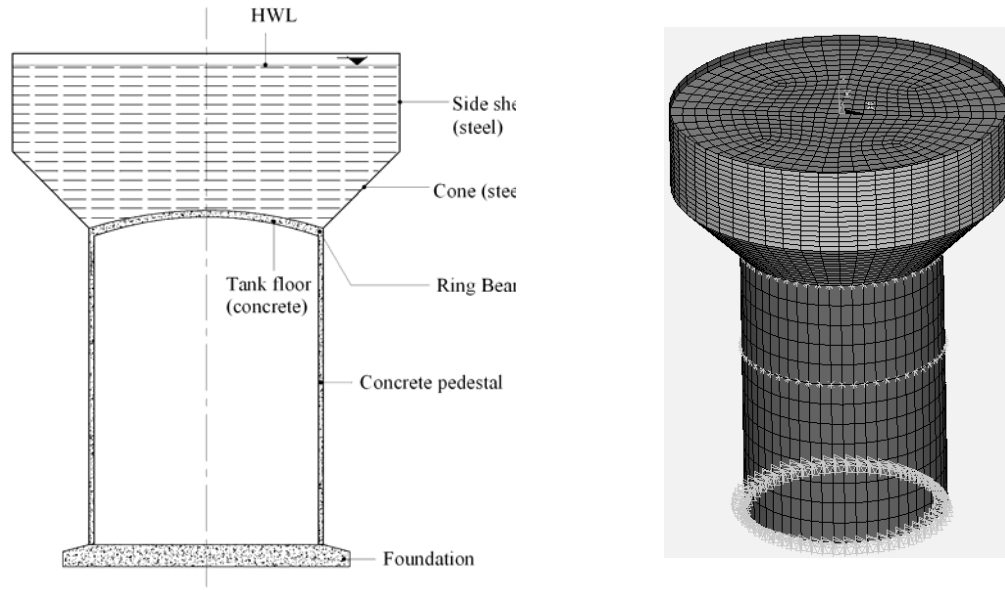
Figure 4.5 Typical elevated tank model

In finite element modeling, tank walls as well as all other structural parts including the supporting shaft in elevated tanks are modeled using four-node quadrilateral shell elements. The element has six degrees of freedom (translations in the nodal x, y, and z directions and rotations about the nodal x, y, and z axes) at each node and both bending and membrane behaviors are permitted. The geometry, node locations, and the coordinate system for this element are shown in Figure 4.6. As shown in the figure, a triangular-shaped geometry is also available for this element. Both normal and in-plane loads are allowed. Pressures may be applied as surface loads on the faces of the element as indicated by the circled numbers in Figure 4.6 (a). Shear deflection is not included in this thin-shell element. In this study, fluid domain is modeled using eight-node isoparametric brick fluid elements in a three dimensional space. Two different types of fluid elements; displacement-based (D-Fluid), and pressure-based (P-Fluid) elements are used for finite element modeling of the fluid through out this research.

80
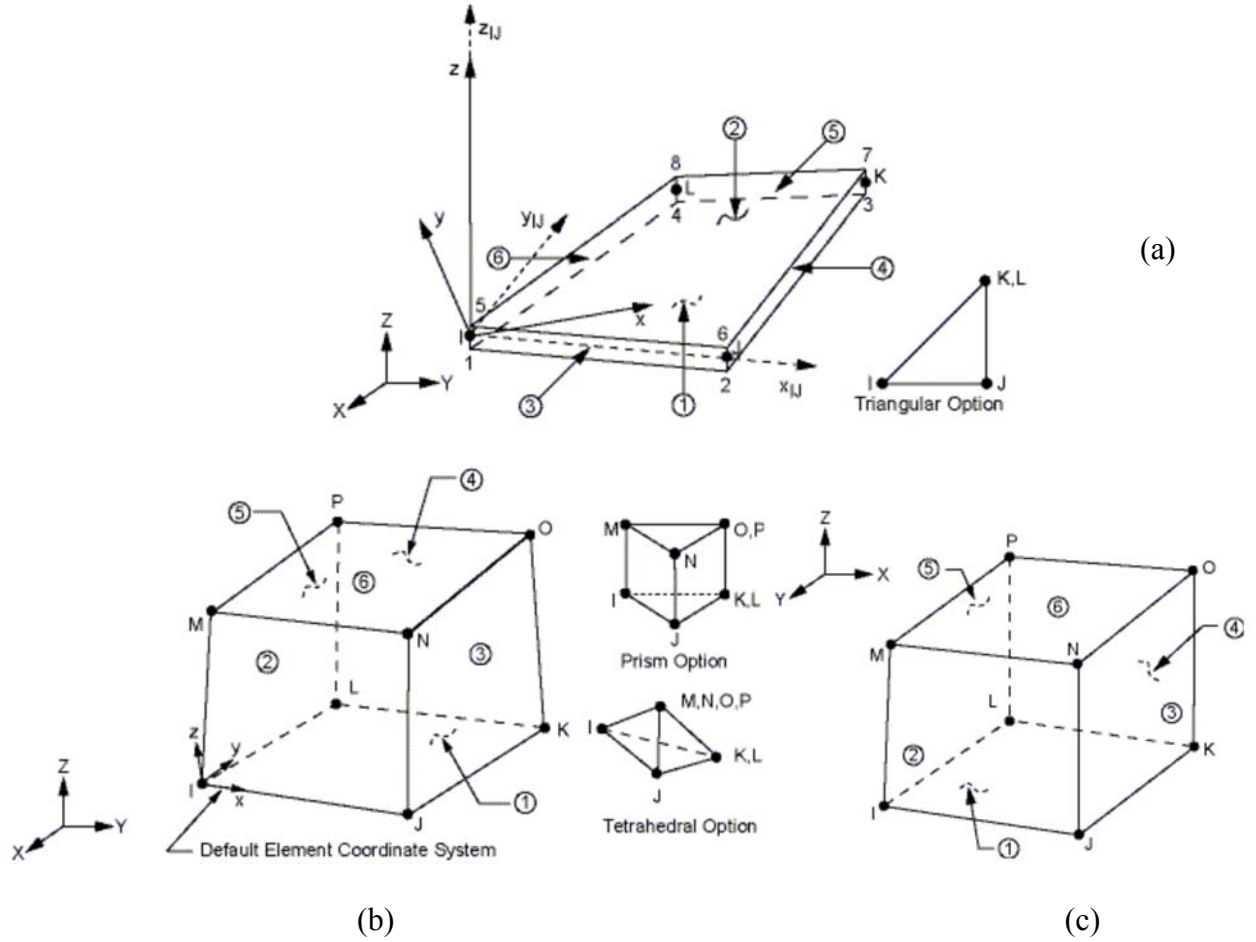
Figure 4.6 Finite elements geometries; (a) Shell element, (b) P-Fluid, (c) D-Fluid

The finite element formulation of P-Fluid elements is described previously in section 4.4. P-Fluid elements used in this study have eight corner nodes with four degrees of freedom per node: translations in the nodal x, y, z directions and pressure. The translational degrees of freedom are only needed for nodes located on the interface. Figure 4.6 shows the geometry, node locations, and the coordinate system for this element. As shown in the figure, prism-shaped and tetrahedron-shaped geometries are also available for this element. Fluid-structure interfaces (FSI) can be flagged by surface loads at the element faces as indicated by the circled numbers in

Figure 4.6. By defining the FSI on desired element faces, the structural motion and fluid pressure at the interface will be coupled.

D-Fluid elements used in this study have eight corner nodes with three degrees of freedom per node: translations in the nodal x, y, z directions. The element is capable of accounting for fluid-structure interactions. Acceleration effects, such as in sloshing problems may be considered using this element. Fluid elements at a boundary should be coupled with the structural elements in the direction normal to the interface. The geometry, node locations, and the coordinate system for this element are shown in Figure 4.6. The finite element formulation of D-Fluid elements is described in the following section.

4.7 D-Fluid finite element formulation

D-Fluid elements use displacements as the variables in the fluid domain. These elements are considered as an extension of structural solid elements in which the element shear modulus is set to zero and the fluid bulk modulus K is used to establish the elastic stress-strain relations. D-Fluid elements are particularly useful in modeling fluids contained within vessels having no net flow rate and can be employed for transient as well as free vibration analyses. The stress-strain relationship of the element is established using the stiffness matrix as follows:

$$
\begin{Bmatrix} \varepsilon_{bulk} \\ \gamma_{xy} \\ \gamma_{yz} \\ \gamma_{xz} \\ R_x \\ R_y \\ R_z \end{Bmatrix} = \begin{bmatrix} 1/K & 0 & 0 & 0 & 0 & 0 & 0 \\ 0 & 1/S & 0 & 0 & 0 & 0 & 0 \\ 0 & 0 & 1/S & 0 & 0 & 0 & 0 \\ 0 & 0 & 0 & 1/S & 0 & 0 & 0 \\ 0 & 0 & 0 & 0 & 1/B & 0 & 0 \\ 0 & 0 & 0 & 0 & 0 & 1/B & 0 \\ 0 & 0 & 0 & 0 & 0 & 0 & 1/B \end{bmatrix} \begin{Bmatrix} P \\ \tau_{xy} \\ \tau_{yz} \\ \tau_{xz} \\ M_x \\ M_y \\ M_z \end{Bmatrix}
\tag{4-33}
$$

where, $\varepsilon_{bulk} = \dfrac{\partial u}{\partial x} + \dfrac{\partial v}{\partial y} + \dfrac{\partial w}{\partial z} = \text{bulk strain}$

82

K = fluid elastic (bulk) modulus

P = pressure

γ = shear strain

$S = K \times 10^{-9}$ (arbitrarily small number to give element some shear stability)

τ = shear stress

R_i = rotation about axis i

$B = K \times 10^{-9}$ (arbitrarily small number to give element some rotational stability)

M_i = twisting force about axis i

Damping matrix of the element that relates the strain rates (strain differentiation with respect to time) to the stresses can also be defined as:

$$
\begin{Bmatrix}
\dot{\varepsilon}_{bulk} \\
\dot{\gamma}_{xy} \\
\dot{\gamma}_{yz} \\
\dot{\gamma}_{xz} \\
\dot{R}_x \\
\dot{R}_y \\
\dot{R}_z
\end{Bmatrix}
=
\begin{bmatrix}
0 & 0 & 0 & 0 & 0 & 0 & 0 \\
0 & 1/\eta & 0 & 0 & 0 & 0 & 0 \\
0 & 0 & 1/\eta & 0 & 0 & 0 & 0 \\
0 & 0 & 0 & 1/\eta & 0 & 0 & 0 \\
0 & 0 & 0 & 0 & 1/C & 0 & 0 \\
0 & 0 & 0 & 0 & 0 & 1/C & 0 \\
0 & 0 & 0 & 0 & 0 & 0 & 1/C
\end{bmatrix}
\begin{Bmatrix}
P \\
\tau_{xy} \\
\tau_{yz} \\
\tau_{xz} \\
M_x \\
M_y \\
M_z
\end{Bmatrix}
\qquad (4\text{-}34)
$$

where, η = viscosity, and $C = .00001\,\eta$

The element does not generate a consistent mass matrix and only the lumped mass matrix is available. The sloshing effects and associated mode characteristics can be studied using this element. To hold the free surface in place, springs having the equivalent stiffness K_s are added to each node of the element. K_s is determined as follows:

$$
K_s = \rho_l A_f (g_x C_x + g_y C_y + g_z C_z) \qquad (4\text{-}35)
$$

where, ρ_l = liquid density, A_f = area of the face of the element, g_i = acceleration in the i direction, and C_i = ith component of the normal to the face of the element. Added springs have positive constants at the nodes on top of the element and have negative constants for those located on bottom surface. Hence, at the interior nodes within the liquid domain, these effects cancel out and they only operate at the fluid free surface.

4.8 Summary

The equation of motion for a typical structural MDOF system subjected to external dynamic forces was derived. The procedure for coupling the fluid and structural domains in finite element modeling of the liquid tanks was discussed. The coupling matrix transferring the structural motion and the hydrodynamic pressure between the structure and the fluid was developed.

The finite element formulation for the coupled system of liquid tanks in the time domain was described. In deriving these formulations, appropriate boundary conditions available in typical liquid tanks were applied. In addition, problems associated with damping characteristics of the fluid domain were discussed. Using the proposed finite element technique, the effects of both impulsive and convective parts and their corresponding damping effects can be taken into account. The proposed technique is general and can be employed for any tank configurations, or any direction of seismic excitation. This method can account for all aspects of structural and fluid components in the time domain.

Some important properties of the elements used in this study for finite element modeling of both ground-supported and elevated tank models were described in this chapter.

CHAPTER 5

DYNAMIC RESPONSE OF CYLINDRICAL GROUND-SUPPORTED TANKS

5.1 Introduction

This chapter deals with the dynamic behavior of cylindrical open top ground-supported water tanks. The main focus of this chapter is to identify the factors having significant effects on the dynamic response of such structures and to address the interaction between these parameters. Examined parameters are sloshing of liquid free surface, tank wall flexibility, vertical ground acceleration, tank aspect ratio, and base fixity. To accurately investigate the dynamic behavior of the tanks, the hydrodynamic response is divided into impulsive and convective components.

In addition, the dynamic results obtained from the rigorous finite element method are compared with those recommended by current practice and thereby the adequacy of current code provisions in estimating the dynamic response of liquid-filled cylindrical containers is investigated. The validity of the proposed finite element method is verified by comparing the results with those calculated from well-proved analytical methods available in the literature.

In the first part of this Chapter, two rigid cylindrical tanks having different aspect ratios are modeled in three-dimensional space and their free vibration results are compared with those obtained through analytical approaches.

Time history response of both rigid and flexible tanks having different conditions at the base; fixed and hinged under both horizontal and vertical components of earthquake is obtained using the direct integration method. Based on the computed results, important conclusions

regarding the seismic behavior of cylindrical ground-supported tanks are drawn and some suggestions to be considered in seismic design of liquid containers are made.

5.2 Tank models properties

Two cylindrical concrete tank models with different aspect ratios, representative of two classes of tanks namely "Shallow" and "Tall" are considered for finite element analysis throughout this chapter. Some information regarding the finite element modeling and geometric properties of the tanks is provided in section 4.6. Dimensions of the tanks are shown in Figure 4.3 and are selected such that the volume of stored water remains unchanged for both tank models. The tanks are assumed to be rigidly anchored to the rigid ground. As a result, the effect of soil-structure interaction is not included. Since only anchored tanks are considered, the tank floor is not included in the FE model. The tank walls are considered to be of constant thickness and connected to the base such that no sliding or uplift may occur.

The tank structure is modeled using elastic shell elements and the fluid domain is modeled using 3D brick-shaped fluid elements. Properties of the concrete and water materials are as follows:

Concrete   Water

Density = 2400 kg/m^3

Young's modulus = 24.86 GPa   Density = 1000 kg/m^3

Poisson's ratio = 0.16

Considered tanks have the aspect ratios of $\dfrac{H_l}{D} = 0.115$ (Shallow tank), and $\dfrac{H_l}{D} = 0.324$ (Tall tank), where H_l and D are as indicated in Figure 4.3. The finite element idealizations of the tanks are also shown in Figure 4.3.

Fluid and shell domains should be meshed in such a way that the location of each node of the fluid domain on the interface coincide exactly with that of the corresponding shell element. Then, these coincident nodes must be coupled in order to get equal displacements in radial direction for both fluid and shell nodes located on the interface. However, tangential relative displacements should be possible to happen. Fluid nodes should be coupled at all interfaces with containing structure; as a result all fluid nodes located at the interface with the tank floor must be restrained in vertical direction.

5.3 Free vibration analysis

Prior to performing time history analysis, free vibration analysis is carried out on the tank models assuming rigid wall boundary condition. The tanks are assumed to have the fixed boundary condition at the base. The natural frequencies and modal responses are obtained using both FE and analytical methods for impulsive and convective modes with the highest participation factors among all modes of vibration.

For each model, the fundamental mode is identified as that with the largest participation factor (β) in the horizontal X direction. Table 5.1 shows computed results determined through FE analysis along with those obtained from analytical methods.

The method introduced by Housner (1963) is used here as an analytical approach for calculating the natural frequency of the fundamental sloshing mode as well as the impulsive and convective mass ratios. Since Housner's method is only applicable to tanks with rigid wall boundary condition, tank models considered in this section are assumed to be rigid as well. A detailed description on Housner's method along with all relevant formulations are given in Appendix A.

Table 5.1. Free vibration analysis results for ground-supported rigid tank models

"Shallow" Model							
Mode		Frequency (Hz)		Effective mass	R_i (%)		β
Number	type	FE	Analytical	(FE) (kN.s²/m)	FE	Analytical	(normalized)
*1	Convective	0.087	0.087	7790.1	78.8	79.8	1.00
2	Convective	0.216	NA	457.6	4.6	NA	0.25
*1	Impulsive	39.410	38.00	1290.7	13.1	13.3	0.40
2	Impulsive	79.670	NA	20.0	0.2	NA	0.05
"Tall" Model							
Mode		Frequency (Hz)		Effective mass	R_i (%)		β
Number	type	FE	Analytical	(FE) (kN.s²/m)	FE	Analytical	(normalized)
*1	Convective	0.149	0.149	5779.0	58.0	59.0	1.00
2	Convective	0.277	NA	197.9	2.0	NA	0.18
3	Convective	0.350	NA	39.3	0.4	NA	0.08
*1	Impulsive	30.530	36.00	3537.2	35.5	37.0	0.78
2	Impulsive	61.780	NA	111.4	1.1	NA	0.14
3	Impulsive	74.060	NA	43.9	0.4	NA	0.09

* Fundamental mode.

The analytical method proposed by Veletsos and Shivakumar (1997) is used to determine the fundamental impulsive frequency of the tank-liquid system as:

$$\omega_i = C_I \frac{1}{H_l} \sqrt{10^3 E_c \frac{g}{\gamma_c}} \tag{5-1}$$

$$C_I = C_w \sqrt{\frac{t_w}{10R}} \tag{5-2}$$

$$T_i = \frac{2\pi}{\omega_i} = \frac{1}{f_i} \tag{5-3}$$

where:

C_l and C_w: coefficients for determining the fundamental frequency of the tank-liquid system

H_l: depth of stored liquid (m)

E_c: modulus of elasticity of concrete (MPa)

g: acceleration due to gravity (9.807 m/s^2)

γ_c: density of concrete (kN/m^3)

t_w: average wall thickness (mm)

R: inside radius of the tank (m)

ω_i: circular frequency of the fundamental impulsive mode of vibration (radian/s)

f_i: natural frequency of the fundamental impulsive mode of vibration (Hz)

For $\dfrac{D}{H_l} > 0.667$:   (5-4)

$$C_w = 9.375 \times 10^{-2} + 0.2039(\frac{H_l}{D}) - 0.1034(\frac{H_l}{D})^2 - 0.1253(\frac{H_l}{D})^3 + 0.1267(\frac{H_l}{D})^4$$
$$- 3.186 \times 10^{-2}(\frac{H_l}{D})^5$$

or, alternatively C_w can be determined from Figure 5.1. These two analytical methods (Housner (1963) and Veletsos and Shivakumar (1997)) are also adapted by ACI 350.3-06 for determining the dynamic characteristics of ground-supported concrete cylindrical tanks.

The ratio (R$_i$) of the effective modal mass in X direction to the total mass of the system for each mode under consideration is also included in Table 5.1. Since the tank wall is modeled as massless shell elements, the obtained modal masses are only contributed by the contained fluid. Therefore, the results obtained from FE analysis are readily comparable with those computed from Housner's method.
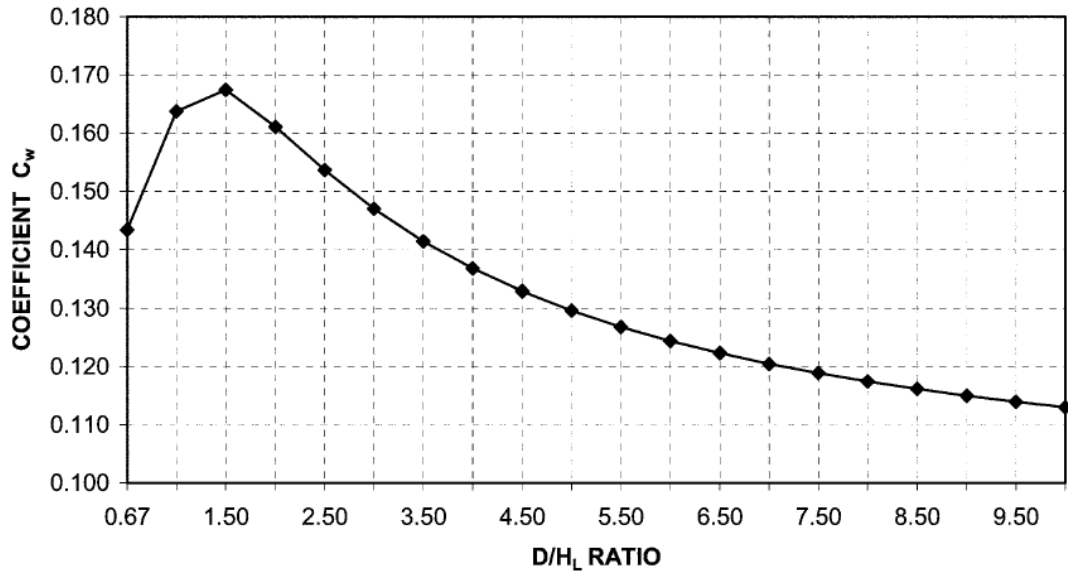
Figure 5.1 Coefficient C_w for ground-supported cylindrical tanks

(adapted from ACI 350.3-06)

The modal participation factors (β) normalized with respect to their largest values for each model are also given in the table. The participation factor corresponding to a specific mode denoted as fundamental mode is much greater than those of other modes. This implies that the response of the system is dominated by these modes when excited horizontally in X direction.

For instance, R_i for the first convective mode of the "Tall" model is 96% of the total R_i obtained by adding those of the three convective modes considered. Regarding the impulsive response of the "Tall" tank, this ratio is again around 96%. The same trend is observed for the "Shallow" tank. Therefore, for practical purposes, only the fundamental impulsive and convective modes (mode numbers 1 in the table) need to be taken into account in order to estimate the dynamic response of such tanks under horizontal excitations.

It is worth noting that all impulsive modes contributing the most to the response to horizontal excitation are cantilever beam type modes with circumferential wave number (n) equal to 1 in which shell cross section remains circular while vibrating.

Results of free vibration analyses show that the participation factors and effective masses associated with the $\cos(n\theta)$ type modes (n > 1) are very small and therefore can be neglected in determining the response to horizontal excitations. This has also been stated by Barton and Parker (1987) for cylindrical tanks having height/diameter ratio larger than 0.5 and also by El Damatty et al. (2005) for conical tanks.

It is important to note that in FE analysis, the tanks can not be modeled as infinitely rigid. This will cause singularity in the solution process. Therefore, the tanks are made relatively rigid by introducing a very large modulus of elasticity for shell material. A Young's modulus of ten times greater than that of a normal concrete is assigned to the shell elements to account for the effect of tank wall rigidity. As a result, as can be observed from Table 5.1, very large impulsive natural frequencies implying the relative rigidity of the tank walls are obtained for FE models.

Considering the wall thicknesses of 300 and 500mm for "Shallow" and "Tall" tanks, respectively, one can use Eqs. (5-1) to (5-4) to compute the natural frequencies of the fundamental impulsive modes. As a result, the fundamental impulsive frequencies of 38 and 36 Hz are calculated for "Shallow" and "Tall" tanks, respectively, which are in close agreement with those obtained from FE.

The mode shapes of "Tall" model listed in Table 5.1 are displayed in Figure 5.2. The sloshing profiles for the first three convective modes of cylindrical containers given by Veletsos (1984) are also shown in the figure. Comparing these two sets of sloshing mode shapes, it is

obvious that they are quite similar in terms of the radial distribution of vertical displacements at liquid free surface.

(a)

FIRST MODE

SECOND MODE

THIRD MODE

1 .8 .6 .4 .2 0 .2 .4 .6 .8 1   1 .8 .6 .4 .2 0 .2 .4 .6 .8 1   1 .8 .6 .4 .2 0 .2 .4 .6 .8 1

r/R   r/R   r/R   r/R   r/R   r/R

(b)

(c)
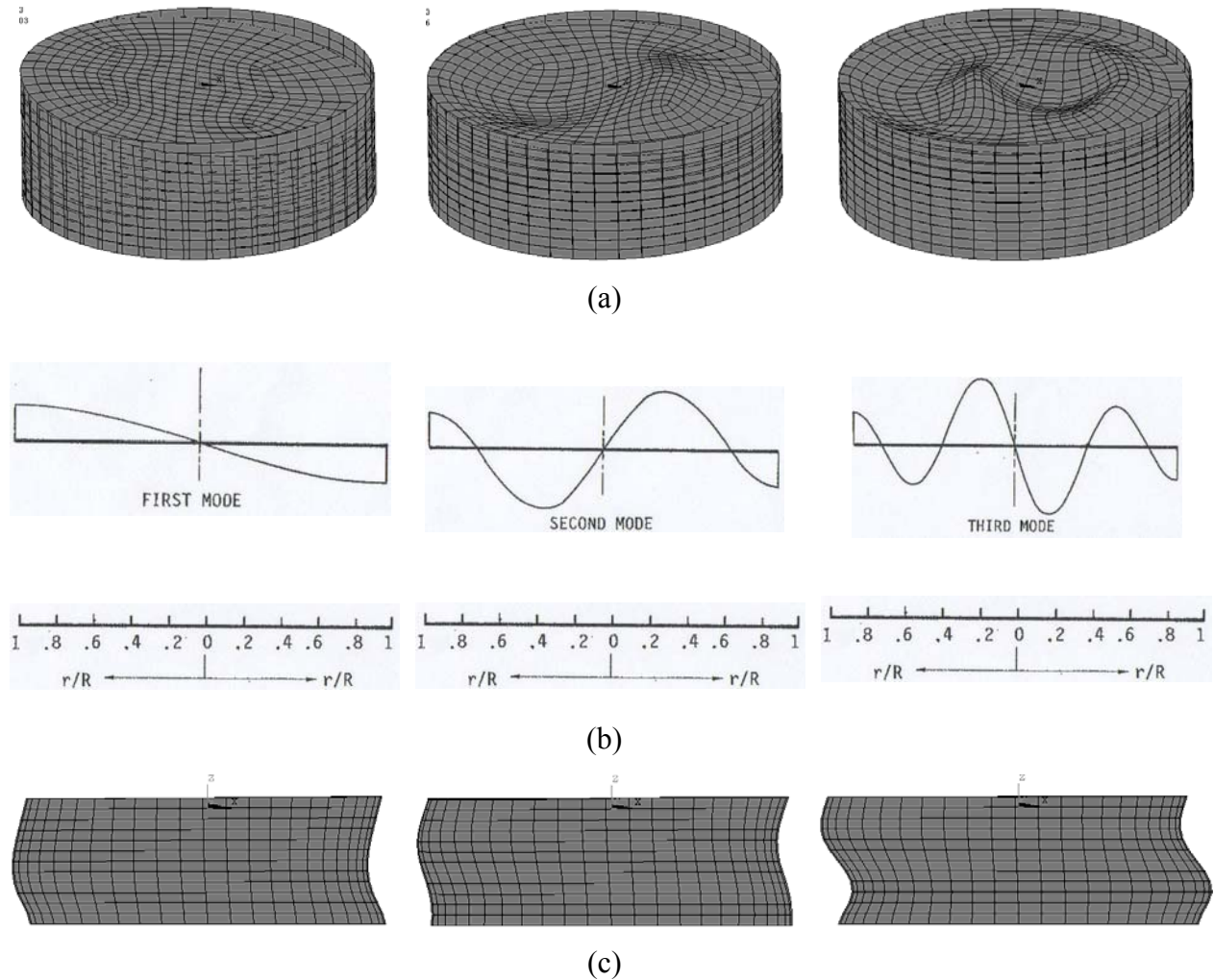
Figure 5.2 Mode shapes of "Tall" model (horizontal motion); (a) First three convective modes (FE), (b) First three convective modes (adapted from Veletsos (1984)), (c) First three impulsive modes (FE)

Comparing the FE and analytical results given in Table 5.1, it can be observed that the finite element results are in excellent agreement with those calculated through analytical approaches verifying that the proposed FE model can be employed with high accuracy to study the fluid-

structure interaction problems of liquid containing structures. A relatively better agreement between results is found for the convective term as compared to the impulsive term especially in terms of the fundamental natural frequencies. The reason could be due to the fact that in both FE and Housner's formulations, the linearized wave equation is employed.

5.4 Verification of numerical model

To further verify the proposed FE technique, the hydrodynamic response of the "Shallow" tank under random seismic excitation is obtained using the FE technique and the results are compared with the analytical solution proposed by Haroun and Housner (1981A). The considered tank is assumed to have fixed condition at the base. Tank walls are assumed to be rigid, and the tank floor is fully anchored to the rigid ground. For comparison purposes, zero damping is assumed for the system.

The horizontal component of 1940 El-Centro earthquake scaled to the peak ground acceleration of 0.4g is used as an excitation and the time history response of the tank-liquid system is obtained. Based on Haroun's study, the analytical impulsive pressure for a rigid cylindrical tank can be obtained using Eq. (3-14) described in detail in Chapter 3. For convenience the equation is rewritten here in the following form:

$$p_1(R,\phi,z,t) = -\frac{2\rho_l \ddot{u}_0(t)}{H_l} \sum_{i=1}^{\infty} \frac{(-1)^{i+1} I_1(\alpha_i R)}{\alpha_i^2 I_1'(\alpha_i R)} \cos(\alpha_i z) \cos(\phi) \qquad (5\text{-}5)$$

where:

α_i are constants given by $\alpha_i = \dfrac{(2i-1)\pi}{2H_l}$ (5-6)

ϕ and z are circumferential and axial coordinates, respectively with the center of the base being the origin.

R = tank radius

ρ_l = liquid mass density

$\ddot{u}_0(t)$ = horizontal ground acceleration

H_l = liquid depth

I_1 = modified Bessel function of the first kind of order 1 and I_1' is its derivative.

In calculating the hydrodynamic pressure by Eq. (5-5), the first fifteen terms of the series ($i = 1$ to 15) are used. More series terms may be included in order to obtain results of higher accuracy. However, for the tank model under consideration, an excellent estimation of the hydrodynamic pressure is obtained using the first fifteen terms. The hydrodynamic impulsive pressure distribution over the height of the rigid tank calculated through analytical solution and FE is shown in Figure 5.3. The impulsive pressure time history at the bottom of the tank adjacent to the wall ($r = R$, $\phi = 0$, $z = 0$) is also shown in Figure 5.4. It is obvious that FE and analytical results are in excellent agreement. This further verifies the validity of the proposed FE technique.
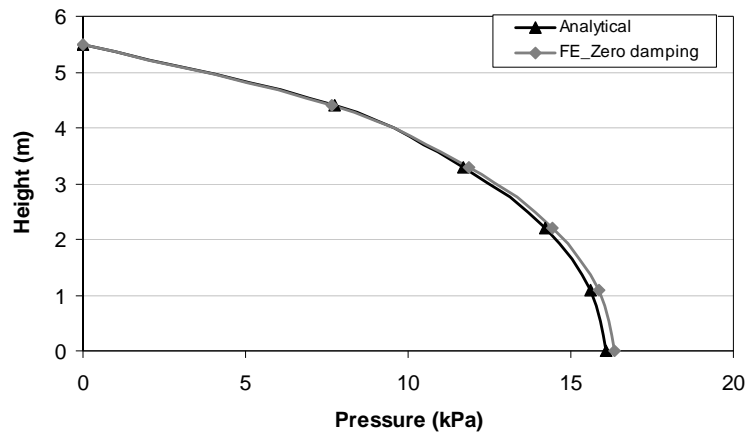
Figure 5.3 Impulsive pressure distribution over the height of the rigid "Shallow" tank
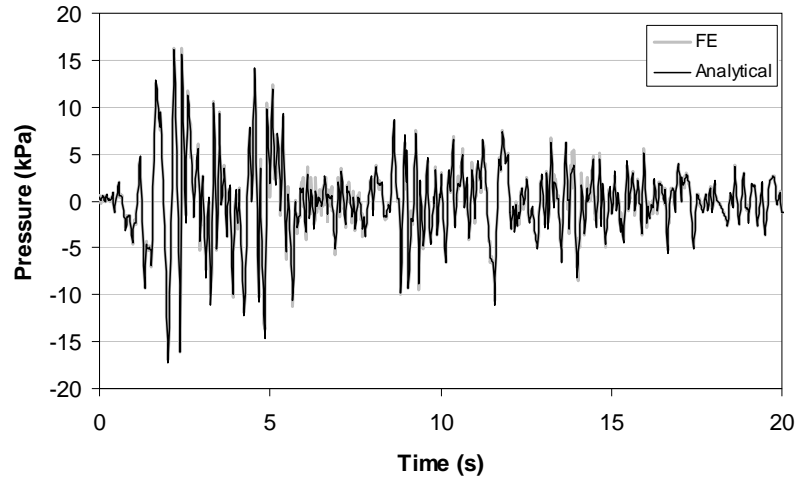
Figure 5.4 Time history of impulsive pressure at ($r = R$, $\phi = 0$, $z = 0$)

5.5 Effect of tank wall flexibility and vertical earthquake component

In order to study the effect of tank wall flexibility, the time history response of tank models having both rigid and flexible walls are calculated and a comparison between the obtained results is made. Furthermore, to investigate the effect of vertical component of earthquake on dynamic behavior of cylindrical tanks, the seismic response of the tanks under both the horizontal component alone and the combined horizontal and vertical components are obtained. In performing the time history analyses, the horizontal and vertical components of 1940 El-Centro earthquake are used as seismic excitations. The components are scaled in such a way that the peak ground acceleration in the horizontal direction reaches 0.4g. The scaled earthquake components are shown in Figure 5.5. The tanks considered in this section are assumed to have hinged boundary condition at their base.

<center>(a)</center><center>(b)</center>
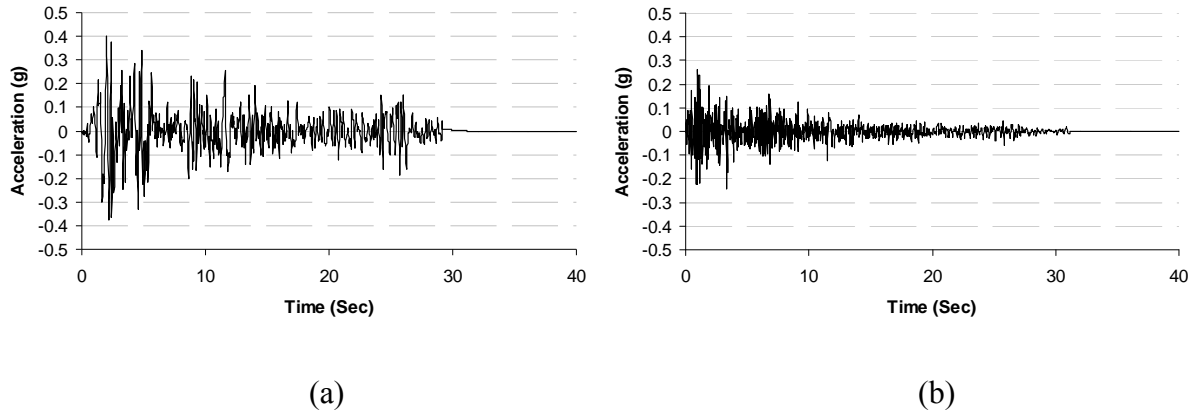
<center>Figure 5.5 Scaled 1940 El-Centro earthquake; (a) Horizontal component,</center>

<center>(b) Vertical component</center>

5.5.1 Dynamic behavior of rigid tanks

(a) Shallow tank

The total time history response of the tanks is separated into impulsive and convective components in order to study the time varying response characteristics of the tank models. The examined responses include the hydrodynamic pressure exerted by the liquid on the tank wall; the associated structural forces including the hoop force, bending moment, and shear force; and the vertical displacement or sloshing height of the liquid free surface.

The transient hoop force, bending moment, and shear force responses for the rigid "Shallow" tank under the horizontal component of El-Centro earthquake are obtained and indicated in Figure 5.6. The structural responses are reported at the locations of maximum response within the tank wall and are calculated per unit width of the wall. The maximum shear occurs at the base of the wall; therefore it will be referred to as base shear. However, for a hinged tank, the maximum hoop force and bending moment occur far from the base and around the mid height of the tank wall.

<center>96</center>
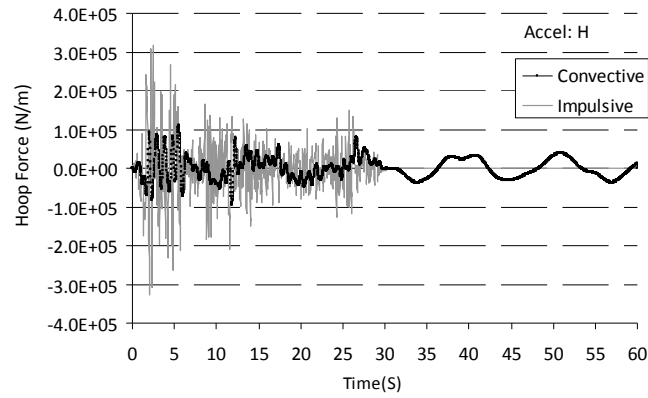
(a)
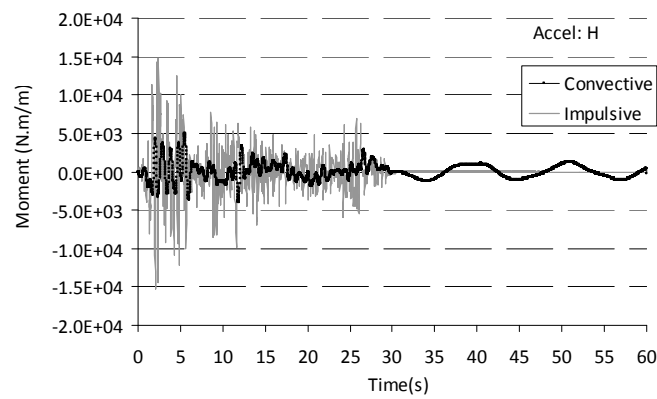
(b)
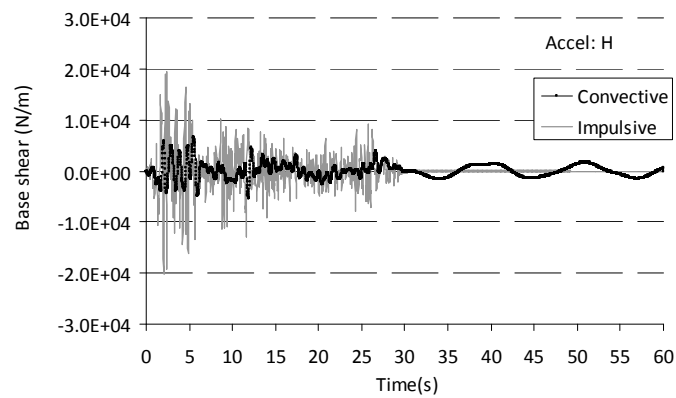
(c)

Figure 5.6 Time history response of the rigid "Shallow" tank due to horizontal excitation;

(a) Hoop force, (b) Moment, (c) Base shear

97

The absolute maximum values for the impulsive hoop force, moment, and base shear due to horizontal excitation are 326 kN/m, 15.2 kNm/m, and 20.2 kN/m, respectively. The corresponding absolute peak values of convective hoop force, moment, and base shear are 109 kN/m, 4.9 kNm/m, and 6.5 kN/m, respectively. As can be observed from Figure 5.6, the impulsive and convective response components do not reach their peaks at the same time. Furthermore, by comparing the convective response values with those of impulsive response, one can conclude that the forces resulting from liquid sloshing have less significant effect on the dynamic response of the liquid-tank system.

Table 5.2 summarizes the peak response values calculated through time history FE analysis. The time history diagram for sloshing of water free surface is shown in Figure 5.7. The sloshing response is reported at $\phi = 0$, adjacent to the tank wall. The maximum positive sloshing height of 248 mm occurs at t = 40.86 sec as a result of horizontal excitation. The peak value of sloshing height occurs far after the peak of the ground acceleration. ACI 350.3-06 predicts the maximum sloshing height of 440 mm which is well above the FE result and is suitable in terms of providing sufficient design freeboard between the water free surface and the roof.

Table 5.2 Summary of peak time history analysis results

				Hoop Force (N/m) $\times 10^3$	Moment (N.m/m) $\times 10^3$	Base Shear (N/m) $\times 10^3$	Sloshing (mm)
Rigid	Shallow	Impulsive	H	326	15.2	20.2	NA
		Convective	H	109	4.9	6.5	248
	Tall	Impulsive	H	685	35.6	47.1	NA
		Convective	H	212	10.9	14.4	931
Flexible	Shallow	Impulsive	H	613 **88%**	27.1 **78%**	33.9 **68%**	NA
			H+V	652	28.2	35.0	NA
			(H+V)/H	1.06	1.04	1.03	NA
		Convective	H	98 **-10%**	4.7 **-4%**	6.1 **-6%**	243 **-2%**
			H+V	105	5.0	6.5	253
			(H+V)/H	1.07	1.06	1.07	1.04
	Tall	Impulsive	H	1331 **94%**	60.3 **69%**	73.1 **55%**	NA
			H+V	1558	75.1	92.9	NA
			(H+V)/H	1.17	1.24	1.27	NA
		Convective	H	201 **-5%**	10.1 **-7%**	13.1 **-9%**	894 **-4%**
			H+V	239	12.7	16.9	965
			(H+V)/H	1.19	1.26	1.29	1.08
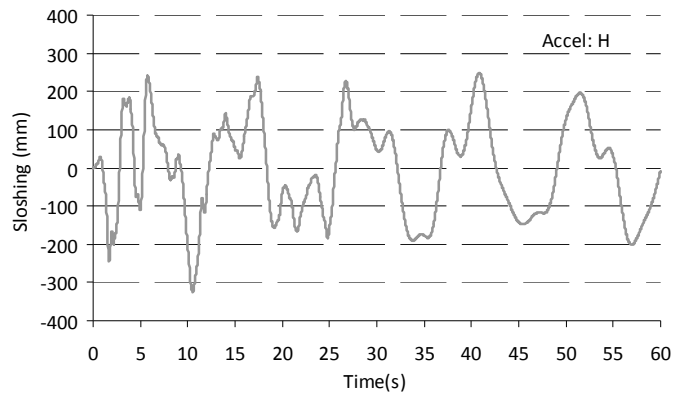
Figure 5.7 Sloshing height time history for rigid "Shallow" tank due to horizontal excitation

(b) Tall tank

The transient hoop force, bending moment, and base shear responses for the rigid "Tall" tank model are shown in Figure 5.8. The absolute maximum values of the resulting hoop force, moment, and base shear corresponding to the impulsive component due to horizontal excitation are 685 kN/m, 35.6 kNm/m, and 47.1 kN/m, respectively. The calculated absolute maximum values of convective hoop force, moment, and base shear are 212 kN/m, 10.9 kNm/m, and 14.4 kN/m, respectively which occur at about 3.1 seconds after peaks of impulsive response. The ratios of convective maximum response values to the corresponding impulsive values are found to be higher in "Shallow" tank as compared to "Tall" tank. This implies that the convective component has somewhat more significant effect on the overall dynamic response of liquid-tank systems in shallow containers compared to tall containers.

The time history of sloshing height at water free surface adjacent to the wall is given in Figure 5.9. Due to horizontal excitation, the maximum positive sloshing height of 931mm occurs at t = 25.14 sec. According to ACI 350.3-06, the design sloshing height of 910mm is obtained which is very close to the calculated FE value.
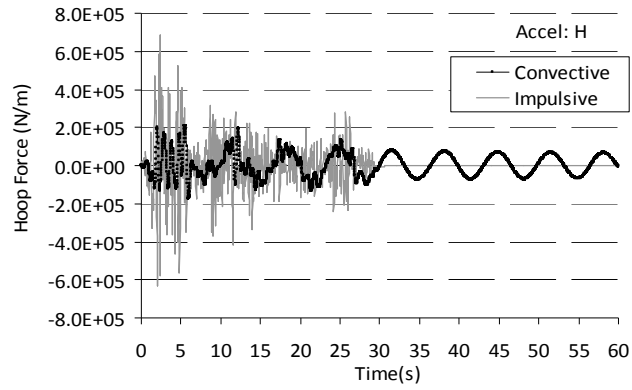
(a)
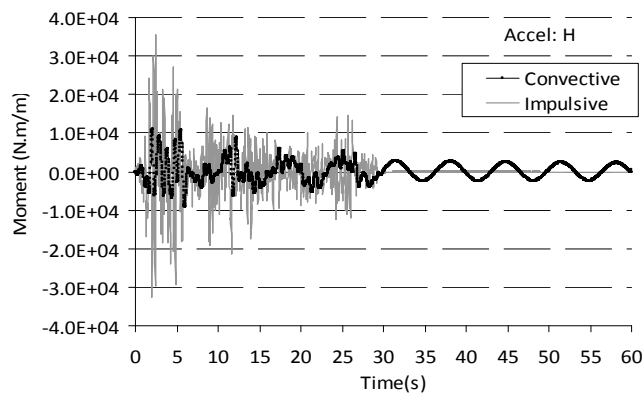
(b)

(c)

Figure 5.8 Time history response of the rigid "Tall" tank due to horizontal excitation;

(a) Hoop force, (b) Moment, (c) Base shear

101
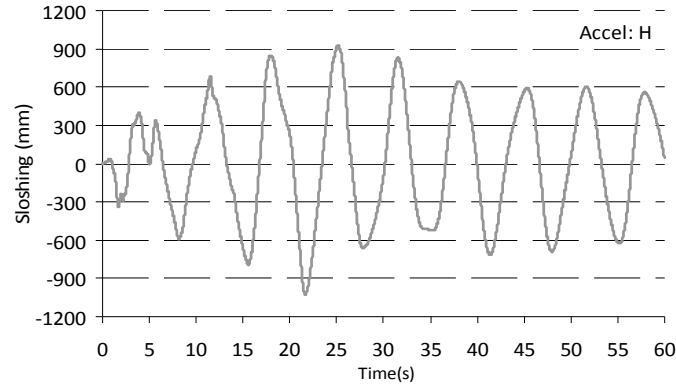
Figure 5.9 Sloshing height time history for rigid "Tall" tank due to horizontal excitation

5.5.2 Dynamic behavior of flexible tanks

(a) Shallow tank

The FE time history results for "Shallow" and "Tall" tank models with flexible wall boundary condition due to both horizontal and combined horizontal and vertical excitations are also presented in Table 5.2. The numbers in bold in the table show an increase (positive) or decrease (negative) percentage over the corresponding rigid tank model. The transient structural responses for flexible "Shallow" tank model are shown in Figure 5.10 and 5.11.

Due to horizontal excitation, the absolute maximum values of hoop force, moment, and base shear are 613 kN/m, 27.1 kNm/m, and 33.9 kN/m, respectively for impulsive component and 98 kN/m, 4.7 kNm/m, and 6.1 kN/m for convective component. As compared to the results obtained for the rigid tank, it can be observed that maximum values of impulsive hoop force, moment, and base shear are increased considerably by 88, 78, and 68 percents, respectively as a result of wall flexibility effect. On the other hand, the obtained results indicate only a negligible decrease in associated convective response values due to the flexibility of tank walls. This shows that the convective part of response is almost independent of tank wall flexibility.

(a)
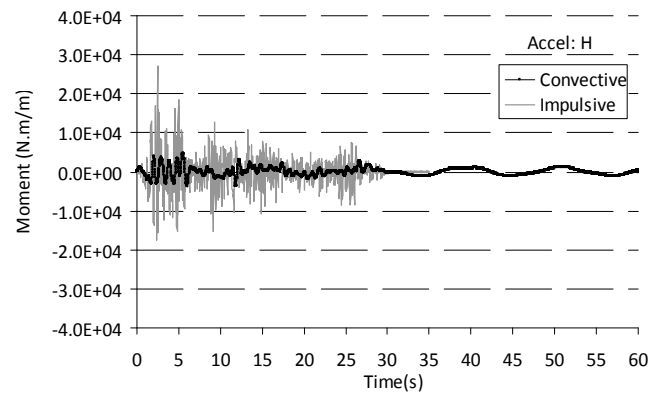
(b)
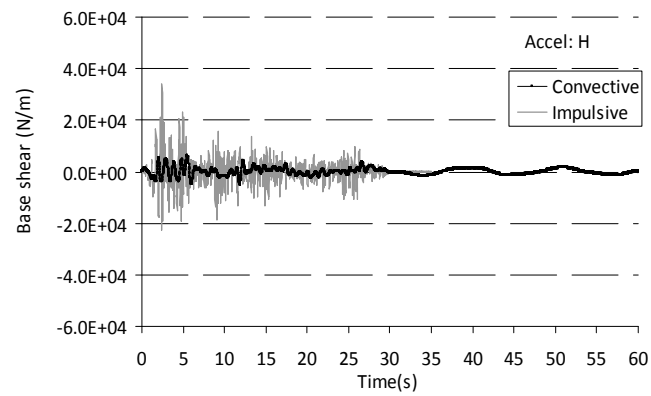
(c)

Figure 5.10 Time history response of the flexible "Shallow" tank due to horizontal

excitation; (a) Hoop force, (b) Moment, (c) Base shear
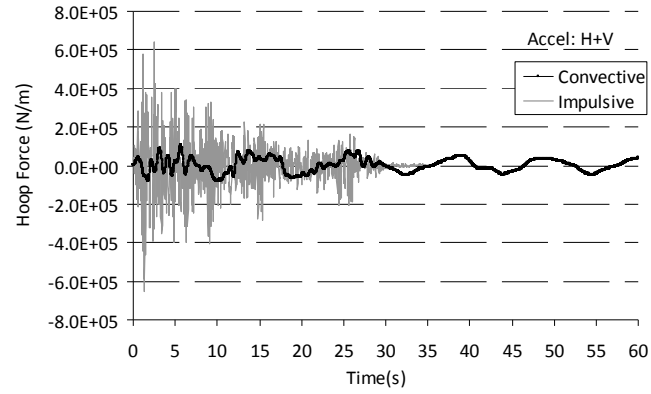
(a)
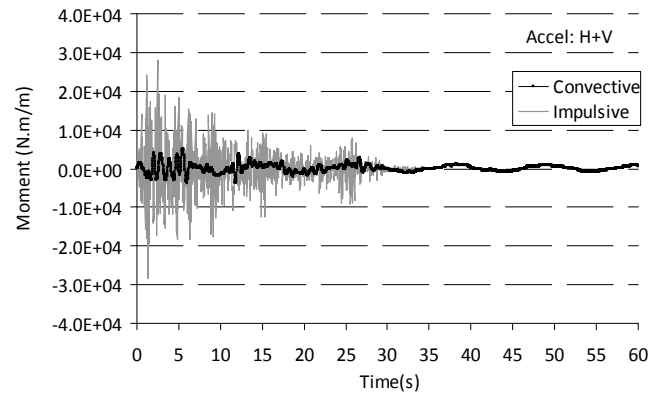
(b)
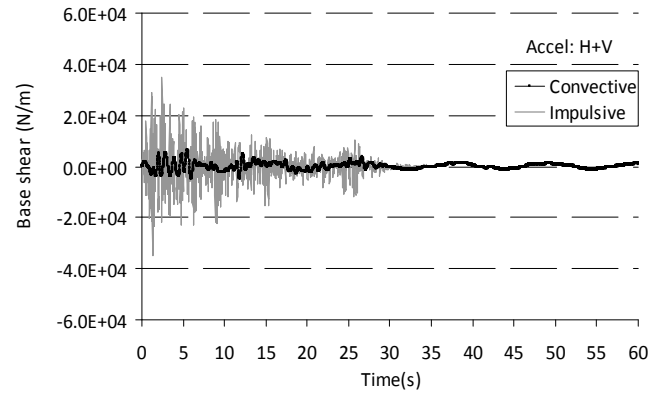
(c)

Figure 5.11 Time history response of the flexible "Shallow" tank due to combined

horizontal and vertical excitation; (a) Hoop force, (b) Moment, (c) Base shear

Considering the combined effect of horizontal and vertical excitations, it can be observed

from the table that the impulsive hoop force, moment, and base shear slightly increase by about

6, 4, and 3 percent, respectively. As compared to the impulsive response, the corresponding convective values increase somehow more drastically by about 7, 6, and 7 percent, respectively. Therefore, it can be concluded that the vertical ground acceleration has a stronger effect on the convective part of response than it has on the impulsive part. It is also found that the effect of vertical ground motion on overall seismic response of the "Shallow" tank model is insignificant.

As a result of vertical acceleration, the peak value of sloshing is increased from 243mm at t = 40.86 sec to 253mm at t = 5.78 sec which shows an increase of around 4 percent compared to the case of horizontal excitation alone. The time history variation of sloshing height is shown in Figure 5.12. Comparing the calculated sloshing height for the flexible tank with that of rigid tank, a reduction of around 2 percent is observed due to the effect of wall flexibility.
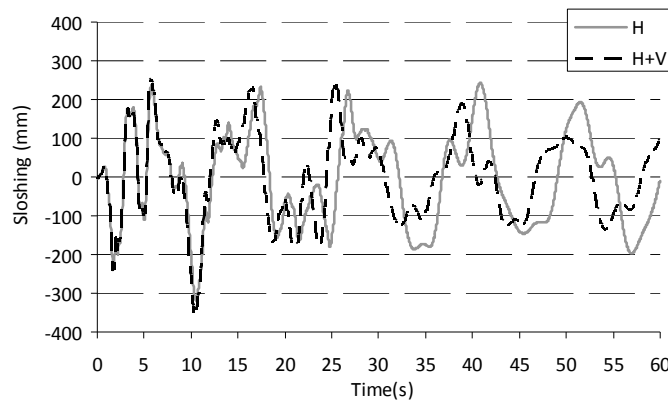
Figure 5.12 Sloshing height time history for flexible "Shallow" tank

The hydrodynamic pressure distribution over the height of the tank wall for both rigid and flexible tank models under horizontal excitation is shown in Figure 5.13. To examine the adequacy of current practice in estimating the hydrodynamic response of liquid-filled cylindrical tanks, the hydrodynamic pressure distribution recommended by ACI 350.3-06 is also indicated in

the figure. It is worth noting that the ACI hydrodynamic pressure values are calculated assuming $I = 1$ and $R = 1$, where I is the ''Importance factor'' and R is the ''Response modification coefficient''. For Code calculations, the design spectrum with a peak ground acceleration of 0.4g to correspond with the horizontal seismic excitation used in FE analyses is used. The mapped spectral accelerations (S_s and S_1) of 1.5 g and 0.6 g, respectively are selected for Imperial Valley location. Moreover, a site with hard rock soil which is categorized as site class "A" as per ASCE 7-05 is assumed in the Code calculations. In obtaining the results based on ACI 350.3-06, the damping ratios of 0.5% and 5% are assumed for convective and impulsive components, respectively.
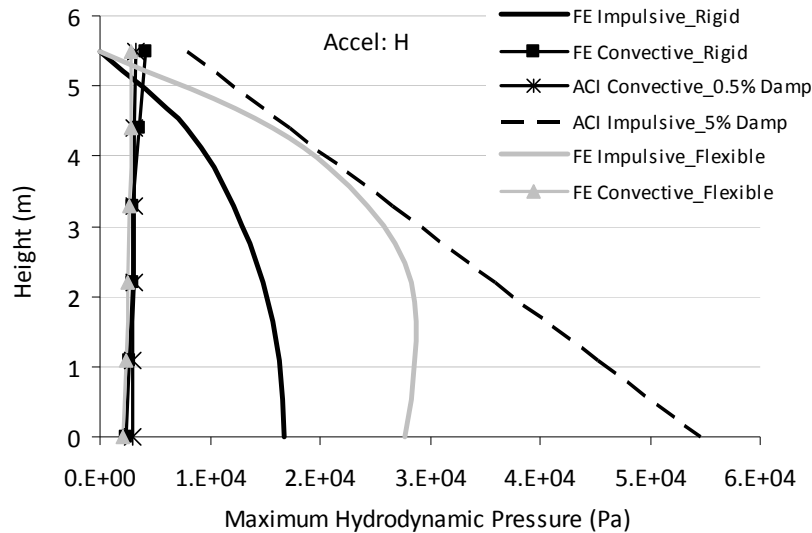
Figure 5.13 Hydrodynamic pressure distribution over the height of "Shallow" tank under horizontal excitation

As obvious from the figure, the impulsive pressure is highly amplified in the flexible tank compared to the rigid tank as a result of tank wall flexibility. However, the convective pressure

does not change significantly due to wall flexibility effect. The maximum impulsive pressure in flexible "Shallow" tank is about 1.7 times greater than that of rigid tank model.

ACI 350.3-06 standard does not distinguish between rigid and flexible wall boundary conditions and thus gives the same pressure distribution for both tanks. This is one of the significant deficiencies of current practice. As a result, ACI values are too conservative for tanks having rigid wall boundary condition. Moreover, because of the linear distribution function used in ACI for distributing the pressure over the tank wall, the values of ACI impulsive pressure are much higher than those of FE even for the case of flexible tank for the sections of the wall near the base. However, the convective pressure values suggested by ACI are in full agreement with those of FE.

In order to examine the pattern of horizontal hydrodynamic pressure distribution around the tank circumference, the hydrodynamic pressure values of the "Shallow" tank model at the water depth of 4.4 m ($z = 1.1m$) under pure horizontal and pure vertical excitations are calculated using both FE and ACI 350.3-06 and are shown in Figure 5.14.

Comparing the results, one can see that the pressure distributions are quite similar. As shown in the figure, under horizontal excitation the pressure distribution can be approximated as a cosine function applied symmetrically about ϕ=0 having outward direction on one half and inward direction on the other half. However, under pure vertical excitation the resulting hydrodynamic pressure has an axisymmetrical distribution around the tank circumference.

The maximum impulsive pressure under horizontal excitation occurs at ϕ=0. According to FE, for "Shallow" tank at the water depth of 4.4m the maximum absolute value of the impulsive pressure is 28.6 kPa, however ACI predicts the maximum pressure of 45.2 kPa.

Under pure vertical excitation, the uniform hydrodynamic pressure having the maximum value of 22.6 kPa is obtained from FE. ACI predicts a higher value of 28.9 kPa at this depth.

(a)

(b)
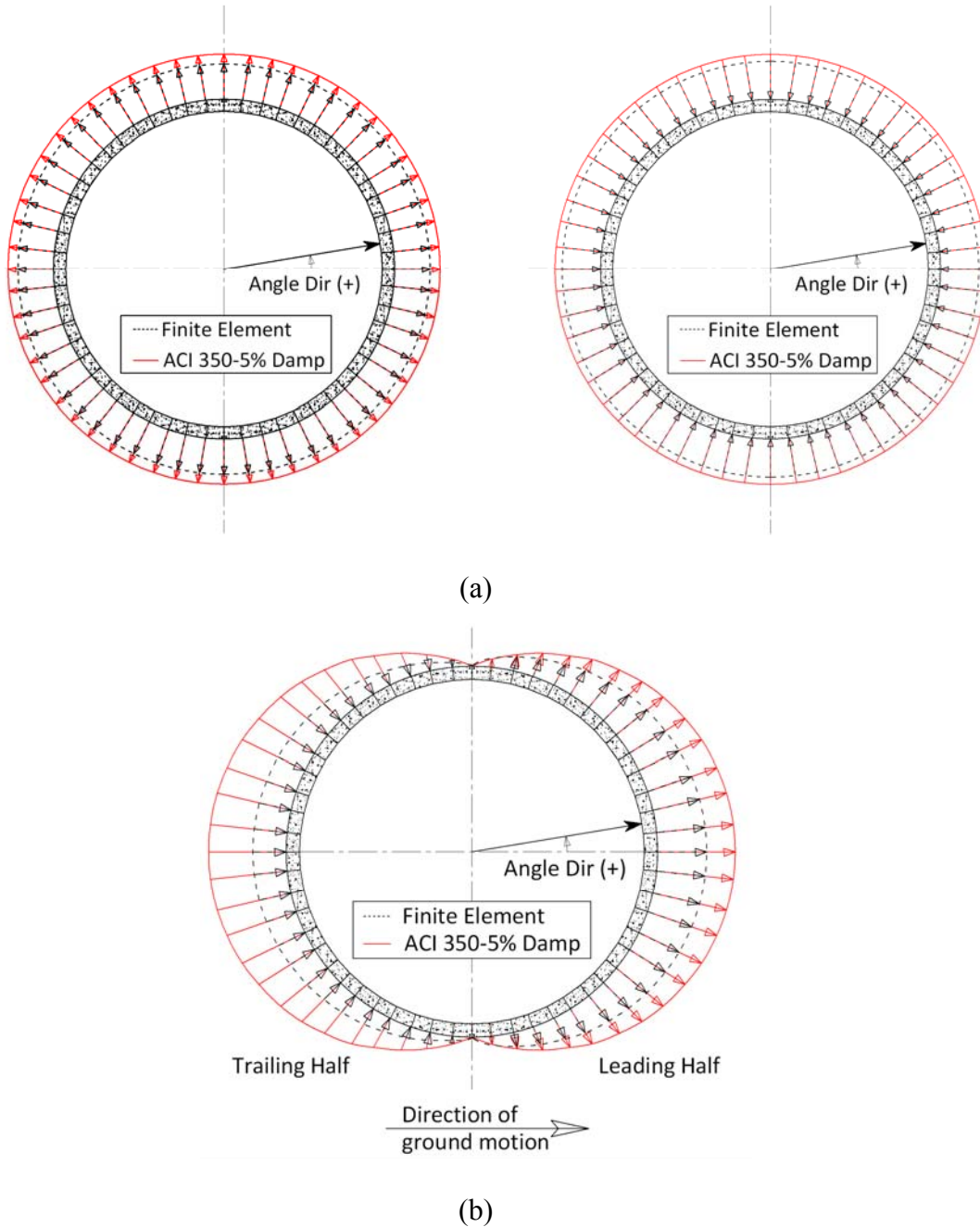
Figure 5.14 Horizontal hydrodynamic pressure distribution on "Shallow" tank at the water depth of 4.4 m ($z = 1.1m$); (a) Total pressure due to pure vertical excitation, (b) Impulsive pressure due to pure horizontal excitation

(b) Tall tank

Figures 5.15 and 5.16 indicate the transient structural responses for flexible "Tall" tank model.
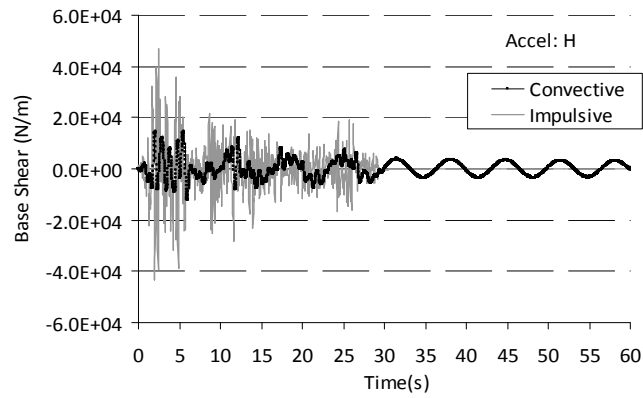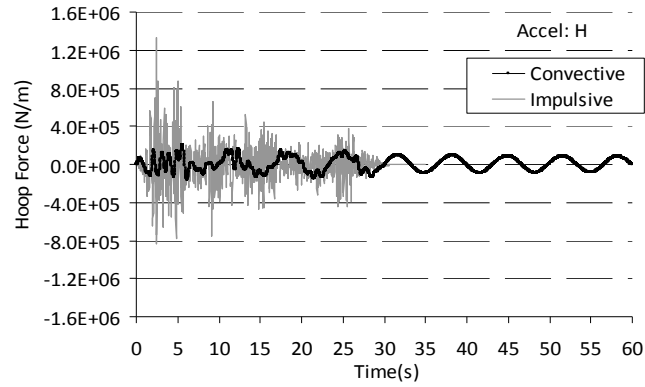

(a)
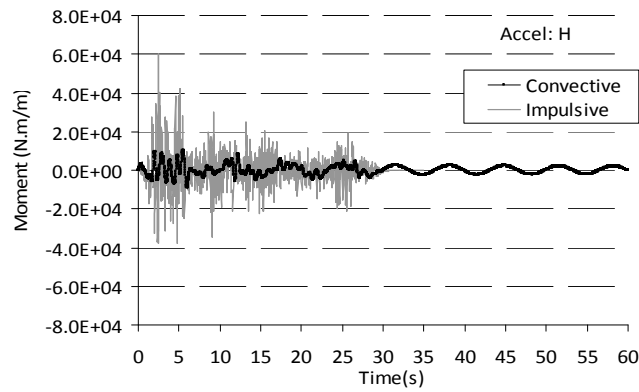
(b)
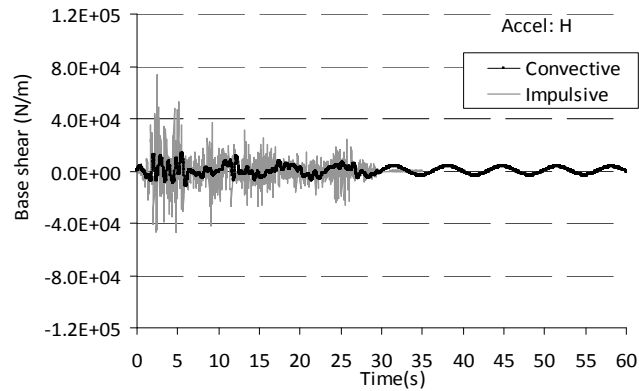
(c)

Figure 5.15 Time history response of the flexible "Tall" tank due to horizontal excitation;

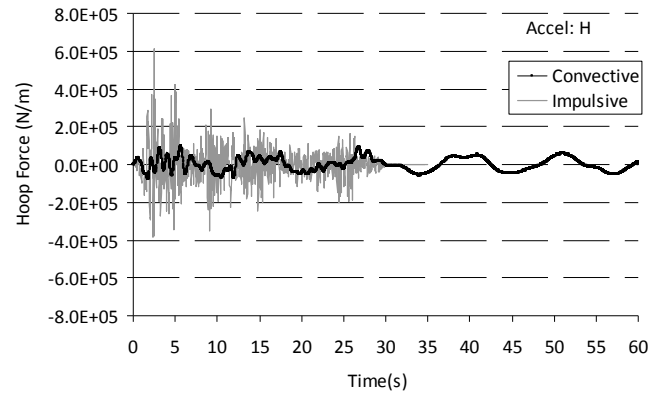(a) Hoop force, (b) Moment, (c) Base shear
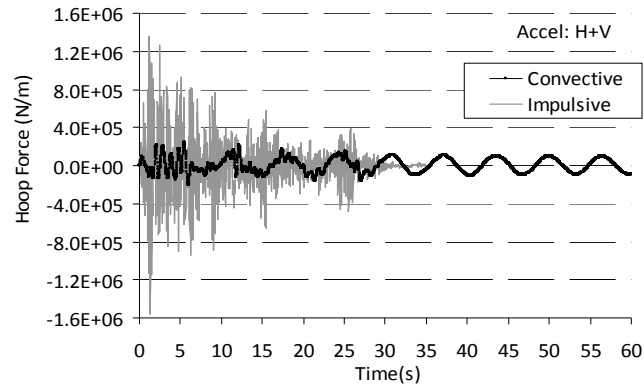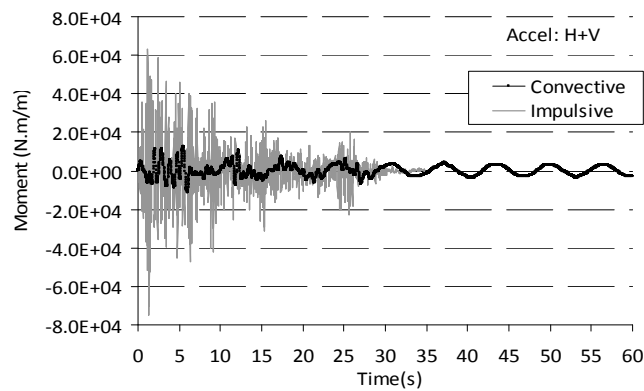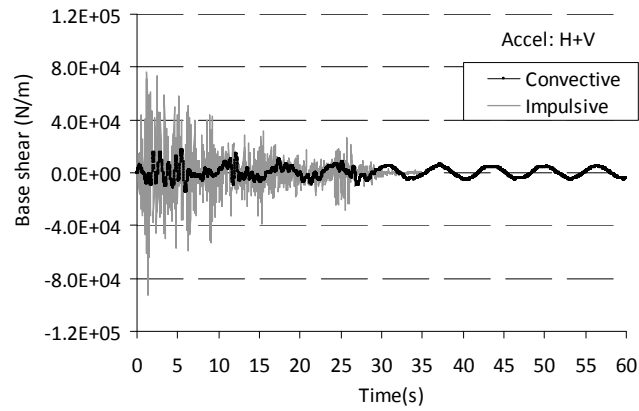
Figure 5.16 Time history response of the flexible "Tall" tank due to combined horizontal

and vertical excitation; (a) Hoop force, (b) Moment, (c) Base shear

As compared to the rigid tank, the maximum impulsive hoop force, moment, and base shear under horizontal acceleration are increased by 94, 69, and 55 percent to the values of 1331 kN/m, 60.3 kNm/m, and 73.1 kN/m, respectively. As a result of wall flexibility, the maximum convective hoop force, moment, and base shear are decreased negligibly by 5, 7, and 9 percent to the values of 201 kN/m, 10.1 kNm/m, and 13.1 kN/m, respectively. As was the case for "Shallow" tank, wall flexibility has a significant effect on the impulsive term of response while it has only a minor effect on the convective term.

Again, as obvious from the obtained time history response diagrams, including the effect of convective term may lead to either an increase or a decrease in overall hydrodynamic response of the tank-liquid system. This can be interpreted as the phase difference between the impulsive and convective components of response.

As presented in Table 5.2 due to vertical acceleration effects, the impulsive hoop force, moment, and base shear are increased by 17, 24, and 27 percent, respectively while the convective terms show comparatively greater increase than those relating to impulsive terms. Obtained results indicate the increase of about 19, 26, and 29 percent in the convective hoop force, moment, and base shear, respectively due to the combined effect of horizontal and vertical excitations as compared to the horizontal excitation alone. This shows that the vertical acceleration has a greater effect on the convective term than it has on the impulsive term. The same trend was observed for "Shallow" tank model. In addition, it is found that the vertical acceleration has a relatively stronger effect on "Tall" tank's impulsive and convective response than it has on "Shallow" tank's response. This trend is also observed for sloshing height response. That is, the increase in sloshing height as a result of vertical acceleration effect is higher in "Tall" tank than "Shallow" tank. Under the combined horizontal and vertical

excitations, the maximum sloshing height of 965 mm occurs at t = 30.74 sec which is about 8 percent higher than the peak sloshing response of 894 mm due to horizontal excitation occurring at t= 25.14 sec. Furthermore, similar to "Shallow" tank model, the wall flexibility has no major effect on sloshing height. The time history variation of sloshing height is shown in Figure 5.17.

Based on the obtained results, it is concluded that the effect of vertical earthquake component needs to be considered in seismic analysis of tall cylindrical tanks. However, it has less effect on the seismic response of shallow tanks.
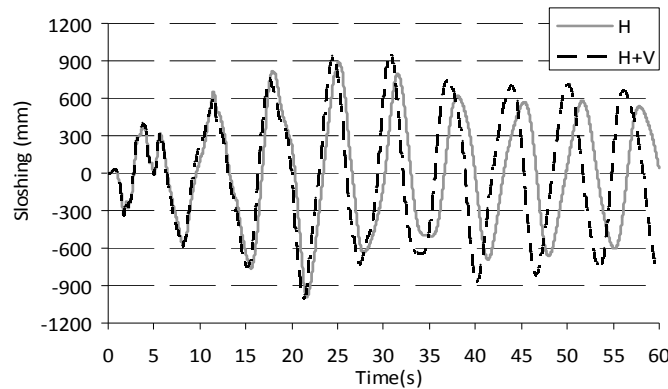
Figure 5.17 Sloshing height time history for flexible "Tall" tank

The hydrodynamic pressure distribution over the height of the tank wall for both rigid and flexible tank models under horizontal excitation is shown in Figure 5.18. It can be observed from Figure 5.18 that the impulsive pressure is highly amplified due to wall flexibility effect and its distribution is different from that of rigid tank. However, the effect of wall flexibility on the convective pressure is negligible. The same trend was observed for "Shallow" tank model. The maximum impulsive pressure in flexible "Tall" tank is about 1.8 times greater than that of rigid tank model. This maximum pressure occurs at the bottom of the tank ($z = 0$) for the rigid tank

while the point of peak impulsive pressure for the flexible tank is located at $z = 3m$ measured from the base of the tank.
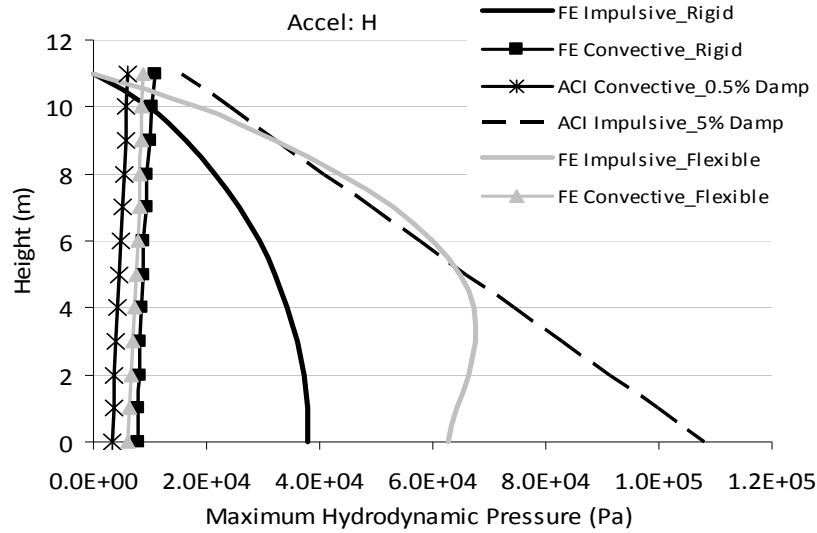
Figure 5.18 Hydrodynamic pressure distribution over the height of "Tall" tank under

horizontal excitation

Again, ACI prediction is too conservative for the tank with rigid wall. However, it gives a reasonable estimation of hydrodynamic pressure values for the flexible tank except at its base. The convective pressure values recommended by ACI are slightly smaller than those of FE analysis. However, since the overall response is dominated by the impulsive term rather than the convective term, the ACI total pressure values are still conservative and thus are suitable for design purposes.

In order to clearly show the effect of vertical acceleration on the dynamic response of the flexible cylindrical tanks, the impulsive hydrodynamic pressure distribution is calculated for the "Tall" tank model under pure horizontal, pure vertical, and combined horizontal and vertical excitations and the obtained results are compared to each other as shown in Figure 5.19.

113
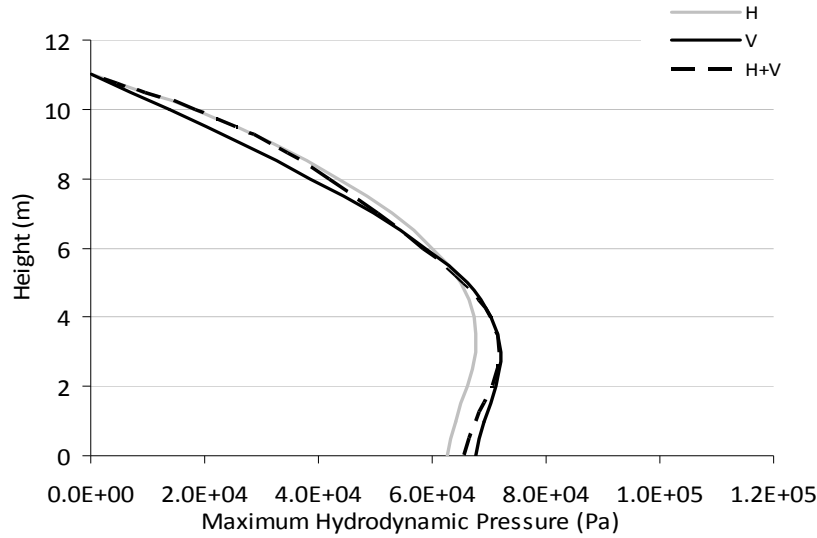
Figure 5.19 Impulsive pressure distribution along the height of the flexible "Tall" tank

It can be observed from the figure that the effect of vertical ground motion could be as high as that of the horizontal motion when considered separately, however this effect is of less significance when horizontal and vertical earthquake components are considered to be applied simultaneously to the structure. Similar trend is also observed in "Shallow" tank model.

The results obtained for "Shallow" and "Tall" tanks also show that very small convective response values are resulted due to pure vertical excitations. This has also been concluded by Haroun and Tayel (1985) who stated that little or no sloshing occurs due to transient vertical motions. Therefore, in obtaining the seismic response of cylindrical tanks to pure vertical random excitations, the effect of convective fluid motion (sloshing) can be neglected and as a result it can be assumed that the overall response of the tank-liquid system is fully dominated by the impulsive term.

5.6 Effect of base fixity

To investigate the effect of base fixity on the dynamic behavior of cylindrical tanks, models having different base conditions; fixed and hinged are subjected to both horizontal and vertical seismic excitations and their dynamic response is calculated. Analyses are performed on both "Shallow" and "Tall" tank models.

Figure 5.20 shows the envelope diagrams of hoop force, bending moment, and shear force along the height of the flexible "Shallow" tank due to horizontal excitation.

Comparing the structural response values given in Figure 5.20 for hinged and fixed tank models, it can be concluded that in general, higher maximum response values are found for tanks having hinged base compared to those having fixed base especially near the mid-height of the wall. However, this is not the case at the base. The maximum absolute values of the base shear and the base moment for the fixed tank are higher than those of the hinged tank. It should be noted that the value of moment at the base of the hinged tank and also hoop force value at the base of tanks having either fixed or hinged conditions is zero.

Under pure vertical and also the combined effect of horizontal and vertical excitations, the same trend as that presented here for pure horizontal excitation is observed. "Tall" tank model also shows a similar trend as "Shallow" tank as described here. For the sake of brevity, those results are not presented here.
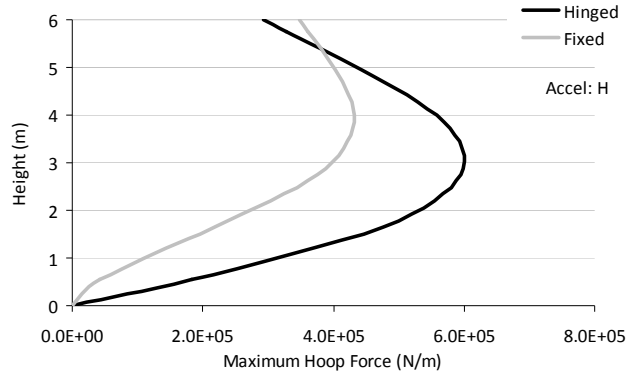
(a)
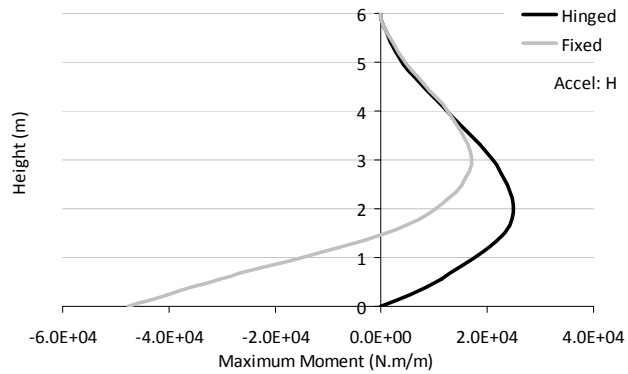
(b)
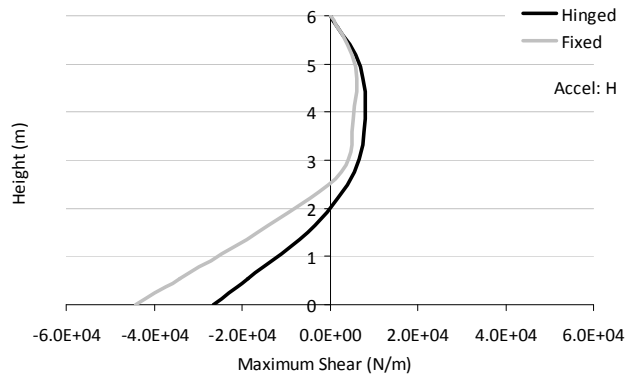
(c)

Figure 5.20 Envelope diagrams for flexible "Shallow" tank model due to horizontal

excitation; (a) Hoop force, (b) Moment, (c) Shear force

Figure 5.21 indicates the hydrodynamic pressure distribution over the height of flexible "Shallow" tank due to horizontal excitation for tanks having fixed and hinged base connections. The corresponding pressure distribution for flexible "Tall" tank model under horizontal

excitation is shown in Figure 5.22. Shown in the figures are also pressure values estimated by ACI 350.3-06 standard.
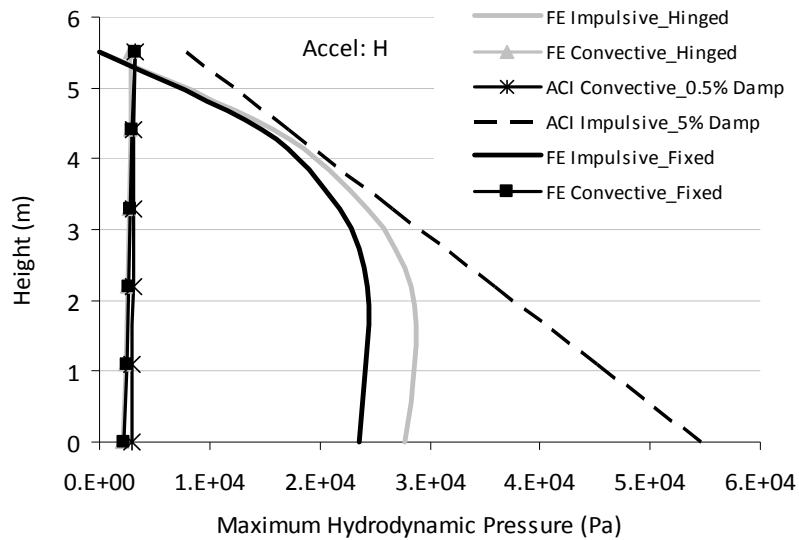
Figure 5.21 Hydrodynamic pressure distribution over the height of flexible "Shallow" tank under horizontal excitation
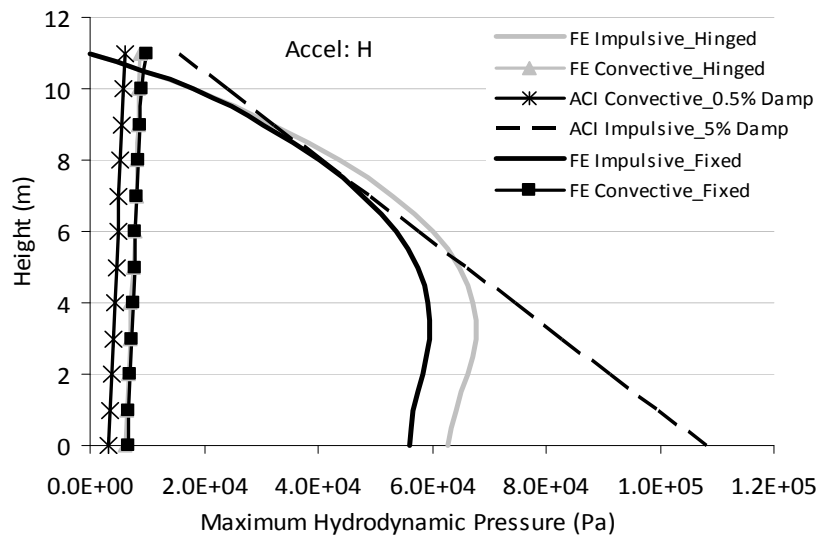
Figure 5.22 Hydrodynamic pressure distribution over the height of flexible "Tall" tank under horizontal excitation

As can be observed from the figures, ACI standard does not distinguish between hinged and fixed boundary conditions and gives the same pressure values for both cases. As indicated in Figure 5.21, ACI standard has overestimated the impulsive pressure at the base of the "Shallow" tank by around 134% for the fixed tank and 99% for the hinged tank. Based on the pressure graphs presented in Figure 5.22, it can be noticed that ACI standard has overestimated the impulsive pressure at the base of the "Tall" tank by around 93% for the fixed tank and 72% for the hinged tank.

Based on the obtained results, it can be concluded that in general higher impulsive pressure values are experienced in hinged tanks compared to the corresponding fixed tanks. However the convective pressure component is not noticeably affected by the base fixity condition. Tanks with different base fixities (hinged or fixed) have slightly different fundamental impulsive frequencies but almost the same convective natural frequencies. This is believed to be the reason for the slight change observed in the impulsive pressure but almost no change in the convective pressure. The obtained results also show that the sloshing height of the water free surface is also not affected by the type of connection at the base. A trend similar to that presented here is observed for the pure vertical as well as the combined horizontal and vertical excitations.

5.7 Summary

In this chapter, the dynamic behavior of cylindrical ground-supported tanks was investigated using FE method in a three dimensional space. Effects of a wide range of parameters such as; tank wall flexibility, vertical component of earthquake, sloshing of liquid free surface, tank aspect ratio, and base fixity on dynamic behavior of such structures were addressed. Both impulsive and convective components were considered in obtaining the results. Results were

calculated for two different aspect ratios, representative of shallow and tall tanks in order to investigate the effect of geometry on the dynamic response of the cylindrical containers. The tanks were assumed to be rigidly anchored to the rigid ground. In order to evaluate the accuracy of current practice, the obtained finite element results were compared with those recommended by the ACI 350.3-06 standard.

The validity of the proposed FE method in both free vibration and time history analyses of cylindrical containers was verified by comparing the calculated FE results with those obtained through analytical approaches available in the literature.

In the first part of the chapter, free vibration analysis was carried out on the rigid tank models. Effect of higher sloshing and impulsive modes and their associated effective mass ratios and mode shapes were investigated. The obtained results including the natural frequencies, and effective modal mass ratios compared very well with those calculated through analytical procedures introduced by Housner (1963) and Veletsos and Shivakumar (1997). It was observed that for practical purposes, only the fundamental impulsive and convective modes are sufficient for characterizing the dynamic response of such tanks to horizontal excitations.

The results also revealed that the $\cos(n\theta)$ type modes ($n > 1$) had a very small effect on the overall dynamic response of the tanks to horizontal excitations. Modes having the highest contributions to the response were cantilever beam type modes with $n = 1$.

In the second part of the chapter, time history analysis was performed on both rigid and flexible tanks having different types of connection at the base; fixed and hinged under both horizontal and vertical components of earthquake using the direct integration method. Appropriate damping ratios corresponding to water components were selected according to ACI 350.3-06. Making use of the proposed finite element method, studying the contribution of both

119

impulsive and convective components of response was made possible. The examined responses were sloshing height, hydrodynamic pressure and the associated structural forces including hoop force, moment, and shear force. The obtained FE results were also compared with those suggested by ACI 350.3-06 standard.

It was shown that the resulting convective forces have less effect on the overall dynamic response of the tanks as compared to the impulsive forces. As a result, the seismic behavior of the tanks was mainly dominated by the impulsive component rather than the convective component.

It was clearly seen that since the sloshing and impulsive components of the response did not reach their peak values at the same time, the effect of considering convective term on the total response might be either increasing or decreasing.

It was also observed that the effect of convective term on the overall dynamic response of liquid containers was rather more significant in shallow tanks compared to tall tanks.

Comparing the results obtained for rigid and flexible tanks revealed that including the wall flexibility resulted in a significant increase on the impulsive part of response and therefore, this effect should be taken into consideration in seismic design of the tanks. However, the convective part of response was found to be almost independent of the tank wall flexibility and instead, it seemed to be dependent on tank's geometrical properties, fluid properties, and ground motion characteristics. Furthermore, it was indicated that the sloshing height of the liquid inside the tanks was not significantly affected by the wall flexibility.

Considering the combined effect of horizontal and vertical excitations, it was shown that including the vertical acceleration effect led to an increase in both impulsive and convective terms of response for "Shallow" as well as "Tall" tank models. It was also observed that the

vertical ground acceleration had a greater effect on the convective component of response than it had on the impulsive component. The overall effect of vertical acceleration was found to be insignificant in "Shallow" tank model. The sloshing height also increased as a result of combined effect of vertical ground motion. It was found that the vertical acceleration had a relatively greater effect on the response of "Tall" tank as compared to the "Shallow" tank. Therefore, the effect of vertical ground motion needs to be taken into consideration appropriately in seismic analysis of tall cylindrical containers and it should not be ignored.

The obtained results also show that the pure vertical ground motion could cause dynamic effects as high as those of the horizontal motion when considered separately, however its effect is found to be of less importance when horizontal and vertical earthquake components are applied together.

It was also concluded that pure vertical transient excitations result in very negligible convective response values for both tank configurations considered. As a result, one can ignore the effect of convective component in determining the seismic response of cylindrical tanks under pure vertical transient motions.

It was indicated that ACI 350.3-06 standard does not appropriately account for the effects of wall flexibility and base fixity. That is, it gives the same hydrodynamic pressure values for rigid and flexible tanks as well as for hinged and fixed tanks. As a result, ACI estimations could be too conservative for the case of rigid tanks. This point needs further consideration in current liquid tank design codes and standards.

Based on the obtained results, one can conclude that in general Code provisions yield a conservative estimation of results, especially for the case of rigid tanks. This was observed for "Shallow" as well as "Tall" tanks. In addition, since the hydrodynamic pressure approximated by

the Code has a linear vertical distribution, the Code estimations of hydrodynamic pressure could be too conservative for the sections near the base.

Studying the dynamic behavior of tanks with different base fixity conditions revealed that generally larger structural response values were developed in the walls of a hinged tank as compared to a fixed tank far from the base. However, the maximum absolute values of the base shear and the base moment were higher in the case of a fixed tank compared to a hinged one. It was also shown that larger impulsive pressure values were exerted on the walls of a hinged tank compared to an analogous fixed tank. However, the base fixity condition had no significant effect on the convective pressure component. Sloshing height was also found to be insensitive to the type of connection at the base.

Results of this study show that the proposed FE procedure can be accurately employed in the transient analysis of cylindrical ground-supported tanks. Using this method, one can account for all aspects in fluid-structure interaction problems including wall flexibility, sloshing motion, damping properties of fluid domain, and the individual effects of impulsive and convective terms in a 3D space.

CHAPTER 6

DYNAMIC RESPONSE OF LIQUID-FILLED ELEVATED TANKS

6.1 Introduction

In this chapter, the dynamic behavior of conical elevated tanks is studied in a three dimensional space. The finite element technique is used to investigate the seismic response of liquid-filled elevated tanks supported on a concrete shaft. The accuracy of this method in analysis of ground-supported cylindrical tanks having different aspect ratios was verified in the previous chapter. This chapter is divided into two main parts.

The primary objective of the first part is to propose a finite element model in order to evaluate the performance of liquid-filled elevated tanks under seismic loading. Moreover, the adequacy of current code provisions in estimating the seismic response of elevated water tanks is studied. To this end, both time history and modal analyses are performed on an elevated tank. Using the proposed FE technique, impulsive and convective response components are obtained separately. Furthermore, the effect of tank wall flexibility and sloshing of the water free surface are accounted for in the FE analysis. The linear free surface boundary condition is used for simulating the sloshing behavior of the contained liquid. In this part of the chapter, also difficulties associated with modeling of the tanks having complex geometries such as conical elevated tanks are discussed.

The main focus of the second part is to investigate the effect of earthquake frequency content on the dynamic behavior of liquid-filled elevated tanks. To do so, a three-dimensional partially filled elevated tank is numerically simulated using FEM and its seismic behavior is analyzed under the effect of different ground motion excitations having different frequency

content characteristics. In order to investigate the effect of earthquake frequency content, four different earthquake records including El-Centro, Northridge, San-Francisco, and San-Fernando are used.

The FE method proposed in this study has some advantages compared to previous analytical research studies done on elevated tanks. One of the main features of the current method is in considering the effect of liquid damping properties and accounting for impulsive and convective terms separately. This has not been addressed previously. As a result, desired damping characteristics corresponding to the two components may be defined separately. In addition, the response of both components can be determined individually.

Furthermore, because of the inclination of the walls in conical elevated tanks, different boundary conditions from those acting on cylindrical tanks exist. For design purposes, usually the whole vessel is modeled as an equivalent cylindrical tank and thus the conical part of the vessel is ignored in modeling. However, using the rigorous technique presented in this study, one can accurately model the effect of fluid-structure interaction in tanks having complex geometries such as conical tanks. In this chapter, also practical instructions to conquer these simulation complexities are addressed.

Through this study, important factors such as the effects of tank wall flexibility, rocking as well as translational motions of the vessel, tank/pedestal interaction, and higher impulsive and convective modes are taken into account in FE modeling of the tanks. The proposed method is capable of accounting for all these effects simultaneously.

6.2 General dynamic behavior of conical elevated tanks

6.2.1 Validity study of current practice

In order to evaluate the validity of current practice in predicting the dynamic response of liquid-filled elevated tanks, the dynamic response of an elevated tank model is determined using both current practice and FE approaches. The obtained results are then compared to each other. Based on the obtained results, important conclusions regarding both the validity of current practice and the general dynamic behavior of such structures are drawn. The procedure employed by current practice for estimating the seismic response of liquid-filled tanks is explained in the next subsection.

6.2.1.1 Seismic design forces based on current practice

For design of elevated water tanks in North America, the ACI 350.3-06 standard in conjunction with ASCE 7-05 are used. These two standards are referred to as "current practice" in this chapter. According to current practice, the seismic base shear (V) is computed from the following equation:

$$V = CW_e \frac{I}{R} \tag{6-1}$$

where, C is the period-dependant seismic response coefficient for impulsive (C_i) or convective (C_c) term, and W_e is the effective weight of the system corresponding to impulsive or convective components which is adapted from Housner's method (Housner 1963). I is the importance factor and R is the response modification factor corresponding to impulsive or convective term. The related formulations for seismic response coefficients and other important information regarding the current practice procedure can be found in section 3.3 of the thesis.

Total base shear (V) and base moment (M) of the structure are determined by taking the square root of the sum of the squares (SRSS) of the impulsive and convective terms.

6.2.1.2 Finite element analysis

A liquid-filled elevated tank is modeled and FE analyses are conducted using 3D fluid elements. The calculated results through free vibration analysis, including natural periods of vibration and effective masses corresponding to each mode of vibration, are compared with those obtained from Housner's method (Housner 1963).

The equation of motion of the system can be solved by the direct integration method. However, since the response of the structure is assumed to be linear, the more efficient analysis using the concept of modal superposition by only including the contribution of significant natural modes is used.

The unidirectional horizontal seismic excitation is applied to the system and the corresponding instantaneous values of shear and moment at the base of the shaft are calculated. The study includes the coupling between the impulsive response of the liquid and the shell and also the sloshing effects.

According to ACI 371R-08 for each model, a sufficient number of modes (both impulsive and convective) to obtain a combined modal mass participation of at least 90% of the actual mass of the structure in the direction under consideration are employed.

The natural periods and associated mode shapes of the structure are computed by solving the eigenvalue problem (Chopra 2000). Using the concept of equivalent simple oscillators, the tank-pedestal system in i^{th} mode of vibration can be idealized with an equivalent single degree of freedom oscillator having an equivalent mass ($\overline{m}_i$), an equivalent height ($\overline{H}_i$), natural frequency

126

(ω_i), and damping ratio (ζ_i). Employing this technique, the equation of motion of the whole system can be converted to "i" independent differential equations corresponding to "i" equivalent single degree of freedom oscillators.

By equating the base shear and kinetic energy of the equivalent simple oscillator with those of the tank-pedestal system, the value of $\overline{m}_i$, known as the effective modal mass as described in most references on structural dynamics can be obtained.

The equivalent height ($\overline{H}_i$) corresponding to each mode is computed as the ratio of base moment reaction (My) obtained by integrating over the vertical reactions (Fz) multiplied by their associated arms (measured from the axis of symmetry at the shaft base) to the base horizontal reaction (Fx).

Having obtained the values of the equivalent mass ($\overline{m}_i$) and the equivalent height ($\overline{H}_i$) corresponding to each mode, one can find the instantaneous base shear and base moment contributed from i^{th} mode as follows:

$$Q_i(t) = \overline{m}_i \ddot{u}_i^t(t) \tag{6-2}$$

$$M_i(t) = \overline{m}_i \overline{H}_i \ddot{u}_i^t(t) \tag{6-3}$$

where, $\ddot{u}_i^t(t)$ is the total acceleration of the equivalent simple oscillator subjected to the known ground acceleration ($\ddot{u}_0(t)$).

The maximum numerical value of $\ddot{u}_i^t(t)$ may be obtained from the pseudo-acceleration response spectrum for the prescribed seismic motion ($\ddot{u}_0(t)$) using the natural frequency (ω_i) and the associated damping ratio (ζ_i) corresponding to the ith mode.

Finally, the total base shear and base moment of the tank-pedestal system can be computed by simply adding the time history values of modal base shears and base moments obtained from equations (6-2) and (6-3) for sufficient number of modes.

Using this technique, base shear and base moment values corresponding to impulsive and convective components of response can be determined separately. The adequacy of current practice in estimating the seismically induced forces in elevated water tanks can be examined by comparing the results from FEM explained here with those provided by the Code.

6.2.2 Numerical model verification

To further verify the current FE technique, the free vibration response of a small-scale aluminum conical tank is obtained using the current FE technique and the results are compared with the experimental values obtained by El Damatty et al. (2005).

In his study, El Damatty has conducted shake table testing as well as numerical analysis to determine the dynamic properties of a conical tank specimen. The geometry and corresponding finite element model used in the current study is indicated in Figure 6.1. Aluminum shell is modeled as linear elastic material with the following properties:

Young's modulus = 69 GPa

Poisson's ratio = 0.33

Density = 2700 kg/m^3

Only displacement degrees of freedom are restrained for nodes located at the base. As a result, the rotations are free to happen at the base nodes. The natural frequencies and effective masses corresponding to both sloshing and liquid-shell vibration modes are obtained using current FE technique and the results are summarized in Table 6.1.
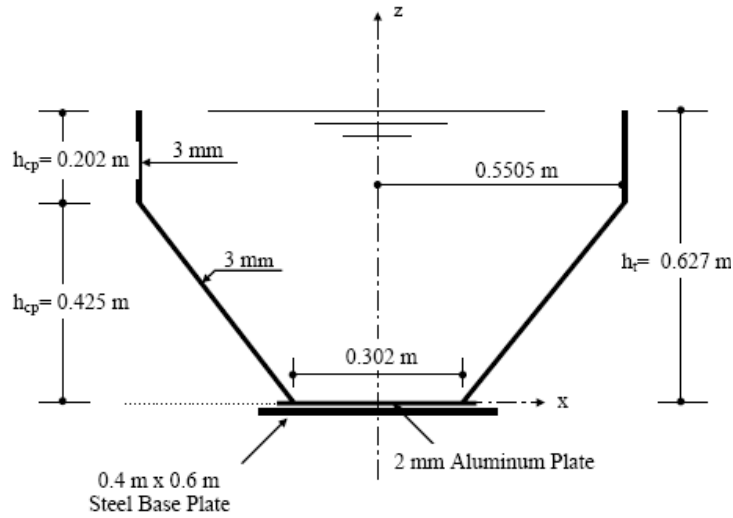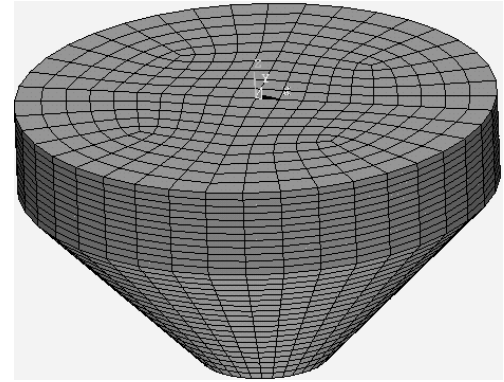
(a)   (b)

Figure 6.1 Geometry of the conical tank model;

(a) Side view, adapted from El Damatty et al. (2005),

(b) Finite Element model used in current study

Table 6.1 Free vibration analysis results for the conical tank model

Mode type	El Damatty et al. (2005)		Current study	
	Frequency (Hz)	R_i (%)	Frequency (Hz)	R_i (%)
Fundamental convective	0.82	58.0	0.84	56.6
First liquid-shell mode	15.60	Negligible	15.11	Negligible
Second liquid-shell mode	18.40		17.97	
First cosθ mode	43.50	40.7	42.36	41.5

In the table, R_i is defined as the ratio of the effective modal mass in the direction under consideration to the total mass of the water. As shown in Table 6.1 the obtained FE results are in excellent agreement with experimental results verifying that the current method can be employed with high accuracy to study the fluid-structure interaction problems of conical liquid containers.

Mode shapes corresponding to the modes listed in Table 6.1 are shown in Figure 6.2. As it is obvious from this figure, the first liquid-shell mode of the considered tank is governed by a $\cos3\theta$ mode while the second liquid-shell mode is dominated by $\cos2\theta$ harmonics. This was also stated by El Damatty et al. (2005).

As presented in Table 6.1, the effective masses corresponding to the $\cos n\theta$ (n > 1) modes are nearly zero. As a result, in determining the impulsive response of such structures, only the effects of $\cos\theta$ modes in which the tank's cross section remains circular need to be considered. These modes are believed to be responsible for the development of base shear and base moment.

To provide further validation of results calculated from FE simulation, the meridional variations of the first two liquid-shell modes evaluated experimentally are plotted in Figure 6.3 and are compared with those obtained from the current study. The plotted drifts are in a radial direction. It can be observed from the figure that there is a significant change in the mode shape pattern between the conical and cylindrical portions of the tank.

It can be observed from the figure that there is an excellent agreement between the results of this study and those reported by El Damatty et al. (2005). Therefore, the same FE technique is employed to study the behavior of liquid-filled conical elevated tanks in this study.
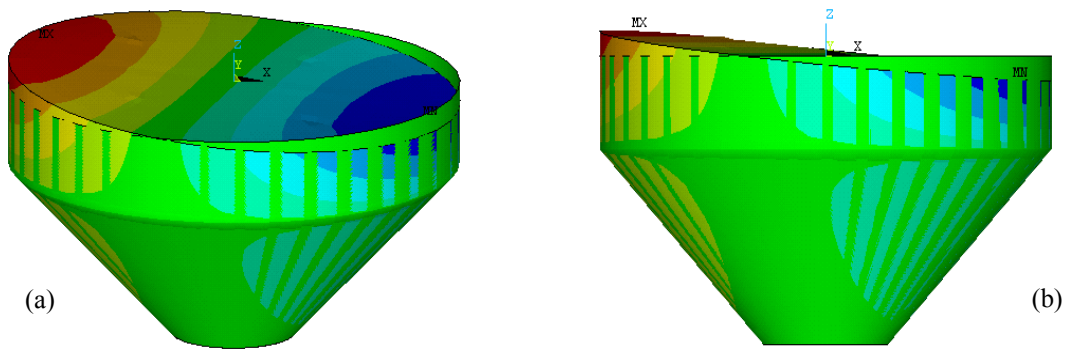
Fundamental convective mode: (a) 3D view, (b) side view
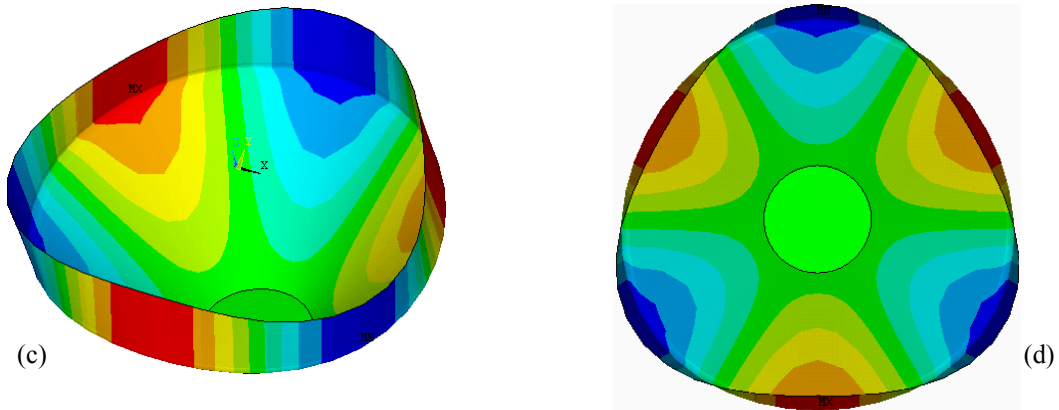
First liquid-shell mode: (c) 3D view, (d) plan view
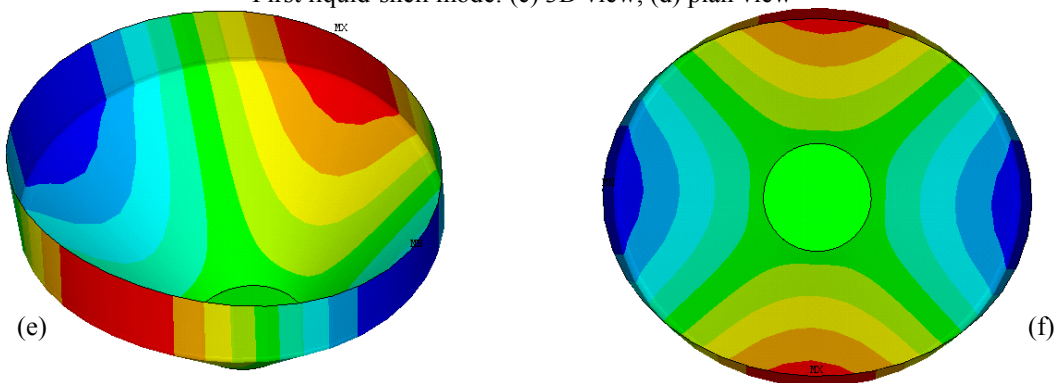
Second liquid-shell mode: (e) 3D view, (f) plan view
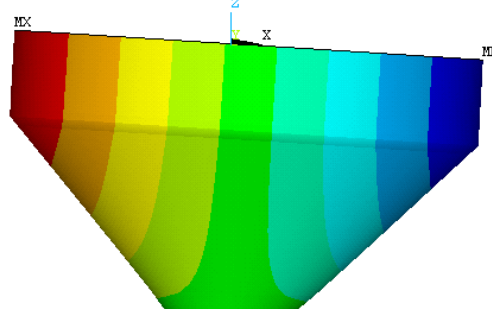
First cosθ mode - side view

Figure 6.2 Conical tank mode shapes

(a) First liquid-shell mode

(b) Second liquid-shell mode
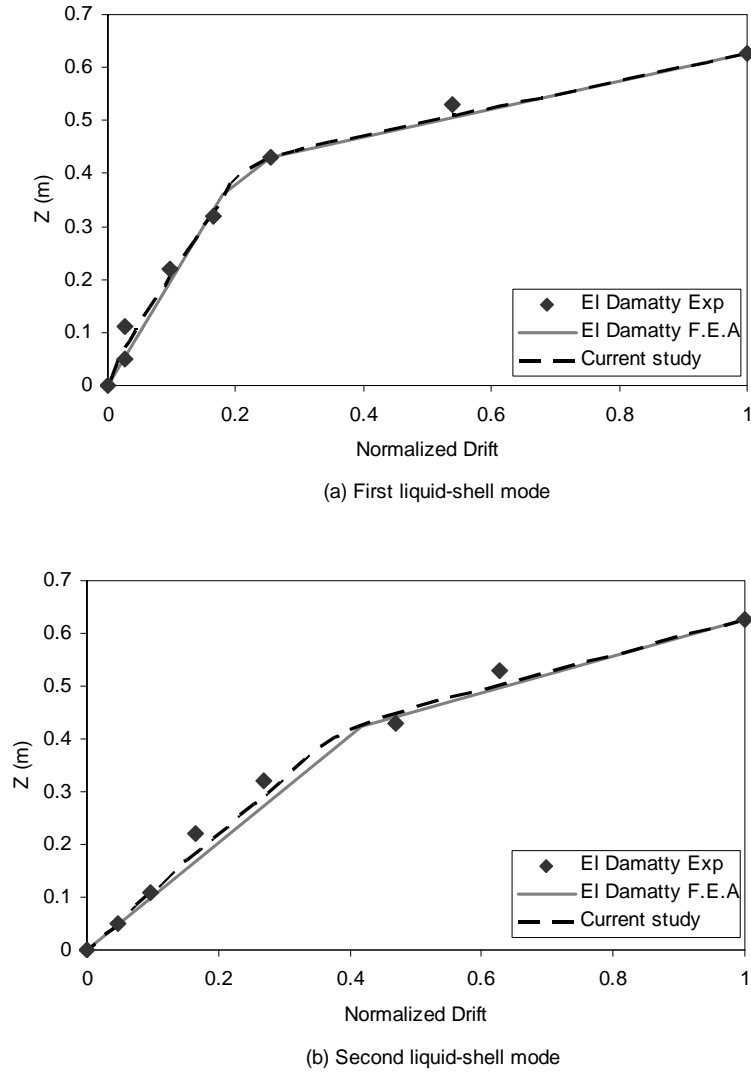
Figure 6.3 Meridional variation of the first two liquid-shell modes

6.2.3 Elevated tank model

In practice both hinged and fixed base connections are used for elevated tanks based on the type of foundation used to support the pedestal. In this study, the tank is assumed to have the hinged boundary condition at the base of the shaft.

Effects of the tank wall flexibility and sloshing of the water are taken into account. The particular tank configuration considered is that of an actual storage tank located in the U.S. with

the full capacity of 7571 m^3 (2 MG). The simplified geometry of the tank is indicated in Figure 6.4. As shown in the figure, the actual tank's floor is a concrete dome. However, because of element shape irregularities occurring during mesh generation of fluid domain located inside the conical portion of the vessel, the floor is modeled as a flat shell.

The effects of such simplification were investigated in this study and it was found to have little effect on the total response. The fundamental mode shapes (both impulsive and convective) of the tank are not generally influenced by the shape of the tank's floor. The properties of the fundamental impulsive mode are mainly dependent on the geometry and stiffness properties of the supporting shaft. In comparison, the fundamental convective mode is mainly affected by the geometry (aspect ratio) of the top cylinder and to a lesser extent by the geometry of the conical portion of the vessel. As a result, such an assumption could only result in a slight increase in the height of the contained water and as a result a slight reduction in the convective mass ratio (W_C/W_L). Furthermore, since the total response is mainly dominated by the impulsive component, the effect of such an assumption on the total response of the model will be negligible.

Other geometric properties not given in Figure 6.4 are as follows:

side shell thickness: 8.8 mm

cone thickness: 24.5 mm

tank floor thickness: 330 mm

shaft thickness: 380 mm
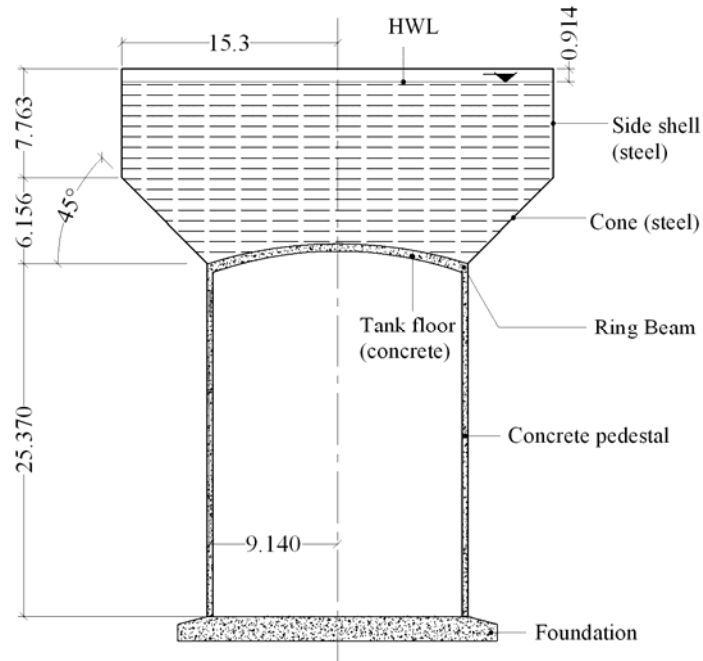
Figure 6.4 Elevated tank geometry

The equivalent weight of platforms inside the shaft with their full live load is accounted for by adding a distributed mass (total mass 715×10^3 kg) applied at 15.6 m above the base. Moreover, a mass balance of 438×10^3 kg corresponding to the weight of the components (e.g. roof, access tube, etc.) is applied around the ring beam as a distributed mass.

The density of water used is 1000 kg/m^3. Concrete and steel elements are modeled as linear elastic material. The following material properties are assumed for the steel and concrete shells:

Steel material:
Young's modulus= 200 GPa
Poisson's ratio= 0.30
Density= 7898 kg/m^3

Concrete material:
Young's modulus= 24.86 GPa
Poisson's ratio= 0.16
Density= 2400 kg/m^3

A total of 16464 fluid elements along with 2996 shell elements are used for modeling the tank. In meshing fluid and shell domains, the nodes of fluid elements located on the interface

134

must be coincident with those of the surrounding shell elements. Then, coupling should be defined between these coincident nodes such that equal displacements could occur in the radial direction. There is no need to define coupling in any other direction. Therefore, tangential relative displacements should be allowed to happen.

Coupling should be defined between the coincident nodes of fluid and structural domains at all interfaces. Therefore, nodes of fluid domain located at the interface with the tank's floor should also be coupled with those of floor elements.

To couple the nodes located at the conical portion of the vessel, first the radial coordinates (in the cylindrical coordinate system) of the fluid-shell nodes located along the cone interface should be rotated by the cone angle ensuring that all nodes are aligned perpendicular to the cone shell. Then, the rotated nodes can be coupled in the direction normal to the surface.

The conical section of the vessel has one interface with the cylindrical side shell at the top and one with the concrete floor at the bottom. In order to define the liquid domain boundary condition correctly, shell nodes located along these two boundary lines should be coupled to the corresponding fluid nodes in two orthogonal directions. This is performed by introducing a new coordinate system at these locations.

In the finite element idealization, the fluid domain is modeled using eight-node brick fluid elements as described previously and the tank's wall is modeled using four-node quadrilateral shell elements. The element has six degrees of freedom (translations and rotations) at each node and both bending and membrane behaviors are permitted. The finite element configuration of the elevated tank model is indicated in Figure 6.5.
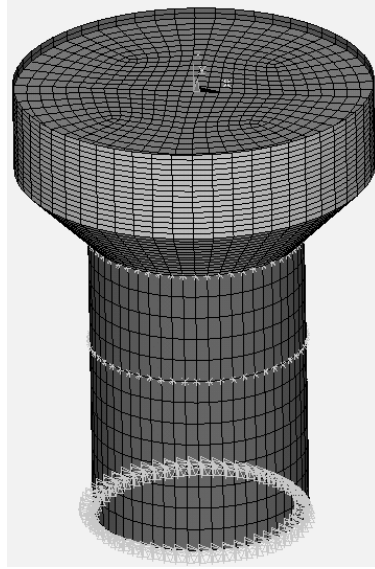
Figure 6.5 FE idealization for the elevated tank model

6.2.4 Results of analysis

6.2.4.1 Free vibration analysis

In this study, free vibration as well as time history analyses are carried out on the three-dimensional elevated tank model. The results of modal analysis are summarized in Table 6.2. The natural frequencies and modal response values are shown for the impulsive and convective modes with the highest participation factors among all modes of vibration. The fundamental sloshing and impulsive modes are identified as those with the largest participation factors (β) in the horizontal X direction.

Given in the table is also the ratio (R_i) of the effective modal mass in X direction to the total mass of the system. The modal participation factors normalized with respect to their largest values are also included in the table. As can be observed from the table, the participation factors corresponding to the fundamental modes are much greater than those of other modes. This

indicates that the response of the system is dominated by the fundamental modes under horizontal excitations.

Included in the table are also water mass ratios and fundamental sloshing frequencies obtained through Housner's method (Housner 1963) assuming vessels to be rigid. To use Housner's formulae, the equivalent cylindrical model of the tank under consideration should be determined. As recommended by some references available in the literature (ACI 371R-08 (2008), and Joshi (2000)), a close approximation for impulsive and convective masses of axisymmetric tanks, other than cylindrical, may be obtained from an equivalent cylindrical tank having the same free surface diameter and an equivalent water depth that results in an equal volume of water for both the original and the equivalent tanks. Using the Housner's formula (Housner 1963), the convective and impulsive mass ratios of 56% and 40.4 % are obtained, respectively.

Table 6.2 Free vibration analysis results for the elevated tank model

Mode		Frequency(Hz)		Effective mass $\times 10^3$ kg (FE)	$\sum R_i$ (%)		β (normalized)
Number	type	FE	Code		FE	Code	
*1	Convective	0.161	0.160	4302.51	58.7	56	1.00
2	Convective	0.161	0.160	235.38	58.7	56	0.23
3	Convective	0.294	NA	141.63			0.18
1	Impulsive	1.955	2.980	918.36	41.3	40.4	0.46
*2	Impulsive	1.955	2.980	3367.52	41.3	40.4	0.88
3	Impulsive	7.470	NA	228.14			0.23
4	Impulsive	7.470	NA	561.35			0.36
5	Impulsive	8.560		308.23			0.15

* Fundamental mode

In the Housner's method, the shell is assumed to be massless and only the mass of water is considered in derivation of equations. Therefore, in order for the finite element results to be comparable with those obtained from the Code (which is based on the Housner's formula), only the water mass contribution is considered in computing R_i, which is listed under the "FE" column.

However, in determining the effective masses listed in the table, the contribution of both fluid and shell element masses are taken into account. Since no shell deflection is observed during the sloshing modes vibration, the entire effective mass obtained from FE contributes from the sloshing liquid and not the non-moving shell. As a result, the convective mass ratio defined as $\sum R_i = \dfrac{\sum W_C}{W_L} = 58.7\%$ is obtained, where $\sum W_C$ is the summation of the modal effective masses corresponding to all sloshing modes and W_L is the total equivalent weight of the stored water. The rest of the liquid mass, i.e. 41.3%, behaves under impulsive modes.

Modes with exactly similar natural frequencies represent the same mode in two orthogonal directions (X and Y). Each of these modes is deviated from X or Y axis by a small angle. The effective masses are given as their projections on X axis.

As shown, the finite element results are in reasonable agreement with those calculated from the Code using the concept of equivalent cylinder model, especially in terms of computed natural frequencies. The difference in the convective mass values is less than 3 percent of the total mass of the fluid. This difference is even smaller for the impulsive masses (less than 1 percent). These findings are in agreement with those reported by Joshi (2000) who stated that for conical (Intze) tanks with the equivalent depth to radius ratios between 0.5 and 1.0 (which is the case here), the maximum errors for the impulsive and convective masses are less than around 5 and 6 percent of

the total liquid mass, respectively. The equivalent depth to radius ratio for the model considered in this study is 0.71.

From the results given in Table 6.2, one can conclude that both impulsive and sloshing behaviors of the considered model are practically dominated by its fundamental modes.

The modes given in Table 6.2 include about 93% of the total mass of the system. This accumulated effective mass ratio is more than the minimum criterion recommended by current practice.

As mentioned before, modes having the same natural frequencies are similar modes but in two orthogonal directions. As a result, the mode shapes and other modal properties remain the same for the first two convective and the first two impulsive modes.

All three sloshing modes given in Table 6.2 are associated with vertical water surface displacements which are antisymmetric about the axis of rotation and change in the circumferential direction as a cosine function. No shell vibration is observed during the animation of these sloshing modes. This is in accordance with the well-known assumption of decoupling the sloshing and the shell motions in liquid-containing structures.

All the impulsive modes presented in Table 6.2 are translational modes. These modes can be classified as the $\cos\theta$-type modes during which the tank's cross-section remains circular. During the first two impulsive modes, the entire tank behaves like a vertical beam.

For higher impulsive modes (modes 3 to 5), the top cylinder of the vessel experiences more pronounced deformation compared to the conical portion. This is partly due to the higher stiffness attributes associated with the conical part compared to the cylindrical part which is in turn because of the thicker shell assigned to the conical part as well as the geometric stiffening effect. The other important factor is that a larger fluid mass per unit height is located at the top

139

portion of the tank compared to the conical section. The top cylinder can be considered as a broad tank with the aspect ratio of H/D = 0.25. Therefore, as is the case for shallow tanks, their mode shape is characterized by a bulge near the mid-height of the cylinder. This is observed in the top cylinder for all higher impulsive mode shapes (modes 3 to 5).

Furthermore, the obtained mode shapes show a drastic change in the mode shape pattern between the conical and the cylindrical portions of the tank in modes 3 to 5. As explained before, this is due to a sudden change in stiffness and geometry at the cone/cylinder interface. This abrupt change results in high localized deformations along the cone/cylinder interface.

For illustration purposes, the convective and impulsive mode shapes are shown in Figures 6.6 and 6.7, respectively. In the next section, the seismic behavior of the elevated tank model is further investigated by performing time history analysis on the model.

(a) side view   (b) 3D view

Fundamental convective mode (Mode 1)

Higher convective mode (Mode 3)
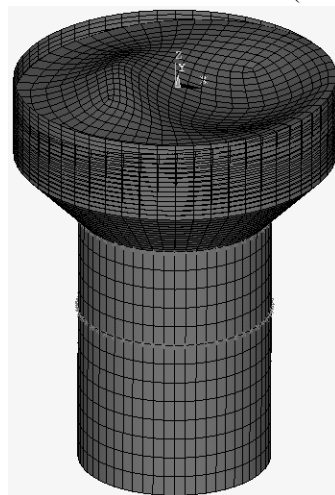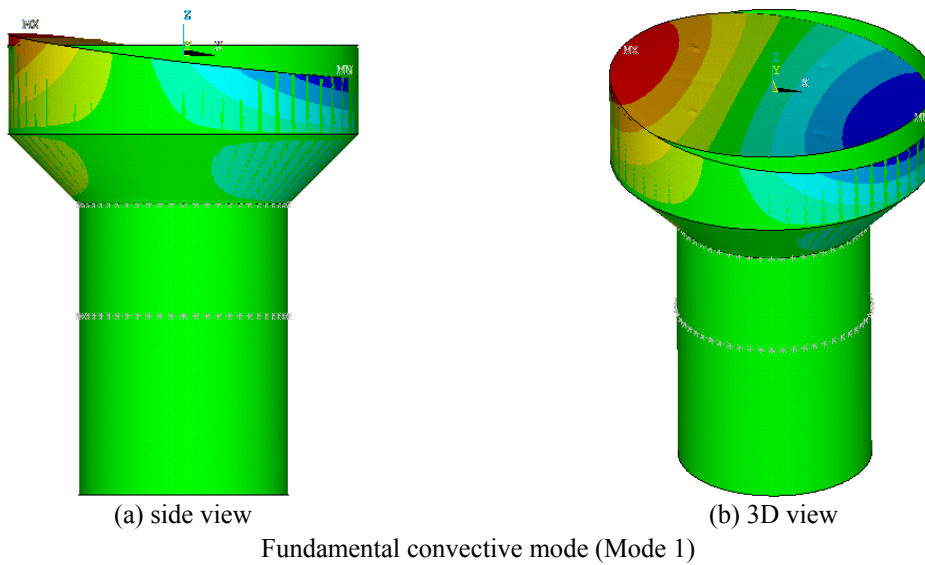
Figure 6.6. Elevated tank mode shapes (convective modes)
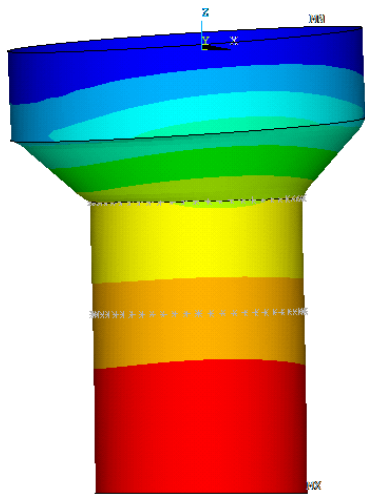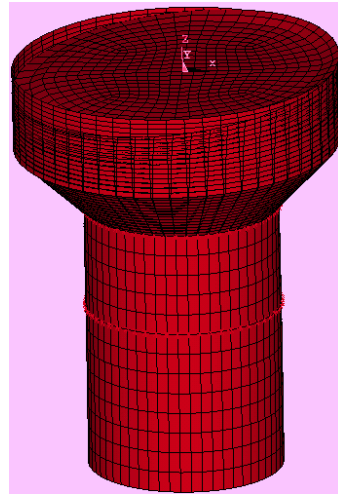
(a) side view   (b) 3D view

Fundamental impulsive mode (Mode 2)
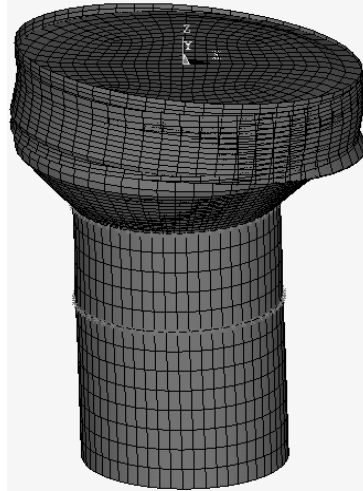
Higher impulsive mode (Mode 4)
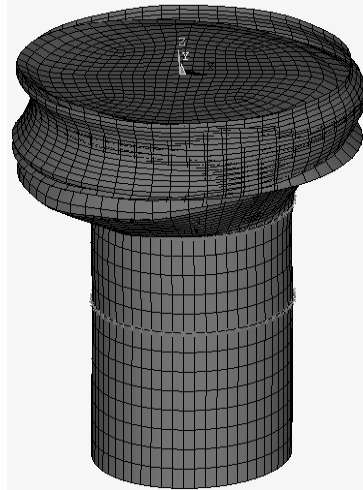
Higher impulsive mode (Mode 5)

Figure 6.7. Elevated tank mode shapes (impulsive modes)

142

6.2.4.2 Time history analysis

The horizontal component of 1940 El-Centro ground motion with the peak ground acceleration of 0.32g as shown in Figure 6.8 is used for time history analysis. Earthquake duration is around 31 seconds with its peak value occurring at 2.02 second. Since the sloshing component of motion continues long after the earthquake ceases and moreover, the maximum sloshing response generally occurs at a later time than that of impulsive response, the ground motion is continued beyond the duration of earthquake and for up to 60 seconds at zero acceleration allowing for the sloshing response to be fully developed.

An integration time step of 0.005 second is used to be small enough to characterize the response. Damping is assigned as a constant damping ratio to each mode considered for modal superposition analysis separately. The damping ratios of 5 and 0.5 percent are used for impulsive and sloshing modes, respectively.

As explained before, a sufficient number of modes are used so that the ratio of the accumulated effective mass to the total mass of the system ($\sum R_i$) reaches at least 90%. Consequently, a total of eight modes (three convective and five impulsive modes) as presented in Table 6.2 are used for time history analysis of the elevated tank model.

For quantitative comparison of the seismic response of the considered model under random ground excitation, the time history values of base shear (V) and base moment (M) of the model subjected to El-Centro earthquake are obtained using the modal superposition technique. The modes listed in Table 6.2 are used to carry out such an analysis.

Time history results have been separated into the impulsive and convective components. Therefore, the maximum response values associated with each component (impulsive or convective) and the instants at which these maxima occur may be determined separately.
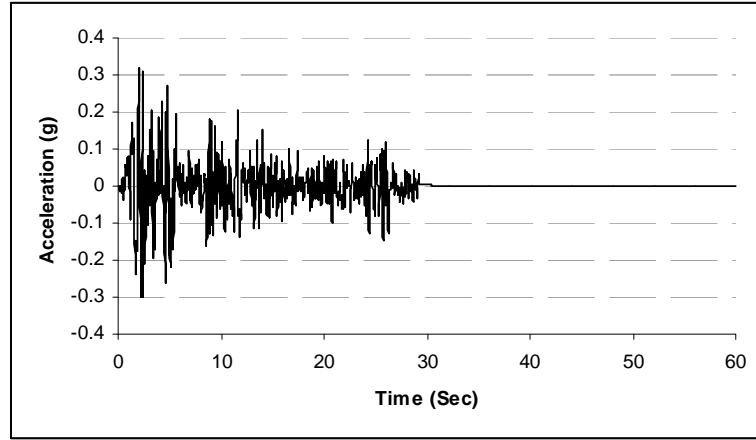
Figure 6.8 1940 El-Centro ground motion, horizontal component (PGA=0.32g)

Figure 6.9 illustrates the time history results for the elevated tank model. The maximum absolute response values computed from the FE analysis are listed in Table 6.3. The maximum absolute response values normalized with respect to the total effective weight of the system (We) are also included in the table. The total effective weight is computed as the sum of the effective masses corresponding to the modes considered for the model (see Table 6.2) multiplied by the acceleration due to gravity (g).
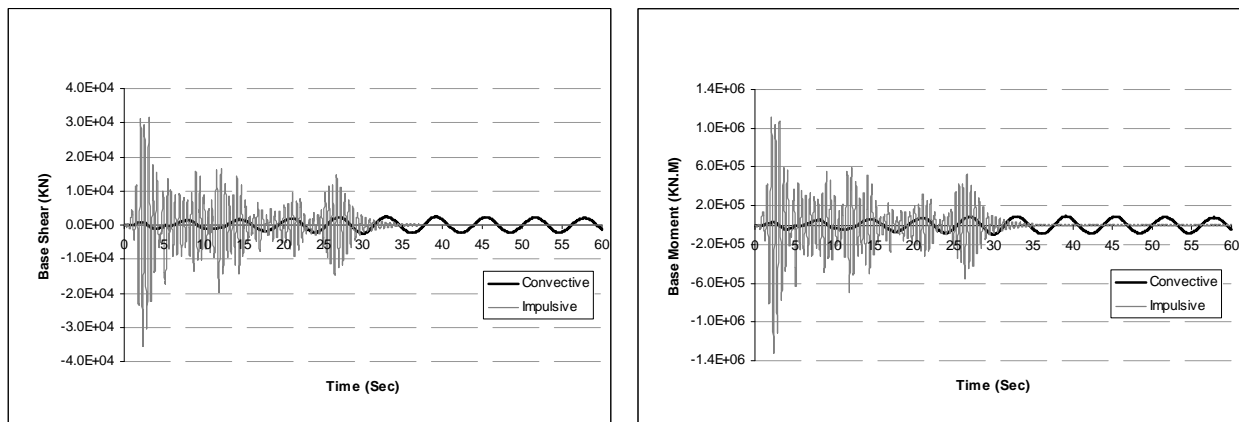
Figure 6.9 Time history results for the elevated tank model

Based on the data provided in Table 6.3, it can be concluded that the contribution of the impulsive component in total seismic response of the elevated tank model is much higher than that of the convective term. Contributions to the base shear and base moment of the shaft from all sloshing modes are found to be negligible because of the very small response spectrum accelerations associated with such low frequency modes. The maximum contribution of sloshing component to the base shear of the shaft is only around 3 percent of the total effective weight of the system while for the impulsive component this contribution could be as high as 36 percent.

Table 6.3 Maximum absolute time history response values for the elevated tank model

	Convective		Impulsive		Total	
Base shear	Max value (kN)	Ratio(%) (Vc/We)	Max value (kN)	Ratio(%) (Vi/We)	Max value (kN)	Ratio(%) (V/We)
	2487	2.52	35548	36.03	34842	35.32
Base moment	Max value (kN.m)	Ratio (Mc/We)	Max value (kN.m)	Ratio (Mi/We)	Max value (kN.m)	Ratio (M/We)
	94023	0.95	1320592	13.39	1293880	13.11

Table 6.3 also shows that adding the sloshing component of the response has resulted in a reduction of forces. This is because of the fact that the water sloshing motion is not in phase with the impulsive motion of the tank-pedestal system.

It is important to note that the peak of the sloshing response occurs far beyond that of the impulsive response. For instance, the maximum impulsive response occurs at $t = 2.34$ s while the sloshing response reaches its peak value at $t = 29.97$ s. As shown in Figure 6.9 when the peak impulsive response occurs, the convective response is at the beginning stage and has not yet fully developed.

At the end of the earthquake's duration, the impulsive motion of the tank-pedestal system is rapidly damped out, in contrast the sloshing part of the response continues at decreasing amplitude for the remainder of the time period considered. This is because of the higher damping ratio ($\zeta = 5\%$) associated with the impulsive component than that of the sloshing component ($\zeta = 0.5\%$).

6.2.5 Comparison of FE results with current practice

To evaluate the accuracy of the current practice in predicting the seismic response of elevated water tanks, the base shear and base moment response values of the elevated tank model are calculated according to the formulations given in section 6.2.1.1.

It should be noted that the response values obtained through current practice are based on the values of I=1.5 and R=3 per ASCE 7-05, where I is the "Importance factor" and R is the "Response modification coefficient". Therefore, to compare these values with those obtained from FE analysis, the calculated time history results (given in Table 6.3) are multiplied by I/R = 0.5.

In calculating the design forces using the current practice, the design spectrum with a peak ground acceleration of 0.32g to correspond with the seismic ground motion used in FE analyses is used. Moreover, the mapped spectral accelerations (S_S and S_1) for Imperial Valley location are chosen as 1.5g and o.6g, respectively. Site class "A", classified as a site with hard rock soil is assumed for the Code analysis.

In obtaining the results using the current practice, first dynamic properties of the model (natural periods of vibration and associated modal masses corresponding to the impulsive and

146

convective modes) are determined using a two-mass idealization approach developed by Housner (1963).

To use Housner's method, initially the conical (Intze) tank under consideration should be converted to an equivalent cylindrical tank having the same volume of water as the original tank. Then, the equivalent lumped masses and the equivalent heights of the impulsive and convective components of the liquid inside the cylinder are calculated using Housner's formulae. In obtaining the effective heights, the effect of hydrodynamic pressure exerted on the bottom of the tank is included.

As shown in Figure 6.10(a), the actual elevated tank model consists of the following mass components; convective mass of water (M_C); equivalent mass M_{tw} which in turn includes the impulsive mass of water and the walls of the vessel; mass of the tank's floor (M_{dr}), and mass of the shaft and interior platforms (M_s). In order to simplify the calculation process, the actual tank model is equated with a two degree of freedom model shown in Figure 6.10(b).

As shown in this figure, the entire mass of the tank-pedestal system is divided into convective (M_C) and impulsive (M_I) components. The convective mass of the contained liquid (M_C) and its location can be readily calculated based on Housner's method. It is assumed to be connected to the walls of the vessel by a spring having the equivalent stiffness of K_1.

M_I represents the impulsive mass of the system and is lumped at distance "a" above the tip of the shaft. It includes the mass components of impulsive water, walls of the vessel, tank floor (M_{dr}), as well as shaft and its interior platforms (M_s).

To determine M_I and its location, initially, the mass components associated with the impulsive water, and the walls of the vessel are equated with the mass M_{tw}, located at an equivalent distance "a" from the top of the shaft. Having obtained the weights of the impulsive

water and the walls of the vessel and the heights corresponding to their centers of gravity, one

can simply calculate the equivalent arm "a" corresponding to the equivalent mass M_{tw}. To present

the entire impulsive weight of the tank-pedestal system as a single equivalent mass (M_I),

impulsive mass components of System (a) which in addition to M_{tw} includes the mass of the

tank's floor (M_{dr}), and that of the shaft and its interior platforms (M_s), may be idealized with

the single-mass M_I as shown in Figure 6.10(b).
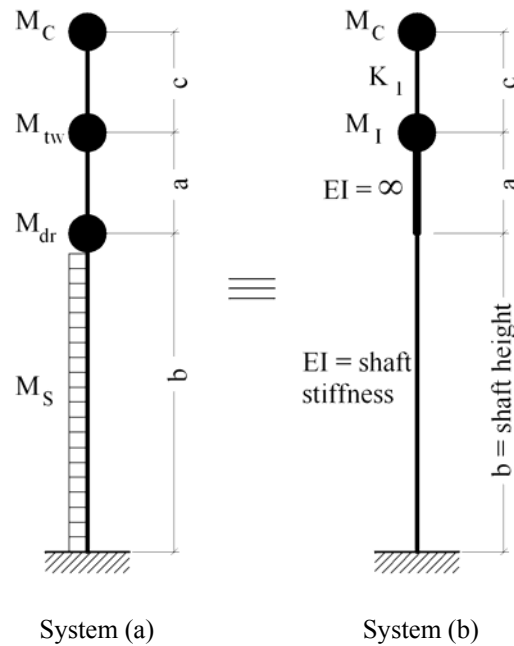
Figure 6.10 Derivation of the total equivalent impulsive mass (M_I)

Mass M_I is considered to be rigidly attached (EI = ∞) to the top of the shaft and is lumped

at the same location as M_{tw}. The amount of mass M_I can simply be determined by equating the

work equations of systems (a) and (b). Using this approach, the elevated water tank is

148

represented as an equivalent two degree of freedom system as shown in Figure 6.11. Mechanical parameters corresponding to this equivalent system are also shown in this figure.

The two modes of vibration with the natural periods of Tc= 6.250 sec and Ti= 0.336 sec are identified for the equivalent two DOF system corresponding to convective and impulsive modes, respectively.

(a) Actual model   (b) Equivalent cylindrical model   (c) Equivalent two DOF model
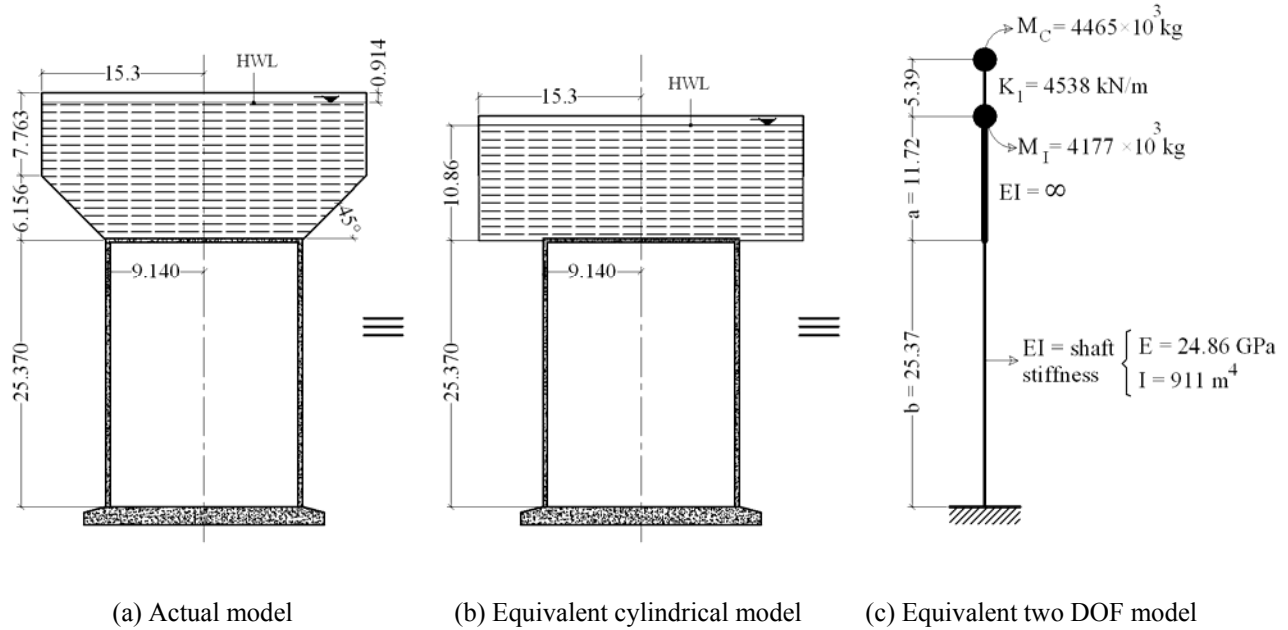
Figure 6.11 Elevated tank model and its equivalent dynamic system

The base shear and base moment corresponding to impulsive and convective components can be obtained using equations described in section 6.2.1.1. The total base shear and base moment can be calculated by combining the impulsive and convective terms using SRSS method (see Table 6.4). The resulting base shear and base moment values are 16425 kN and 609557 kNm, respectively.

Comparing these results with those obtained from FE analysis, it can be concluded that estimated responses are in reasonable agreement. The difference between two sets of data is only

6 percent for both base shear and base moment. The main reason for this difference is that based on the current practice the effects of tank wall flexibility and rocking component of the motion on seismic response cannot be accounted for appropriately and also only the contribution of first sloshing and impulsive modes are included while the effect of higher modes are ignored.

Table 6.4 Comparison of FE time history with current practice

	Current practice			FE time history	Response ratio
	Impulsive	Convective	Total (SRSS)		
Base shear (kN)	16389	1078	16425	17421	1.06
Base moment (kN.m)	607834	45794	609557	646940	1.06

As an alternative approach, the fundamental impulsive period of the elevated tank model can be estimated assuming the pedestal acting as a cantilever column with the entire vibrating mass of the system lumped as a single mass at its end. Using this approach, a single mass is assumed to be located at the centroid of the contained liquid. The lateral stiffness of the tank/pedestal system can be determined assuming a cantilever beam type deflection for the pedestal. The results yield to the fundamental impulsive frequency of 2.198 Hz which is in close agreement with the natural frequency of 1.955 Hz obtained from FE analysis.

6.2.6 Comparison of FE results with "equivalent lateral force procedure" of ACI 371R-08

In order to evaluate the accuracy of the "equivalent lateral force procedure" recommended by ACI 371R-08 guide, the base shear and base moment of the elevated tank model is computed using this method and is compared with those obtained from FE analysis. It is important to note

that in this approximate procedure, the sloshing behavior of the stored liquid is ignored and the entire mass of water is considered as an impulsive mass.

According to "equivalent lateral force procedure", the seismic base shear (V) is determined from:

$$V = C_s W_e \tag{6-4}$$

where, W_e is the total effective weight of the system. C_s is the seismic response coefficient and is determined as follows:

$$C_s = S_{DS} \frac{I}{R} \tag{6-5}$$

C_s should not be greater than

$$C_s = S_{D1} \frac{I}{T_f R} \tag{6-6}$$

but should not be taken less than

$$C_s = 0.044 S_{DS} I \tag{6-7}$$

where, I, R, S_{DS}, and S_{D1} are as defined previously in sections 6.2.1.1 and 3.3 of the thesis. T_f is the fundamental period of the tank/pedestal system which is determined assuming that the entire vibrating mass of the system is represented by a single lumped mass located at the centroid of the contained water. Assuming the pedestal acting as a cantilever beam of length L_g having uniform stiffness with a single mass lumped at its end, T_f can be determined as follows:

$$T_f = 2\pi \sqrt{\frac{W_e}{g k_c}} \tag{6-8}$$

where, k_c is the tank lateral stiffness which is determined as:

$$k_c = \frac{3E_c I_c}{L_g^3} \tag{6-9}$$

in which, E_c is the modulus of elasticity of concrete; I_c is the moment of inertia of the gross concrete section about the centroidal axis, neglecting reinforcement and L_g is the distance from base to centroid of the stored water. For a thin cylinder of thickness h_r and mean diameter d_w, the cross-sectional area A_c and moment of inertia I_c are calculated as:

$$A_c = \pi d_w h_r \tag{6-10}$$

$$I_c = 0.125\pi (d_w)^3 h_r = 0.125 A_c (d_w)^2 \tag{6-11}$$

Substituting for I_c, one can obtain the following approximate equation for fundamental period T_f:

$$T_f = 2\pi \sqrt{\frac{8 W_e L_g^3}{3 A_c E_c d_w^2 g}} \tag{6-12}$$

As was mentioned previously, this assumption will lead to the fundamental frequency of 2.198 Hz. Once the seismic base shear is obtained, the lateral seismic force F_x induced at any level is determined by distributing the total lateral seismic force over the height of the structure as follows:

$$F_x = C_{vx} V \tag{6-13}$$

$$C_{vx} = \frac{W_x h_x}{\sum_{i=1}^{n} W_i h_i} \tag{6-14}$$

where, C_{vx} is the vertical distribution factor, W_i and W_x are portion of the total effective weight of the structure W_e located or assigned to level i or x; h_i and h_x are height from the base to level i or x. The calculated lateral seismic forces F_x for the elevated tank model under consideration are shown in Figure 6.12. In calculating these lateral seismic forces, the design spectrum as described previously in section 6.2.5 in conjunction with Eqs. (6-4) to (6-7) is used.
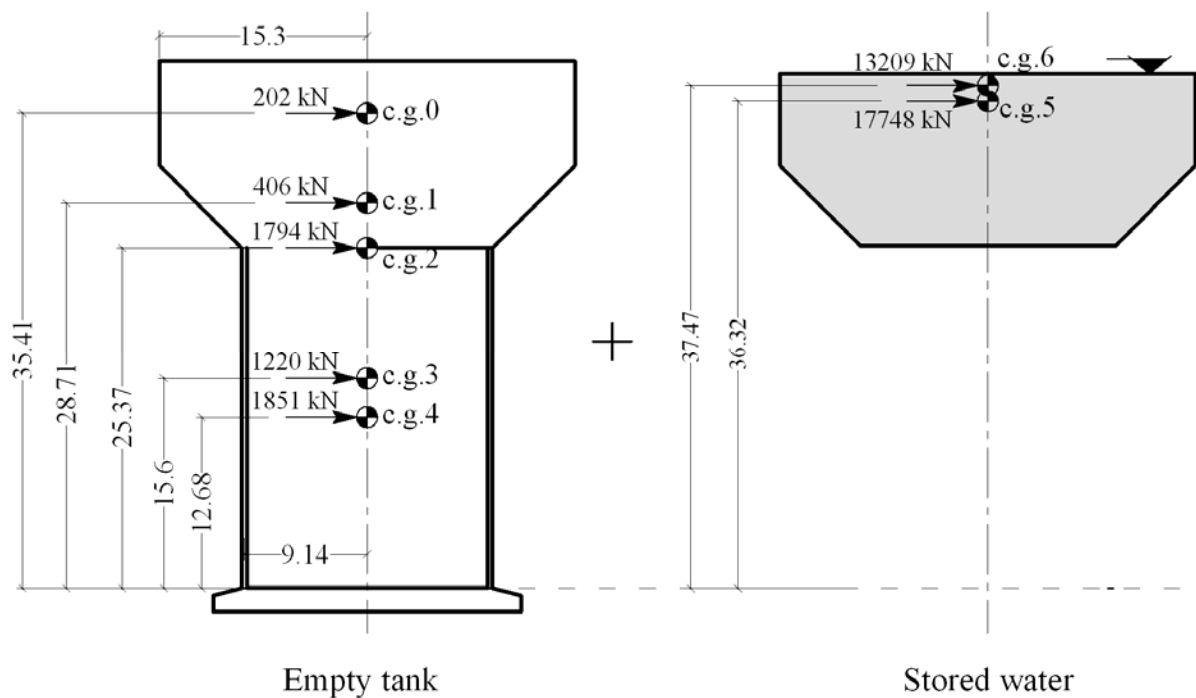
Figure 6.12 Lateral seismic forces obtained from "equivalent lateral force procedure"

In Figure 6.12, c.g.0 to c.g.6 are centers of gravity for different portions of the tank-pedestal system defined as follows:

c.g.0:   Center of gravity for cylindrical steel shell

c.g.1:   Center of gravity for conical steel shell

c.g.2:   Center of gravity for tank's floor + Ring beam + other accessories

c.g.3:   Center of gravity for interior platforms

c.g.4:   Center of gravity for concrete pedestal

c.g.5 and c.g.6:   Centers of gravity for impulsive and convective water components

The lateral seismic shear V_x and overturning moment M_x acting at level x is determined by:

$$V_x = \sum_{i=1}^{x} F_i \tag{6-15}$$

$$M_x = \sum_{i=1}^{x} F_i (h_i - h_x) \tag{6-16}$$

where, F_i is the portion of the seismic base shear induced at level i and is from the top of the structure to the level under consideration.

Eqs. (6-15) and (6-16) lead to the base shear and base moment values of 36,430 kN and 1,246,402 kN.m, respectively for the elevated tank model under consideration. These values are greater than those obtained from FE by a factor of 2.09 and 1.93, respectively. As expected, seismic response values are highly overestimated using the "equivalent lateral force procedure" recommended by ACI 371R-08, leading to an overdesign of the shaft structure and supporting foundation. As a result, this procedure does not seem to be appropriate for evaluating the seismic response of liquid-filled elevated tanks.

6.2.7 Comparison of FE results with "combined Code/FE" method

The seismic base shear and overturning moment at the base of the elevated tank may also be computed using the modal response values obtained from FE analysis in combination with response spectrum in accordance with current practice as defined under section 6.2.1.1.

As a result, dynamic properties of the model including the equivalent weights of the impulsive and convective modes, natural periods of vibration, and associated moment arm for each considered mode are first determined from a fluid-structure interaction analysis performed using the ANSYS computer program. Then, the seismic response coefficients corresponding to each mode under consideration are determined using the current practice as explained before. Eq. (6-1) can then be used to calculate the seismic base shear contributed by each mode. The corresponding overturning moment for each mode can be simply evaluated by multiplying the computed base shear by the moment arm obtained from FE modal analysis.

The total impulsive response is obtained by combining the response values corresponding to impulsive modes using the SRSS method. The same combination method may be used to obtain the total convective response. Finally, computed impulsive and convective terms are again combined using SRSS method to obtain the total base shear and base moment of the structure. This leads to the total base shear and base moment values of 13,611 kN and 484,880 kNm, respectively.

Comparing the contributions of impulsive and convective components, one can observe that the contribution of convective term in total response is much smaller than that of impulsive.

Comparing the results of combined method with those obtained from FE analysis, it can be observed that the combined method underestimates the base shear by 21% and base moment by 25% which is not desirable for design applications.

Comparing the results obtained through current practice presented in section 6.2.5 with those of combined method, it can be seen that following the provisions of current practice lead to relatively higher response values (21% for base shear and 26% for base moment).

These higher response values obtained from current practice are resulted from higher seismic coefficient (C_i) associated with the fundamental impulsive mode. This is in fact due to lower period corresponding to fundamental impulsive mode estimated using current practice compared to that obtained through FE analysis.

6.3 Effect of earthquake frequency content on the dynamic behavior of liquid-filled elevated tanks

In order to investigate the effect of earthquake frequency content on the dynamic behavior of liquid-filled elevated tanks, the same elevated tank model is subjected to four different ground motions with different frequency content properties and the time history response values are obtained.

It should be noted that in the previous section the time history response of the model was determined using the modal superposition technique, however in the current section the direct integration method is used for obtaining the transient response of the model. Furthermore, since the sloshing component was found to have a negligible effect on the overall seismic behavior of the tank, only the impulsive part of response is considered in this section and the effect of sloshing term is neglected. Studied responses are shear and overturning moment at the base of the pedestal.

The longitudinal components of 1940 El-Centro, 1994 Northridge, 1971 San-Fernando, and 1957 San-Francisco earthquakes are used as horizontal excitations for the elevated tank model. Only the first 15 seconds of the records are used in time history analyses.

The El-Centro record is scaled in such a way that its peak ground acceleration reaches 0.4g. Other records are scaled in such a way to have the same value of Power index (P_a) (Housner 1975) as that of the scaled El-Centro record. Various indices have been proposed so far to characterize the intensity of earthquake motions including: peak ground acceleration, Arias intensity (Arias 1970), Power index (Housner 1975), Spectrum intensity (Housner 1952), and so on.

Among all these indices, it is well known that the Power index is one of the most appropriate indices to be used for scaling of the earthquake motions and as a result the intensity of motions can be satisfactorily characterized by this parameter. The earthquake motions are usually characterized by parameters related primarily to the amplitude of the shaking, such as peak ground acceleration however, research studies show that it is not a reliable measure by itself (Housner 1975). The single peak on an accelerogram can not be considered as an accurate representation of the earthquake record as a whole.

Housner (1975) proposed that a measure of seismic intensity could be defined by the average rate of buildup of the total energy per unit mass input to the structure. Taking into consideration that the integral of the squared ground acceleration is proportional to the total input energy, he introduced the Power index as:

$$P_a = \frac{E(D)}{D} = \frac{1}{D} \int_{t_0}^{t_0+D} a(t)^2 \, dt \qquad (6\text{-}17)$$

where,

$E(D)$ is the total energy input during time D

D is the "significant duration" of earthquake

t_0 is the time at the beginning of the strong shaking phase

$a(t)$ is the base acceleration

In other words, the Power index can be considered as a measure of the rate at which energy would be fed into the system. In Eq. (6-17), t_0 and $t_0 + D$ are the limits of the strong portion of motion. Eq. (6-17) can be interpreted as the average value of the squared acceleration over the significant duration interval D.

Arias intensity (Arias 1970) relates to the sum of the energies dissipated per unit of mass by a population of damped oscillators of all natural frequencies ($0 < \omega < \infty$):

$$AI = \frac{\pi}{2g} \int_0^{t_r} a(t)^2 dt \qquad (6\text{-}18)$$

where, t_r is the total duration of the ground motion and g is the acceleration due to gravity. If the strong shaking is considered to start at the beginning of the record, i.e. t_0 is zero, the following relation may be derived:

$$AI = \frac{\pi}{2g} E(t_r) \qquad (6\text{-}19)$$

As it is obvious from this equation, the Arias intensity is actually representative of the total energy in the record.

The popular definition of significant duration of motion proposed by Trifunac and Brady (1975) is adopted in this study where the significant duration is defined as the interval between instants t_5 and t_{95} at which 5% and 95% of the total integral in Eq. (6-18) is attained, respectively:

$$D = t_{95} - t_5 \tag{6-20}$$

The concept of significant duration has the benefit of considering the properties of the whole accelerogram and defining a continuous time interval during which the shaking may be considered as strong.

Finally, the earthquake Power can be defined as:

$$P_a = \frac{1}{t_{95} - t_5} \int_{t_5}^{t_{95}} a(t)^2 \, dt \tag{6-21}$$

The scaled earthquake records are shown in Figure 6.13. The Arias intensity versus time (known as Husid plot) is also indicated in Figure 6.14 for all the earthquake records considered. As it is obvious from this figure, all curves have equal initial slopes over the time interval D (significant duration), implying that all scaled records have the same level of Power.
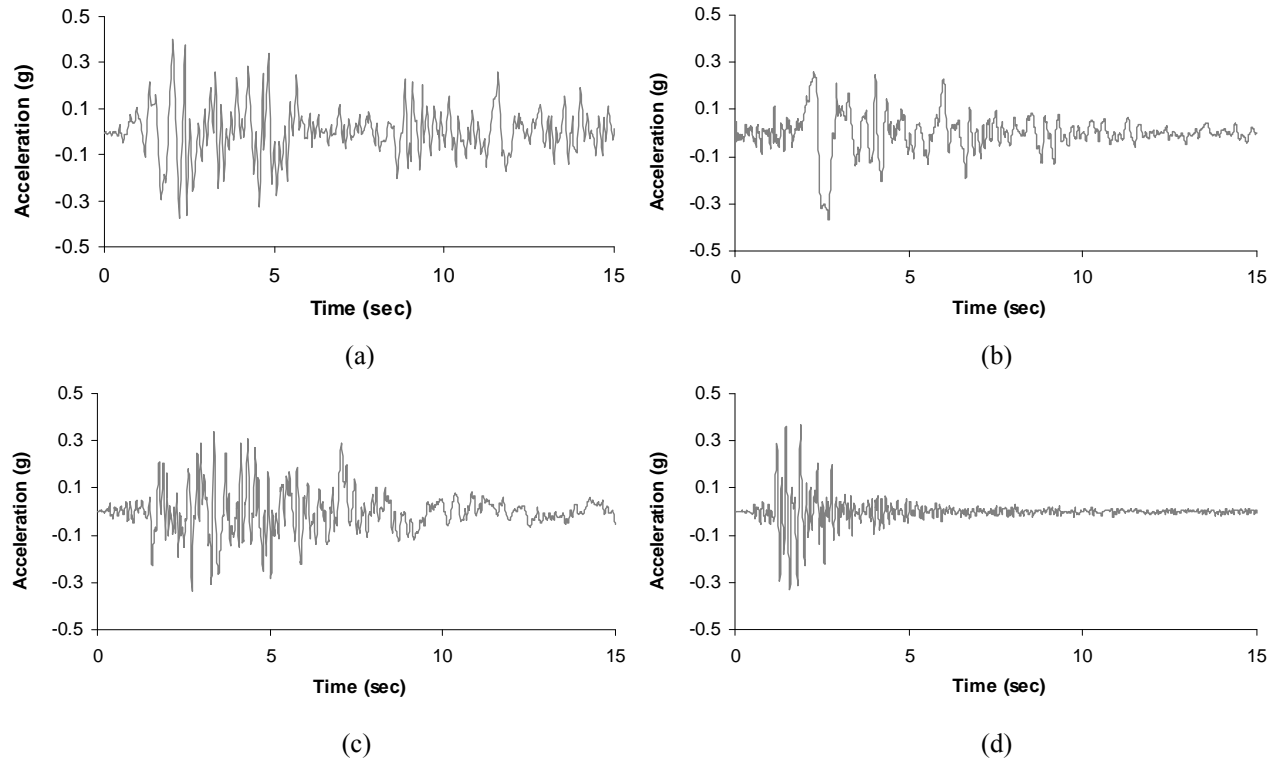
Figure 6.13 Scaled earthquake records (horizontal component); (a) El-Centro,

(b) Northridge, (c) San-Fernando, (d) San-Francisco
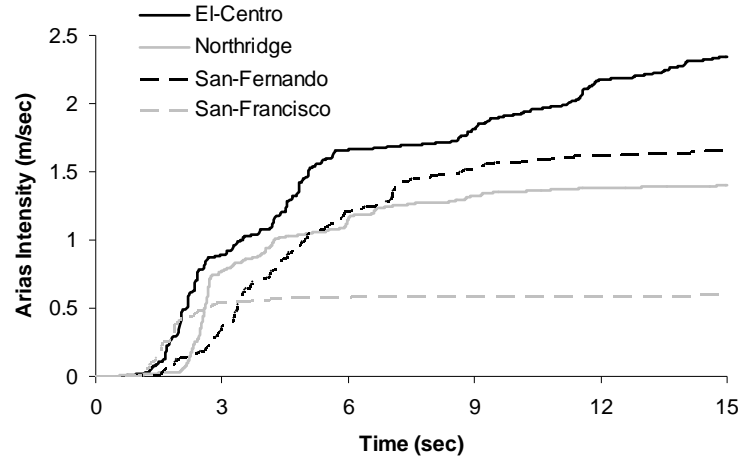
Figure 6.14 Arias Intensity versus time (Husid plot) of the earthquake records

The characteristics of the scaled records are listed in Table 6.5. The predominant frequency (f_p) of each record is also given in the table.

Table 6.5 Ground motions properties

Earthquake	$t_5(s)$	$t_{95}(s)$	$D(s)$	$P_a(m^2/s^4)$	$f_p(Hz)$	$\dfrac{PGA}{PGV}$
El-Centro	1.63	13.25	11.62	1.13	2.000	0.88
Northridge	2.12	9.14	7.02	1.12	1.282	0.51
San-Fernando	1.75	10.08	8.33	1.12	4.160	1.11
San-Francisco	1.18	4.15	2.97	1.13	4.545	2.44

The predominant frequency is defined as the frequency corresponding to the highest peak in a response spectrum. For instance, the Pseudo-acceleration (PSA) response spectra corresponding to 5% of critical damping are calculated for Northridge and San-Francisco records, as shown in Figure 6.15. From this figure, one can determine the predominant frequencies of 1.282 Hz and 4.545 Hz for Northridge and San-Francisco ground motions,

160

respectively. Using the same approach, the predominant frequencies of 2.00 Hz and 4.16 Hz are found for El-Centro and San-Fernando records, respectively.
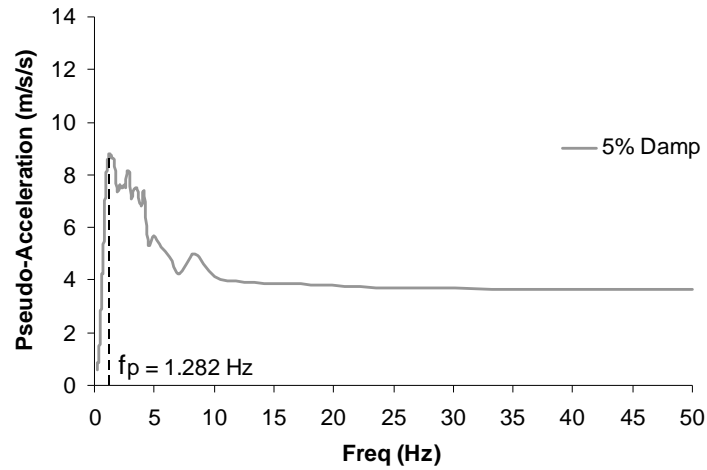
(a)
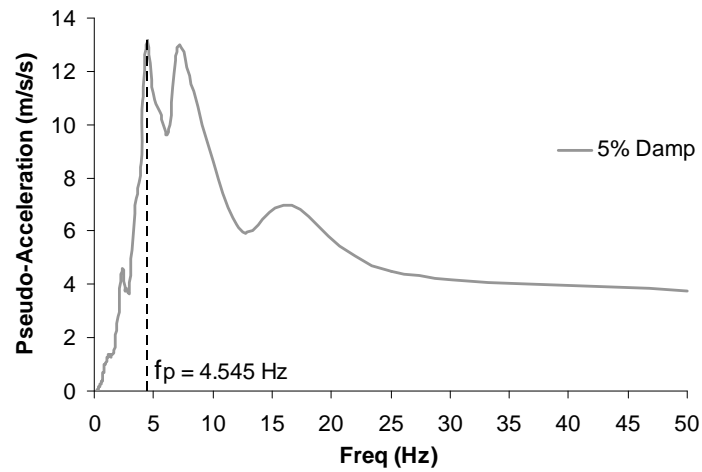
(b)

Figure 6.15 Response spectra for horizontal earthquake components (5% damping);

(a)Northridge, (b) San-Francisco

The ratio of peak ground acceleration (in units of g) to peak ground velocity (in units of m/s) ($\frac{PGA}{PGV}$) is believed to be a good indicator of the frequency content characteristics of the

ground motion. As a result, ground motions with $\dfrac{PGA}{PGV}$ <0.8 are classified as low frequency

content, earthquake records with 1.2> $\dfrac{PGA}{PGV}$ >0.8 are classified as intermediate frequency

content, and those with $\dfrac{PGA}{PGV}$ >1.2 can be classified as high frequency content. Therefore, the

Northridge record is categorized as low frequency content, the El-Centro and San-Fernando

records are categorized as intermediate frequency content and the San-Francisco record is

categorized as high frequency content.

The transient base shear and base moment for the elevated tank model due to horizontal

excitation are calculated using the proposed method. As mentioned before, four different seismic

excitations are applied to the model to investigate the effect of frequency content on the seismic

response of the tank-pedestal system. The time history base shear and base moment responses of

the tank subjected to these records are presented in Figures 6.16 and 6.17, respectively. It should

be noted that these values correspond with the total force and moment acting at the base of the

pedestal.
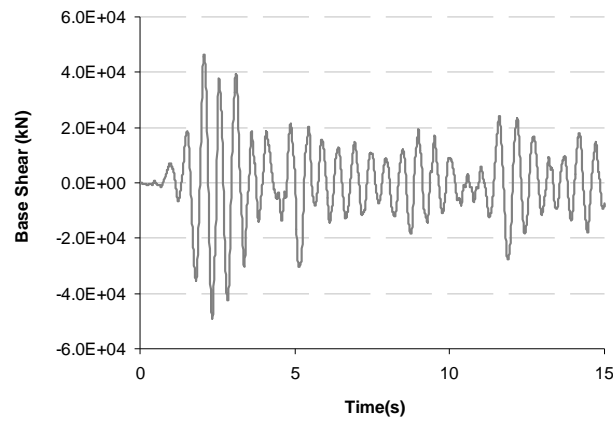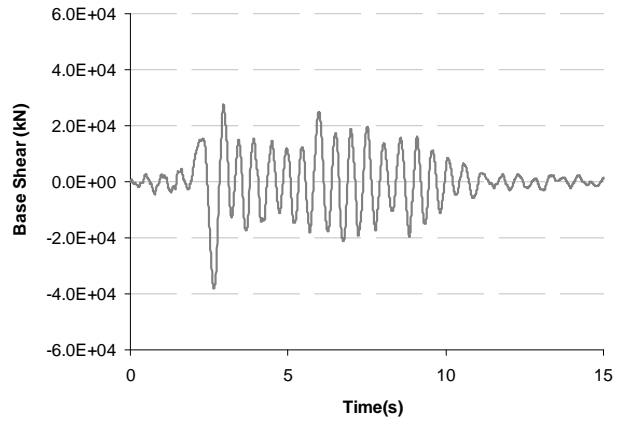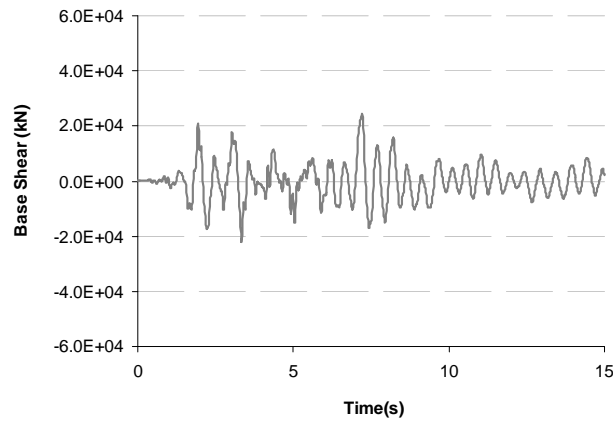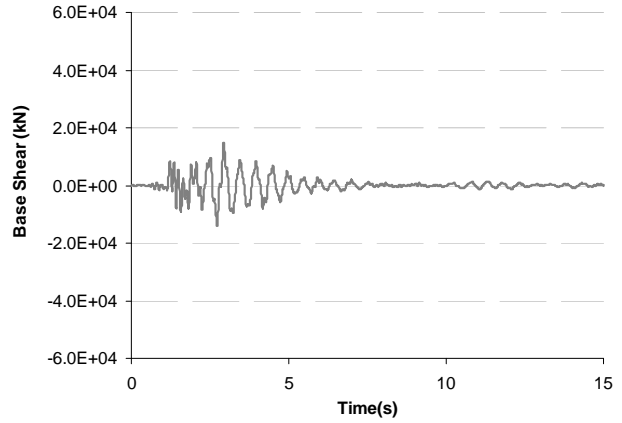
Figure 6.16 Time history of base shear response for the elevated tank model under

horizontal excitation (impulsive component); (a) El-Centro, (b) Northridge,

(c) San-Fernando, (d) San-Francisco
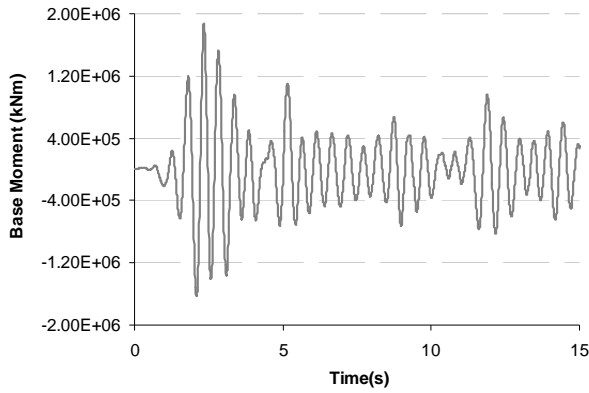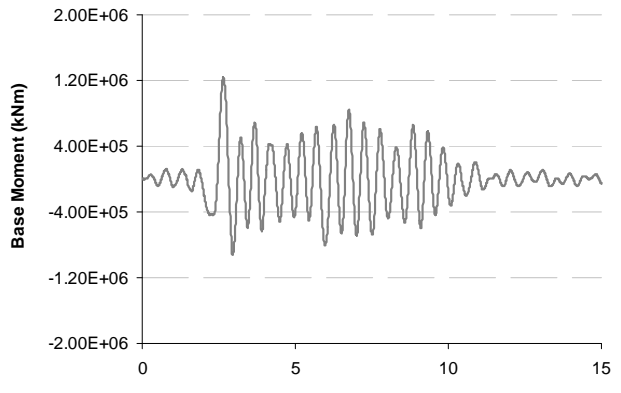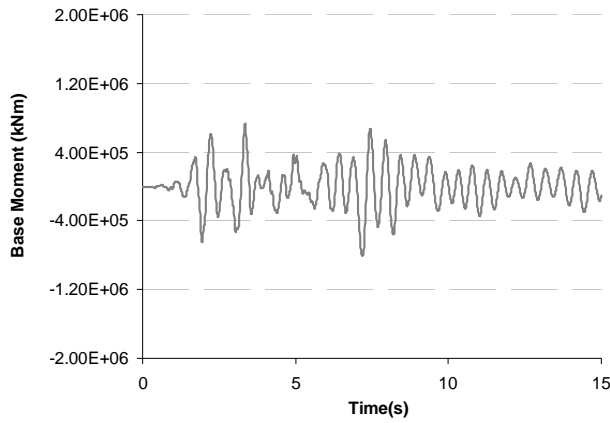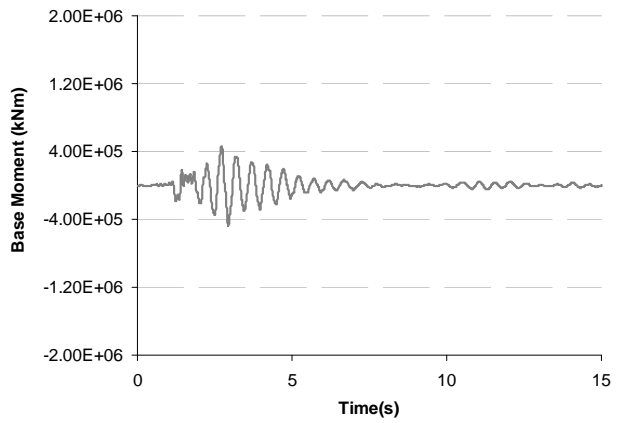
Figure 6.17 Time history of base moment response for the elevated tank model under

horizontal excitation (impulsive component); (a) El-Centro, (b) Northridge,

(c) San-Fernando, (d) San-Francisco

For comparison purposes, the peak FE results for various ground motions are normalized with respect to the peak response values corresponding to the record producing the highest response among four records considered. The variation of the dynamic response in terms of the normalized peak base shear and base moment for different earthquake records is shown in Figure 6.18.

(a)   (b)
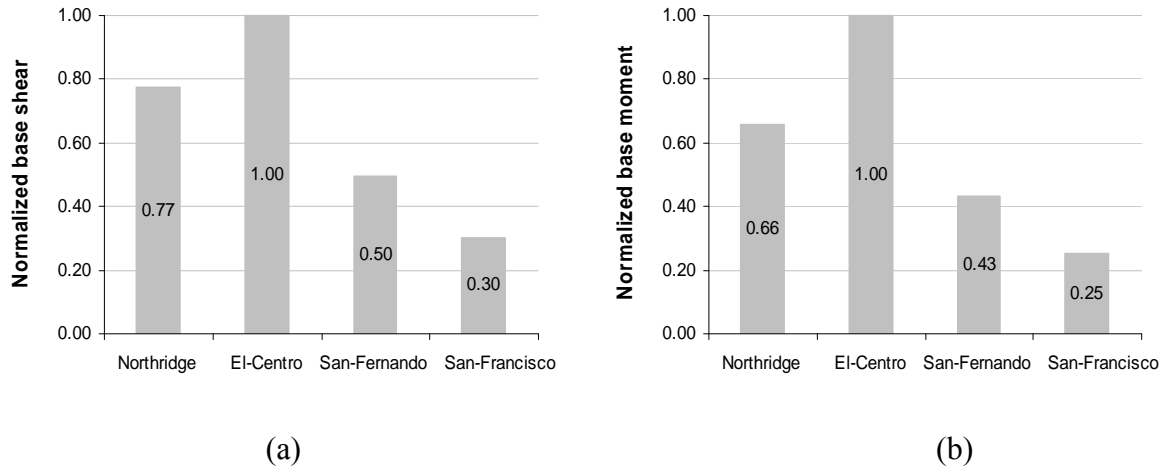
Figures 6.18 FE structural responses of the elevated tank model;

(a) normalized peak base shear, (b) normalized peak base moment

As shown in this figure, the intermediate frequency content earthquake of El-Centro results in the highest response values compared to all other records. On the other hand, the lowest response values are observed for the high frequency content record of San-Francisco. The base shear and base moment response values due to San-Francisco record are approximately one-third and one-fourth of those calculated under El-Centro record, respectively. This shows that the effect of earthquake frequency content on the dynamic response of tank-pedestal systems could be very significant and thus may cause a considerable increase in time-domain peak response values. As is the case in this study, the base shear and base moment values are increased by about 233% and 300%, respectively due to the effect of earthquake frequency content.

Based on the obtained results, it can be concluded that the response values due to El-Centro record are highly amplified as a result of the similarity between the frequency characteristics of the tank-pedestal system and the earthquake motion. It is expected that the record with the nearest predominant frequency to the fundamental impulsive frequency of the system may cause the highest response values compared to other records. Comparing the fundamental impulsive

frequency of the elevated tank model, 1.955 Hz (see Table 6.2) with the predominant frequencies of the earthquake records listed in Table 6.5, it can be observed that the El-Centro record has the closest predominant frequency, 2.00 Hz to the natural frequency of the fundamental impulsive mode of the system. This justifies the much higher response values calculated under El-Centro earthquake compared to other ground motions having predominant frequencies well separated from the fundamental frequency of the system.

6.3.1 Comparison of FE results with current practice

To further examine if the current practice is capable of accounting for the effect of earthquake frequency content, the seismic response of the elevated tank model is obtained using the "current practice" method as explained previously in section 6.2.1.1.

The Code coefficients S_S and S_1 are determined in accordance with ASCE 7-05 for the location of each seismic event. These coefficients can be determined more easily from the national seismic hazard mapping project website, http://eqhazmaps.usgs.gov/ (U.S. Geological Survey). This web site contains electronic versions of the hazard maps. It also contains software which allow determination of map values and Code coefficients by either latitude-longitude or zip code. This software is used here for determination of all Code coefficients. The mapped spectral accelerations (S_S and S_1) corresponding to the location of each seismic event are reported in Table 6.6. Moreover, site class "A", classified as a site with hard rock soil is assumed for all locations.

In order for the current practice results to be comparable with those obtained from FE, the values of I=1 and R=1 are chosen for Code calculations, where I is the "Importance factor" and R is the "Response modification coefficient".

Table 6.6 Mapped spectral accelerations (S_S and S_1) for the considered earthquakes

Earthquake	Zip Code	S_S (g)	S_1 (g)
El-Centro	92243	1.50	0.60
Northridge	91324	1.84	0.66
San-Fernando	91340	2.36	0.82
San-Francisco	94101	1.50	0.67

As was also mentioned previously in section 6.2.5, current practice results compare very well with FE results under the intermediate frequency content record of El-Centro.

Under the low frequency content Northridge earthquake, current practice method leads to the base shear value of 37901 kN which is almost equal to the value obtained through FE with the difference less than 1%. However, the obtained base moment value of 1405616 kNm from current practice is about 14% higher than the value given by FE.

Based on current practice, the base shear and base moment values of 34828 kN and 1291647 kNm are found due to San-Fernando earthquake. These values are higher than those calculated through FE by about 43% and 59%, respectively.

Using the method recommended by current practice, one can obtain the base shear and base moment values of 37901 kN and 1405616 kNm, respectively under the high frequency content earthquake of San-Francisco. Comparing these values with those obtained from FE, it can be observed that current practice has highly overestimated the base shear and base moment by about 155% and 195%, respectively. This seems to be too conservative for design applications leading to an overdesign of the shaft structure.

According to current practice, the highest response values among four earthquake records considered are obtained under El-Centro ground motion, similar to what was observed through FE calculations. For comparison purposes, the current practice response values corresponding to

167

different earthquakes are normalized with respect to the response values obtained for El-Centro record. Figure 6.19 indicates the normalized base shear and base moment for different earthquake records considered.

Unlike the trend observed for FE results, current practice predicts the lowest response values for the intermediate frequency content record of San-Fernando. In addition, exactly the same response values are determined for both the low frequency content record of Northridge and high frequency San-Francisco record using current practice approach.

As indicated in Figure 6.19, current practice predicts an increase of around 18% for both base shear and base moment due to the effect of earthquake frequency content. This is much lower than the increase percentages of 233% and 300% obtained through FE calculations for base shear and base moment, respectively.

(a)   (b)
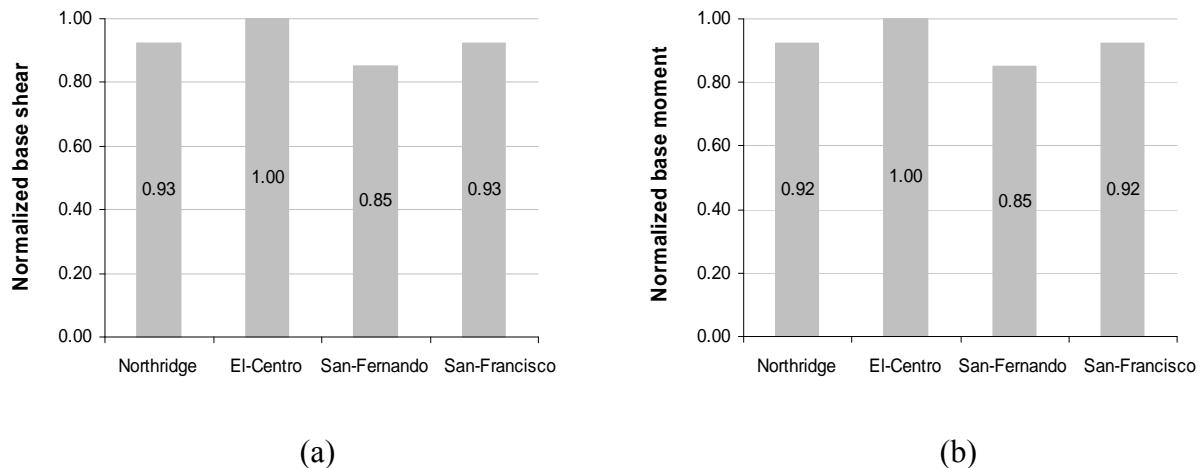
Figures 6.19 Structural responses of the elevated tank model based on "current practice"; (a) normalized base shear, (b) normalized base moment

Finally, based on the comparison made between current practice and FE results, it can be concluded that current practice can not appropriately account for the effect of earthquake

frequency content on the seismic response of liquid-filled elevated tanks. This seems to be a significant issue indicating the need for further consideration in design codes and standards.

6.4 Summary

In this study, a detailed finite element method was employed to study the fluid-structure interaction for liquid-filled conical elevated tanks. The liquid inside the tank was modeled using 3D fluid finite elements.

This study showed that the proposed finite element technique was capable of accounting for the fluid-structure interaction in conical liquid containers. Using this method the study of liquid sloshing effects in tanks with complex geometries such as conical tanks was made possible.

During this study, free vibration analysis as well as transient analysis using both modal superposition and direct integration methods were carried out to investigate the fluid-structure interaction problem in elevated water tanks. Studied responses were shear and overturning moment at the base of the shaft structure. Effects of tank wall flexibility and water sloshing were taken into consideration in the proposed FE analysis. Different damping factors corresponding to different parts of response (impulsive and convective) were assigned to the model. In addition, the instantaneous values of sloshing and impulsive terms were determined separately.

The results of the study compared very well with both analytical and experimental results, indicating the validity of the proposed FE method in studying the fluid-structure interaction effects in conical elevated tanks. Modal FE analyses resulted in natural frequencies and effective water mass ratios very close to those obtained from Housner's formulations with differences for water mass ratios smaller than 3% of the total mass of the fluid for all cases. Both impulsive and

convective terms of response of the elevated tank model considered were mainly dominated with the fundamental modes.

As mentioned before, in order to verify the validity of the proposed numerical model, the free vibration response of a small-scale aluminum conical tank was determined by the proposed FE method and the results were compared with the experimental values reported by El Damatty et al. (2005). The obtained FE results were in full agreement with experimental results. All identified impulsive modes with high contributions to the response of the considered aluminum tank model were $\cos\theta$ type modes (circumferential wave number of 1). Modes with n>1 were found to have negligible contribution to the response and therefore can be ignored. The obtained results also showed a significant change in the mode shape pattern between the conical and cylindrical portions of the tank.

It was shown that the effect of considering sloshing term on the total response might be either increasing or decreasing. This is due to the fact that in general the sloshing and impulsive components of the response do not reach their peak values at the same time.

Studying the results of analysis for the elevated tank model also revealed that the impulsive component had a much bigger contribution to the total response than the convective term. Therefore, for the specific model and ground motion considered in this study, it can be concluded that for practical purposes an accurate estimation of the actual response may be obtained by only including the effect of impulsive term and neglecting the sloshing component.

In the first part of the chapter, the "current practice" results were compared with those obtained from the FE time history analysis of the model subjected to El-Centro ground motion and a very good agreement was observed. The difference between two sets of data was only 6 percent for both base shear and base moment responses. This verifies the validity of the "current

practice" in estimating the seismic response of liquid filled elevated water tanks. However, the results of the study showed that the "current practice" was not capable of accounting for the effect of earthquake frequency content on the dynamic response of such structures appropriately.

In order to examine the accuracy of "equivalent lateral force procedure" recommended by ACI 371R-08, the response values were computed using this procedure and were compared with those of FE analysis. The response values were highly overestimated using the "equivalent lateral force procedure". Therefore, it can be concluded that this procedure does not provide an accurate estimation of seismic response for elevated water tanks and in general leads to an overdesign of the shaft-foundation system.

As an another approach, the seismic response of the elevated tank model was obtained using FE modal analysis results in combination with Code response spectrum (i.e. "combined Code/FE" method) and the results were compared with those of FE analysis. The combined method underestimated the base shear and base moment by 21% and 25%, respectively. This shows the inadequacy of this method for design applications. Comparing the results obtained through different methods, one can say that the "current practice" method provides more accurate results compared to the "equivalent lateral force procedure" and the "combined Code/FE" method.

The effect of earthquake frequency content on the dynamic behavior of elevated water tanks was also investigated in the second part of the chapter by performing time history analyses on an elevated tank model using four different ground motions having different frequency content characteristics. The chosen earthquake records had low to high frequency contents. It was observed that the response values due to the intermediate frequency content record of El-Centro

were significantly amplified as a result of the similarity between the frequency characteristics of the tank-pedestal system and the earthquake record.

The obtained results also showed that the effect of earthquake frequency content on the seismic response of conical elevated tanks could be very significant and therefore may result in a substantial increase in transient response values.

It should be noted that this study was restricted to only one elevated tank subjected to specific ground motions. As a continuation of this research study, a parametric study is carried out to determine the effect of various tank and shaft dimensions on response (see Chapter 7).

CHAPTER 7

PARAMETRIC STUDY AND DESIGN APPLICATION

7.1 Introduction

In this chapter, the dynamic behavior of elevated water tanks is further investigated by performing a comprehensive parametric study on liquid-filled conical elevated tanks using the finite element technique. Using this technique, impulsive and convective pressure components are determined separately in a three-dimensional space. In addition, the effects of tank wall flexibility and sloshing of the liquid free surface are considered. Again, the sloshing behavior of the stored liquid is simulated based on the assumption of linear sloshing.

Through this parametric study, a wide range of tank parameters and geometries typically found in practice is considered. In order to perform this study, a parametric model capable of building any finite element models of a three-dimensional liquid container either conical elevated or cylindrical ground-supported is developed. The parametric model input file is written using ANSYS® command lines and is then incorporated into the ANSYS® software. Varying parameters such as: shaft radius, shell thickness, tank radius, shaft height, tank height, liquid depth, etc. have been defined in this parametric model allowing us to create any FE tank model desired. The text command file of the parametric model is given in Appendix B.

The detailed parametric model proposed is capable of accounting for all deciding parameters and estimating the relative importance of each parameter on the overall dynamic response of elevated water tanks. This is accomplished by performing a set of sensitivity studies on principal parameters and thereby examining the variation trend of the resultant hydrodynamic pressure components.

As a result of this parametric study, pressure distribution graphs corresponding to both impulsive and convective hydrodynamic pressures are generated by carrying out spectral analyses on a large number of conical elevated tanks having different geometrical properties. It will be shown later in this chapter that these pressure graphs can be utilized simply in design applications for liquid-filled conical elevated tanks.

The accuracy of the proposed pressure graphs is verified by comparing the results obtained through the application of these pressure graphs with those calculated using the previously verified FE time-history analysis and also the "current practice" method described in Chapter 6. To this end, two typical elevated tanks are randomly selected and their seismic response is estimated using three different approaches mentioned above.

7.2 Effect of inclusion of roof on dynamic response of elevated tanks

In this section, the effect of inclusion of roof on dynamic response of the conical elevated tanks is investigated by performing spectral analyses on an elevated tank model with and without the roof and then comparing their corresponding hydrodynamic pressure values. The elevated tank model considered for this purpose is the same tank that was described in Chapter 6, section 6.2.3. The corresponding FE model of the tank with the roof included is shown in Figure 7.1.

The design spectrum per ASCE 7-05 is defined as an input response spectrum in ANSYS® for performing the spectral analyses. Only the contribution of fundamental impulsive and convective modes is included in calculating the dynamic response values.

The studied responses are the maximum impulsive and convective pressure values on both the wall and the floor of the water-filled vessel. The peak pressure values corresponding to impulsive and convective components are reported separately. Reported pressure values are the

174

maximum values per row of elements. These maximum values are identified along the cylindrical side shell, cone shell, and tank floor by post-processing the obtained pressure values using three post-processor algorithms written by the author; "POST-CYL", "POST-CON", and "POST-FLOOR", respectively. These algorithms are written using the ANSYS® command lines. The text command files for these post-processors are given in Appendix B.

<table>
<tr><td>(a)</td><td>(b)</td></tr>
</table>
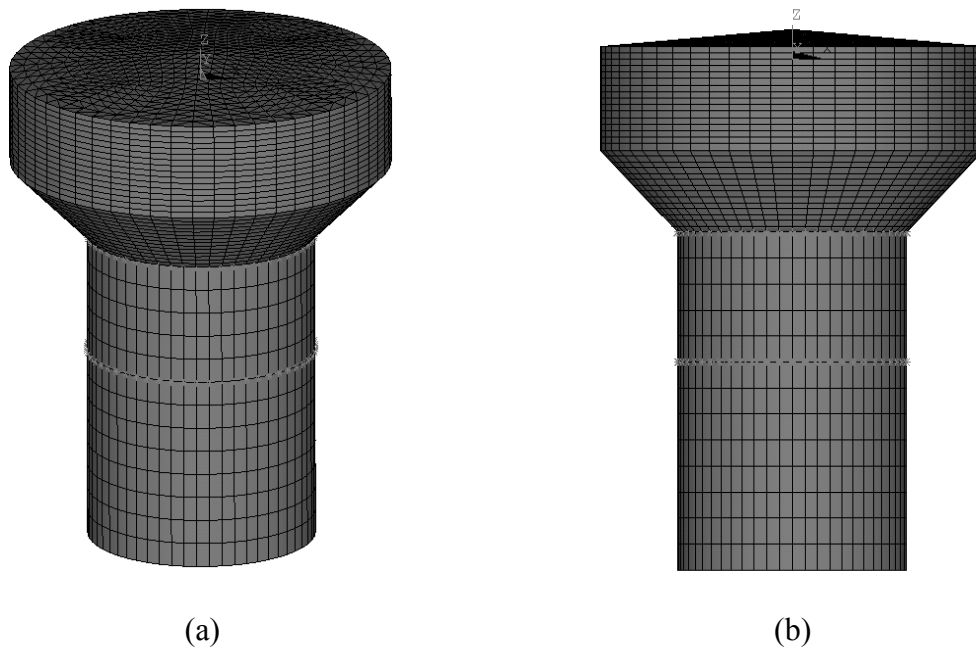
Figure 7.1 FE idealization for the roofed elevated tank model; (a) 3D view, (b) side view

All modal response values including the natural periods of vibration, mode shapes, effective modal masses, etc. are obtained through a FE free-vibration analysis. The real response values such as hydrodynamic pressure values corresponding to each mode under consideration are then calculated by introducing the ASCE 7-05 design spectrum as an input response spectrum and carrying out a FE spectral analysis.

In defining the design response spectrum per ASCE 7-05, the values of I=1 and R=1 are assumed where I is the "Importance factor" and R is the "Response modification coefficient". In addition, the mapped spectral accelerations (S_S and S_1) are chosen as 1.5g and o.6g, respectively. Moreover, site class "A", classified as a site with hard rock soil is assumed.

The obtained FE results show that the natural frequency corresponding to the fundamental convective mode remains unchanged due to inclusion of the roof. However, the natural frequency of the fundamental impulsive mode is negligibly decreased from 1.955 Hz (without roof) to 1.942 Hz (with roof) as a result of including the roof in finite element modeling of the tank. The fundamental impulsive mode shape of the tank with the roof mounted at the top is indicated in Figure 7.2.
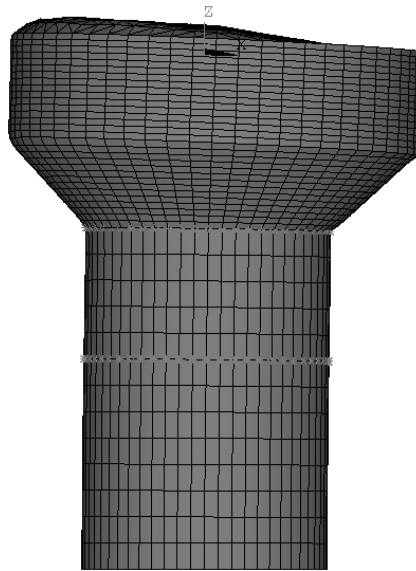
Figure 7.2 Fundamental impulsive mode shape (with roof)

The peak hydrodynamic pressure values corresponding to convective and impulsive components acting on the wall and the floor of the vessel are shown in Figure 7.3. The parameter "Rroot" in the figure denotes the radius of the shaft structure.

176

As obvious from the figure, the effect of inclusion of the roof on peak hydrodynamic pressure values is quite negligible. Both convective and impulsive pressure distributions of the tank model having no roof are virtually identical with those of the roofed tank. Moreover, inclusion of the roof would also result in generation of a large number of spurious modes relating to membrane vibrations. Therefore for the sake of simplicity, in performing the parametric study, the roof can be excluded in FE modeling of the tanks. However, the roof mass effect is included in the simplified models by applying an equivalent distributed mass at the ring beam level using 3D point mass elements.
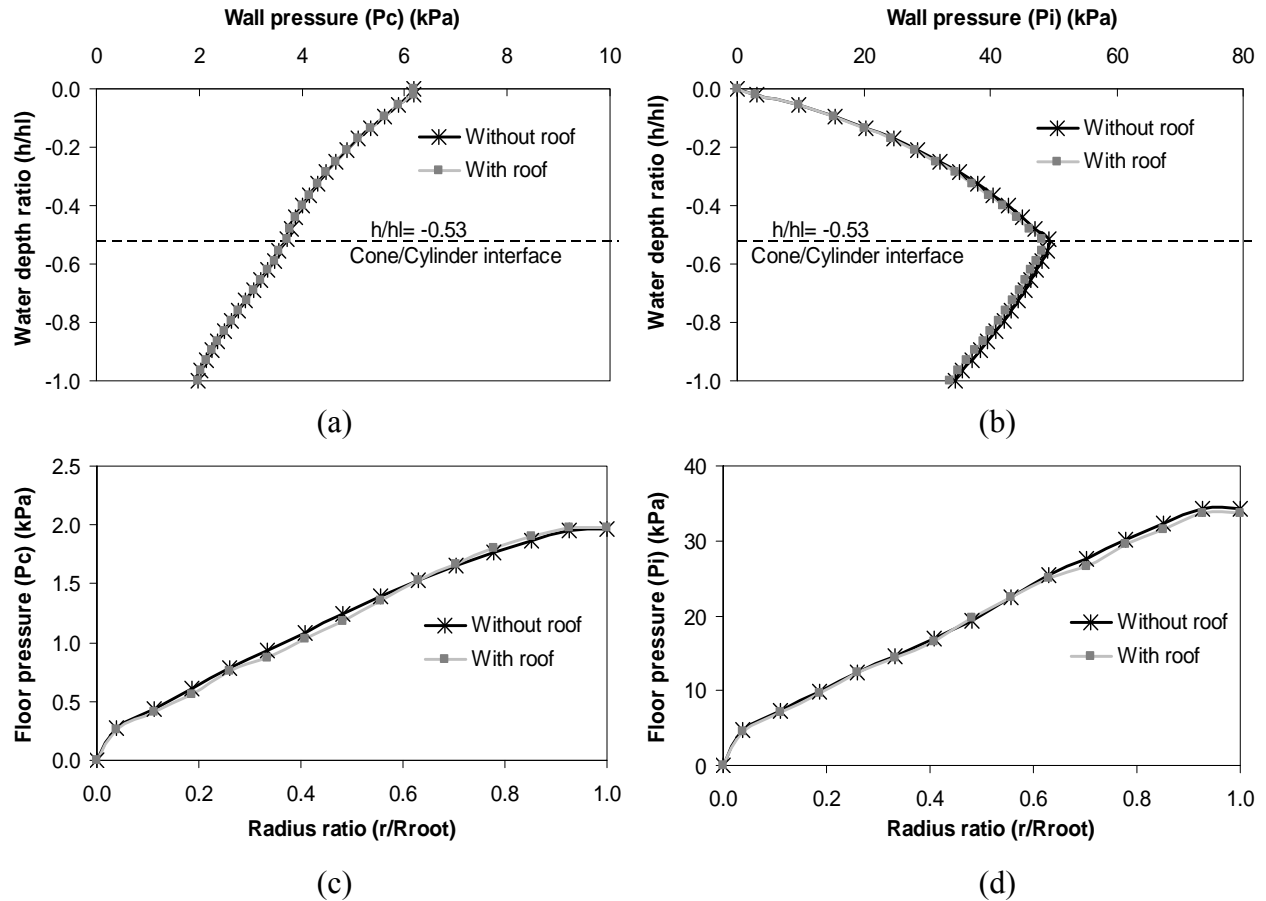
Figure 7.3 Hydrodynamic pressure distribution; (a) Convective pressure over the tank wall, (b) Impulsive pressure over the tank wall, (c) Convective pressure over the tank floor, (d) Impulsive pressure over the tank floor

7.3 Pressure distribution patterns

In this section, the pressure distribution patterns on the wall and the floor of a conical elevated tank corresponding to the fundamental convective and impulsive modes are determined by performing a modal analysis on an elevated tank model. The same elevated tank model explained in Chapter 6, section 6.2.3 is used here. The obtained modal pressure distributions corresponding to the fundamental convective and impulsive modes are plotted in Figures 7.4 and 7.5, respectively. Shown in the figures are also the horizontal pressure distributions around the tank's circumference at the water depths of 3.18m and 10.14m which represent random sections within the cylindrical and conical portions of the vessel, respectively.

As obvious from these figures, under both convective and impulsive mode vibrations, a cosine distribution pattern is observed for the horizontal hydrodynamic pressure along both the cylindrical and the conical sections of the vessel. As shown in the figures, horizontal pressure is exerted symmetrically about the centroidal axes of the vessel having outward direction on one half and inward direction on the other half. Based on the obtained pressure distribution diagrams, the maximum horizontal pressure under lateral excitation occurs along $\phi = 0$.

The vertical pressure distribution corresponding to the fundamental convective mode indicated in Figure 7.4(a), points out that the convective pressure has a maximum magnitude at the water free surface and decreases gradually moving toward the lower sections of the vessel with the minimum magnitude occurring adjacent to the tank floor.

According to Figure 7.5(a), illustrating the vertical pressure distribution related to the fundamental impulsive mode, one can observe that the impulsive pressure begins at zero value at the water fee surface then increases gradually moving toward the bottom of the tank. The

impulsive pressure reaches its maximum magnitude at the cone/cylinder interface then decreases steadily moving further down toward the bottom of the tank.

(a)

(b)   (c)
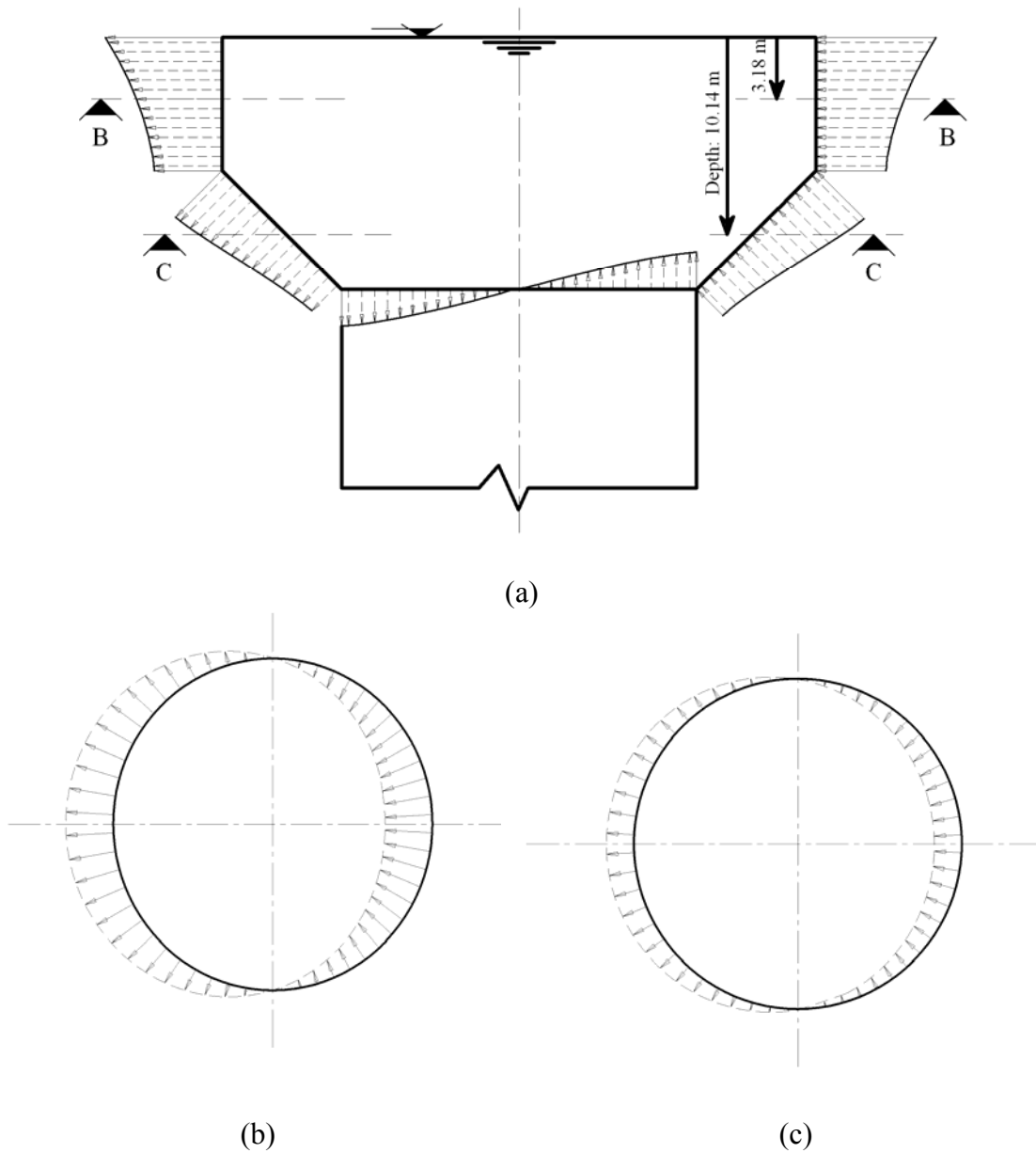
Figure 7.4 Pressure distribution corresponding to the fundamental convective mode

(obtained from FE modal analysis, pressure scale: 1/1); (a) Tank elevation, (b) Section B-B,

(c) Section C-C

(a)

(b)   (c)
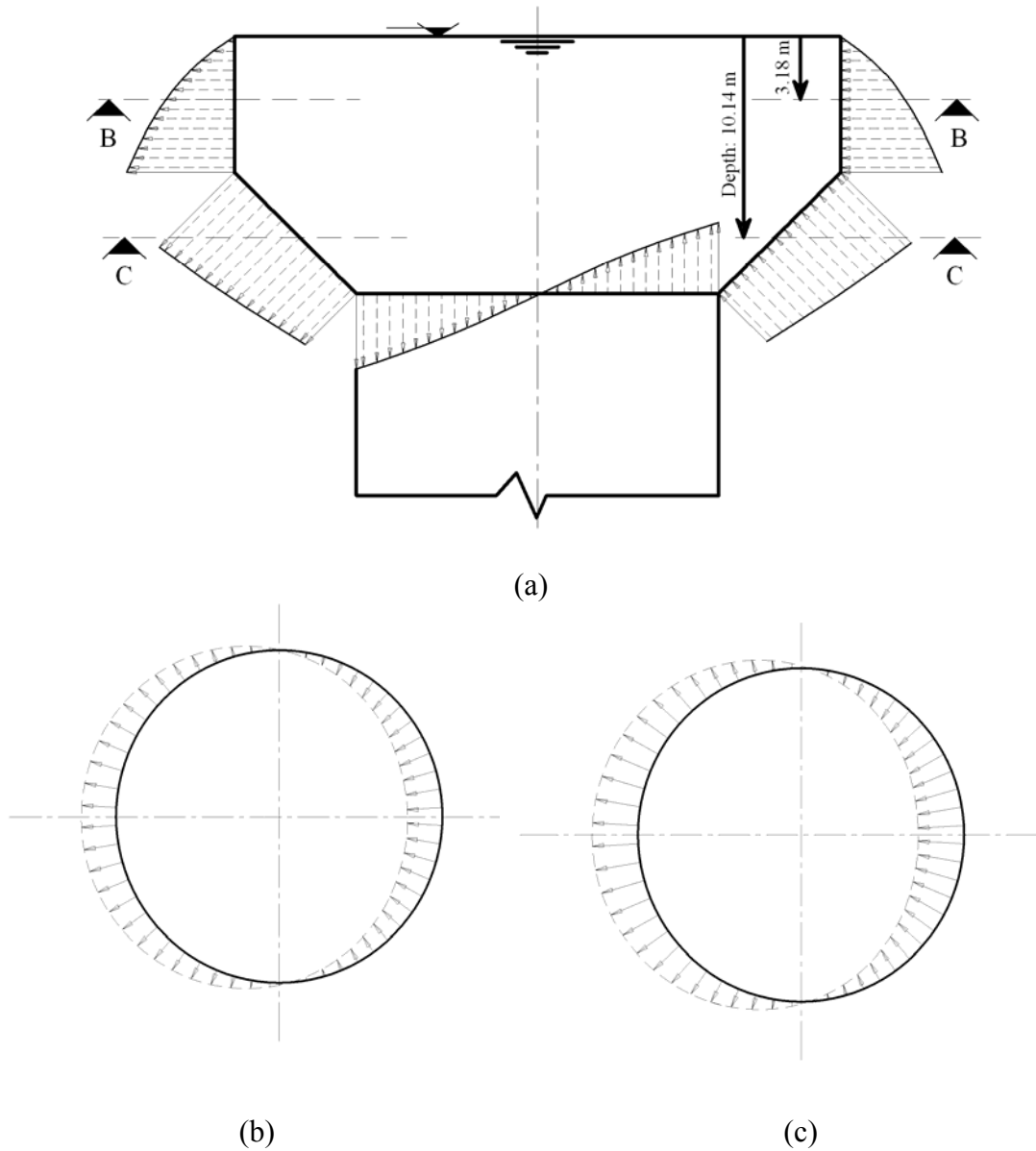
Figure 7.5 Pressure distribution corresponding to the fundamental impulsive mode (obtained

from FE modal analysis, pressure scale: 1/100); (a) Tank elevation, (b) Section B-B,

(c) Section C-C

The hydrodynamic pressure distribution on the tank floor shows an anti-symmetric variation

pattern about the centroidal axis of the shaft in both convective and impulsive fundamental

modes. As indicated in the figures, the pressure applied on the tank floor has an upward direction

on one half and downward direction on the other half with the maximum magnitudes occurring along the cone/floor interface and a zero value occurring along the centroidal axis of the tank floor.

7.4 Parametric study methodology

As mentioned before the FE spectral analysis using the ASCE 7-05 design spectrum is used to carry out this parametric study. The validity of this finite element technique in seismic analysis of conical elevated tanks was verified in Chapter 6. Using this technique, the hydrodynamic pressure distribution in a three-dimensional space corresponding to the convective and impulsive terms is determined separately. Important factors such as tank wall flexibility and liquid sloshing effects are also included in the analysis. The liquid sloshing behavior inside the vessel is modeled assuming a linear sloshing theory. The damping ratios of 5 and 0.5 percent are assumed for impulsive and convective modes of vibration, respectively.

Tank models used for this parametric study are assumed to have hinged connection at their base. Concrete shafts of three different ranges of stiffness; lower range (K_s= 1.3E8 N/m), median range (K_s= 4.5E9 N/m) and upper range (K_s= 1.4E10 N/m) are chosen for this study. The considered stiffness range covers a wide spectrum of shaft stiffness variation typically found in practice today. The parameters selected for this study are shown in Figure 7.6. The parameters are defined as follows:

r_t : Radius of the cylindrical steel shell

R_{root} : Radius of the supporting shaft

h_{top} : Freeboard (distance between the water free surface and the roof)

h_3 : Height of water in the cylindrical portion of the tank

h_c : Height of the conical portion of the tank

181

hshaft : Height of the supporting shaft

tcyl : Average thickness of the cylindrical portion of the tank

tcon : Average thickness of the conical portion of the tank

tfloor : Thickness of the tank's floor

tshaft : Thickness of the concrete shaft wall

teta : Cone angle
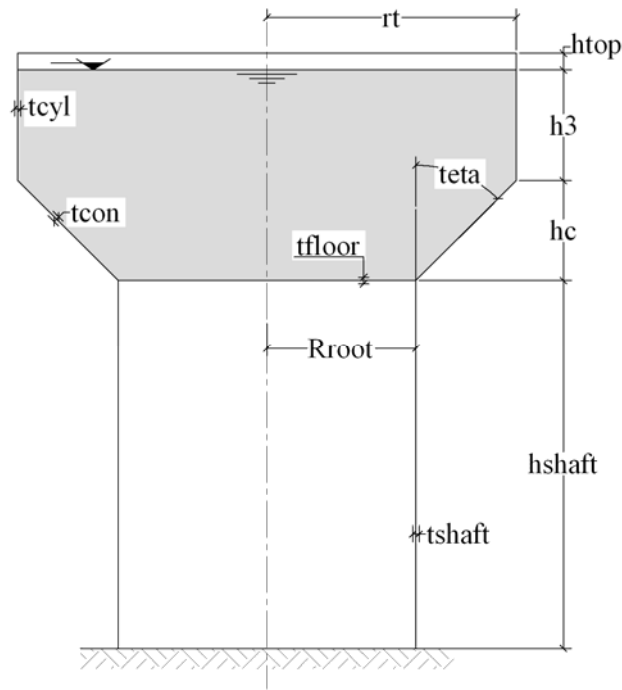
Figure 7.6 Parameters defined for the parametric study

In total, 243 elevated tank models were created throughout this parametric study. On each model, two different types of analysis; modal and spectral were performed. The tank configurations considered for this study cover "Rroot/h3" ratios varying from 0.40 to 1.30, and "hc/h3" ratios varying from 0.40 to 1.00. This results in a wide range of tank capacities encompassing form the smallest to the largest conical elevated tanks ever built in practice. It should be noted that for the cone angle "teta" to remain at 45°, the ratio of "rt/h3" should be

selected equal to the summation of the ratios "hc/h3" and "Rroot/h3" for each tank configuration under consideration.

The value of parameter "htop" is considered to be equal to 0.50 m for all elevated tank models analyzed. In addition, the value of parameter "teta" is kept constant at 45° for all models considered throughout this parametric study.

FE models are created using the parametric model specifically written for this parametric study using the ANSYS command lines. Detailed discussion on this parametric model can be found in Appendix B.

For all models, the mass densities of 1000 kg/m^3, 7898 kg/m^3, and 2400 kg/m^3 are assumed for water, steel, and concrete materials, respectively. All structural parts are modeled assuming linear elastic material. The Young's modulus of 200 GPa and 24.86 GPa are used for steel and concrete materials, respectively. Furthermore, Poisson's ratios corresponding to steel and concrete materials are assumed to be 0.30 and 0.16, respectively. The stored fluid is modeled using eight-node brick fluid elements and the structural domain is modeled using four-node quadrilateral shell elements having six degrees of freedom (translations and rotations) per node.

Based on the results obtained from this parametric study, a number of pressure graphs presenting the pressure distribution along the height of the tank wall are determined for both convective and impulsive components. The graphs are plotted as normalized wall pressure (Pc/Sac/WL) or (Pi/Sai/WL) versus water depth ratio (h/hl), where "Pc" and "Pi" represent the convective and impulsive pressure values in N/m^2, respectively. "Sac" and "Sai" are the spectral accelerations in m/s^2 corresponding to the convective and impulsive modes, respectively. "WL" is the weight of the contained water in Newton (N) and "hl" is the height of the water inside the tank in meter (m).

In plotting these pressure graphs, the values of spectral accelerations (Sai and Sac) were calculated based on the ASCE 7-05 design spectrum using the natural periods of impulsive and convective modes, respectively obtained from the FE modal analysis. In doing so, the values of "Importance factor" I=1 and "Response modification coefficient" R=1 were chosen as per ASCE 7-05. Furthermore, the mapped spectral accelerations (S_S and S_1) were selected as 1.5g and o.6g, respectively. Site class "A", representing a site with hard rock soil was also assumed in determining these accelerations.

7.5 Sensitivity studies

Prior to performing the parametric study, a set of sensitivity analyses were carried out to investigate the sensitivity of the proposed quantities (Pc/Sac/WL) and (Pi/Sai/WL) to different parameters such as floor thickness "tfloor" and plate thickness along the cylindrical "tcyl" and conical "tcon" portions of the vessel.

7.5.1 Effect of floor thickness variation

In order to examine the effect of floor thickness variation on the normalized pressure distribution, three different tank models having different floor thicknesses are considered. The assumed tank models have the following properties in common:

h3 = 6.85 m,   hc = 4.28 m,   hshaft = 22.0 m,   htop = 0.5 m,   rt = 12.42 m,

Rroot = 8.13 m,   tcyl = 8.83 mm,   tcon = 24.51 mm,   tshaft = 381 mm.

The tank has the full capacity of 4755 m^3 (1.26 MG). Three different values of floor thickness "tfloor" equal to 250 mm, 330 mm, and 450 mm are chosen and the resulting

normalized pressure distribution corresponding to the convective (Pc/Sac/WL) and impulsive
(Pi/Sai/WL) components along the height of the tank wall are calculated (see Figure 7.7).

(a)

(b)
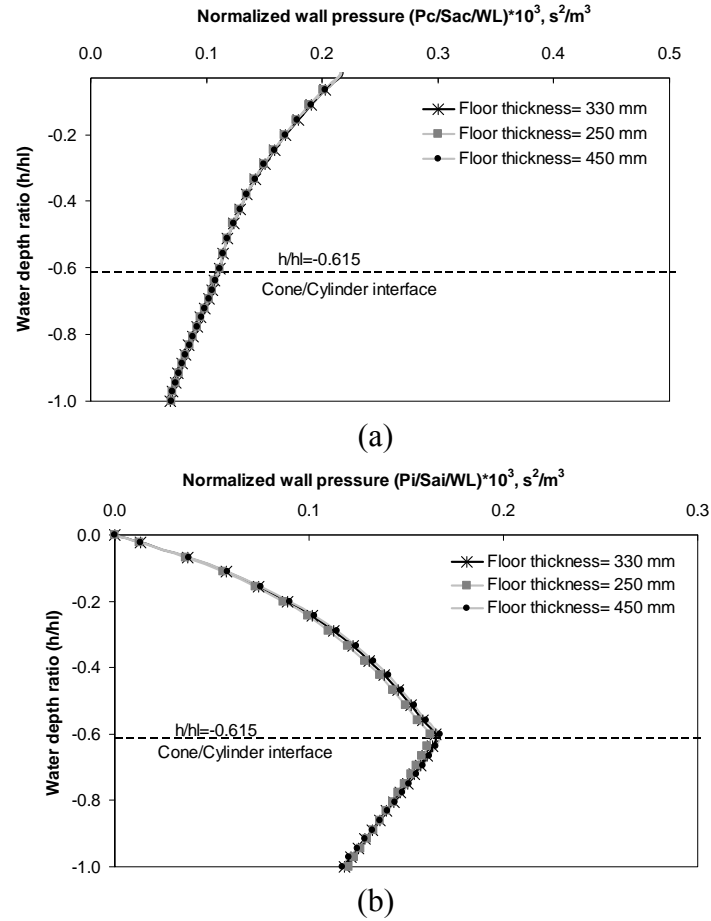
Figure 7.7 Pressure distribution over the tank wall (Effect of floor thickness variation);

(a) Convective pressure, (b) Impulsive pressure

As obvious from Figure 7.7, normalized pressure distribution is almost independent of the
floor thickness variation. This trend is observed for both convective and impulsive response
components.

7.5.2 Effect of plate thickness variation

In this section the effect of plate thickness variation on the normalized pressure distribution is investigated by selecting three different tank models having different plate thicknesses. The following properties are common to the three elevated tank models considered:

h3 = 6.85 m,   hc = 4.28 m,   hshaft = 22.0 m,   htop = 0.5 m,   rt = 12.42 m,

Rroot = 8.13 m,   tshaft = 381 mm,   tfloor = 330 mm.

The geometry of the tank is the same as that explained in the previous subsection. However, in order to examine the effect of plate thickness variation on the proposed normalized pressure quantity, three different values of plate thicknesses "tcyl" and "tcon" are chosen.

As mentioned above, three different tank models are created by doubling (2t) and halving (0.5t) the plate thicknesses "tcyl" and "tcon". The original plate thicknesses (t) corresponding to the cylindrical and conical portions of the vessel are 8.83 mm and 24.51 mm, respectively. The resulting normalized pressure distributions along the height of the tank wall corresponding to these three models are indicated in Figure 7.8. Consequently, as indicated in Figure 7.8, the proposed normalized pressure quantity can be considered independent of the plate thickness variation. This is true for both convective and impulsive terms.

As a result, it can be concluded that by normalizing the obtained pressure values with respect to the spectral accelerations (Sac and Sai), one can omit the sensitivity of the hydrodynamic pressure to the variation of floor and plate thicknesses. This reduces the number of parameters required to perform the parametric study yielding considerable reduction in computational efforts.

186
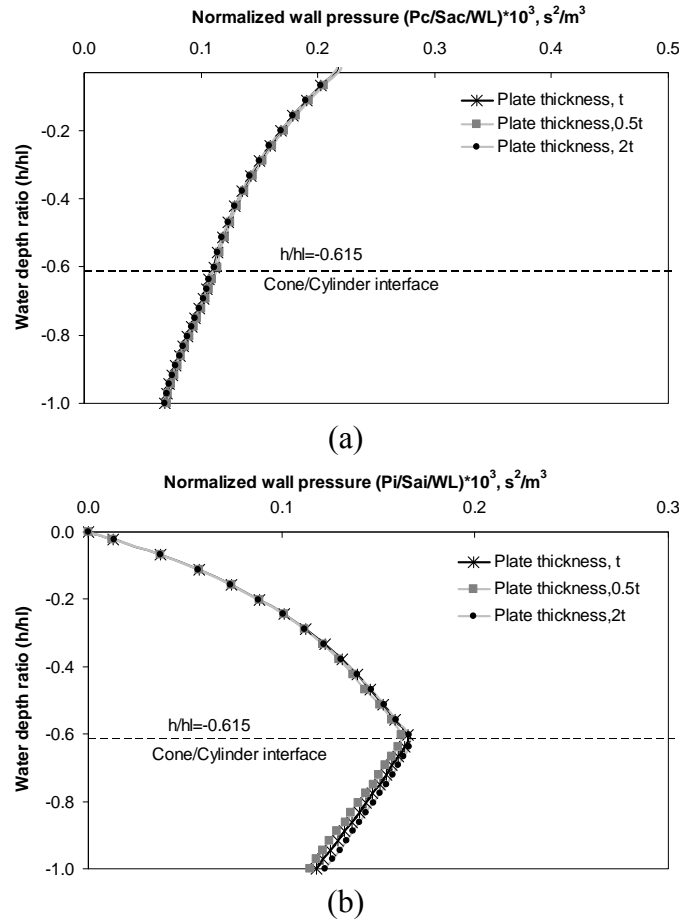
Figure 7.8 Pressure distribution over the tank wall (Effect of plate thickness variation);

(a) Convective pressure, (b) Impulsive pressure

The normalized convective and impulsive pressure graphs obtained through this parametric study corresponding to the three different ranges of shaft stiffness considered are given in Figure 7.9 and Figures C.1 through C.26 in Appendix C. The pressure graphs are calculated for "Rroot/h3" ratios varying from 0.40 to 1.30, and "hc/h3" ratios varying from 0.40 to 1.00. The graphs show the normalized pressure distribution along the height of the tank wall. The heights corresponding to the cone/cylinder interfaces are also shown in the figures by horizontal dashed lines.
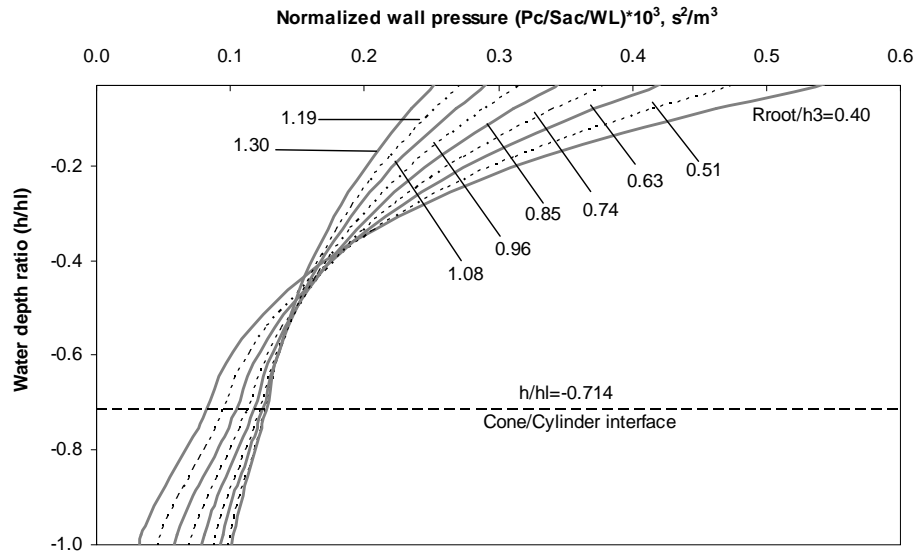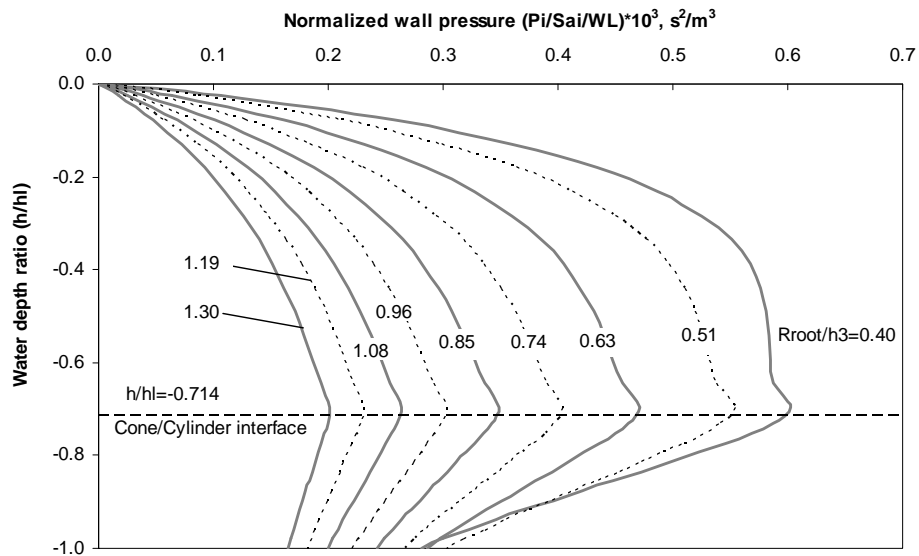
Figure 7.9 Pressure distribution over the tank wall for Ks= 4.5E9 N/m and hc/h3=0.4;

(a) Convective, (b) Impulsive

As shown in the figures, it can be noticed that as the Rroot/h3 ratio increases, the normalized impulsive wall pressure decreases gradually while keeping a similar pressure distribution pattern over the tank height. Observing the given convective pressure graphs, it can be noted that an

increase in the Rroot/h3 ratio results in a decrease in the normalized convective wall pressure for the upper sections of the tank, whereas a reverse trend is observed for the lower sections. Moreover, it can be noticed that the convective pressure reaches its maximum value at the water free surface while the impulsive pressure reaches its peak value at the cone/cylinder interface with the zero magnitude occurring at the fee surface.

7.6 Verification study

In order to examine if the proposed pressure graphs are capable of estimating the seismic response of liquid-filled conical elevated tanks accurately; a verification study is conducted on two randomly selected elevated tank models.

7.6.1 Elevated tank model A

The tank configuration considered for this part of verification study is that of an actual elevated tank situated in the U.S. The selected tank is a 1945 m^3 elevated water storage tank with dimensions as specified in Figure 7.10. Hinged boundary condition is assumed at the base of the tank. Other geometric properties not indicated in the figure are expressed below:

side shell thickness: 6.9 mm

cone thickness: 11.4 mm

tank floor thickness: 533 mm

shaft thickness: 300 mm

A distributed mass (total mass 115×10^3 kg) accounting for the equivalent mass of the platforms inside the pedestal with their full live load is applied at 20.3 m above the base. In addition, a distributed mass balance of 111×10^3 kg accounting for the mass of the components of

189

the tank (e.g. roof, access tube, etc.) is assigned at the ring beam level. The material properties defined for water, concrete and steel parts of the model are as explained before under section 7.4 of this chapter. The finite element idealization of the tank is also indicated in Figure 7.10.

(a)   (b)
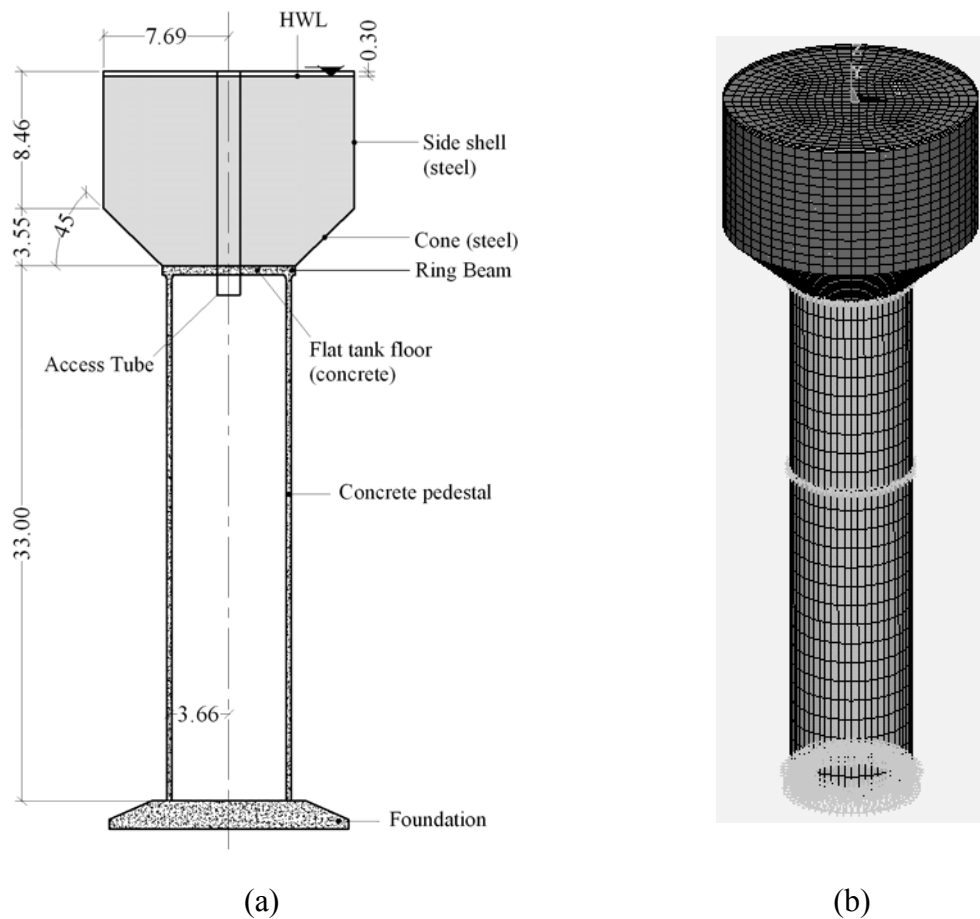
Figure 7.10 Elevated tank model A; (a) Tank geometry, (b) 3D FE model

The peak values of shear and overturning moment at the base of the tank due to lateral seismic excitation are obtained using three different methods; FE time-history analysis, "current practice" method (described under section 6.2.1.1), and finally the method presented in this chapter using the proposed parametric pressure graphs. The response values are obtained for

convective and impulsive components separately. The results of FE-time history analysis are used to assess the adequacy of the other two methods mentioned above.

The same FE technique as that explained previously in Chapter 6 is utilized here for determining the transient response of the selected elevated tank model under a random ground excitation. The validity of this method was verified formerly in Chapter 6.

The tank is subjected to the horizontal component of 1940 El-Centro ground motion with the peak ground acceleration of 0.32g. The earthquake record is shown in Figure 6.8. The direct integration method with an integration time step of 0.005 second is used. Sloshing effect is also included in the time history analysis. The damping ratios of 5 and 0.5 percent are assigned for impulsive and convective components, respectively. Moreover, the damping ratios of 5 and 2 percent are assumed as structural damping for concrete and steel parts of the tank model, respectively. Figure 7.11 illustrates the time history results for the elevated tank model. The maximum absolute response values obtained through FE time-history analysis are given in Table 7.1.

(a)   (b)

Figure 7.11 Impulsive time history results for the elevated tank model A; (a) Base shear,

(b) Base moment

191

Table 7.1 Peak base shear and base moment response values for the elevated tank model A

| | FE time-history | | | | Current practice | | | | Pressure graphs | | | |
| | Convective | | Impulsive | | Convective | | Impulsive | | Convective | | Impulsive | |
	Max value	Ratio	Max value	Ratio	Max value	Ratio	Max value	Ratio	Max value	Ratio	Max value	Ratio
Base shear (kN)	723	**1.00**	4865	**1.00**	687	**0.95**	4968	**1.02**	743	**1.03**	5332	**1.09**
Base moment (kN.m)	30747	**1.00**	182080	**1.00**	30208	**0.98**	195727	**1.07**	30942	**1.01**	200275	**1.10**

Using the two-mass idealization approach recommended by "current practice", two modes of vibration with the natural periods of 4.21 sec and 1.01 sec corresponding to the fundamental convective and impulsive modes, respectively are identified. These period values are in excellent agreement with the natural periods of 4.23 sec and 1.11 sec obtained from a modal FE analysis.

In calculating the response values using the current practice method, the values of "Importance factor", I=1 and "Response modification coefficient" R=1 are used. Furthermore, the design spectrum scaled to a peak ground acceleration of 0.32g to correspond with the earthquake record used in FE time-history analysis is employed. The mapped spectral accelerations (S_S and S_1) for Imperial Valley location are determined as 1.5g and o.6g, respectively per ASCE 7-05. Moreover, site class "A" representing a site with hard rock soil is chosen to correspond with the rigid ground boundary condition assumed in FE modeling of the tank.

Using the formulations given in section 6.2.1.1, one can calculate the base shear values of 687 kN and 4968 kN corresponding to the convective and impulsive terms, respectively. Furthermore, based on the current practice approach, the base moment values of 30208 kNm and 195727 kNm are found for convective and impulsive components, respectively. The calculated

convective and impulsive terms may be combined by SRSS method to determine the total response values of the tank-pedestal system.

As a third and final method, the seismic response of the elevated tank model is calculated by applying the appropriate pressure values obtained from the proposed pressure graphs. The selected tank model has the shaft stiffness of about 1.3E8 N/m, and the aspect ratios Rroot/h3 and hc/h3 of 0.43 and 0.42, respectively. Therefore, the appropriate pressure values are obtained by interpolating between the values determined from the curves corresponding to the aspect ratios of Rroot/h3=0.4 and 0.51 and also hc/h3=0.4 and 0.475. In interpolating the pressure values, graphs corresponding to the shaft stiffness of Ks= 1.3E8 N/m are used.

Entering the natural periods of 4.23 sec and 1.11 sec corresponding to the fundamental convective and impulsive modes, respectively into the El-Centro response spectrum, the spectral acceleration of Sai=0.27g for impulsive and Sac=0.06g for convective mode are obtained. The 5% and 0.5%-damped response spectra scaled to the peak ground acceleration of 0.32g are used for impulsive and convective modes, respectively. Substituting these spectral accelerations (Sai and Sac) along with the weight of stored water (WL) into the normalized pressure values obtained from interpolation, the actual hydrodynamic pressure values can be computed. The resulting convective and impulsive pressures are shown in Figure 7.12.

As shown in the figure, the convective pressure has the peak value of 6.2 kPa at water free surface, while the impulsive pressure has the peak value of 21.8 kPa at cone/cylinder interface. For the sake of simplicity, the equivalent linear approximation may be used instead of the exact pressure distribution by equating the area under the exact pressure distribution curve to the area under the idealized linear approximation curve, as indicated in Figure 7.12.

Figure 7.12 Pressure distribution over the tank wall (elevated tank model A);

(a) Convective pressure, (b) Impulsive pressure

The obtained pressure values are applied to the model with a cosine variation pattern around the tank circumference and the corresponding values of base shear and base moment due to convective and impulsive water components are obtained by performing a simple static analysis. The empty tank's inertial effects are included by performing a spectral analysis on the empty structure using the El-Centro response spectrum. Using only the fundamental mode having the natural period of T= 0.42 sec is sufficient to accurately estimate the seismic response of the empty tank.

The response of the empty tank is considered to be in phase with the response due to the vibration of the impulsive water. As a result, the total impulsive response may be determined by simply adding these two response components together. However, the total response of the tank may be calculated by combining the total impulsive response explained above with the response due to convective behaviour using a SRSS combination method. The obtained impulsive and convective response values are given in Table 7.1.

As presented in Table 7.1, in general using both "current practice" and proposed pressure graphs has resulted in a precise estimation of base shear and base moment values under both convective and impulsive vibrations. However, current practice has underestimated the convective base shear and base moment by about 5% and 2%, respectively.

Utilizing the proposed pressure graphs has led to a slight overestimation of the convective base shear and base moment by only 3% and 1%, respectively. This approach also produces a reasonable overestimation of the impulsive base shear and base moment of approximately 9% and 10%, respectively which seems appropriate for design applications.

7.6.2 Elevated tank model B

The elevated tank model considered for this part is the same tank that was described in Chapter 6, section 6.2.3. The chosen tank has the water storage capacity of 7571 m^3. All properties of the tank model are given in Chapter 6. Similar to previous section, the peak values of base shear and base moment are determined using three different approaches; FE time-history analysis, "current practice" method, and the method presented in this chapter using the proposed parametric pressure graphs. The horizontal component of 1940 El-Centro ground motion with the peak ground acceleration of 0.32g is applied to the model as lateral excitation. The damping ratios of 5 and 0.5 percent are used for impulsive and sloshing components, respectively. The maximum absolute response values obtained through three different approaches are given in Table 7.2.

Similar to the procedure described in previous section, one can calculate the base shear values of 2156 kN and 32778 kN using current practice corresponding to the convective and

impulsive terms, respectively. Based on the current practice approach, the base moment values of 91588 kNm and 1215668 kNm are obtained for convective and impulsive terms, respectively.
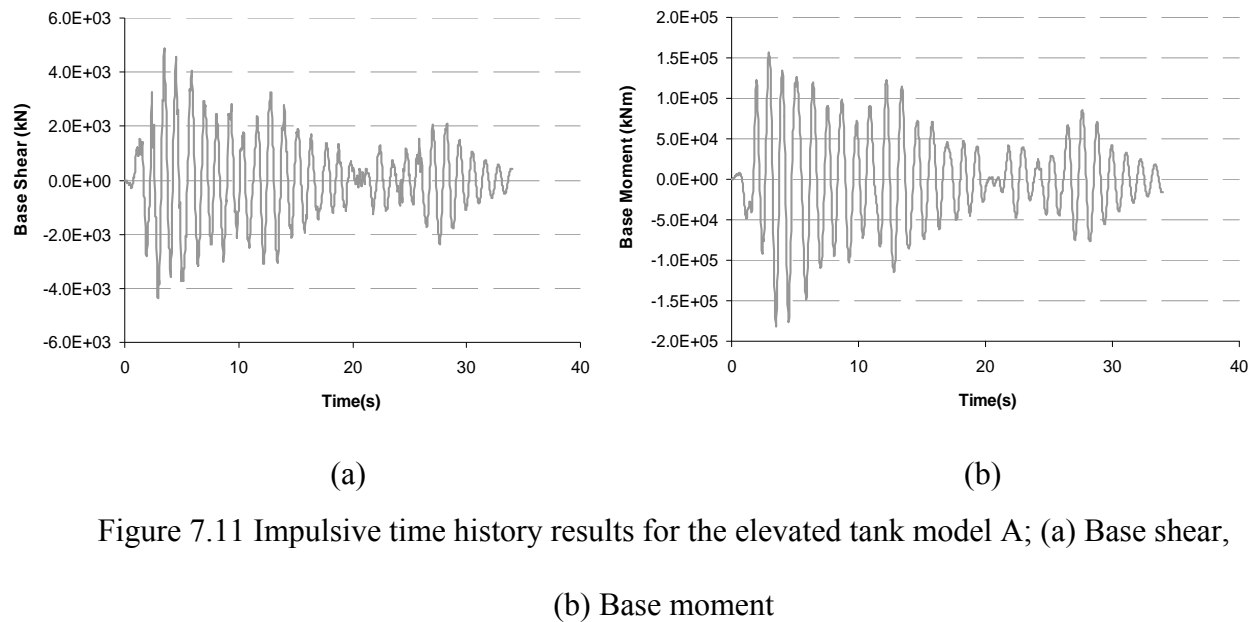
Table 7.2 Peak base shear and base moment response values for the elevated tank model B

	FE time-history				Current practice				Pressure graphs			
	Convective		Impulsive		Convective		Impulsive		Convective		Impulsive	
	Max value	Ratio	Max value	Ratio	Max value	Ratio	Max value	Ratio	Max value	Ratio	Max value	Ratio
Base shear (kN)	2487	**1.00**	35548	**1.00**	2156	**0.87**	32778	**0.92**	2661	**1.07**	38036	**1.07**
Base moment (kN.m)	94023	**1.00**	1320592	**1.00**	91588	**0.97**	1215668	**0.92**	98724	**1.05**	1465857	**1.11**

As a third approach, the seismic response of the elevated tank model is determined by applying the appropriate pressure values obtained from the proposed pressure graphs. The selected tank model has the shaft stiffness of about 4.5E9 N/m, and the aspect ratios $R_{root}/h3$ and $h_c/h3$ of 1.3 and 0.90, respectively. Therefore, the appropriate pressure values are calculated by interpolating between the values determined from the curves corresponding to the aspect ratios of $h_c/h3$=0.85 and 0.925. In interpolating the pressure values, graphs corresponding to the shaft stiffness of K_s= 4.5E9 N/m and aspect ratio of $R_{root}/h3$=1.3 are used.

Entering the natural periods of 6.2 sec and 0.51 sec corresponding to the fundamental convective and impulsive modes, respectively into the El-Centro response spectrum, the spectral acceleration of S_{ai}=0.88g for impulsive and S_{ac}=0.067g for convective mode are obtained. The 5% and 0.5%-damped response spectra scaled to the peak ground acceleration of 0.32g are used for impulsive and convective modes, respectively. Substituting these spectral accelerations (S_{ai} and S_{ac}) along with the weight of stored water (W_L) into the normalized pressure values

obtained from interpolation, the actual hydrodynamic pressure values can be computed. The resulting convective and impulsive pressures are shown in Figure 7.13.
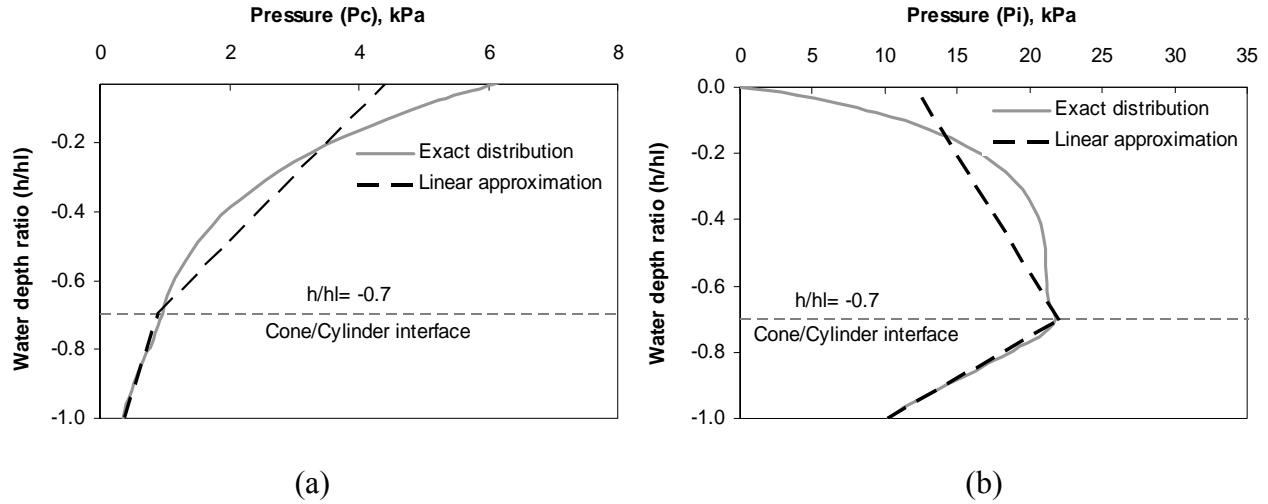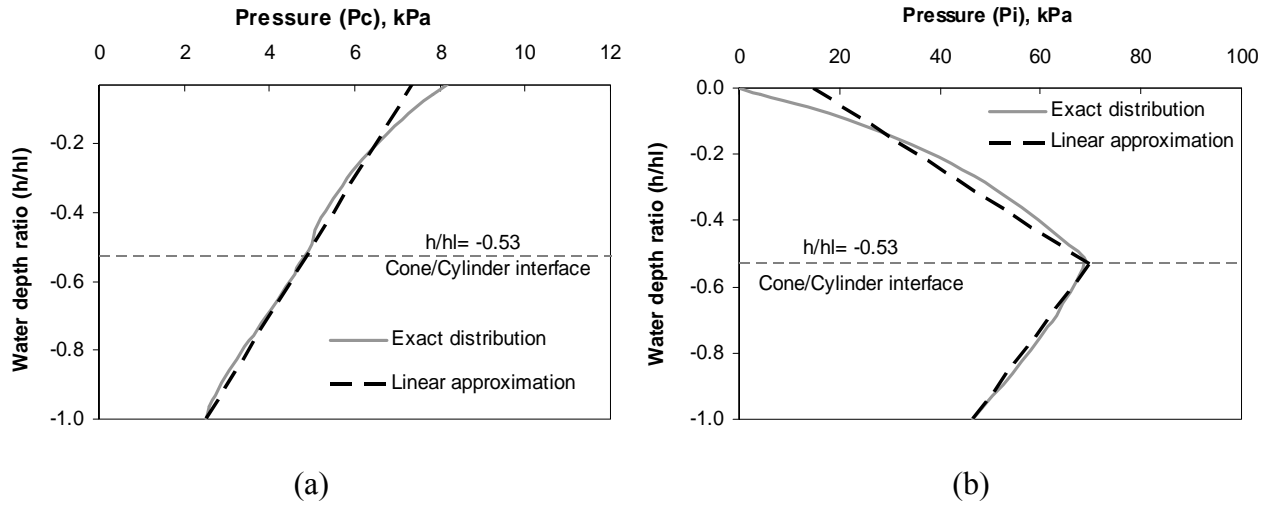

Figure 7.13 Pressure distribution over the tank wall (elevated tank model B);

(a) Convective pressure, (b) Impulsive pressure

As shown in the figure, the convective pressure has the peak value of 8.2 kPa at water free surface, while the impulsive pressure has the peak value of 68.6 kPa at cone/cylinder interface. The equivalent linear approximation is also indicated in the figure. Similar to the procedure described in the previous section, one can calculate the corresponding values of base shear and base moment due to convective and impulsive components by applying the obtained pressure values to the model. The calculated values are listed in Table 7.2.

As presented in Table 7.2, an accurate estimation of results is obtained using the proposed pressure graphs for both convective and impulsive response components of the medium-capacity tank model under consideration. Employing the proposed pressure graphs has resulted in a slight overestimation of the convective base shear and base moment by only 7% and 5%, respectively.

A reasonable overestimation of around 7% and 11% is also obtained using this procedure for impulsive base shear and base moment, respectively. As a result, a designer can use this approach with confidence to accurately estimate the response values in seismic design of liquid-filled conical elevated tanks.

7.7 Summary

In this chapter, a comprehensive parametric study was carried out on liquid-filled conical elevated tanks using a detailed FE technique in a three-dimensional space. Based on the results of this study, the convective and impulsive pressure values can be separately determined along the height of the tank wall for typical elevated water tanks found in practice today.

In performing this parametric study, the effects of tank wall flexibility and sloshing of the water free surface were considered. The study covered a wide range of tank dimensions and geometries commonly found in current practice. The effects of deciding parameters such as shaft stiffness, tank radius, shaft radius, height of contained water, tank height and so on were taken into consideration in this parametric study.

Through this parametric study, the normalized pressure distribution graphs corresponding to the convective and impulsive components were obtained for a wide range of varying parameters by carrying out FE spectral analyses on a large number of conical elevated tanks. Spectral analyses were performed using ASCE 7-05 design spectrum. The graphs were plotted as normalized wall pressure (Pc/Sac/WL) or (Pi/Sai/WL) against water depth ratio (h/hl).

Based on the results of the sensitivity studies conducted, it was concluded that the proposed normalized pressure quantities (Pc/Sac/WL and Pi/Sai/WL) were almost insensitive to the variations of plate thickness along the cylindrical and conical portions of the vessel. This study

also demonstrated the independence of the proposed normalized pressure quantities from the variations of tank's floor thickness. Thus, it was concluded that the sensitivity of the hydrodynamic pressure to the floor and plate thickness variations can be removed by normalizing the hydrodynamic pressure with respect to the spectral accelerations.

In the first part of the chapter, the effect of inclusion of the roof on dynamic response of the conical elevated tanks was investigated by carrying out FE analyses on an open-topped and a roofed tank model and comparing the obtained response values. It was observed that the effect of inclusion of the roof on dynamic response of such structures was insignificant and as a result its effect was neglected throughout the parametric study.

A detailed explanation was provided on the exact pressure distribution patterns on the wall and the floor of conical elevated tanks under lateral seismic excitations. This was achieved by conducting a free vibration FE analysis on a typical liquid-filled elevated tank. Both convective and impulsive modes of vibration were included for this part of the study.

The validity of the calculated pressure graphs was verified by performing a comparison study between the proposed pressure graph method as the investigated method and the pre-verified FE time history method as the control method. For comparison purposes, the obtained results were also compared with those recommended by current practice. Based on the results of this verification study, it was concluded that the proposed normalized pressure graphs could be utilized with high level of accuracy for seismic design of liquid-filled conical elevated tanks.

CHAPTER 8

APPLICATION OF PERIOD ADJUSTMENT AND SEISMIC

ISOLATION TECHNIQUES TO CONICAL ELEVATED TANKS

8.1 Introduction

In the present chapter, the applicability of two techniques to liquid-filled conical elevated tanks is investigated. These techniques are proposed by Kumieda (1976) which are used for reducing the effect of seismic excitation being input to the structure. Two different techniques will be proposed and their application to elevated water tanks will be addressed.

The chapter is divided into two main parts. In the first part of the chapter, the first technique called *"Natural period adjustment method"* is introduced. In this technique, the seismic response of the elevated tank model can be reduced by increasing its natural period far beyond the predominant period of the input motion. This can be achieved by providing some soft portion within the tank structure itself to extend its natural period. In other words, the earthquake induced response of the structure is reduced by providing a more flexible structural design which can in turn be accomplished by making alterations in tank's configuration/geometry. The effect of such modification on dynamic response of elevated water tanks is investigated in this study by performing FE time-history analyses on various tank-pedestal models having different configurations/geometries.

The second part of the chapter addresses the application of "*isolation method*" to liquid-filled conical elevated tanks. In this technique, the supporting shaft structure is isolated either from the ground or the vessel mounted on top by means of seismic isolators such as lead-rubber

and elastomeric bearings. Devices such as lead-rubber bearings may also be considered as energy dissipaters which are capable of absorbing the input seismic energy.

The application of these two innovative menshin (earthquake reduction) techniques for elevated water tanks will be investigated in detail throughout this chapter using a rigorous finite element method (FEM). The proposed FEM is capable of simulating the accurate 3D behavior of the isolated elevated tanks involving the nonlinear hysteretic behavior of seismic isolators.

8.2 Natural period adjustment method

The main focus of this section is on the effect of cone angle on the seismically induced response of the supporting structure in liquid-filled conical elevated tanks. Finite element (FE) technique is used to investigate such effect. This FE technique was explained in detail in previous chapters in this thesis. Using this technique, the seismic behavior of elevated water tanks having different cone angles under random excitation is investigated.

Effects of tank wall flexibility, damping properties of impulsive and convective components of water, sloshing of the water free surface and both translational and rocking motions of the supporting shaft are accounted for in the FE analysis. Moreover, the contribution of impulsive and convective components of the response is accounted for separately.

The primary objective of this part of study is to evaluate the effect of the inclined cone angle of the lower portion of the combined vessel on the dynamic behavior of the entire structure. In the construction of vessels, the slope is usually assumed as 45°. The effect of varying slope ranging from 45° to 90° is examined. To do so, the time history response of the considered tank-pedestal models with different cone angles is obtained using modal superposition technique. The selected elevated tank models are subjected to a unidirectional horizontal seismic excitation and

the corresponding transient base shear and base moment response values at the base of the shaft structure are determined. Furthermore, to examine the accuracy of current practice a comparison between the finite element results and those recommended by current practice is also made. The current practice method is explained in detail under sections 6.2.1.1 and 6.2.5.

As per ACI 371R-08 (2008) for all models under consideration, a sufficient number of modes (both impulsive and convective) to reach a cumulative modal mass participation of at least 90% of the total mass of the system in the excitation direction are used.

In total, five elevated tank models are employed for FE analyses. The geometry and other considerations taken into account in modeling of the tanks are described below.

8.2.1 Tank models

The elevated tank models considered in this study are assumed to have hinged condition at the base. The original model (Model A) is a 7571 m^3 (2 MG) actual elevated water tank located in the U.S. Five different models are considered in which they have different cone angles but with constant depth of water. Model A has a cone angle of 45°. Models B, C, D, and E are created by increasing the angle (α) measured from the inclined cone interface of model A around point A by 15, 30, 37.5, and 45 degrees, respectively. This results in cone angles (β) of 45, 60, 75, 82.5, and 90 degrees corresponding to models A, B, C, D, and E, respectively. The heights of the cylindrical and conical portions of the vessels are kept constant. The tank floor cantilever length (X) is then determined as a distance between the intersection point of cone-tank floor center layers and the outer surface of the shaft. Therefore, by increasing the cone angle, the tank floor cantilever length (X) is increased as shown in Figure 8.1. All models have the same shaft height, shaft radius, and shaft thickness. Moreover, steel vessels of different models have similar

202

plate thicknesses, top cylinder radius, and cylindrical and conical heights. The simplified geometry of the model is shown in Figure 8.1. All dimensions shown are in meters. Both modal and time history analyses are carried out. Other properties of the model not indicated in the figure including the properties assumed for the contained water, steel and concrete shell materials are the same as those described in Chapter 6 under section 6.2.3.

For modeling the tanks, 16464 three-dimensional fluid elements along with a number of shell elements ranging from 2996 to 3220 are used. For the sake of brevity, only the finite element configurations of models A and C are indicated in Figure 8.2.
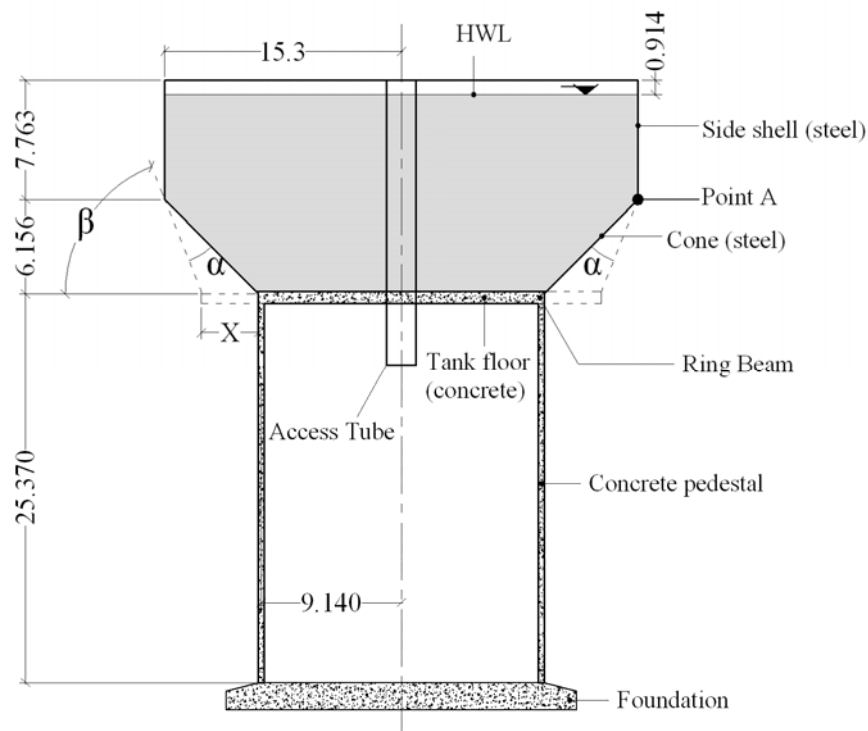
Figure 8.1 Simplified geometry of the elevated tank model

<div align="center">(a)   (b)</div>
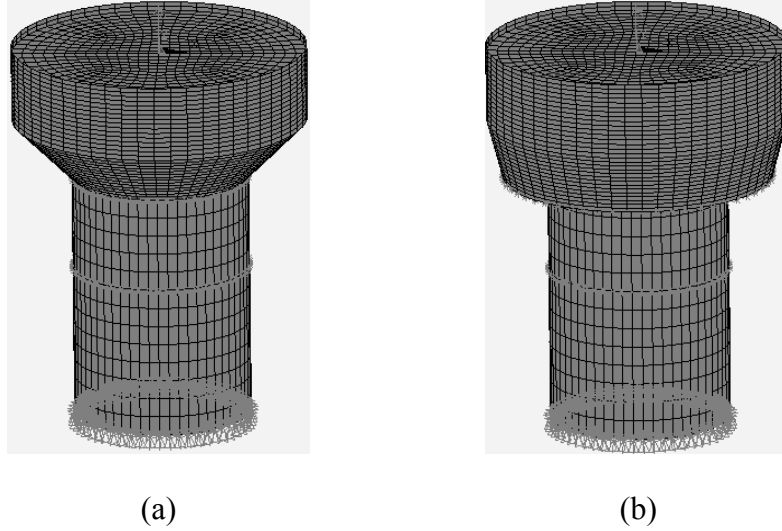
Figure 8.2 FE idealizations of the models; (a) Model A, (b) Model C

8.2.2 Time history-modal analysis

The ground motion used for the time history analysis is the horizontal component of 1940 El-Centro earthquake scaled to the peak ground acceleration of 0.4g as shown in Figure 8.3. An integration time step of 0.005 second is used for time history analysis of the tanks. In performing the modal superposition analysis, the constant damping ratios of 3 and 0.5 percent are assigned for impulsive and convective modes, respectively.
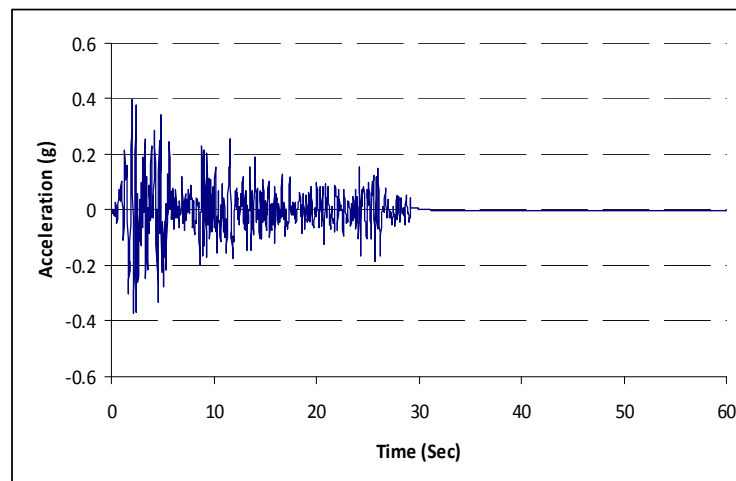
Figure 8.3 Scaled 1940 El-Centro ground motion, horizontal component (PGA=0.4g)

The free vibration analysis results are listed in Table 8.1. The fundamental sloshing and impulsive modes can be readily identified based on their high modal participation factors (β), as indicated in the table. The modal participation factors are normalized with respect to the largest participation factor among all modes of vibration. The ratio (R_i) given in the table is defined as the ratio of the effective modal mass to the total mass of the system in the direction under consideration. Water mass ratios and fundamental sloshing frequencies calculated from Housner's method (Housner (1963)) are also given in the table. In using Housner's method, the vessels are assumed to be rigid.

Comparing the mass ratios obtained for different models, it can be observed that by increasing the cone angle from 45° to 90°, the convective mass ratio decreases gradually while an inverse trend is observed for the impulsive mass ratio. This trend is similar for both FE and Housner's methods. This is due to the fact that as the cone angle increases, the equivalent depth of water (corresponding to the equivalent cylindrical model) increases too. As a result, a higher aspect ratio (liquid height to diameter ratio "Hl/D") is obtained for a model with a larger cone angle which results in an increase in the impulsive mass and a decrease in the convective mass ratios. This is a well-established relationship reported by many researchers (Housner (1963), Haroun and Housner (1981A), and Veletsos (1984)) and standards (ACI 350.3-06).

By reviewing the table, it can be observed that the calculated FE results compare very well with those given by Housner's method which is based on the concept of equivalent cylinder model. Such agreement is especially more noticeable between the computed natural frequencies. In all cases considered, the difference in convective mass values is less than 5 percent of the total mass of the contained water. A smaller difference of around 2 percent is observed for impulsive masses.

Table 8.1 Free vibration analysis results for elevated tank models

Model A (45°)						
Mode		**Frequency(Hz)**		**Effective mass**	**∑R$_i$ (%)**		**β**
Number	**type**	**FE**	**Housner**	**× 10^3 kg (FE)**	**FE**	**Housner**	**(normalized)**
*1	Convective	0.161	0.160	4302.51	58.7	56	1.00
2	Convective	0.161		235.38			0.23
3	Convective	0.294	NA	141.63			0.18
1	Impulsive	1.955	NA	918.36	41.3	40.4	0.46
*2	Impulsive	1.955		3367.52			0.88
3	Impulsive	7.470		228.14			0.23
4	Impulsive	7.470		561.35			0.36
5	Impulsive	8.560		308.23			0.15
Model B (60°)							
Mode		**Frequency(Hz)**		**Effective mass**	**∑R$_i$ (%)**		**β**
Number	**type**	**FE**	**Housner**	**× 10^3 kg (FE)**	**FE**	**Housner**	**(normalized)**
1	Convective	0.162	0.163	48.63	57	53.3	0.10
*2	Convective	0.162		4696.61			1.00
3	Convective	0.294	NA	83.93			0.13
4	Convective	0.294		69.03			0.12
*1	Impulsive	1.189	NA	3813.45	43	43.2	0.90
2	Impulsive	1.189		45.79			0.10
3	Impulsive	5.136		654.12			0.37
4	Impulsive	6.148		1410.52			0.55
Model C (75°)							
Mode		**Frequency(Hz)**		**Effective mass**	**∑R$_i$ (%)**		**β**
Number	**type**	**FE**	**Housner**	**× 10^3 kg (FE)**	**FE**	**Housner**	**(normalized)**
1	Convective	0.161	0.164	402.45	55.1	51.3	0.30
*2	Convective	0.161		4608.58			1.00
1	Impulsive	0.816	NA	452.44	44.9	45.4	0.31
*2	Impulsive	0.816		2541.24			0.74
3	Impulsive	0.818		351.28			0.28
4	Impulsive	4.656		652.25			0.38
5	Impulsive	4.656		1546.66			0.58
6	Impulsive	5.683		440.91			0.31

* Fundamental mode

Table 8.1 Free vibration analysis results for elevated tank models (continued)

Model D (82.5°)							
Mode		Frequency(Hz)		Effective mass × 10³ kg (FE)	∑R$_i$ (%)		β
Number	type	FE	Housner		FE	Housner	(normalized)
*1	Convective	0.161	0.165	5110.99	54.9	50.46	1.00
1	Impulsive	0.723	NA	129.54	45.1	46.4	0.16
*2		0.735		2895.07			0.75
3		0.740		177.19			0.19
4		4.354		2683.43			0.72
5		5.630		321.41			0.25
Model E (90°)							
Mode		Frequency(Hz)		Effective mass × 10³ kg (FE)	∑R$_i$ (%)		β
Number	type	FE	Housner		FE	Housner	(normalized)
*1	Convective	0.160	0.165	3621.79	54.6	49.6	1.00
2		0.160		1608.83			0.67
1	Impulsive	0.662	NA	55.09	45.4	47.4	0.12
2		0.665		463.00			0.36
3		0.665		61.23			0.13
4		0.673		1888.41			0.72
5		0.675		389.36			0.33
6		0.675		81.81			0.15
7		4.098		1099.53			0.55
*8		4.098		1938.09			0.73
9		5.608		217.11			0.24
10		10.325		91.15			0.16

* Fundamental mode

It is important to note that all fundamental sloshing modes corresponding to models under consideration have very close natural frequencies, however the effect of cone angle variations on the natural frequencies of the impulsive modes is more pronounced. This is because of the significant influence of cone angle variation on the relative stiffness distribution of structural

components which results in introducing new types of modes with different dynamic characteristics to the tank-pedestal system.

From the results given in Table 8.1, one can conclude that for all considered models, the sloshing behaviors of the models are almost dominated by their fundamental sloshing modes. However, this is not the case for the impulsive response of the models having relatively large cone angles (models C, D, and E). Calculated results show that for models A and B, fundamental impulsive modes dominate the impulsive response. However, in models C, D, and E with larger cone angles there are some modes having high contributions to the response that are not necessarily fundamental modes (having the highest participation factor). For example, in model D, the 4th mode has an impulsive mass participation very close to that of the fundamental mode (2nd mode). Therefore considering more impulsive modes other than the fundamental mode seems necessary in predicting the response of such models to horizontal ground motions.

It is found that all obtained impulsive modes for models A and B are translational modes. On the other hand, the fundamental modes of models C and D and also 4th mode of model E which has a very close effective mass and participation factor to that of the fundamental mode (mode 8 which is translational) are rocking type modes. The 5th mode of model C and 4th mode of model D which have the second highest participation factors among all impulsive modes are translational modes.

Considering the modal information given, one can conclude that the increase of cone angle (which corresponds to the increase of the unsupported cantilever length between the shaft wall and the cone shell) leads to introducing some rocking type modes (models C, D, and E) with high values of participation factors and effective mass ratios to the system.

As shown in Table 8.1, these rocking modes with high contributions to the response have relatively low natural frequencies compared to the typical translational modes and therefore have small associated response spectrum accelerations. Consequently, it is expected that the resultant base shear and overturning moment values of models with dominant rocking components (models C, D, and E) be smaller than those with dominant translational components (models A and B). This is further investigated in the next section by performing time history analyses on the models. For the sake of brevity, only a few number of mode shapes are presented in Figure 8.4. For a better view of the rocking mode shapes, only the associated shell deformations are displayed.

For quantitative comparison of the seismic response of considered models under random excitations, the time history values of base shear (V) and base moment (M) of the tank models subjected to El-Centro earthquake are obtained using the modal superposition technique. The modes listed in Table 8.1 are used to carry out such analyses. Time history results are separated into impulsive and convective terms. As a result, the maximum response values associated with each component (impulsive or convective) can be determined separately. Figures 8.5 and 8.6 illustrate the obtained time history results for all elevated tank models considered. The maximum absolute response values computed from the FE analysis are listed in Table 8.2. Given in the table, are also the maximum absolute response values normalized with respect to the total effective weight of the system (We).

Reviewing the obtained results listed in Table 8.2 reveals that cone angle variations could have a significant effect on the impulsive response of the system, however this effect is found to be negligible for the convective component. Comparing the normalized base shear and base moment ratios, it is further concluded that as expected model A with total base shear and base

209

moment ratios of 53.15% and 19.74 has the highest reaction forces compared to other models. On the other hand, model C with total base shear and base moment ratios of 22.84% and 6.58 has the lowest response values. The base shear and base moment of model C are only 43 and 33 percent of those of model A, respectively.

(a)

(b)

(c)

(d)
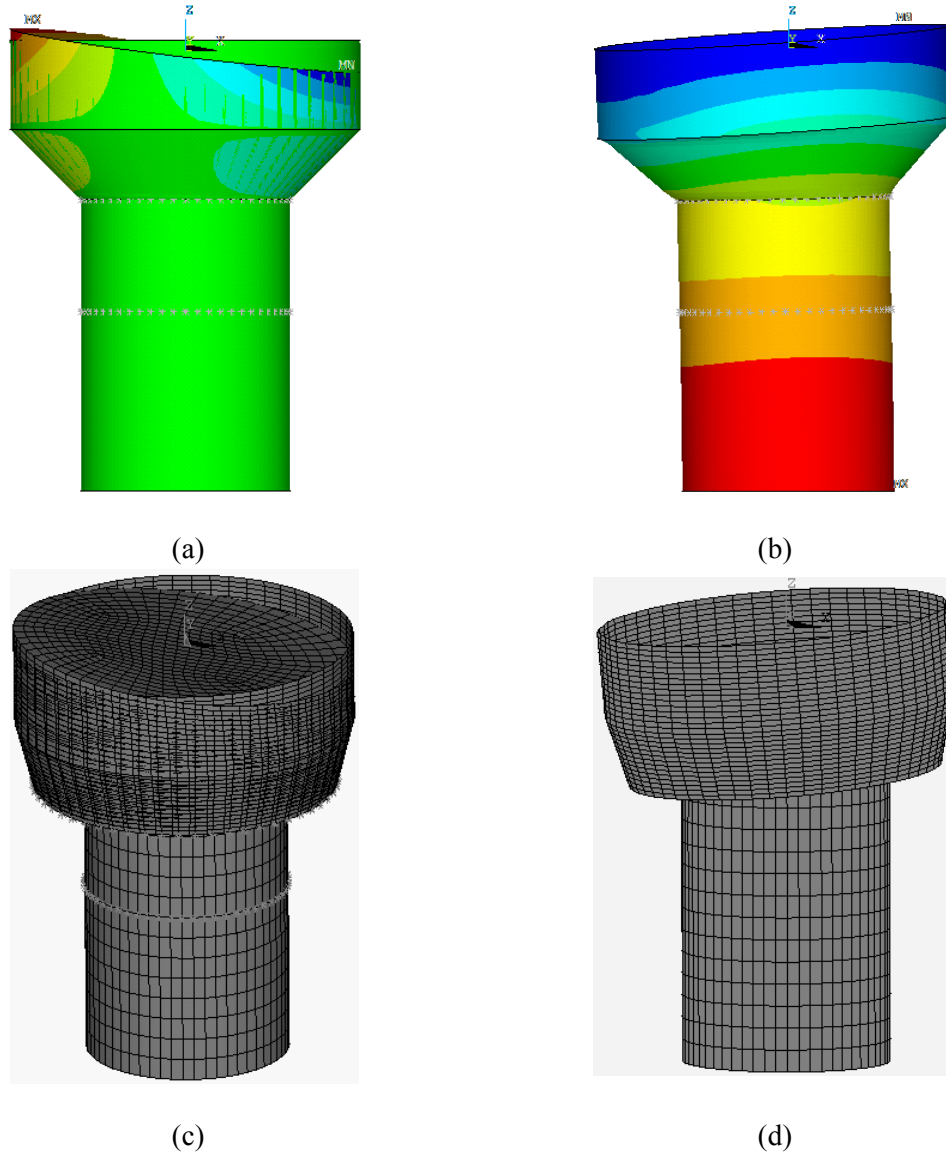
Figure 8.4 Fundamental mode shapes of elevated tanks; (a) Convective mode of Model A (side view), (b) Impulsive mode (Translational) of Model A, (c) Convective mode of Model C (3D view), (d) Impulsive mode (Rocking) of Model C
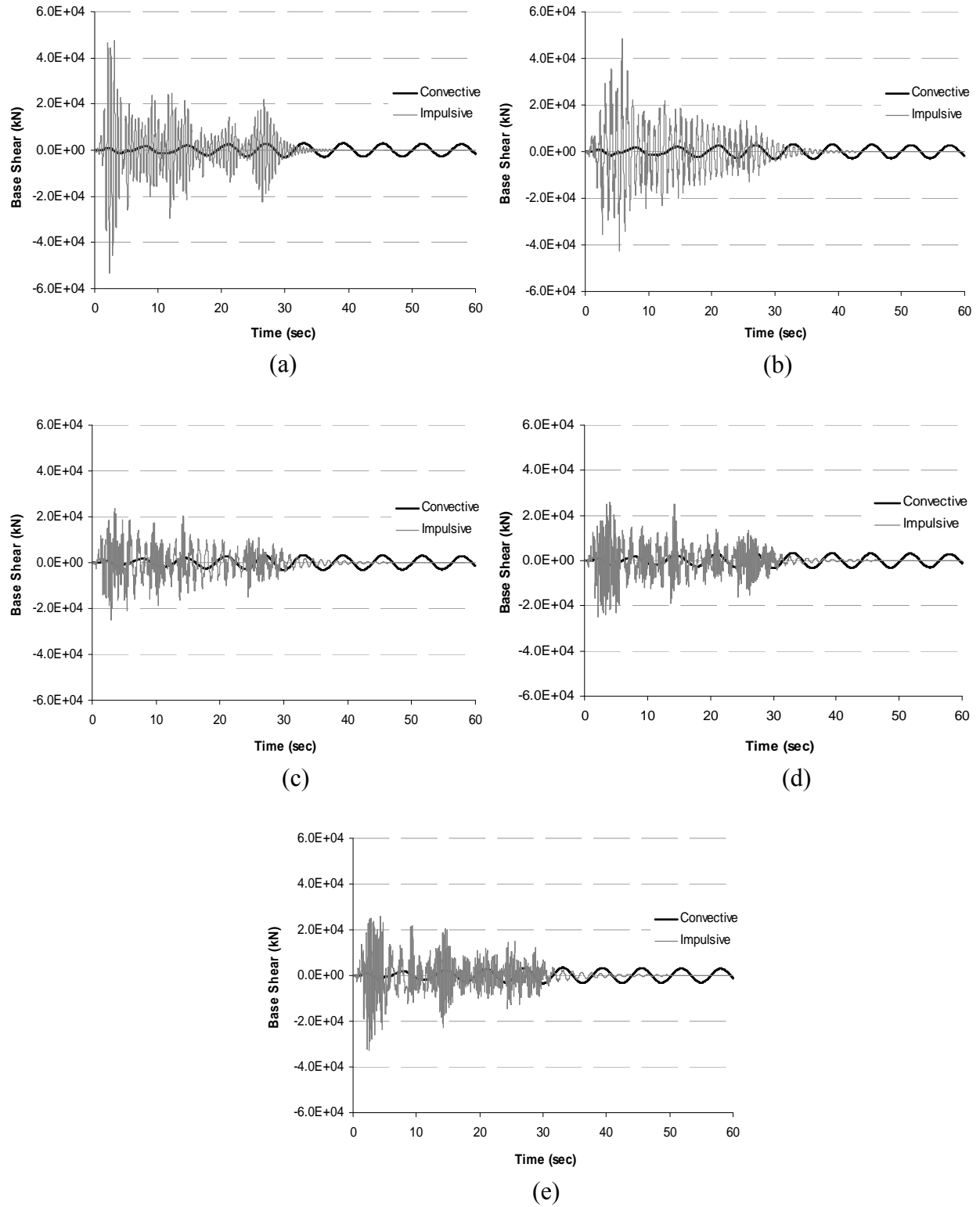
Figure 8.5 Time history results for base shear; a) Model A, b) Model B, c) Model C,

d) Model D, e) Model E

211
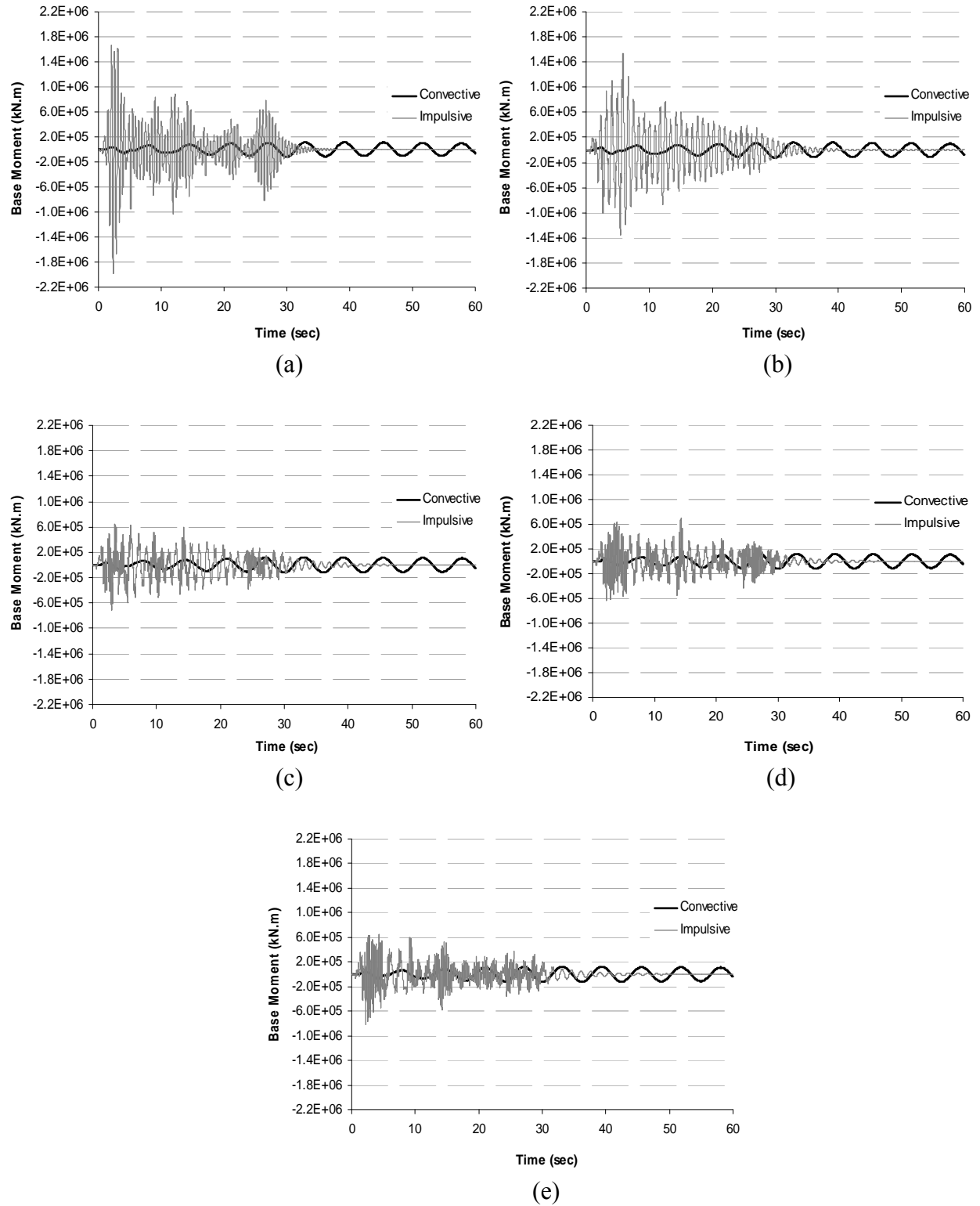
Figure 8.6 Time history results for base moment; a) Model A, b) Model B, c) Model C,

d) Model D, e) Model E

212

Table 8.2 Maximum absolute time history response values

Model	Base Shear (kN)					
	Convective		Impulsive		Total	
	Max value	Ratio(%) (Vc/We)	Max value	Ratio(%) (Vi/We)	Max value	Ratio(%) (V/We)
A	3108	3.15	53322	54.05	52440	53.15
B	3258	3.07	48530	45.73	48196	45.41
C	3315	3.07	24818	23.02	24627	22.84
D	3366	3.03	25741	23.19	27264	24.56
E	3432	3.03	32606	28.85	31624	27.98
Model	Base Moment (kN.m)					
	Convective		Impulsive		Total	
	Max value	Ratio (Mc/We)	Max value	Ratio (Mi/We)	Max value	Ratio (M/We)
A	117529	1.19	1980888	20.07	1947499	19.74
B	121358	1.14	1541155	14.52	1528799	14.40
C	122526	1.13	716878	6.65	709801	6.58
D	124011	1.11	704841	6.35	782770	7.05
E	125973	1.11	819312	7.25	782356	6.92

8.2.3 Effect of tank geometry

Table 8.2 shows that the selected models may be categorized into high (models A and B) and low (models C, D, and E) range of response values according to their normalized shear and moment ratios. In model A, the shaft, the floor and the cone center layers intersect at a common interface and as a result no relative rotations can occur between them. Because of the rigidity of the supporting shaft in the axial direction relative to its lateral direction, no rocking mode can be developed for such models (Model A and to some extent model B). The restraint against the rotation at the tip of the shaft, provided due to the overturning moment exerted at the top of the shaft, tends to increase the stiffness of the shaft. This increase in stiffness results in low natural

periods and therefore high response spectral accelerations (as can be observed for models A and B in Table 8.1).

When the cantilever length of the tank floor is large enough (models C, D, and E), dominant rocking modes with low natural frequencies and thus associated low response spectral accelerations are formed.

The fundamental mode type (translational or rocking) associated with each model, mainly depends on the proportion of lateral to rotational (at the base of the vessel) stiffness. Therefore, the judgment of fundamental mode type needs a rigorous analysis as done here. For models C and D, the rotational stiffness at the base of the vessel is smaller compared to the lateral stiffness of the shaft, while model E has relatively smaller lateral stiffness in comparison with its rotational stiffness. This is believed to be the reason as why the fundamental mode types of models C and D are rocking while that of model E is translational. This justifies the slight increase of normalized response ratios of model E relative to models C and D.

For all models considered, sloshing modes have a negligible contribution to the base shear and base moment response values. Among all models considered, the maximum contribution to the base shear response due to sloshing modes is observed in model A with the sloshing contribution of around 3% of the total effective weight of the system. However, for the same model the impulsive term is found to have a much higher contribution of around 54%.

Since the sloshing motion of the contained water is not in phase with the impulsive vibration of the tank-liquid system, in some of the cases including the sloshing effects has led to a slight reduction in the total response.

For comparison purposes, the peak base shear and base moment values obtained for all the models are normalized with respect to those of model A for which the highest response values are calculated (see Figure 8.7).
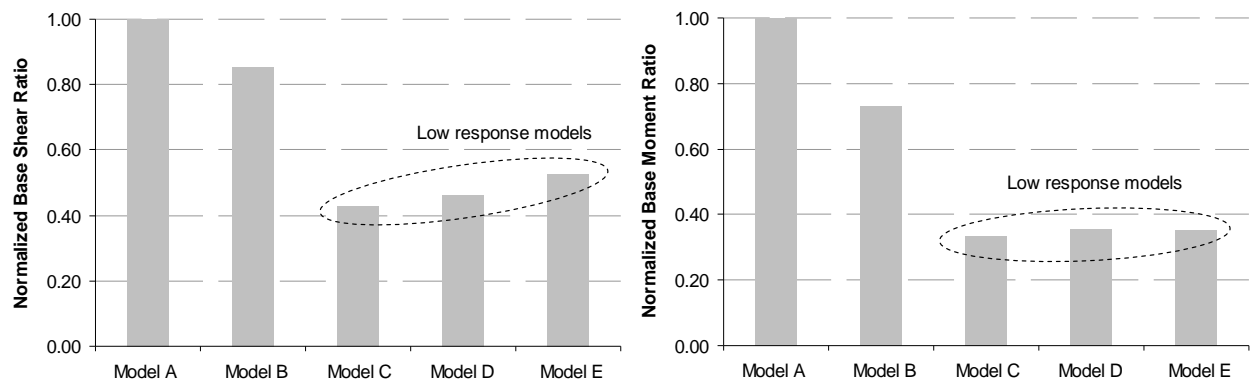
Figure 8.7 Normalized base shear and base moment ratios

Figure 8.7 shows that among the selected models, model C with the cone angle of 75° may be introduced as the optimum case with its base shear and base moment values being the lowest response values among all considered models. As presented in Table 8.2, the base shear and base moment response of the shaft may be decreased by a factor of 2.3 and 3.0 respectively by only increasing the cone angle from 45° (as in model A) to 75° (as in model C). This could lead to a more economical design of the shaft structure and the supporting foundation system. However, design considerations allowing for the probably large rotations associated with the rocking component of the response should be accounted for.

8.2.4 Comparison with current practice

In this section a comparison study is carried out between the FE method and the current practice in order to estimate the accuracy of the current practice in calculating the seismic response of the elevated tanks.

In computing the results using the current practice approach, the design spectrum scaled to the peak ground acceleration of 0.4g to match the seismic excitation used in FE time history analyses is used. The values of "Importance factor" I and "Response modification coefficient" R are considered as unity. Moreover, the mapped spectral accelerations (S_S and S_1) for Imperial Valley location are selected as 1.5g and o.6g, respectively. Site class "A", representing the hard rock soil is also assumed.

Following the current practice procedure explained in sections 6.2.1.1 and 6.2.5 leads to the total base shear and base moment values of 49243 kN and 1827092 kN.m, respectively for model A. Comparing these values with those of FE method given in Table 8.2, it can be observed that the current practice estimations are in reasonable agreement with those calculated through FE analysis for model A. For both base shear and base moment, the difference between the estimated results is only 6 percent. However, for models with dominant rocking behavior (models C, D, and E), the current practice highly overestimates the results, for instance as high as 2.2 times greater than those of FE for the base shear response of model C. The reason for such overestimation is that the current practice approach is not capable of accounting for the effect of rocking component of motion on the dynamic response of the tanks. Therefore, designing such models according to current practice will lead to an overdesign of the shaft structure and the supporting foundation system. To avoid this, a detailed dynamic analysis capable of accounting

for both translational and rotational (rocking) degrees of freedom of the shaft seems to be essential.

8.3 Seismic isolation method

8.3.1 Passive control bearings

Among different types of passive control devices, lead-rubber and elastomeric bearings are more widely used in today's practice. They offer a simple and economical solution for seismic isolation of structures. They have many features suiting them for use as efficient seismic isolators.

Elastomeric bearings are usually made with alternating relatively thin horizontal layers of rubber bonded to horizontal steel plates. They are generally preferred over plain rubber pads because of their superiority under compressive loads. The vertical stiffness of bearing is increased by the presence of these steel plates resulting in a relatively large overall vertical stiffness. However, a low level of horizontal stiffness is provided by the rubber layers under the lateral loads such as earthquake, wind, etc. Steel plates do not considerably change the shear stiffness.

A lead-rubber bearing is manufactured by inserting a lead plug down the centre of a laminated elastomeric bearing. This introduces a significant amount of hysteretic damping to the bearing leading to further improvement in the reduction of forces and moments. The lead material yields under a rather low level of shear stress and shows nearly an elastic-plastic behavior (Robinson (1982)). It also shows a good fatigue behavior under cyclic loading. Rubber bearings (both elastomeric and lead-rubber bearings) also increase the resonant period of the structure to a value out of the range of the ground motion's strong excitation. Lead-rubber

bearings provide the required amount of damping and the seismic isolation solution both in a single unit. This yields a cheap solution to the problems of seismic isolation.

There have been a number of experimental studies on the behavior of lead-rubber bearings in the past. However, only a few analytical research studies have been carried out on this type of isolators. This is because of the difficulties associated with modeling the lead-rubber bearings. Lead-rubber bearings consist of three different materials having different characteristics and behaviors. The main difficulty encountered in the modeling process of lead-rubber bearings results from the high nonlinearity of lead and rubber materials, incompressibility of rubber material, and also geometric nonlinearities associated.

8.3.2 Nonlinear modeling of rubber material

The behavior of rubber-like material is very complex. They usually behave elastically isotropic and can undergo large strains during a seismic event. The stress-strain relationship of rubber material can be highly nonlinear. The behavior of such materials can be accurately simulated by utilizing the hyperelastic models. Hyperelasticity is used for the materials capable of experiencing large elastic strain that is recoverable to the initial state. As a result, elastomers such as rubber and many other polymer materials can be considered in this category. Modeling of the nonlinear characteristics of rubber material can be achieved based on the theory of finite deformation.

There are several material constitutive models for modeling the isotropic behavior of the rubber material. The strain energy potentials are usually used to define the constitutive behavior of hyperelastic materials. The material is assumed to be purely incompressible. Assuming that the material behavior is isotropic, the strain energy potential can be conveniently expressed in

terms of principal stretch ratios (Simo and Hughes (1997)). In this study, the Ogden Potential constitutive model is used for large-strain analysis of rubber-like material (Ogden (1984) and Ogden (1986)). In hyperelastic models, the strain energy potential function (W) can be assumed to be a scalar function of one of the strain or deformation tensors. The derivative of the strain energy potential with respect to a strain component gives the corresponding stress component. The Ogden type of strain energy potential is expressed as:

$$W = \sum_{i=1}^{N} \frac{\mu_i}{\alpha_i} (\bar{\lambda}_1^{\alpha_i} + \bar{\lambda}_2^{\alpha_i} + \bar{\lambda}_3^{\alpha_i} - 3) + \sum_{k=1}^{N} \frac{1}{d_k} (J-1)^{2k} \tag{8-1}$$

where,

N = the order of the Ogden Potential function

μ_i, α_i, d_k = material constants

J = the ratio of the deformed elastic volume over the undeformed volume of material (for incompressible material $J = 1$)

$\bar{\lambda}_1, \bar{\lambda}_2, \bar{\lambda}_3$ = modified principal stretch ratios

Usually, a higher N result in a better fit the exact solution; however orders of N > 3 may cause numerical difficulty in fitting the material constants. In this study, the Ogden Potential model of order 3 (N = 3) is used.

The principal stretch ratio is expressed as:

$$\lambda_i = 1 + \varepsilon_i \tag{8-2}$$

where, ε_i is the principal value of the engineering strain tensor in the ith direction.

The initial shear modulus of the material (μ) is defined as:

$$\mu = \frac{1}{2} \sum_{i=1}^{N} \alpha_i \mu_i \tag{8-3}$$

The initial bulk modulus is given as:

$$K = \frac{2}{d_1} \qquad\qquad (8\text{-}4)$$

Constant d_1 can thus be considered as material incompressibility parameter. It is obvious that the accurate estimation of results during a hyperelastic analysis highly depends on the accurate assessment of the material constants given in Eq. (8-1). Rubber material constants are usually derived using experimental stress-strain data. In the current study, the test data reported by Treloar (Treloar (1944) and Treloar (1975)) are used to characterize the rubber material constants. Treloar performed three different types of experiments; uniaxial tension, equibiaxial tension, and pure shear on samples cut from a sheet of Vulcanized natural rubber. These test data cover several modes of deformation and a wide range of strain values. The rubber material constants are then fit using these test data in all three deformation states simultaneously. Combination of test data from multiple deformation states improves the simulation of the hyperelastic behavior of the material.

The nonlinear least squares fit analysis is performed in this study in order to determine the rubber material constants. By carrying out this analysis, the Ogden Potential constants can be calculated from experimental stress-strain data given by Treloar. In the least squares fit analysis method, the sum of the squared error between experimental and theoretically predicted stress values is minimized. The sum of the squared error can be expressed as follows:

$$E = \sum_{i=1}^{n} (T_i^{E} - T_i(C_j))^{2} \qquad\qquad (8\text{-}5)$$

in which:

E = least squares residual error

T_i^{E} = experimental stress values

$T_i(C_j)$ = engineering stress values (function of material constants)

n = number of experimental data points

In order to minimize the above equation, the variation of the squared error should be set to zero i.e. $\delta E = 0$. This results in a set of equations which can be solved simultaneously to determine the hyperelastic material constants;

$$\frac{\partial E}{\partial C_1} = 0 \, , \; \frac{\partial E}{\partial C_2} = 0 \, , \, \ldots \, , \text{ etc.}$$

The optimum material constants were calculated using the least squares fit optimization methodology for the three types of Treloar's test data (uniaxial tension, equibiaxial tension, and pure shear) simultaneously. The optimal values of μ_i and α_i are given in Table 8.3. Since the incompressible material is assumed here for hyper rubber under consideration (i.e. $J = 1$), the parameters d_k in Eq. (8-1) have no effect on the stress computations and therefore need not to be determined. Utilizing these constants, one can calculate the nominal stress (engineering stress) for different values of engineering strain (ε) which are depicted in Figure 8.8 for the three different deformation states. Indicated in the figure, are also the experimental data measured by Treloar. As evident from these figures, the considered rubber material parameters lead to superior fit to all three test data for the entire range of strains. This verifies the validity of the assumed hyperelasticity model, the parameter identification scheme and the estimated rubber material constants listed in Table 8.3.
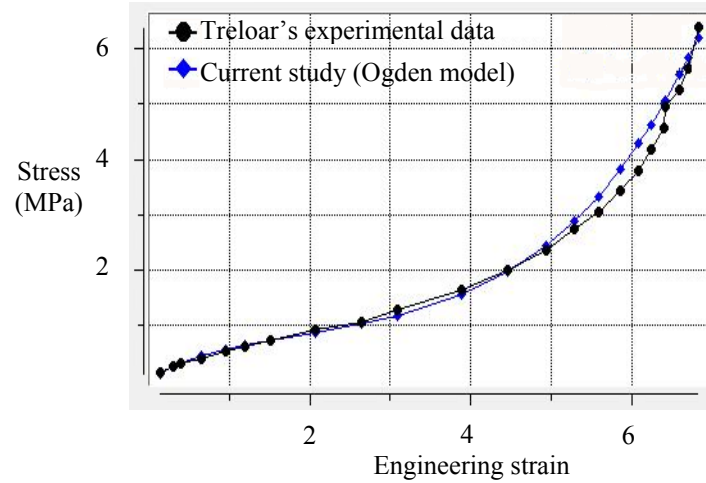
(a)
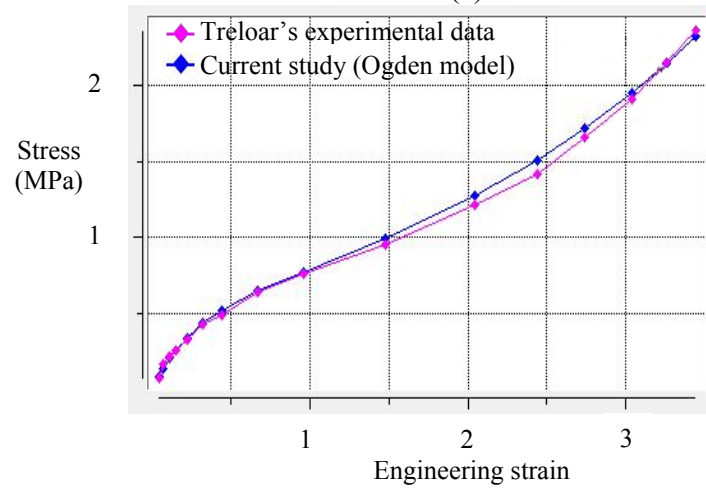
(b)
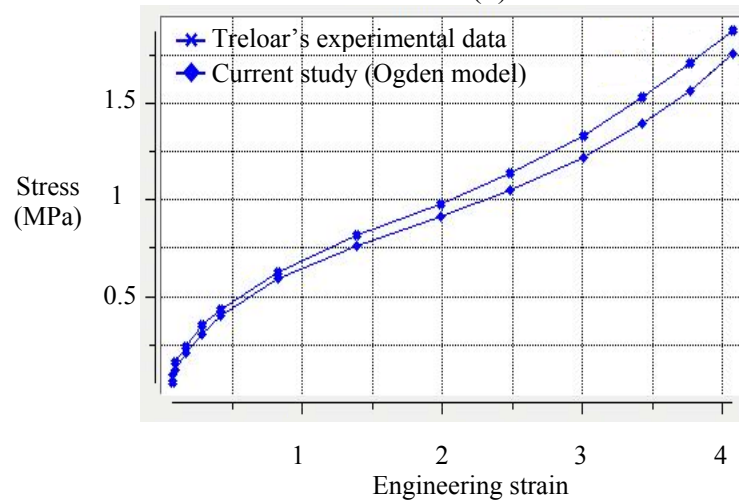
(c)

Figure 8.8 Stress-strain results for rubber material using three types of test data (N=3),

(a) uniaxial tension, (b) equibiaxial tension, (c) pure shear

222

Table 8.3 Optimal values of rubber constants using three test data simultaneously (N=3)

Material constant (Pa)	Value
μ_1	483387
α_1	1.52
μ_2	-21634
α_2	-1.78
μ_3	188
α_3	5.93

8.3.3 Verification study

8.3.3.1 FE modeling of lead-rubber and elastomeric bearings

In this section, numerical analysis using an elaborate finite element technique is performed to analyze the behavior of rubber bearings subjected to a combination of compression and shear forces. Solid 185 element from the ANSYS® library of elements is used for the 3D FE modeling of the lead, steel, and rubber parts of the bearings. The element has eight nodes and three degrees of freedom at each node (translations in x, y, and z directions). The element is capable of modeling both plasticity and hyperelasticity behaviors. Solid 185 element is particularly designed for simulating material behavior with high incompressibility such as purely or nearly incompressible hyperelastic materials (high poisson's ratio) and elastoplastic materials (experiencing large plastic deformations). The element offers a variety of options in handling incompressible hyperelastic material behavior. The Ogden type constitutive model explained in the previous section is used here for simulating the nonlinear behavior of rubber.

The "classical bilinear kinematic hardening" plasticity algorithm is adopted to capture the nonlinear behavior of mild steel and lead materials. This plasticity algorithm uses the Von Mises yield criterion together with the kinematic hardening rule. The stress-strain behavior corresponding to this plasticity option is plotted in Figure 8.9 (a). Indicated in the figure is also

the stress space for this plasticity algorithm. The surfaces indicated in Figure 8.9 (b) are the yield

surfaces, that is, any stress state inside the surface leads to an elastic response of the material (no

plastic strain is developed). In kinematic hardening rule, it is assumed that the size of yield

surface remains unchanged and as the yielding progresses the yield surface translates into stress

space, as shown in Figure 8.9 (c). The following properties are assumed for the steel, lead, and

rubber materials:

| Steel material:	Lead material:	* Rubber material:
Young's modulus= 205 GPa	Young's modulus= 16 GPa	Poisson's ratio= 0.499
Tangent modulus= 20.5 GPa	Tangent modulus= 45 MPa	Density= 1150 kg/m^3
Yield stress= 275MPa	Yield stress= 12 MPa	Initial shear modulus= 0.39MPa
Poisson's ratio= 0.28	Poisson's ratio= 0.44	
Density= 7850 kg/m^3	Density= 11300 kg/m^3	* Other properties for rubber
		material are given in Table 8.3.

(a)   (b)

(c)
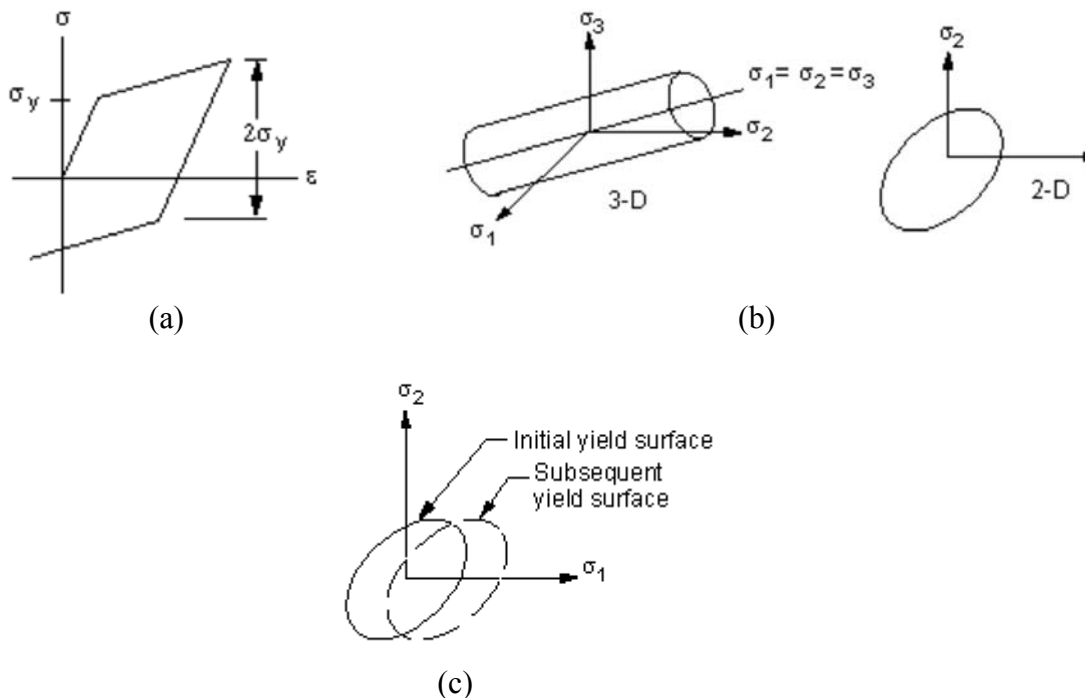
Figure 8.9 Bilinear kinematic hardening plasticity algorithm; (a) stress-strain behavior,

(b) yield surfaces, (c) kinematic hardening rule

8.3.3.2 Comparison of results with experimental data

In order to validate the FE implementation process, the results obtained through FE analysis are compared with those measured through experiments. The boundary conditions defined for the FE models are in conformity with the actual conditions of the test.

Two full-scale lead-rubber bearings with the experimental data available are analyzed here using the proposed 3D FE procedure. The first bearing is a lead-rubber shear damper consisting of a 100 mm-diameter lead core inserted in the center of a 356×356×140 mm elastomeric bearing. The role of the lead core is to increase the initial stiffness of the bearing and also to increase the capacity of the isolator to dissipate energy. The bearing consists of seven mild steel plates with the thickness of 3-mm and six rubber layers with the thickness of 16mm. Two steel plates with the thickness of 20 mm are attached to the top and bottom faces of the bearing. These plates are intended to connect the bearing to the structure and also help distribute the applied forces. The experiment on this bearing was reported by Robinson and Tucker (1981). The simplified geometry of the bearing along with its corresponding FE model are shown in Figure 8.10.

First, an incremental load of 400 kN is applied vertically to the bearing. Then a lateral force of 100 kN is applied on the uppermost steel plate with a given compressive load (400 kN) being retained. All degrees of freedom of the nodes located on the lowermost steel plate boundary are restrained. Automatic time stepping feature of the software is used during the solution process. This feature automatically optimizes the number of loading sub steps required for obtaining the solution according to the response frequency and the nonlinearity effects experienced during the solution phase. If the convergence is not obtained during a specific load step, the algorithm automatically retreats to the previous converged solution and adjusts the load increment size

225

accordingly so that convergence is reached. The force-displacement curves corresponding to the experimental and numerical approaches are indicated in Figure 8.11. As shown in the figure, a good correlation between FE and experimental results has been generally obtained. The FE approach predicts a relatively stiffer response for the unloading part of the hysteretic loop.
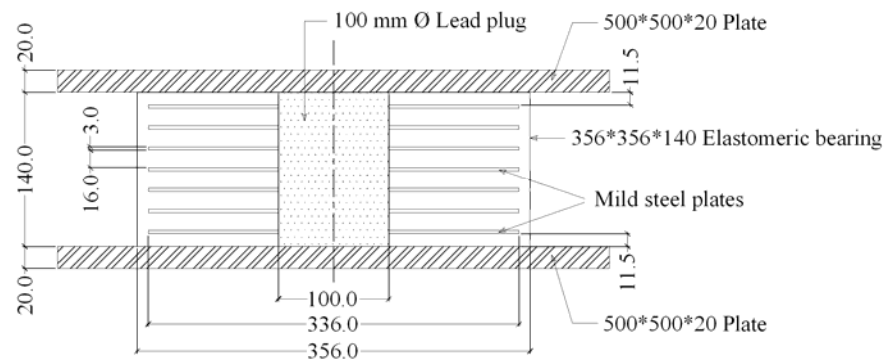
(a)
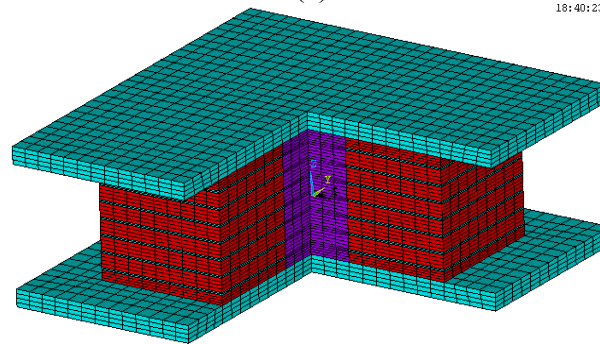
(b)

Figure 8.10 "356×356×140" mm lead-rubber bearing; (a) simplified geometry, (b) 3D finite element model

The deformed shape of the bearing corresponding to loading points A, B, and C indicated on the force-displacement curve of the bearing is shown in Figure 8.12. Figure 8.12(a) indicates the deformed shape of the bearing under pure compression. Figures 8.12(b) and (c) present the

deformed shapes of the model subjected to a combination of compression and shear. The presented deformed meshes show the considerable geometric nonlinearities involved in the analysis of rubber bearings. As evident from the figures, rubber layers are excessively bulged under the applied loads.
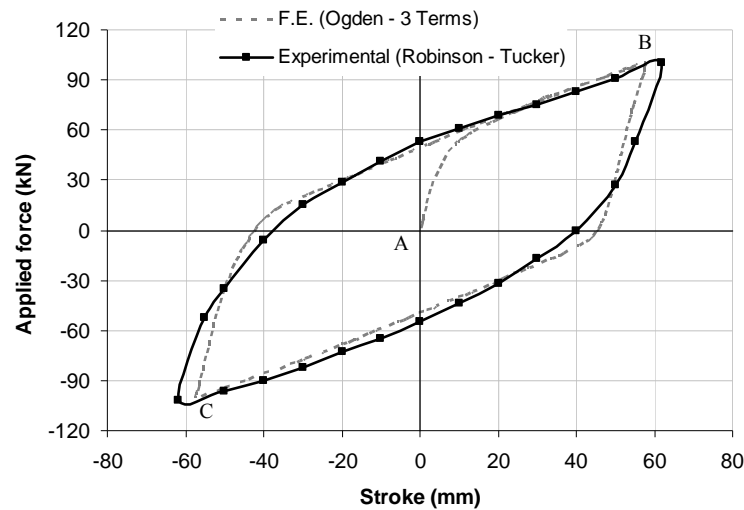

Figure 8.11 Force-displacement diagram for "356×356×140" mm lead-rubber bearing
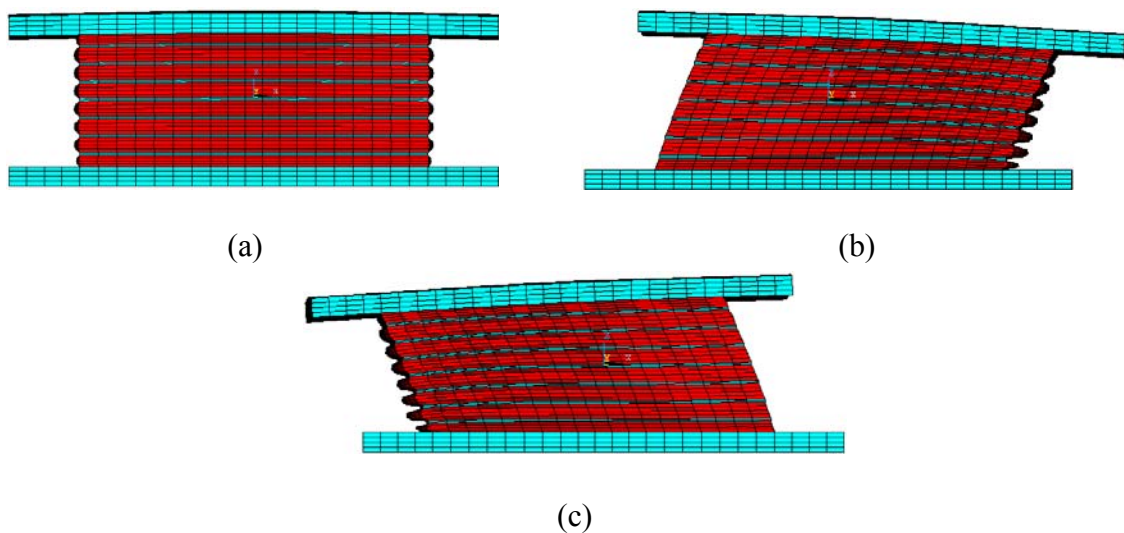

(a)

(b)

(c)

Figure 8.12 Deformed shape of the "356×356×140" mm lead-rubber bearing at

(a) point A, (b) point B, (c) point C

The second bearing is a large circular lead-rubber shear damper with the diameter of 650 mm and the height of 197mm. The bearing has a lead plug of 170 mm inserted in its center. The simplified geometry of the bearing is presented in Figure 8.13. It consists of ten mild steel plates with the thickness of 5-mm and nine rubber layers with the thickness of 15 mm. The experiment on this bearing was reported by Robinson (1982). A high vertical load of 3.15 MN is applied first using the automatic load increment size algorithm followed by the lateral force. The force-displacement hysteretic loops corresponding to the experimental and numerical approaches are shown in Figure 8.14. As obvious from the figure, a good agreement is generally obtained, however the FE method estimates a stiffer behavior for the initial part of the loop (loading path) but softer behavior for the unloading part.

The reasonable correlation between the FE simulation and the experimental results show the adequacy of the employed hyperelasticity model, estimated material parameters, and employed numerical procedure. As a result, when the experimental results are not available for the bearings which are to be used in the structure, the proposed elaborate FE method can be used with reasonable level of accuracy to predict the behavior of the isolator. This removes the need for conducting tedious analytical and/or experimental studies.
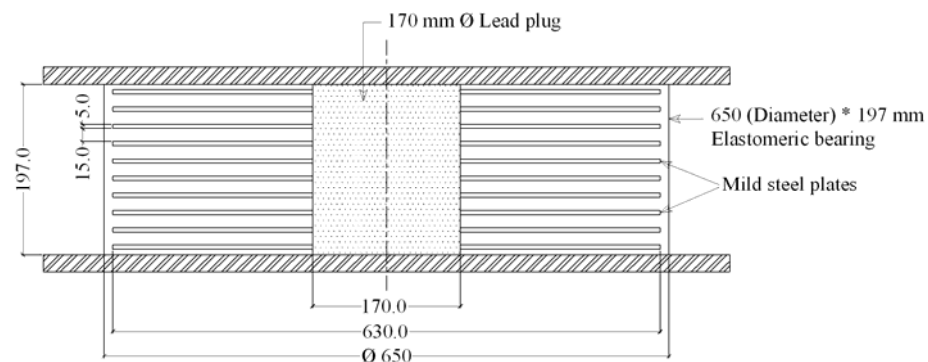

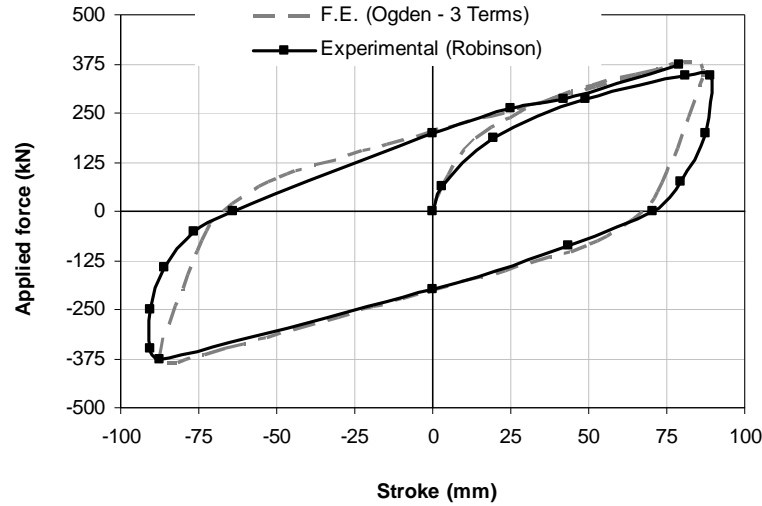Figure 8.13 Geometry of the 650 (Diameter) × 197 mm lead-rubber bearing

Figure 8.14 Force-displacement diagram for 650 (Diameter) × 197 mm

lead-rubber bearing

8.3.4 Simplified simulation of bearings

Including the elaborate FE models of bearings in seismic analysis of isolated elevated water tanks leads to numerical difficulties due to a large number of degrees of freedom resulted and is therefore not computationally efficient. As a result, a practical idealization for modeling the seismic behavior of passive control bearings is proposed based on the numerical (FE analysis) and/or experimental data obtained for the isolator. After verifying this simplified model against experimental results, the model will be implemented for seismic isolation of liquid-filled elevated water tanks in the next section.

Here, a simplified two-node link element model (Link 180) is used for simulating the shearing behavior of the dissipation devices. Link 180 is a 3D finite strain spar element with two nodes and three degrees of freedom at each node (translations in x, y, and z directions). The element has plasticity, and large strain capabilities.

The axial (vertical) behavior of the bearings (both elastomeric and lead-rubber bearings) is modeled using a linear elastic spring element (Combin 14). The element has two nodes with up to three degrees of freedom at each node (translations in x, y, and z directions). This allows the effect of rocking motion to be accounted for in dynamic analysis of the tanks. Only a uniform stress is allowed in the spring.

Based on the proposed simplified modeling technique, only a vertical stiffness (Kv) is sufficient to characterize the axial behavior of the bearings. The horizontal (shearing) behavior of the bearings is modeled using a bilinear kinematic hardening plasticity algorithm explained before. As a result, three main parameters are needed to define the horizontal behavior of the bearings; namely the yield strength (Qy), and the elastic (Ke) and plastic (Kp) stiffnesses. Comparing to a typical stress-strain based plasticity algorithm, Qy corresponds to the yield stress, and Ke and Kp correspond to the initial Young's modulus and tangent modulus, respectively. A simplified hysteretic loop for lead-rubber bearings with the above parameters indicated on is presented in Figure 8.15. The model parameters may be determined from an elaborate FE analysis and/or an experimental study.
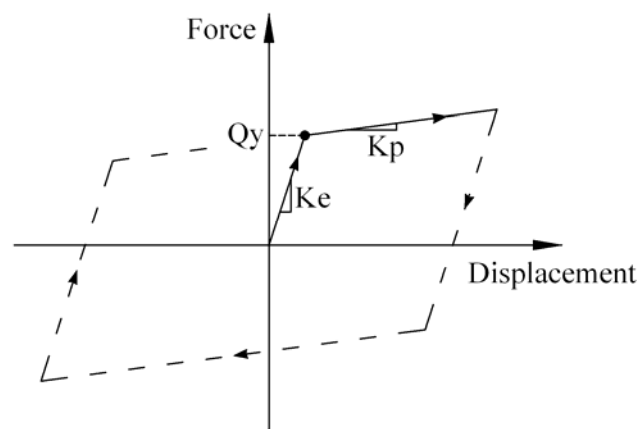

Figure 8.15 Simplified hysteretic loop for lead-rubber bearings

In the next section, the circular 650 (Diameter) × 197 mm lead-rubber bearings will be incorporated for seismic isolation of elevated water tanks. The bearings will be simulated using the simplified modeling technique explained here. Based on the experimental study by Robinson (1982), the following parameters are suggested for simplified modeling of the bearing:

$$Qy = 224 \ kN, \qquad Ke = 17 \ \frac{kN}{mm}, \qquad Kp = 2 \ \frac{kN}{mm}, \text{ and } \qquad Kv = 600 \ \frac{kN}{mm}.$$

The hysteretic behavior of the bearing is indicated in Figure 8.16 as determined by the simplified approach and compared to the Robinson's experimental data. As evident from the figure, a reasonable agreement is observed between the results predicted by the simplified model and experimental observations. As a result, this simplified model may be used for simulating the behavior of rubber bearings without great loss of accuracy. The proposed model is practical, straightforward and easy to use.
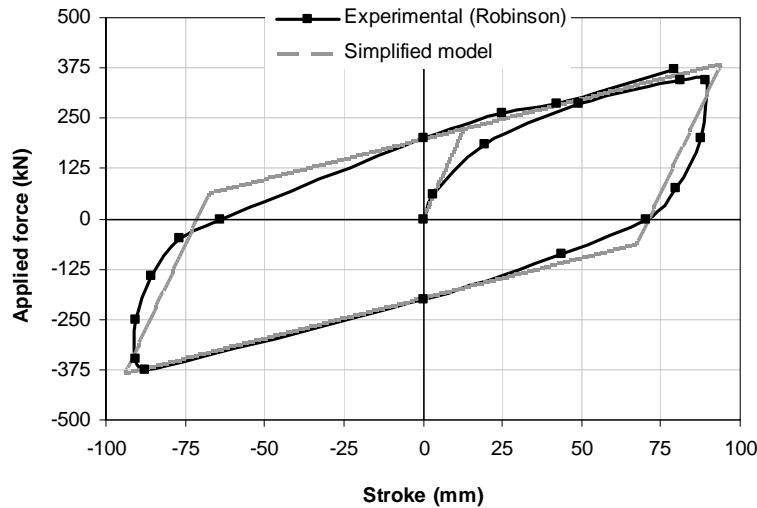

Figure 8.16 Hysteretic loop for 650 (Diameter) × 197 mm lead-rubber bearing (Simplified model)

8.3.5 Application to liquid-filled conical elevated tanks

8.3.5.1 General considerations

The application of passive control technique to liquid-filled conical elevated tanks, using lead-rubber and elastomeric bearings in particular will be investigated in this section of the thesis. The elevated tank model considered for this study is the same as that used in Chapter 6. The properties of the model are described in detail under section 6.2.3. As explained in detail in previous chapters, the fluid domain is modeled using eight-node 3D fluid elements and the structural domain is modeled using four-node quadrilateral shell elements. Effects of both impulsive and sloshing components of the stored water are included in the finite element modeling of the tanks.

A total of forty eight 650 (Diameter) × 197 mm lead-rubber bearings are used for seismic isolation of the tank models in this study. The hysteretic behavior of the bearing is explained in the previous section and is indicated in Figure 8.16. It is worth noting that two nodes should be defined at the locations of isolators in order to accommodate the isolation device where needed.

The number and properties of the bearings are chosen based on the Meggett (1978) recommendations that reasonable values for the plastic shear stiffness and the yield strength of lead-rubber pads should be taken as:

$$K_p = (1 \text{ to } 2) \, W \, m^{-1} \tag{8-6}$$

$$Q_y = (0.05 \text{ to } 0.10) \, W \tag{8-7}$$

where, W is the part of the weight carried by the bearing. In the current study, the bearings are measured with $K_p \approx 1.1 \, W \, m^{-1}$ and $Q_y \approx 0.1 \, W$. In a research study on the dynamic behavior of isolated multi-storey buildings, Lee and Medland (1981) also suggested similar values to those concluded by Meggett for plastic stiffness and yield strength of the bilinear hysteretic dampers.

Regarding the seismic isolation of bridges, Blakeley et al. (1980) proposed isolation parameters close to those determined by Meggett.

Both modal and time history analyses are carried out on isolated and non-isolated elevated tanks. The ground motion used for the time history analysis of the tanks is the horizontal component of 1940 El-Centro ground motion with the peak ground acceleration of 0.50g. The first 20 seconds of the record is used in dynamic analyses. Direct integration method is used for transient analysis of the tanks.

As explained in detail in Chapter 4, the natural frequencies corresponding to the fundamental convective and impulsive modes are used to determine the damping constants (α and β) in non-isolated tank problems. However, in the case of isolated tanks, since the response is mainly dominated by the isolation mode, the natural frequency corresponding to this mode should be used in determining the associated damping constant. The damping constant associated with the sloshing component is determined using the natural frequency of the fundamental convective mode, similar to what is done for non-isolated tanks. As will be discussed later in this chapter, the fundamental sloshing frequency does not change significantly due to seismic isolation.

The damping ratios equal to 0.5 and 5 percent are considered for the convective and impulsive water components, respectively. The stiffness proportional damping equivalent to 5 and 2 percent of critical damping is considered as structural damping for concrete and steel segments of the tank, respectively. In addition, the physical elastic-plastic hysteresis loss in energy dissipation devices introduces a significant amount of damping to the system. The effect of such damping is accounted for by defining an appropriate bilinear plasticity model for the isolators. However, the viscous damping of isolators was neglected in FE modeling of the tanks

as the major part of the input seismic energy is dissipated by the hysteretic behavior of the isolators.

In order to investigate the sensitivity of conical elevated tank response to seismic isolation system, effects of various parameters such as lateral versus vertical isolation, location of isolators, shaft stiffness, tank aspect ratio, and yield strength of isolators will be investigated and discussed in the next sections of this chapter. This will provide some useful information regarding the dynamic behavior of isolated conical elevated tanks which can help in obtaining an optimum design for the tank and its seismic isolation system.

8.3.5.2 Effect of lateral and vertical isolation on dynamic response

The effect of lateral and vertical isolation on seismic response of elevated water tanks is considered in this section. The geometry of the non-isolated tank model is shown in Figure 8.17. All dimensions are given in "mm". The considered tank model is isolated at top of the shaft structure (immediately below the ring beam) using two different techniques; lateral as shown in Figure 8.18 and vertical isolation as shown in Figure 8.19. The construction detail proposed for the case of lateral isolation is shown in Figure 8.18(b). Two possible construction details are also recommended for vertical isolation case as presented in Figures 8.19 (b) and (c). As shown in these figures, in vertically isolated tank, isolators are fully restrained against radial movement by means of either rollers or joint fillers. This horizontal restraint may also be provided by other means such as seismic cables, tie downs, or concrete ring cage. In this isolation scheme, the system flexibility is provided by rocking motion of the tank due to vertical deformability of rubber pads supporting the tank.

It is assumed that isolators are firmly attached to the structure at top and bottom through anchor bolts and connector plates. Lead-rubber bearings are used for lateral isolation of the tank while elastomeric bearings are employed for the case of vertical isolation. The dimensional properties of the elastomeric bearings used in this study are similar to those of lead-rubber bearings (as indicated in Figure 8.13) except that they do not have a lead plug at the center. The vertical stiffness of elastomeric bearings are assumed to be the same as that of lead- rubber bearings (Kv = 600 $\frac{kN}{mm}$). Furthermore, the same number of isolators (n = 48) is used in both lateral and vertical isolation cases.
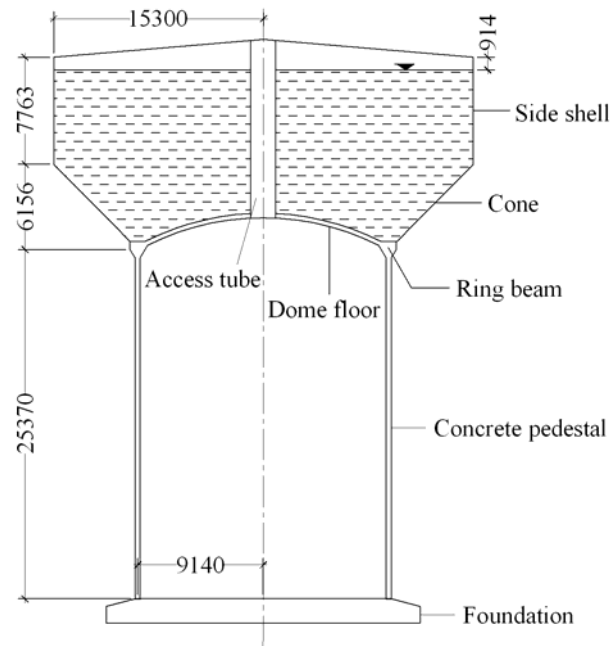

Figure 8.17 Simplified geometry of the non-isolated tank model

(a)

(b)
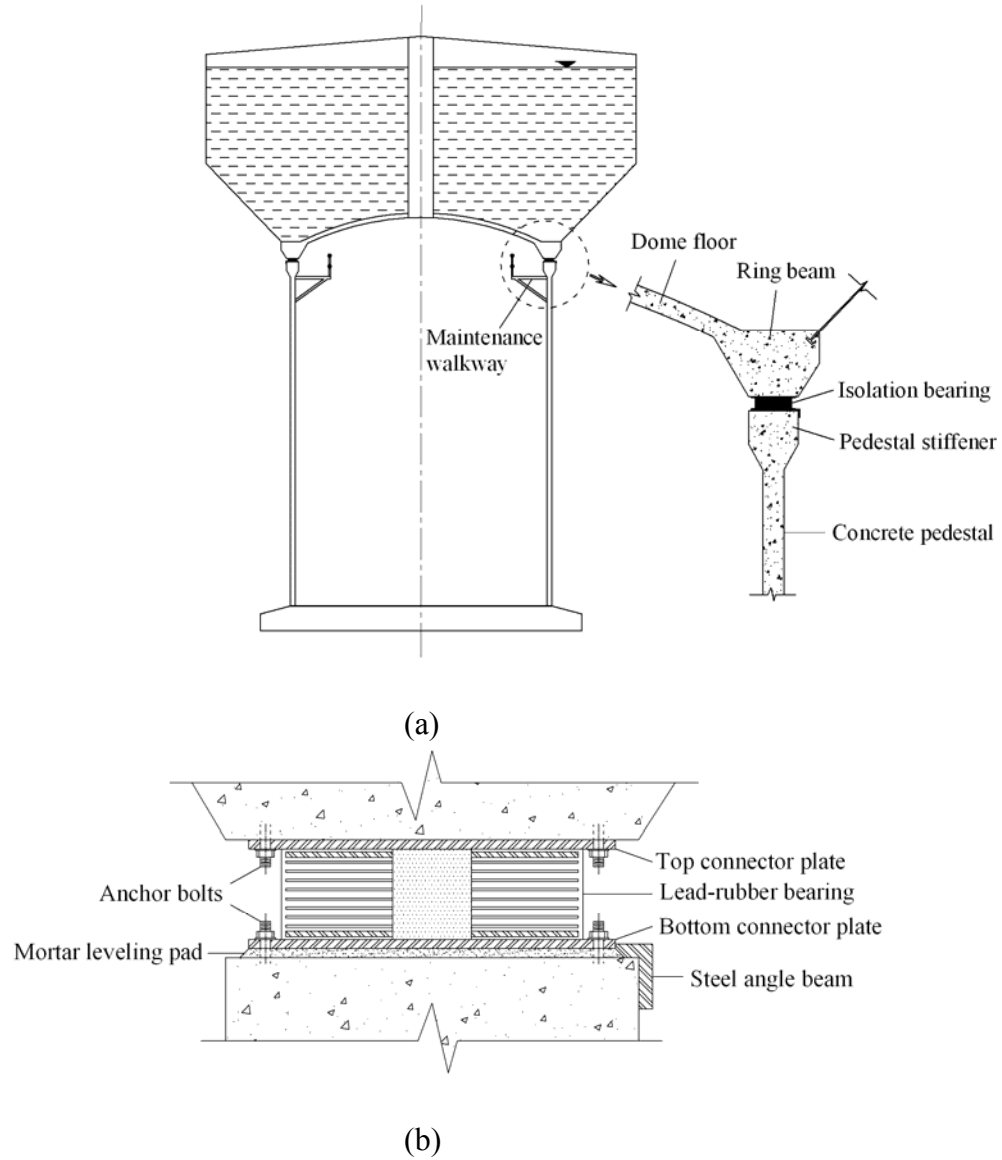
Figure 8.18 Proposed lateral isolation scheme; (a) side view of the tank, (b) isolation detail

The time-history response of the tank isolated laterally and vertically, subjected to El-Centro ground motion (PGA=0.50g) is calculated using the proposed FE technique. The obtained response values are then compared with those of non-isolated tank. The response quantities of interest are base shear, base moment, lateral displacement at top of the shaft below the isolators (i.e. tower drift), and lateral displacement at tank floor level top of the isolators.
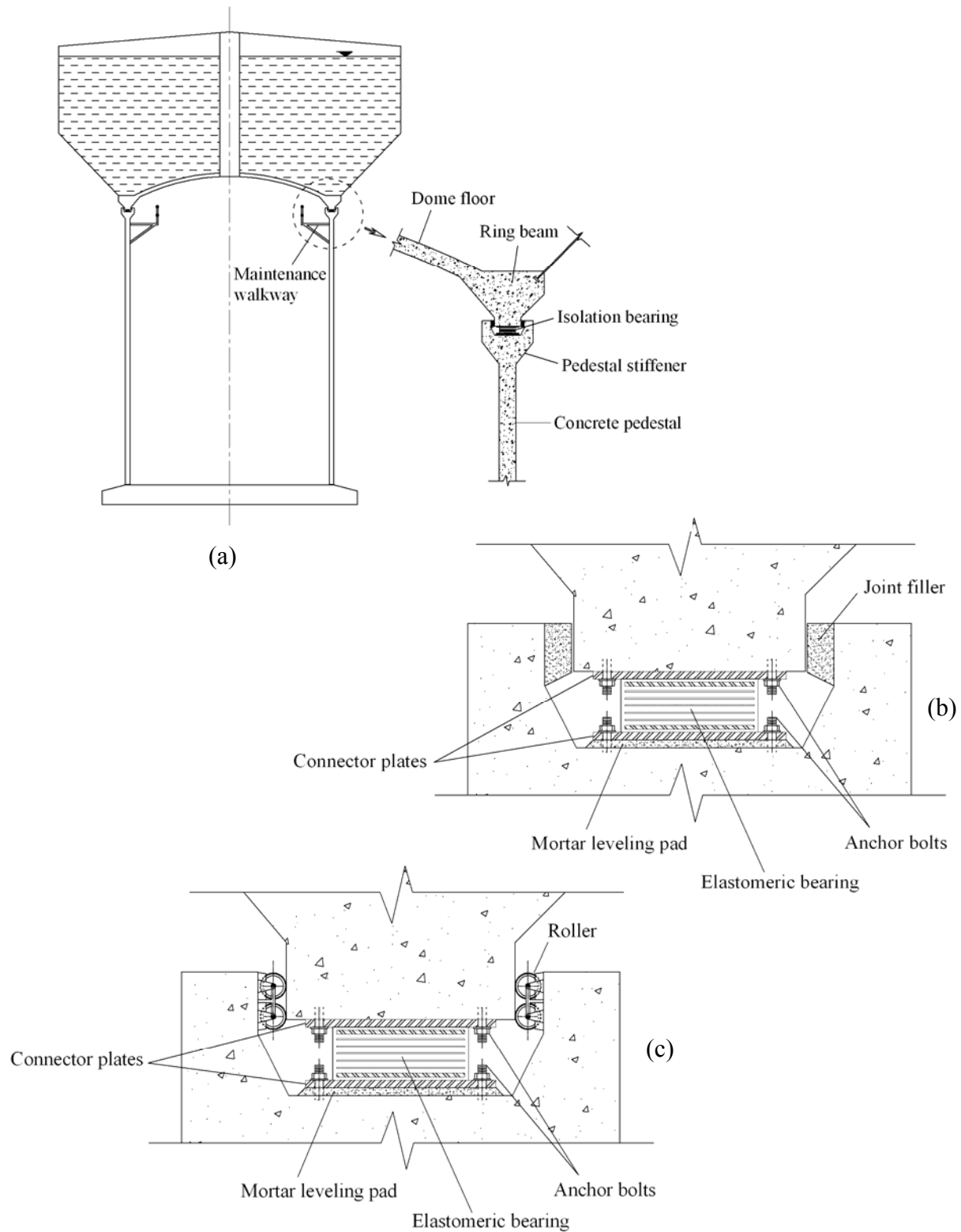
Figure 8.19 Proposed vertical isolation scheme; (a) side view of the tank, (b) isolation detail I,

(c) isolation detail II

Figure 8.20 shows the obtained time history responses of both laterally and vertically isolated tanks against those corresponding to the non-isolated tank for comparison purposes.

(a)

(b)

(c)

(d)
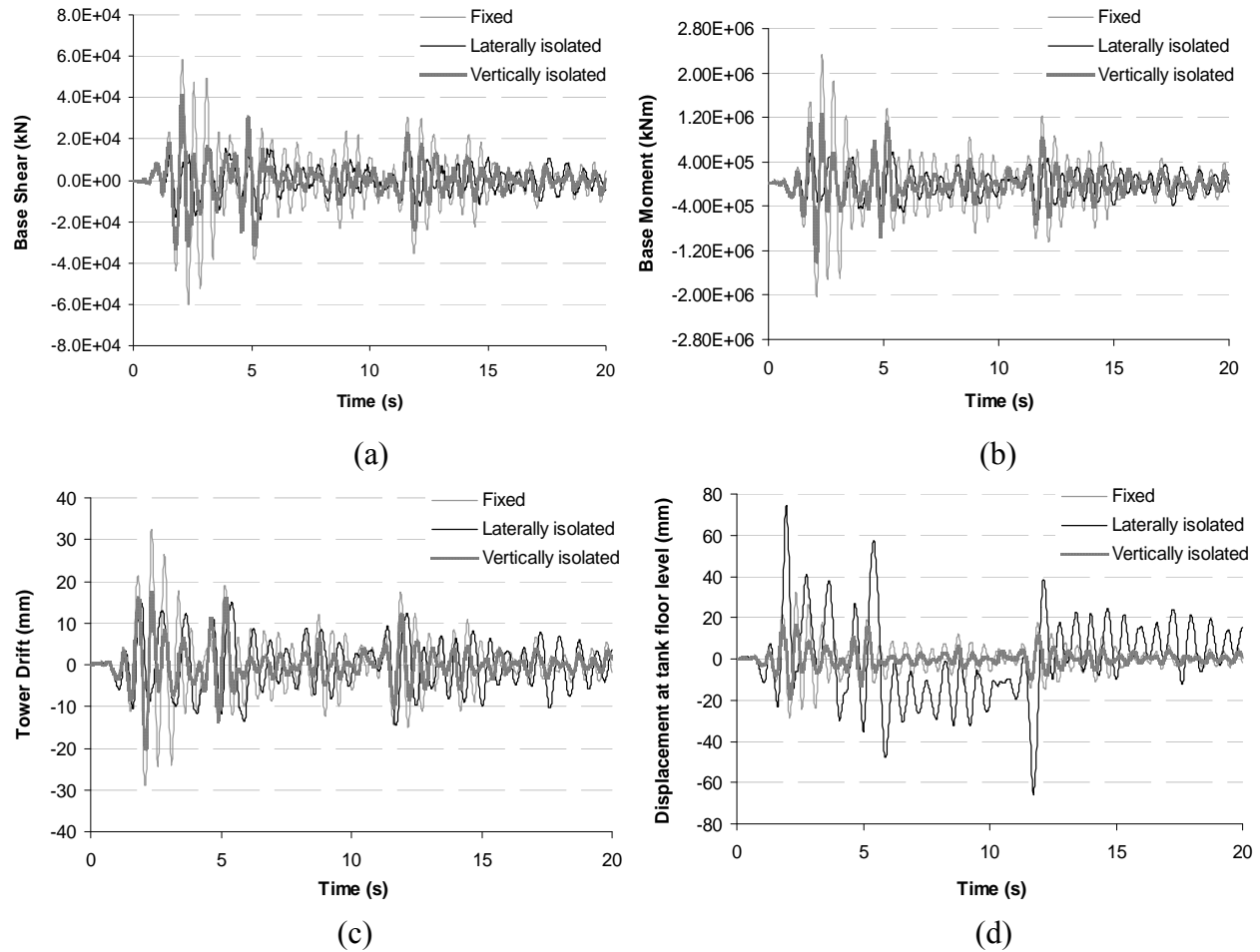
Figure 8.20 Time-history response of the elevated tank model under El-Centro earthquake (PGA=0.5g); (a) base shear, (b) base moment, (c) tower drift, (d) lateral displacement at tank floor level (at top of the isolators in isolated models)

The comparisons among the response variations calculated for the fixed and isolated models clearly show the period elongation effect in the time-history response of the isolated tank models due to seismic isolation. Moreover, it can be observed from the figure that the base shear, base

moment and tower drift response values are significantly reduced due to seismic isolation in both laterally and vertically isolated models. This verifies the effectiveness of seismic isolation in liquid-filled conical elevated tanks. Examining the obtained results, it can be observed that in general more reduction is achieved by the lateral isolation strategy as compared to the vertical isolation technique. This is partly due to an additional damping effect resulting from hysteretic energy absorption of lead-rubber bearings and partly due to the horizontal flexibility of the bearings in laterally isolated case compared to the case of vertical isolation. However, as indicated in Figure 8.20 (d), a different trend is observed in terms of the lateral displacement response at tank floor level. As shown in this figure, the absolute maximum value of lateral displacement is increased from 32.4 mm in the fixed tank case to 74.3 mm in lateral isolation case while it is decreased to 19.4 mm in vertical isolation case. This can be the main advantage of vertical isolation over lateral isolation strategy which offers a beneficial solution to the difficulties which arise from the excessive deformations usually experienced in isolated structures. This issue is especially of great importance in elevated water tanks because of the piping system failure that may be experienced as a result of excessive deflections.

It can be concluded that when excessive deformation due to lateral isolation is not of concern, lateral isolation strategy is usually a better option leading to a more effective solution to the problem. On the other hand, if additional structural movements cannot be accommodated by existing tank design, vertical isolation scheme is preferred over lateral isolation.

The absolute maximum time history response values corresponding to the isolated and non-isolated tank models are summarized in Table 8.4. The numbers in bold show an increase (positive) or decrease (negative) percentage over the corresponding non-isolated tank model.

239

Table 8.4 Summary of peak time history response values

Response	Fixed	Laterally isolated	Vertically isolated
Base Shear (kN)	60251	19250 **-68%**	40830 **-32%**
Base Moment (kNm)	2326509	583244 **-75%**	1416708 **-39%**
Tower Drift (mm)	32.4	15.0 **-54%**	20.3 **-37%**
Displacement at tank floor level (mm)	32.4	74.3 **+129%**	19.4 **-40%**

For comparison purposes, the maximum response values corresponding to different isolation schemes considered are normalized with respect to those of non-isolated tank model, as shown in Figure 8.21.

In order to investigate the effect of seismic isolation on the sloshing response of conical elevated tanks, the time history sloshing height is calculated for laterally isolated tank model and is compared against that of non-isolated case, as shown in Figure 8.22.

The maximum sloshing height in the fixed base tank is 761 mm. As a result of seismic isolation, the free-surface displacement increases by about 25% to a value of 955mm. This in turn results in an increase in the magnitude of convective pressure by about 33% at the water free surface. Figure 8.23 shows the total hydrodynamic pressure distribution along the height of the tank wall for both isolated and non-isolated cases. Overall, the total hydrodynamic pressure decreases considerably due to seismic isolation of the tank.
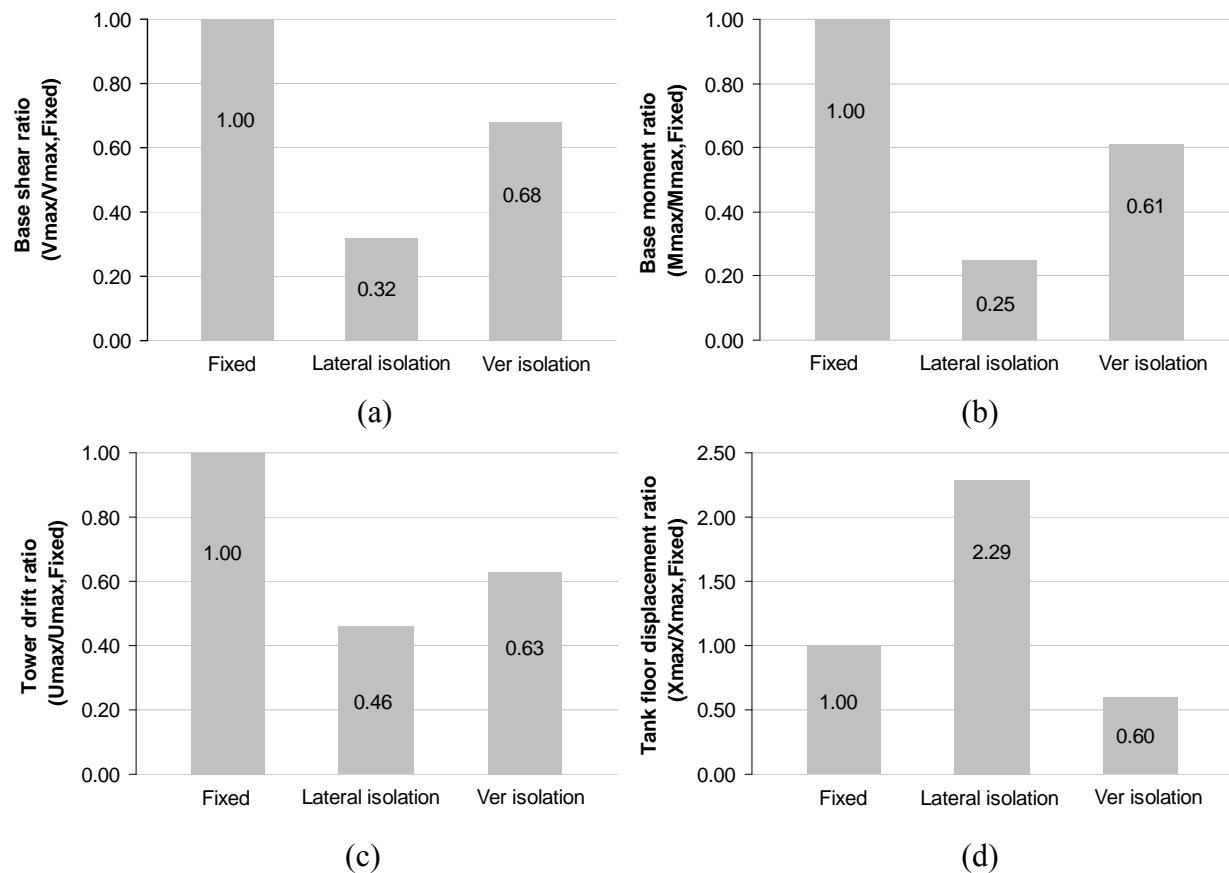
Figure 8.21 Normalized peak time history response values; (a) base shear, (b) base moment,

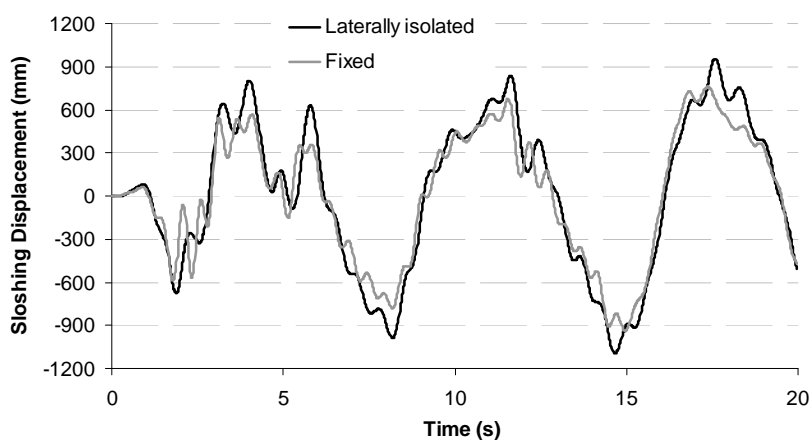(c) tower drift, (d) displacement at tank floor level

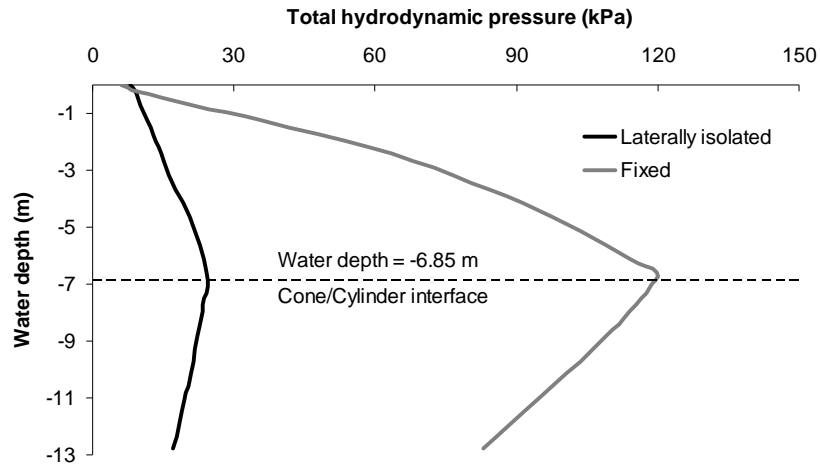Figure 8.22 Time history of sloshing height at water free surface

Figure 8.23 Hydrodynamic pressure distribution over the tank wall

The maximum total hydrodynamic pressure reduces by about 80% due to lateral seismic isolation. A similar trend was observed in the experimental study carried out by Chalhoub and Kelly (1990) on cylindrical ground-supported water tanks. Malhotra (1997C) and Shekari et al. (2009) also found a similar trend in response for cylindrical ground-supported tanks isolated by rubber bearings. This could be interpreted as a stronger coupling observed between the longer period dominant isolation mode and the fundamental convective mode in the isolated tank case in comparison to the totally uncoupled (well-separated natural periods) fundamental impulsive and convective modes usually observed in typical fixed base tanks. As will be discussed later in this chapter, this long-period content isolation mode together with the fundamental convective mode characterize the motion of isolated elevated tanks. Nonetheless, the observed increase in sloshing response due to isolation of the tank is negligible and can be overcome by the proper choice of the isolation design and/or by the installation of dampers at the location of peak free-surface sloshing.

242

The reduction in total hydrodynamic pressure due to seismic isolation can be considered as another measure of the effectiveness of the seismic isolation system.

The magnitude of the impulsive component of pressure is mainly dependent on the absolute acceleration of the impulsive water mass. As a result of seismic isolation, this acceleration is reduced significantly leading to a considerable reduction in the magnitude of impulsive pressure. This reduction in impulsive pressure offsets the increase in convective pressure due to seismic isolation which thus results in a significant net decrease in the total hydrodynamic pressure, as shown in Figure 8.23.

8.3.5.3 Effect of isolation location on response

To consider the effect of isolators' location on the dynamic response of conical elevated tanks, the considered tank model is laterally isolated using two different isolation schemes as follows:

1) Isolation type A in which isolators are located at the base of the shaft as shown in Figure 8.24 (a).

2) Isolation type B in which isolators are provided at top of the shaft immediately below the concrete ring beam as shown in Figure 8.24(b).

The elevated tank model considered for this part of study is the same as that used in the previous section. Figure 8.17 shows the geometrical properties of the corresponding non-isolated tank model.
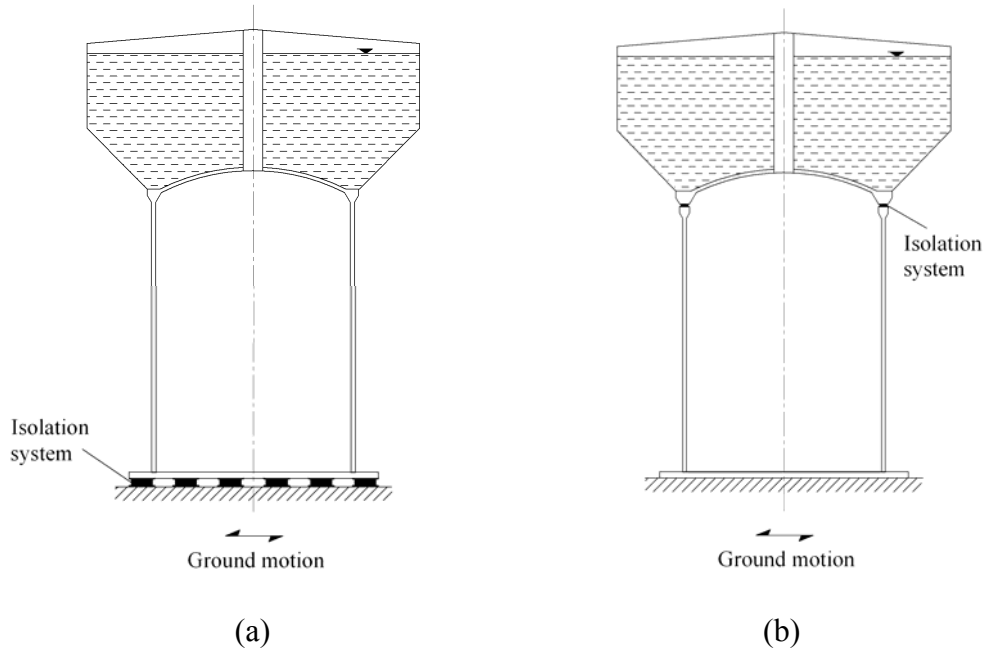
Figure 8.24 Schematic geometries of the isolated tank models; (a) Isolation type A,

(b) Isolation type B

Figure 8.25 shows the time history variation of response of the elevated tank model in fixed and isolated conditions considering the two locations for seismic isolators. As obvious from the figure, different response variations are obtained for isolation types A and B.

The absolute maximum time history response values corresponding to the isolated and non-isolated tank models are summarized in Table 8.5. The numbers in bold show an increase (positive) or decrease (negative) percentage over the corresponding non-isolated tank model.

For comparison purposes, the maximum response values corresponding to different isolation types considered are normalized with respect to those of non-isolated tank model, as shown in Figure 8.26.
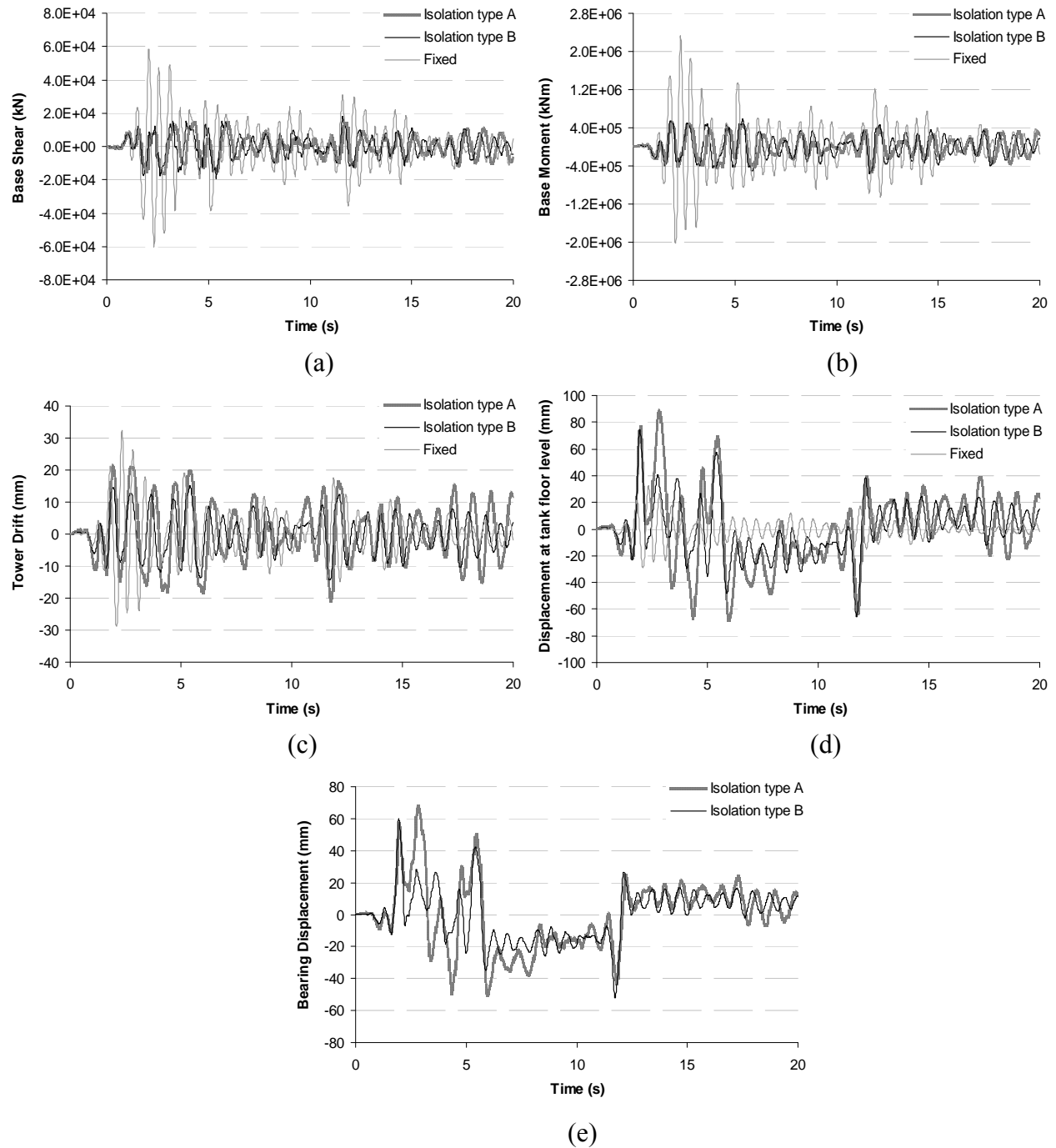
Figure 8.25 Time-history response of the elevated tank models considering different locations for isolators; (a) base shear, (b) base moment, (c) tower drift, (d) lateral displacement at tank floor level, (e) bearing displacement

Table 8.5 Peak time history response values considering different locations for isolators

Response *	Fixed	Isolation type B	Isolation type A
Base Shear (kN)	60251	19250 **-68%**	16278 **-73%**
Base Moment (kNm)	2326509	583244 **-75%**	515243 **-78%**
Tower Drift (mm)	32.4	15.0 **-54%**	21.2 **-35%**
Displacement at tank floor level (mm)	32.4	74.3 **+129%**	88.3 **+173%**

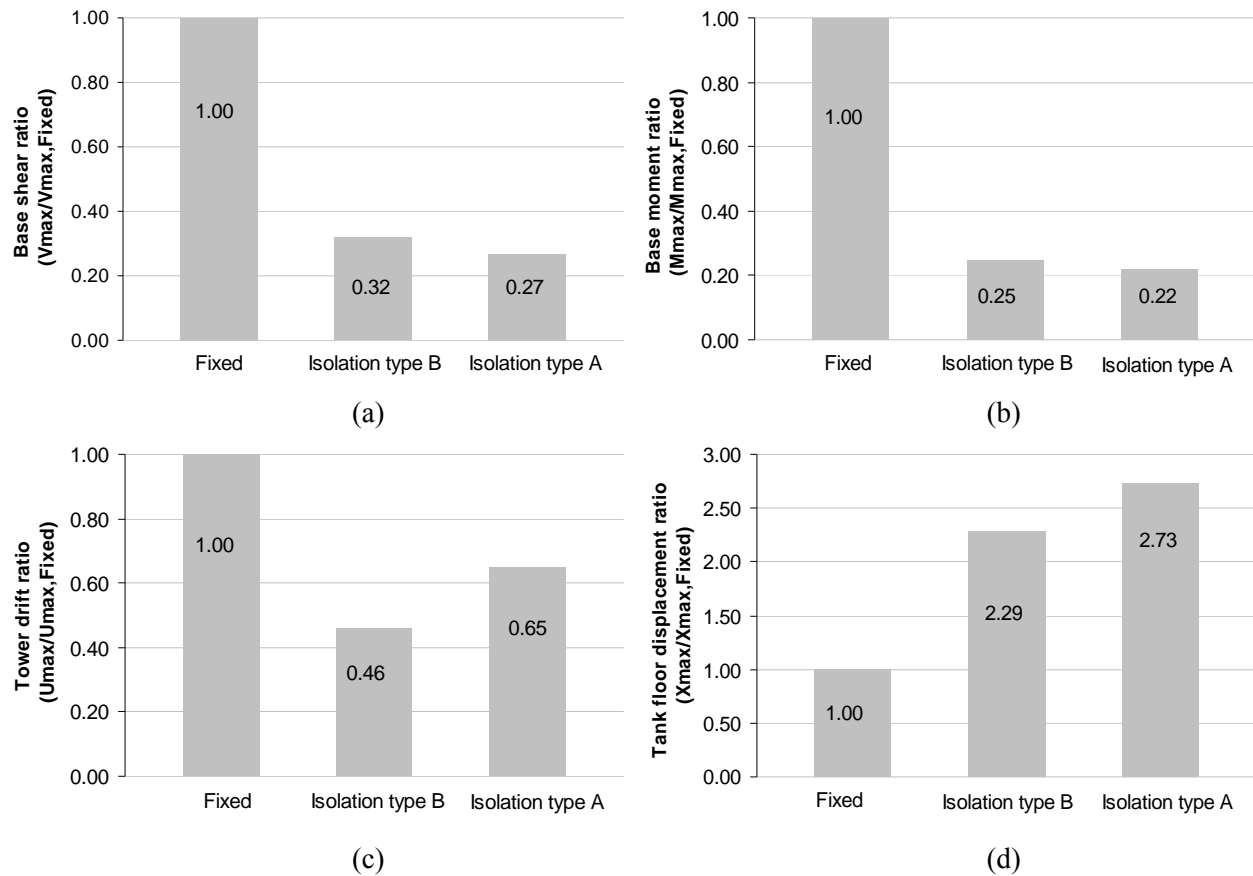* All response values given in the table are maximum absolute values.

Figure 8.26 Normalized peak time history response values considering different locations for seismic isolators; (a) base shear, (b) base moment, (c) tower drift, (d) displacement at tank floor level

246

As presented in Table 8.5, in both isolation types, the values of base shear and base moment are reduced significantly. However, generally, more reduction is achieved by isolation type A as compared to isolation type B. A different trend is observed for tower drift response. Isolation type B results in a reduction percentage of around 54% in tower drift response value while only 35% reduction is achieved by isolation type A. In terms of displacement at tank floor level, isolation type B is considered more advantageous over isolation type A, as less increase percentage is observed in isolation type B (129%) in comparison to the increase percentage of 173% calculated for isolation type A.

The maximum absolute bearing displacements calculated for isolation types A and B are 68 mm and 60 mm, respectively. This indicates that the bearing displacement is slightly smaller in the tank with isolation type B in comparison to the isolation type A since the weight applied on isolation type B is comparatively less than that in isolation type A. This is obvious in Figure 8.27 which shows the force-displacement hysteretic loops during the considered earthquake motion corresponding to isolation types A and B. The given hysteretic diagram is for one isolator. The enclosed area in a force-displacement hysteretic loop implies the energy dissipated in a cycle.

According to the calculated hysteretic loops indicated in this figure, one can notice that the total amount of energy absorbed during the earthquake increases when isolators are located at the base of the tank compared to the case where bearings are installed at top of the shaft. This could be considered as another advantage for isolation type A over isolation type B. The reason is believed to be the increase in vertical loads applied to the isolators due to the self weight of the shaft, weight of platforms inside the shaft and their live load, and the weights of all other accessories attached to the shaft structure. This phenomenon has also been noticed experimentally in research works by Robinson (1982) and King (1980).
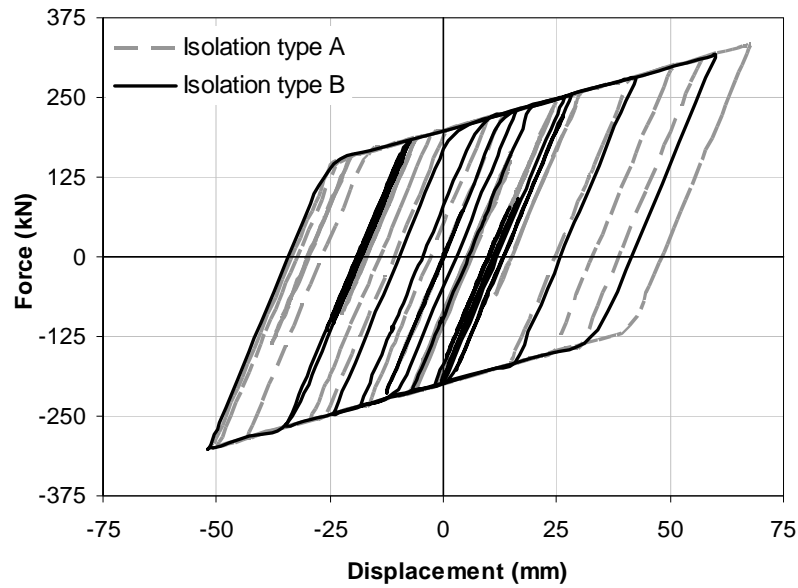
Figure 8.27 Force-displacement diagram for seismic isolation types A and B

8.3.5.4 Effect of stiffness of the shaft structure (natural period of the shaft structure)

To study the effect of shaft stiffness on the effectiveness of seismic isolation, two elevated tank models having different shaft stiffness characteristics namely; stiff and flexible are considered and their time history response is calculated using the proposed methodology.

The two tanks are assumed to be laterally isolated at top of the shaft structure and the same isolation properties are considered for both stiff and flexible models. The properties of the considered isolation system are as explained before under section 8.3.5.1. The elevated tank model considered for this part of study is the same as that used in the previous section. See Figure 8.17 for the geometrical properties of the corresponding tank model. The flexible tank model is created by reducing the shaft thickness to 127 mm such that the resulting shaft stiffness reaches as low as one third of that of the original model (stiff model). As mentioned before, the

thickness of the shaft structure in the original model (stiff model) is 380 mm. All other properties of the two tank models are assumed to be the same.

Table 8.6 lists the peak time history response values of the isolated stiff and flexible tank models against corresponding non-isolated tanks. The numbers in bold show an increase (positive) or decrease (negative) percentage over the corresponding non-isolated tank model.

Table 8.6 Peak time history response values for stiff and flexible tank models

Response *	Original shaft stiffness (Stiff model)		Low shaft stiffness (Flexible model)	
	Fixed	Isolated	Fixed	Isolated
Base Shear (kN)	60251	19250 **-68%**	35182	16156 **-54%**
Base Moment (kNm)	2326509	583244 **-75%**	1266423	518286 **-59%**
Tower Drift (mm)	32.4	15.0 **-54%**	59.5	45.3 **-24%**

* All response values given in the table are maximum absolute values.

Table 8.6 shows that for stiff model, the reduction percentages in base shear, base moment, and tower drift, as a result of isolation, are 68%, 75%, and 54%, respectively, while the corresponding reductions for flexible model are 54%, 59%, and 24%. The obtained results show a considerable reduction in dynamic response of the tanks due to seismic isolation in both stiff and flexible cases. However, this reduction is comparatively more pronounced in stiff model in comparison to flexible model. As a result, it can be concluded that seismic isolation is comparatively more effective in tanks with stiffer shaft structure compared to those having more flexible shaft structures given that all other properties are the same.

Comparing the results obtained for non-isolated stiff and flexible tanks, it can be noticed that smaller seismic forces are transmitted by the flexible shaft structure resulting in smaller base shear and base moment response values. However, this flexibility has resulted in an increase of around 84% in tower drift.

The peak base shear and base moment response values calculated for the isolated tanks are compared against those of non-isolated tanks for two different values of shaft stiffness, as indicated in Figure 8.28.

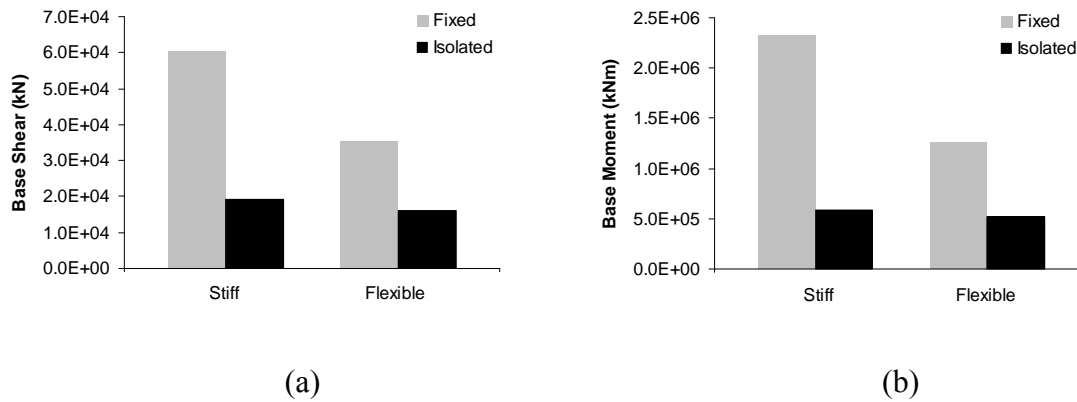<center>(a)   (b)</center>

<center>Figure 8.28 Comparison of results between stiff and flexible tank models</center>

As obvious from the figure, the response of isolated tanks is obviously less sensitive to the flexibility of the shaft structure as compared to the corresponding non-isolated tanks. In other words, the dynamic response of isolated tanks is not significantly influenced by the stiffness properties of the supporting shaft structure.

8.3.5.5 Effect of tank aspect ratio

In order to investigate the sensitivity of seismic isolation to the tank's geometry, the transient response of two elevated tank models having different aspect ratios namely; broad and

slender is determined in both isolated and non-isolated conditions using the proposed FE scheme. The effectiveness of seismic isolation is then examined by comparing the results obtained for broad and slender configurations.
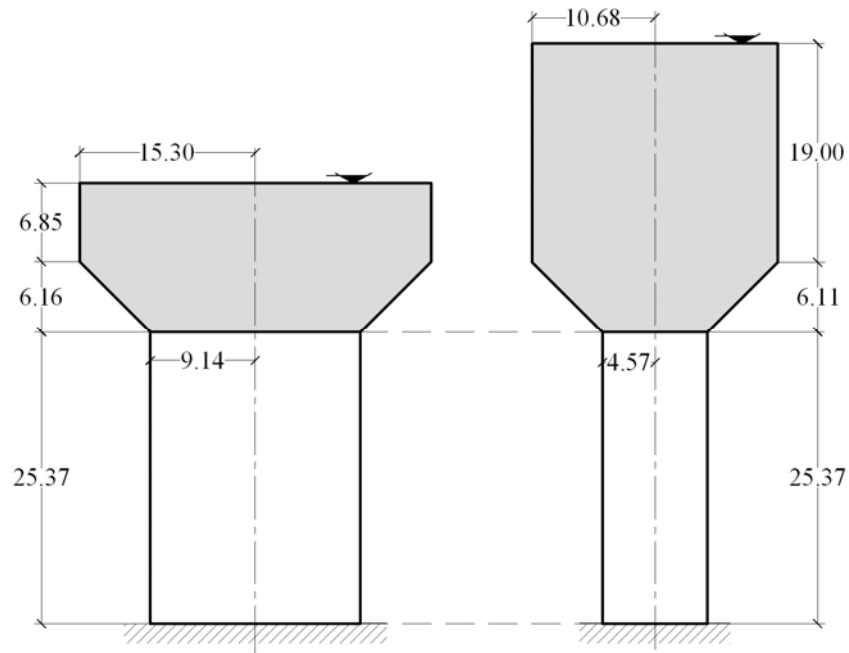
The considered broad and slender tank models have the aspect ratios of 0.7 and 2.1, respectively. Tank aspect ratio (A.R.) is defined as the ratio of equivalent water height (based on the concept of equivalent cylinder model) to the radius of the cylindrical part of the vessel.

The broad tank model considered in this section is the same as that used in Chapter 6, section 6.2.3 and elsewhere throughout this chapter (see Figure 8.17). The simplified geometries of the tanks along with their FE models are indicated in Figure 8.29.

The tanks are assumed to be laterally isolated at top of the shaft structure, and the same isolation properties are considered for both broad and slender models. The properties of the considered isolation system are as explained before under section 8.3.5.1.

The volume of contained water is the same in both cases. Furthermore, the stiffness and mass distributions along the height of the shaft, and conical and cylindrical side shells are similar in both tank models. The mass distributions are made equivalent by adjusting the mass density of each section (shaft, cone, and cylinder parts) of the tank appropriately. As a result of this adjustment, the total mass of broad and slender tank models will also be the same.

The stiffness distributions are also made equivalent by altering the thickness of each shell section (shaft, cone, and cylinder parts) of the tank properly such that the resulting stiffness matches that of broad tank model. These adjustments result in equal values of shaft period, isolation time period, and isolation yield strength in broad and slender tank models. Thus, the obtained time history results are readily comparable.

251

(a)
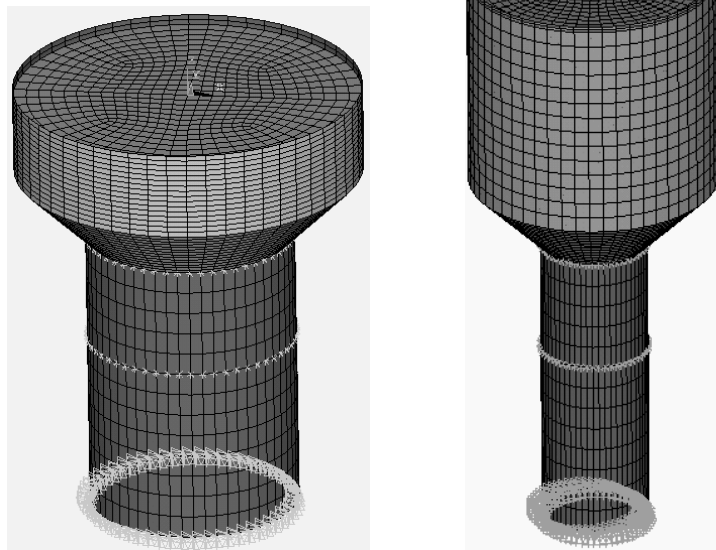
(b)

Figure 8.29 Broad and slender tank models; (a) simplified geometries, (b) FE models

Table 8.7 lists the peak time history response values of the isolated broad and slender tank models against corresponding non-isolated tanks. The numbers in bold show an increase (positive) or decrease (negative) percentage over the corresponding non-isolated tank model.

As presented in the table, the base shear and base moment values of slender tank model are greater than those of broad tank in both fixed and isolated conditions. This reveals the significant effect of tank's geometry on the dynamic response of the elevated tanks in both fixed and isolated conditions.

Table 8.7 shows that for broad model, the reduction percentages in base shear, base moment, and tower drift, as a result of isolation, are 68%, 75%, and 54%, respectively, while the corresponding reductions for slender model are 77%, 79%, and 78%. Therefore, it can be concluded that comparatively greater reductions in dynamic response can be achieved due to seismic isolation in slender tank as compared to broad tank.

Table 8.7 Peak time history response values for broad and slender tank models

Tank model		Bearing Disp. (mm) *	Sloshing Disp. (mm)	Base Shear (kN) *	Base Moment (kNm) *	Tower Drift (mm) *
Broad	Fixed	NA	761	60251	2326509	32.4
	Isolated	60	955 +25%	19250 -68%	583244 -75%	15.0 -54%
Slender	Fixed	NA	844	88810	3211956	36.9
	Isolated	83	1148 +36%	20785 -77%	690779 -79%	8.2 -78 %

* Values given for these response quantities are maximum absolute values.

The time variation of sloshing displacement is calculated for isolated slender tank model and is compared against that of non-isolated case, as shown in Figure 8.30. The time-history of sloshing displacement corresponding to broad tank model is indicated in Figure 8.22.
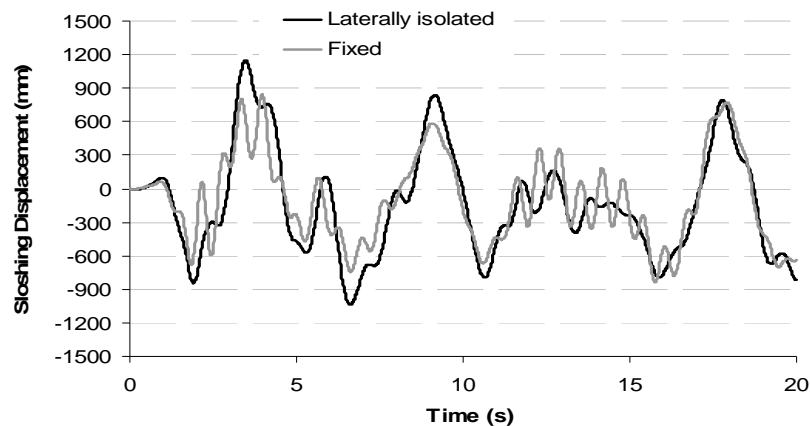

Figure 8.30 Time history of sloshing height at water free surface (slender tank)

The maximum sloshing height in fixed base slender tank is 844 mm. As a result of seismic isolation, the free-surface displacement increases by around 36% to the value of 1148mm. Comparing these values with those obtained for broad tank model, it can be observed that the magnitude of sloshing height produced in slender tank model is greater than that of broad tank model in both fixed and isolated conditions. Moreover, the increase in sloshing displacement resulted from the seismic isolation of the tank is relatively higher in the case of slender tank as compared to broad tank. This may be due to stronger coupling between the fundamental sloshing mode and the isolation mode in tanks with higher aspect ratios (slender tank) as compared to those with lower aspect ratios (broad tank). The sloshing period decreases as the tank's aspect ratio increases and therefore the sloshing and isolation mode periods get closer to each other for the slender tank (high aspect ratio) than for the broad tank model (low aspect ratio). Because of

the possible interaction between the sloshing and isolation modes of vibration, especially in slender tanks, the contributions of both modes should be considered for an accurate analysis of isolated elevated tank models. Therefore, a single mode solution (based on the "isolation mode" only) recommended for most of the isolated systems (such as in buildings) is not adequate to accurately estimate the seismic response of isolated elevated tanks.

The maximum absolute bearing displacements for broad and slender tank models are 60 mm and 83 mm, respectively. This reveals that bearing displacement is relatively smaller in broad tank as compared to slender tank or in other words, the bearing displacement increases as the aspect ratio increases.

Figure 8.31 shows the force-displacement hysteretic loops during the earthquake corresponding to broad and slender tank models. As obvious from this figure, the total amount of absorbed energy increases as the tank's aspect ratio increases. This could be considered as another advantage for slender tanks over broad tanks in seismic isolation applications.
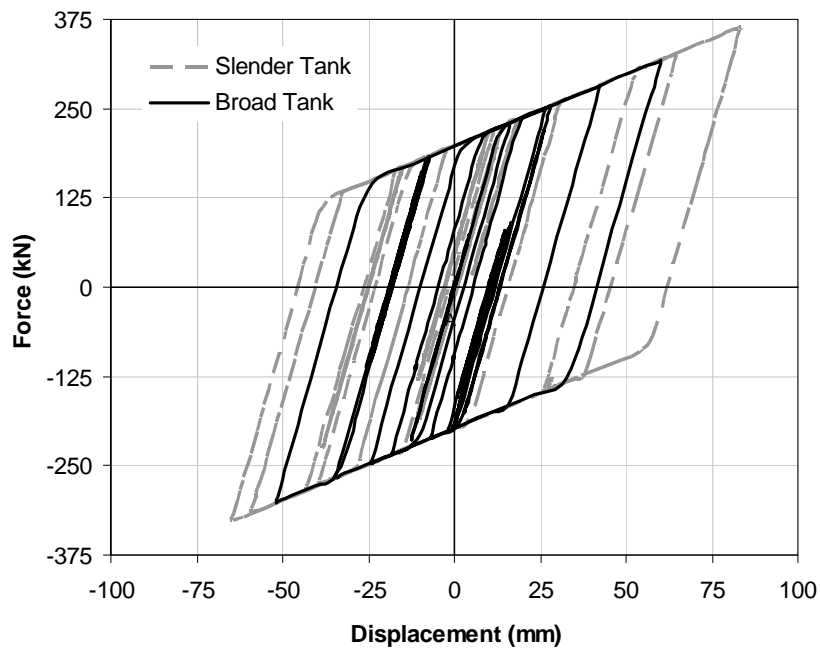

Figure 8.31 Force-displacement diagram for broad and slender tank models

Overall, comparing the total amount of absorbed energy between two cases, and also the reduction percentages achieved in the considered response quantities through seismic isolation, it can be concluded that seismic isolation is comparatively more effective in slender tanks in comparison to broad tanks.

8.3.5.6 Effect of yield strength of isolators

In this section, the influence of the yield strength of bearings on seismic response of isolated conical elevated tanks is investigated. The elevated tank model considered for this part of study is the same as that used in sections 8.3.5.2 to 8.3.5.4 of this chapter. See Figure 8.17 for the geometrical properties of the corresponding non-isolated tank model. Furthermore, the considered tank models are assumed to be laterally isolated at top of the shaft structure.

Figure 8.32 shows the variation of normalized base shear (V_{max}/W) versus normalized yield strength of isolators (Q_y/W), where, W is the weight supported by the bearings. In obtaining this graph, five different isolation systems having different yield strength ratios (Q_y/W) are considered. All other properties of the considered isolation systems are the same. The tank models analyzed previously had the Q_y/W ratio of 0.125.

The Figure initially shows a decreasing trend in the base shear as the yield strength ratio increases up to about 5% at which the minimum base shear is attained. Beyond this point, any further increase in yield strength ratio result in increase in base shear ratio. As a result, it can be said that there is an optimum value for the yield strength of isolators leading to a minimum value of the seismic response. For the specific tank and earthquake record considered in this study, this optimum value is found to be about 5% of the weight carried by isolators.
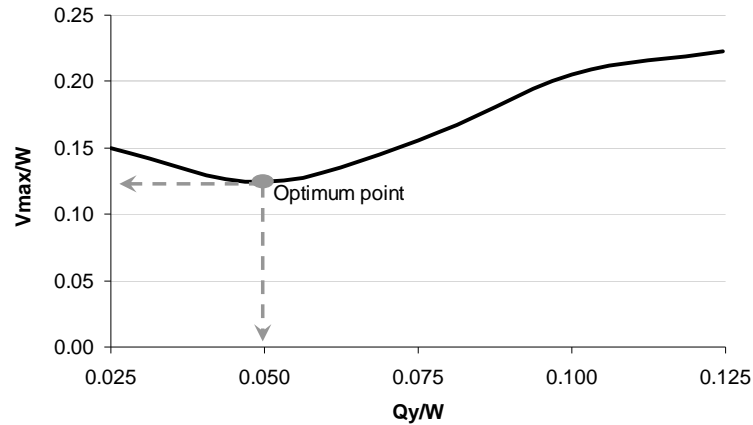
Figure 8.32 Effect of the yield strength of isolators on the dynamic response of

elevated tank model

A proper choice of the yield strength of isolators plays an important role in achieving the minimum dynamic response in isolated elevated tanks. However, attention should be drawn to the fact that any decrease in the yield strength of bearings will result in an increase in the bearing displacement which might not be desirable based on the specific design requirements for both the tank and the bearings. Therefore, in selecting the appropriate properties of the isolation system, both the seismic forces transmitted to the structure and the displacement to be accommodated by the bearings should be taken into account.

8.3.5.7 Free vibration analysis of isolated elevated tanks

Free-vibration analysis is performed on an isolated elevated tank model in order to investigate the properties of the modes having major contributions to the response. The tank model considered for this part of study is shown in Figure 8.17. The tank is assumed to be laterally isolated at the base. The properties of the considered isolation system are as explained previously under section 8.3.5.1.

Table 8.8 lists natural frequencies for the convective, impulsive, and base-isolation modes of the isolated tank model as well as those of non-isolated tank. In addition, the modal participation factors (β) normalized with respect to their largest values for each model are also given in the table.

As given in the table, the period of the isolated tank model (1.65 sec) is several times longer than the impulsive period of the corresponding non-isolated model (0.51 sec). In an effective isolation design, the period of the isolation mode should be greater than the period of the fundamental impulsive mode in the corresponding fixed-base tank model. However, this extended period should not be in close vicinity to the fundamental sloshing period as this may cause an excessive increase in sloshing height due to resonance effect. This is not expected to occur since the sloshing period is usually very large.

Generally, seismic isolation systems should be designed in such a way that their dominant frequency be in the range of 0.25 to 1.00 Hz (Kim and Lee (1995)). This range is referred to as the effective frequency range resulting in an effective seismic isolation of the structure. As shown in Table 8.8, the natural frequency of the base-isolation mode (0.606 Hz) for the tank model under consideration is in the effective frequency range for seismic isolation systems. Furthermore, it can be observed from the table that the natural frequency corresponding to the impulsive mode has been shifted from 1.955 Hz to a higher value of 3.095 Hz as a result of base isolation. However, no frequency shift is observed in convective modes indicating that base isolation has no significant effect on sloshing modes. This phenomenon reveals that impulsive modes are more significantly influenced by the properties of seismic isolation system as compared to convective modes.

Table 8.8 Comparison of free-vibration analysis results between fixed-base and base-isolated elevated tank models

Mode type	Fixed-base model		Base-isolated model	
	Frequency, Hz (Period, sec)	β (normalized)	Frequency, Hz (Period, sec)	β (normalized)
Convective	0.161 (6.21)	1.00	0.157 (6.37)	0.74
Impulsive	1.955 (0.51)	0.88	3.095 (0.32)	0.05
Base-isolation	NA	NA	0.606 (1.65)	1.00

Figure 8.33 shows normalized modal participation factors (β) for the base-isolated tank model. As shown in the figure, the modal participation factor of the base-isolation mode is largest implying that this mode dominates the total dynamic response of the base-isolated tank model. Convective mode has the second highest modal participation factor among all modes of vibration. The participation factor corresponding to the impulsive mode is very small compared to the other modes suggesting that this mode does not contribute significantly in the overall seismic response of the model. As a result, to accurately capture the dynamic response of isolated elevated tanks, the contributions of both isolation and convective modes of vibration should be taken into account.

Similar to fixed-base tank models, convective mode in isolated elevated tanks is associated with the fluid motion at the tank's free surface. No significant motion is observed in the shaft, tank shell, and isolation system in the convective mode. The isolation mode is associated with a large displacement in the isolation system and very small tower drift amplitude. This is typically referred to as a rigid body motion. The obtained impulsive mode shape indicates considerable deflections in the shaft, tank shell, and isolation system.
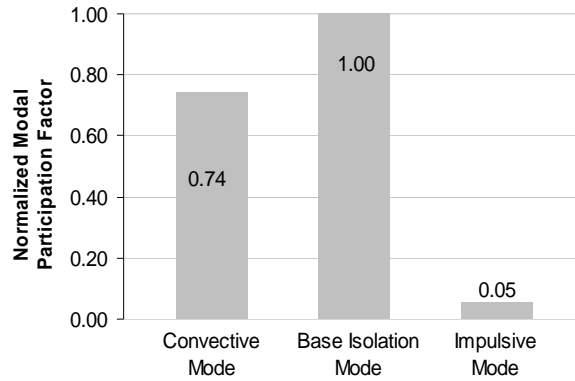
Figure 8.33 Normalized modal participation factors (β) for the base-isolated tank model

8.4 Summary

In the first part of this chapter, a detailed finite element method was employed to study the fluid-structure interaction for liquid-filled conical elevated tanks with varying cone angles. Transient analyses using modal superposition technique were carried out to investigate the effect of cone slope angle on the base shear and base moment response of the supporting structure in elevated water tanks. Effects of tank wall flexibility, water sloshing and the rocking component as well as the lateral translational component were taken into consideration in the proposed FE analysis. Different damping ratios corresponding to the different parts of response (impulsive and convective) were assigned to the model. In addition, the instantaneous values of the sloshing and impulsive terms were determined separately.

Free vibration FE analyses resulted in natural frequencies and effective water mass ratios very close to those obtained from Housner's formulations with differences for water mass ratios smaller than 5% of the total mass of the fluid for all cases considered.

The sloshing response of the elevated water tanks considered was mainly dominated with the fundamental sloshing mode. However the results showed that the impulsive response of the tank models having large cone angles could not be accurately predicted by only considering the

fundamental impulsive mode. As a result, more impulsive modes other than the fundamental impulsive mode are needed in studying the dynamic behavior of such models.

Time history analyses of the elevated water tanks with different geometries showed that the effect of cone angle variations could be significant on the impulsive component of the response but not on the convective part. Increasing the cone angle and thereby increasing the unsupported cantilever length of the tank floor resulted in new dominant rocking modes having high participation factors and effective mass ratios. These rocking modes characterized with their relatively small natural frequencies had smaller associated response spectrum accelerations compared to those of typical lateral translational impulsive modes. Therefore, smaller shear forces and overturning moments were exerted at the shaft base of the elevated tanks having large cone angles (namely models C, D, and E in the current study). For instance, by only increasing the cone angle from 45° to 75°, the base shear and base moment of the shaft structure were decreased by a factor of 2.3 and 3.0, respectively. This allows much slimmer and lighter design of all supporting structures, including the shaft structure and the foundation system.

The computed FE time history results were also compared with those obtained from current practice. The current practice provided reasonable estimations for models with translational dominant behavior. However, the results were too conservative for models having dominant rocking behavior leading to an overdesign of the structure. As a result, it is recommended that a dynamic model having the capability to consider both lateral translational and rotational degrees of freedom be employed for the analysis of such structures.

In the second part of this chapter, some important aspects on elastomeric and lead-rubber bearings, their elaborate FE modeling, and their force-displacement behavior were addressed. Using the proposed FE technique, modeling of the nonlinear behavior of rubber material was

made possible. Optimum rubber material parameters were estimated successfully using a robust parameter identification scheme from several available experimental data simultaneously. The obtained set of material parameters resulted in an excellent correlation between experimental and analytical results under different deformation states and from low to high strain levels.

The load-deformation response of two typical full-scale lead-rubber bearings under the combined action of compression and shear was obtained up to moderate strain levels using the proposed FE procedure. The calculated FE results correlated well with those of the experimental study ensuring the adequacy of the proposed FE model. Employing this numerical model can result in a significant reduction in the amount of experimental and/or analytical work required to accurately characterize the hysteretic behavior of this type of isolators. Moreover, this elaborate FE model can be used to determine the global parameters of the simplified two-node model proposed for the practical simulation of the seismic behavior of rubber bearings in this study.

It was observed that the proposed simplified model was capable of accurately estimating the hysteretic response of energy dissipation devices with less computational efforts. The proposed simplified modeling approach is practical, accurate enough, and easy to use in 3D FE applications.

In the last part of this chapter, an attempt was made to apply seismic isolation using lead-rubber and elastomeric bearings to liquid-filled conical elevated tanks.

To investigate the effectiveness of seismic isolation for this type of structures, the dynamic response of both fixed and isolated conical elevated tanks partially filled with water was investigated using a three-dimensional numerical procedure under horizontal seismic excitations. Various studies were carried out to investigate the effects of different parameters on the effectiveness of the seismic isolation system. The examined parameters included: lateral versus

vertical isolation, different locations of isolators, shaft stiffness, tank aspect ratio, and yield strength of isolators.

Two possible construction details for vertical isolation and one detail for lateral isolation of conical elevated tanks were considered. It was observed that the application of passive control devices to conical elevated water tanks could offer a substantial benefit for the earthquake-resistant design of such structures. The magnitude and distribution of seismically induced forces, moments and displacements could be controlled through appropriate selection of device properties, isolators' locations, and tank's structural and geometrical characteristics.

The results of this study show the effectiveness of seismic isolation technique for these types of structures. In general, it can be concluded that the magnitude of tower drift, total hydrodynamic pressure, and seismically induced forces and moments is reduced significantly due to the presence of seismic isolation system whose dominant frequency is within the effective frequency range of seismically isolated systems. However, an increase in displacements in laterally isolated tanks seems to be inevitable unless providing additional damping is considered. The extra cost imposed by installing seismic isolators is expected to be offset by the additional savings achieved due to seismic isolation in the shaft structure, foundation and anchorage system, and tank material.

In general it was observed that more reduction in seismic shear, moment, and tower drift was achieved due to the lateral isolation scheme as compared to the vertical isolation. However, a different trend in response was observed in terms of lateral displacement at tank floor level. Vertical isolation resulted in a considerable reduction in lateral displacement while a significant increase in lateral displacement was experienced in the laterally isolated tank model. This could be the main advantage of vertical isolation over lateral isolation system. As a result, it can be

263

concluded that when excessive deformation due to lateral isolation is not of concern, this isolation strategy is usually a better option leading to a more effective solution to the problem. On the other hand, if additional structural movements can not be accommodated by existing tank design, vertical isolation scheme is preferred over lateral isolation.

Despite the foregoing advantages, it was observed that the sloshing height was amplified due to seismic isolation of the tanks in both broad and slender tank configurations. However, a greater amplification in sloshing displacement was noticed in the case of slender tank as compared to broad tank. This may be considered as a drawback for the isolated elevated tank systems as compared to the typical fixed-base tanks. It was also observed that the contribution of convective pressure component was negligibly increased as a result of seismic isolation, however the total hydrodynamic pressure was reduced significantly.

To determine the optimum location of seismic isolators for elevated water tanks, two different isolated models (isolation type A and B) were selected and base shear, base moment, tower drift, lateral displacement at tank floor level, bearing displacement, and absorbed energy were examined under the horizontal component of 1940 El-Centro record. In isolation type A, isolators were located at the base of the tank while in isolation type B, isolators were provided at top of the shaft structure immediately below the concrete ring beam. Isolation types A and B predicted different response variations. More reduction in base shear and base moment response values was achieved by isolation type A as compared to isolation type B. However, a different trend was noticed for tower drift response. In terms of displacement at tank floor level, isolation type B was found to be more advantageous over isolation type A. In addition, a slightly smaller bearing displacement was obtained for isolation type B as compared to isolation type A. In addition, the amount of energy dissipated during the seismic excitation was increased where

isolators were located at the base of the tank compared to the case where isolators were placed at top of the shaft structure.

Higher isolation efficiency was observed in tanks having stiffer shaft structure in comparison to those with more flexible shaft structure. It was shown that the seismic response of isolated tanks was not considerably affected by the flexibility of the shaft structure.

The seismic isolation resulted in significant advantages for both broad and slender tank configurations. However, slender tanks were found to be better candidates in terms of more effective application of seismic isolation. Sloshing displacement in slender tank was comparatively greater than that of broad tank in both isolated and non-isolated conditions.

Due to a potential coupling between the sloshing and isolation modes of vibration, especially in slender tanks, an accurate estimation of seismic response of isolated elevated tanks is achievable by considering the contributions of at least two modes of vibration; convective mode and isolation mode. It was also observed that the bearing displacement increased as the tank's aspect ratio increased resulting in an increase in the total amount of absorbed energy.

The results of the study also revealed that there was an optimum value for the yield strength of isolators at which the seismic response (base shear) of the tank reached its minimum value. For the specific tank and seismic excitation used in this study, this optimum value was determined to be about 5% of the weight applied on the isolators.

Based on the results of free-vibration analysis performed on a base-isolated elevated tank model, it was observed that impulsive modes were significantly affected by the properties of seismic isolation system in comparison to sloshing modes. Based on the calculated modal participation factors, it can be concluded that the base-isolation mode dominates the total dynamic response of the base-isolated tank model. The second highest modal participation factor

265

among all modes of vibration was found for the convective mode. The participation factor corresponding to the impulsive mode was found to be very small implying that this mode does not contribute considerably in the overall seismic response of isolated elevated tanks.

CHAPTER 9

SUMMARY, CONCLUSIONS AND RECOMMENDATIONS

9.1 Summary

The main focus of the current study was to evaluate the performance of cylindrical ground-supported as well as conical elevated water tanks under seismic excitations using a rigorous and efficient finite element technique.

As a result of major advances in computer science and the development of rigorous numerical codes, academic and industrial interest in the use of finite element technique as a tool to investigate the fluid-structure interaction problems has greatly increased in recent years. Using this technique, more precise and realistic results are generally obtainable. In this research study, the fluid-structure coupling formulations were solved using a finite element technique. Various kinds of analysis including modal, spectral and time history analysis using both modal superposition and direct integration methods were carried out using the general-purpose finite element analysis program ANSYS®. Throughout this study, the effects of important factors on dynamic behavior of such structures were addressed. The examined parameters were sloshing of liquid free surface, tank wall flexibility, vertical ground acceleration, tank aspect ratio, base fixity, and higher impulsive and convective modes.

The accuracy of the proposed numerical model was verified by comparing the obtained results with other analytical and experimental results available in the literature.

According to the methodology commonly used in current design standards, the dynamic response of partially filled liquid tanks is calculated using simplified mechanical models and a frequency-based approach. The Housner's method is the most well-known procedure employed

in current design practice for seismic analysis and design of liquid tanks. In this technique, the tank hydrodynamic response is divided into two components; "impulsive" and "convective". In order to investigate the validity of current code provisions in seismic analysis and design of liquid containing structures, the obtained FE results were compared with those recommended by current practice and important conclusions were drawn.

Furthermore, the effect of earthquake frequency content on the seismic behavior of liquid-filled elevated tanks was investigated. To do so, a typical elevated tank model was numerically simulated using FEM in a three-dimensional space and its seismic response was determined under the effect of different seismic excitations having different frequency content characteristics.

The seismic behavior of elevated water tanks was further studied by carrying out a comprehensive parametric study on liquid-filled conical elevated tanks using the finite element technique. Through this parametric study, a broad range of tank capacities and geometries typically found in use today was covered. This parametric study led to generation of pressure distribution graphs corresponding to both impulsive and convective components for a large number of conical elevated tanks having different geometrical properties. It was also indicated that the proposed pressure graphs could be employed simply in design applications for liquid-filled conical elevated tanks.

The applicability of two different menshin techniques to liquid-filled conical elevated tanks was investigated. As a first menshin technique, "Natural period adjustment method" was introduced and its effectiveness was investigated using a rigorous finite element method in a three-dimensional space. In this technique, the natural period of the elevated tank model was extended far beyond the predominant period of the input seismic motion by making alterations in

tank's configuration/geometry. This was achieved by increasing the inclined cone angle of the lower portion of the vessel. As a second menshin technique, the application of seismic isolation method to conical elevated tanks was examined. In this technique, the shaft structure was isolated either at top immediately below the ring beam level or at the base by means of elastomeric and lead-rubber bearings.

9.2 Conclusions

Based on the results of this research study, the following conclusions are made regarding the dynamic behavior of ground-supported cylindrical containers:

1. The proposed FE procedure can be accurately employed in dynamic analysis of liquid containers. Using this method, all aspects in fluid-structure interaction problems can be considered including wall flexibility, sloshing motion, damping properties of fluid domain, and the individual effects of impulsive and convective terms in a three-dimensional space.

2. For practical purposes, only the fundamental impulsive and convective modes are sufficient for characterizing the dynamic response of ground-supported cylindrical tanks to horizontal excitations. Moreover, the $\cos(n\theta)$ type modes ($n > 1$) have a negligible effect on the overall dynamic response of the tanks to horizontal excitations. Modes having the highest contributions to the response are cantilever beam type modes with $n = 1$.

3. Since the sloshing and impulsive components of the response do not reach their peak values at the same time, the effect of considering sloshing term on the total response might be either increasing or decreasing.

4. The effect of convective term on the overall dynamic response of cylindrical ground-supported containers is rather more significant in shallow tanks compared to tall tanks.

5. Including the wall flexibility result in a significant increase on the impulsive component of response. However, the convective component of response is found to be almost independent of the tank wall flexibility. Furthermore, the sloshing height of the liquid inside the tanks is not significantly affected by the wall flexibility.

6. Considering the combined effect of horizontal and vertical excitations, it is concluded that including the vertical acceleration effect leads to an increase in both impulsive and convective terms of response for "Shallow" as well as "Tall" tank models. The combined ground acceleration has a greater effect on the convective component of response than it has on the impulsive component. The overall effect of combined acceleration is found to be insignificant in "Shallow" tank model. The sloshing height is increased as a result of combined effect of vertical and horizontal ground motions. The combined acceleration has a relatively greater effect on "Tall" tank's response than it has on "Shallow" tank's response. As a result, the combined effect of horizontal and vertical ground motions needs to be taken into consideration appropriately in seismic analysis of tall cylindrical containers.

7. The pure vertical ground motion can cause dynamic effects as high as those of the horizontal motion when considered separately, however its effect is found to be of less importance when horizontal and vertical earthquake components are applied together.

8. Pure vertical transient excitations result in very negligible convective response values for both tank configurations considered. As a result, the effect of convective component in

determining the seismic response of cylindrical tanks under pure vertical transient motions can be ignored.

9. ACI 350.3-06 standard is not capable of appropriately accounting for the effects of wall flexibility and base fixity. That is, it gives the same hydrodynamic pressure values for rigid and flexible tanks as well as for hinged and fixed tanks. As a result, ACI estimations could be too conservative for the case of rigid tanks.

10. In general, ACI 350.3-06 (2006) provisions yield a conservative estimation of results, especially in the case of rigid tanks. This is observed for "Shallow" as well as "Tall" tanks. In addition, since the hydrodynamic pressure approximated by the Code has a linear vertical distribution, the Code estimations of hydrodynamic pressure could be too conservative for the sections near the base.

11. Generally larger structural response values are developed in the walls of a hinged tank as compared to a fixed tank far from the base. However, the maximum absolute values of the base shear and base moment are higher in the case of a fixed tank compared to a hinged one. In addition, larger impulsive pressure values are exerted on the walls of a hinged tank compared to an analogous fixed tank. However, the base fixity condition has no significant effect on the convective pressure component. Sloshing height is also found to be insensitive to the type of connection at the base.

The following conclusions can be stated regarding the dynamic behavior of liquid-filled conical elevated tanks:

1. The proposed finite element technique is capable of accounting for the fluid-structure interaction in conical liquid containers. Using this method the study of liquid sloshing effects in tanks with complex geometries such as conical tanks is made possible.

2. A very good agreement is observed between the "current practice" and FE time history results for the elevated tank models under consideration subjected to a ground motion. This verifies the validity of the "current practice" in estimating the seismic response of liquid filled elevated water tanks. However, the results of the study show that the "current practice" is not capable of accounting for the effect of earthquake frequency content on the dynamic response of such structures appropriately.

3. The response values are highly overestimated using the "equivalent lateral force procedure" recommended by ACI 371R-08. Therefore, it can be concluded that this procedure does not provide an accurate estimation of seismic response for elevated water tanks and in general leads to an overdesign of the shaft-foundation system.

4. The "combined Code/FE" method (i.e. FE modal analysis results in combination with Code response spectrum) results in an underestimation of seismic response values. This indicates the inadequacy of this method for design applications. Comparing the results obtained through different methods, it can be concluded that the "current practice" method provides more accurate results compared to the "equivalent lateral force procedure" and the "combined Code/FE" methods.

5. The effect of earthquake frequency content on the seismic response of conical elevated tanks could be very significant and therefore may result in a substantial increase in transient response values. It is found that the response values due to the intermediate frequency content record of El-Centro are significantly amplified as a result of the similarity between the frequency characteristics of the tank-pedestal system and the earthquake record.

6. Based on the results of the parametric study, the convective and impulsive pressure values along the height of the tank wall under lateral seismic excitations for typical conical elevated tanks found in practice today can be separately determined. The proposed pressure graphs can be utilized with high level of accuracy for seismic design of liquid-filled conical elevated tanks.

7. The effect of inclusion of the roof on dynamic response of conical elevated tanks is insignificant and as a result its effect can be neglected.

8. The effect of variations of cone angle of the tank could be significant on the impulsive component of the response but not on the convective component. By increasing the cone angle and thereby increasing the unsupported cantilever length of the tank floor, the shear force and overturning moment exerted at the shaft base of the elevated tanks can be reduced significantly. For instance, by only increasing the cone angle from 45° to 75°, the base shear and base moment are reduced by factors of 2.3 and 3.0, respectively. This could lead to a more economical tank design.

9. The current practice provides reasonable estimations for tanks with translational dominant behavior. However, the results are too conservative for tanks having dominant rocking behavior leading to an overdesign of the structure. It is recommended that a dynamic model having the capability to consider both lateral translational and rotational degrees of freedom be employed for the analysis of such structures.

10. The load-deformation response of typical rubber bearings under the combined action of compression and shear can be obtained accurately using the proposed FE procedure. This elaborate FE model can also be employed to determine the global parameters of the simplified two-node model proposed for the practical simulation of the seismic behavior

of rubber bearings in this study. The proposed simplified model is capable of accurately estimating the hysteretic response of energy dissipation devices with less computational efforts. The proposed simplified modeling approach is practical, accurate enough, and easy to use in 3D FE applications.

11. The results of the study show the effectiveness of seismic isolation technique for elevated water tanks. The magnitude of tower drift, total hydrodynamic pressure, and seismically induced forces and moments is reduced significantly by the effect of seismic isolation system whose dominant frequency is in the effective frequency range of seismically isolated systems. However, an increase in displacements in laterally isolated tanks seems to be inevitable unless a larger amount of damping is provided.

12. More reduction in seismic shear, moment, and tower drift is achieved by the lateral isolation scheme as compared to the vertical isolation. However, a different trend is observed in terms of the lateral displacement response at tank floor level. Vertical isolation results in a considerable reduction in lateral displacement while a significant increase in lateral displacement is experienced in laterally isolated tank models.

13. The sloshing height is amplified due to seismic isolation of the tanks in both broad and slender tank configurations. However, a greater amplification in sloshing displacement is noticed in the case of slender tank as compared to broad tank. This may be considered as a drawback for the isolated elevated tank systems as compared to the typical fixed-base tanks. It is also found that the contribution of convective pressure component is negligibly increased as a result of seismic isolation however the total hydrodynamic pressure is reduced significantly.

14. Providing isolators at the base of the shaft (type A) and at top of the shaft (type B) result in different response variations. More reduction in base shear and base moment response values is achieved by isolation type A as compared to type B. However, a different trend is noticed for tower drift response. In terms of displacement at tank floor level, isolation type B is found to be more advantageous over isolation type A. In addition, a slightly smaller bearing displacement is obtained for isolation type B as compared to type A. In addition, the amount of energy dissipated during the seismic excitation is increased where isolators are located at the base of the tank compared to those are placed at top of the tower structure.

15. Higher isolation efficiency is observed in tanks having stiffer shaft structure in comparison to those with more flexible shaft structure. In addition, the seismic response of isolated tanks is not considerably affected by the flexibility of the shaft structure.

16. The seismic isolation results in significant advantages for both broad and slender tank configurations. However, slender tanks are concluded to be better candidates in terms of more effective application of seismic isolation. It is also observed that the bearing displacement increases as the tank's aspect ratio increases resulting in an increase in the total amount of absorbed energy.

17. Due to a potential coupling between the sloshing and isolation modes of vibration, especially in slender tanks, an accurate estimation of seismic response of isolated elevated tanks is achievable by considering the contributions of at least two modes of vibration; convective mode and isolation mode.

18. There is an optimum value for the yield strength of isolators at which the seismic response of the tank reaches its minimum value. For the specific tank and seismic

excitation used in this study, this optimum value is determined to be about 5% of the weight applied on the isolators.

19. Impulsive modes are more significantly affected by the properties of seismic isolation system in comparison to sloshing modes. The base-isolation mode dominates the total dynamic response of the base-isolated tank model. The second highest modal participation factor among all modes of vibration is found for the convective mode. The participation factor corresponding to the impulsive mode is found to be very small implying that this mode does not contribute considerably in the overall seismic response of isolated elevated tanks.

9.3 Recommendations for future studies

Based on this research study, some suggestions for further research on dynamic behavior of cylindrical ground-supported and conical elevated water tanks can be made as follows:

1. More case studies with varying tank capacity, liquid depth, tank aspect ratio, shaft geometry, and ground excitation properties can be carried out through a careful selection of wide range of liquid storage tanks in order to verify the effects of these parameters on the dynamic response of such structures.

2. The dynamic response of liquid-filled conical elevated tanks under vertical ground accelerations can be investigated using the proposed numerical procedure.

3. The effect of deformable foundation on dynamic behavior of liquid containing structures can be investigated by simulating the soil-structure interaction (SSI) effect in a rigorous numerical model. Moreover, the effect of different support conditions such as un-anchored connections can be further studied.

276

4. The sloshing behavior of liquid tanks can be further investigated using nonlinear free surface boundary condition.

5. The effect of inclusion of the access tube, wall openings, and interior platforms on seismic response of conical elevated tanks can be further investigated.

6. It is suggested that the nonlinear behavior of steel and reinforced concrete materials be included in numerical modeling of the tanks.

7. Effects of lateral and vertical stiffness properties of elastomeric and lead-rubber bearings on seismic response of isolated elevated water tanks can be further studied.

8. The application of other types of isolation and energy dissipation devices such as friction-pendulum, lead extrusion dissipater, and torsional/flexural beam/plate devices to liquid storage tanks can be studied in future research.

9. The dynamic behavior of isolated elevated tanks under wind load is recommended to be investigated in the future studies.

APPENDIX A

LAMINA FLUID THEORY

A.1 Housner's method

Lamina fluid theory was used as the basis by Housner (1957; 1963) to calculate the hydrodynamic pressure components in rectangular and cylindrical liquid containers. He separated the hydrodynamic pressures into impulsive and convective parts and proposed practical formulations for predicting the dynamic behavior of each part separately. In the proposed analysis, the fluid was assumed to be incompressible and the fluid displacements were considered to be small. The tank was assumed to be rigid and subjected to horizontal acceleration.

A.1.1 Impulsive pressure

Figure A.1(a) shows a liquid tank having vertical walls and horizontal floor. The tank is symmetrical with respect to the x-y and z-y planes. As the tank undergoes an acceleration $\ddot{u}_0$ in the horizontal x direction, acceleration components $\ddot{u}$, $\ddot{v}$, and $\ddot{w}$ will be generated in the fluid domain in x, y, and z directions, respectively. It is assumed that $\ddot{w}$ is either zero or very small that it can be neglected. As a result of this assumption, the fluid domain can be assumed as a series of lamina of dz thickness which are separated by thin vertical membranes. This will force the fluid to vibrate in the x-y plane only. Therefore, for simplification it can be considered that the hydrodynamic pressures are generated in a lamina of fluid.

(a)

(b)
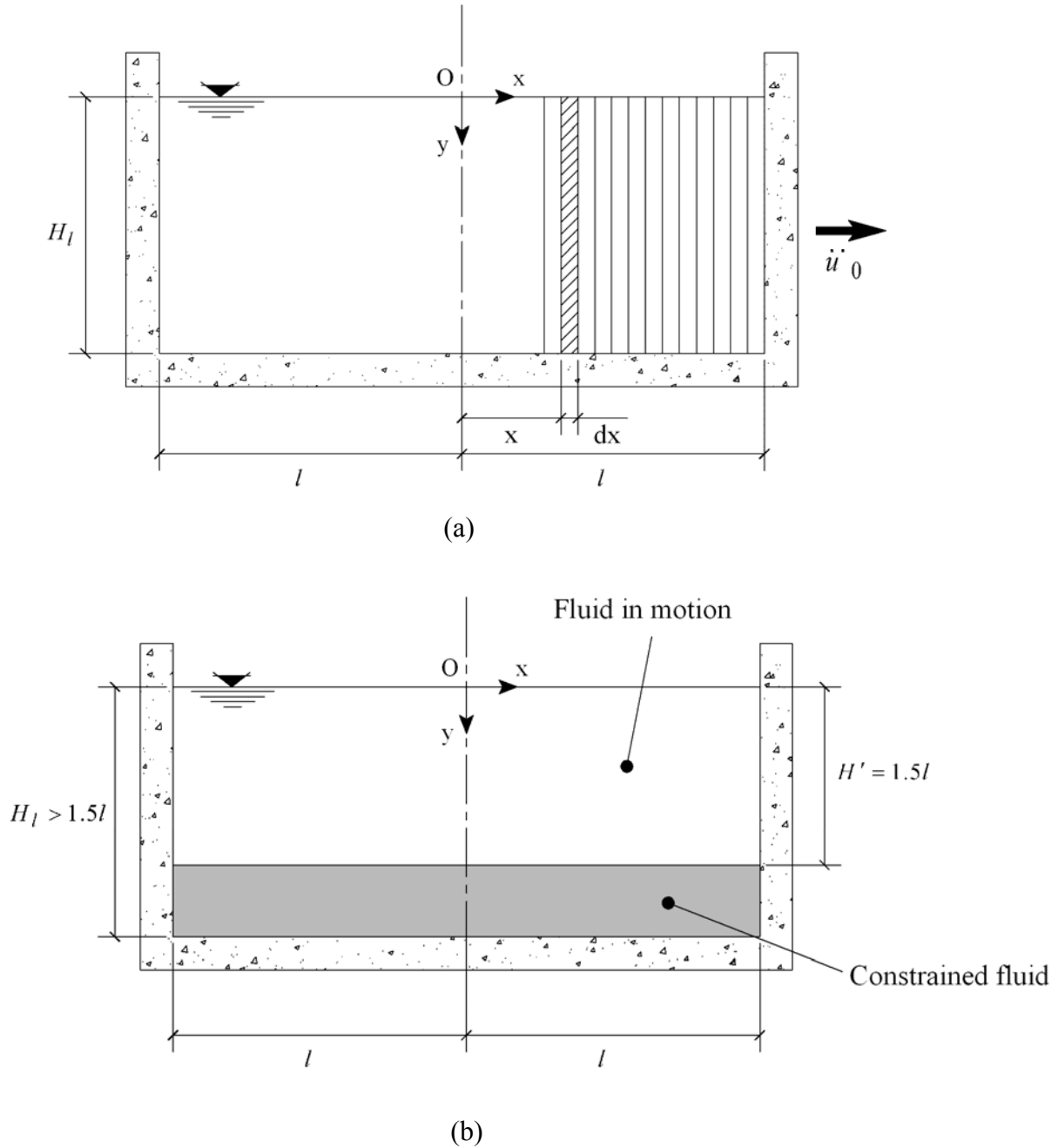
Figure A.1 Generalized symmetrical tank model (for cylindrical tanks $l = R$); (a) x-y view,

(b) Slender tank special case with $H_l > 1.5l$

A lamina of fluid of unit thickness in the x-y plane is shown in Figure A.1(a). As a result of

the horizontal vibration of the tank, a horizontal and a vertical component of acceleration will be

imparted to the contained fluid. As a reasonable assumption, the horizontal component of fluid velocity $\dot{u}$ can be considered independent of the y coordinate. Physically, this is equivalent to assuming that the fluid is constrained by thin, massless, vertical membranes which can move freely along x direction. As shown in the figure, the original distance between the membranes is assumed to be dx. As the tank experiences base excitation, the membranes together with the fluid will be accelerated. The fluid will also be squeezed in vertical direction with respect to the membranes. Using the mass balance criterion on the lamina shown in Figure A.2, one can obtain the relation between the horizontal and vertical velocity components, $\dot{u}$ and $\dot{v}$, as follows:

$$\dot{v}dx + \dot{u}(H_l - y) = (\dot{u} + \frac{\partial \dot{u}}{\partial x}dx)(H_l - y) \qquad \text{or} \qquad (A\text{-}1)$$

$$\dot{v} = (H_l - y)\frac{\partial \dot{u}}{\partial x}$$

Differentiating with respect to time results in:

$$\ddot{v} = (H_l - y)\frac{\partial \ddot{u}}{\partial x} \qquad (A\text{-}2)$$
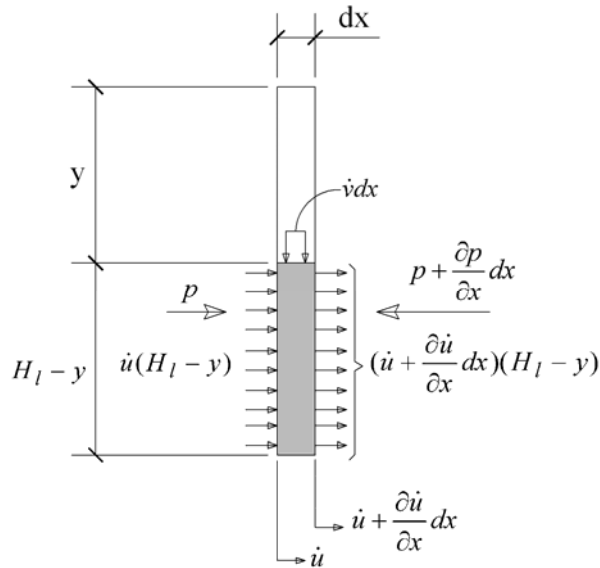
Figure A.2 Fluid element under consideration

Applying Newton's law to a differential fluid element shown in Figure A.3, one can obtain the equation of motion in the vertical direction:

$$-\frac{\partial p}{\partial y}dxdy = \rho_l dxdy\frac{d\dot{v}}{dt} \qquad \text{or} \qquad (A-3)$$

$$\frac{\partial p}{\partial y} = -\rho_l\frac{d\dot{v}}{dt} = -\rho_l(\frac{\partial \dot{v}}{\partial t} + \frac{\partial \dot{v}}{\partial x}\frac{dx}{dt} + \frac{\partial \dot{v}}{\partial y}\frac{dy}{dt})$$

where, p is the hydrodynamic impulsive pressure, and ρ_l is liquid density; $\frac{dx}{dt}$ and $\frac{dy}{dt}$ represent $\dot{u}$ and $\dot{v}$, respectively. As mentioned before the fluid displacements were assumed to be small. As a result, the derivatives of the velocities with respect to x and y are also considered to be small and may be omitted from Eq. A-3 resulting in:

$$\frac{\partial p}{\partial y} = -\rho_l(\frac{\partial \dot{v}}{\partial t}) \qquad (A-4)$$
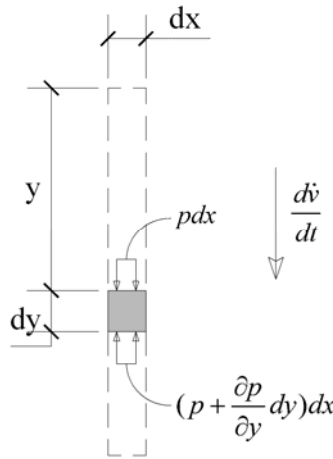
Figure A.3 Differential fluid element

The total horizontal impulsive force acting on one membrane is obtained by the following integration:

$$P = \int_0^{H_l} p\,dy \tag{A-5}$$

Substituting Eq. A-2 into Eq. A-4, integrating from zero to y, and taking into consideration that $p|_{(y=0)} = 0$ and $\ddot{u} \neq \ddot{u}(y)$, the impulsive pressure is determined as follows:

$$p = -\rho_l \frac{\partial \ddot{u}}{\partial x} \int_0^y (H_l - \bar{y})d\bar{y} = -\rho_l H_l^2 \left[\frac{y}{H_l} - \frac{1}{2}(\frac{y}{H_l})^2 \right] \frac{\partial \ddot{u}}{\partial x} \tag{A-6}$$

Impulsive force can be obtained by substituting Eq. A-6 into Eq. A-5,

$$P = -\rho_l H_l^2 \frac{\partial \ddot{u}}{\partial x} \int_0^{H_l} \left[\frac{y}{H_l} - \frac{1}{2}(\frac{y}{H_l})^2 \right] dy = -\frac{1}{3}\rho_l H_l^3 \frac{\partial \ddot{u}}{\partial x} \tag{A-7}$$

By applying the Newton's rule to the fluid element shown in Figure A.2, one can obtain the equation of motion in the x direction. It is important to note that all higher order terms arising from the time derivative of $\dot{u}$ are ignored in obtaining this equation,

$$\frac{\partial P}{\partial x} = -\rho_l H_l \ddot{u} \tag{A-8}$$

Substituting the impulsive force (P) from Eq. A-7 into Eq. A-8,

$$\frac{\partial^2 \ddot{u}}{\partial x^2} - \frac{3}{H_l^2} \ddot{u} = 0 \tag{A-9}$$

It should be noted that $\ddot{u}$ is considered as a dependant variable which is only a function of x. As a result, Eq. A-9 may be considered as a total differential equation with its solution given as:

$$\ddot{u} = C_1 \cosh \sqrt{3}\, \frac{x}{H_l} + C_2 \sinh \sqrt{3}\, \frac{x}{H_l} \tag{A-10}$$

Eq. A-6 together with Eq. A-10 will be used to determine the impulsive fluid pressure. However, care should be taken that these equations are only applicable when the surface is

horizontal. Nevertheless, considering the small displacements of fluid, the equations can still be used even when the fluid surface has been excited into oscillations.

For slender tanks with $\dfrac{H_l}{R} > 1.5$, better results for impulsive pressure distribution may be obtained by applying the equations A-6 and A-7 to the upper part of the fluid domain ($H' = 1.5R$) and considering the lower portion of the fluid as a constrained fluid (see Figure A.1(b)). As a result, it can be assumed that the upper and lower portions of the fluid domain are separated from each other by means of a fixed rigid membrane located at $y = H'$. The equation of motion for the constrained portion of fluid in the horizontal direction is obtained by applying the Newton's law to a differential element as before. Assuming a tank wall acceleration of $\ddot{u}_0$, we have:

$$\frac{\partial p}{\partial x} = -\rho_l \ddot{u}_0 \tag{A-11}$$

Integrating Eq. A-11 and considering that because of symmetry $p\big|_{(x=0)} = 0$, we have:

$$p = -\rho_l \ddot{u}_0 x \tag{A-12}$$

A.1.2 Convective pressure

When the tank walls undergo seismic accelerations, the fluid surface is excited into motion and as a result of this motion, hydrodynamic convective pressures will be produced on the wall and floor of the tank. In order to determine the convective pressures associated with the first mode of fluid vibration, it is assumed that the fluid domain is restrained by horizontal, rigid membranes which are free to rotate as depicted in Figure A.4. Again, $\dot{u}$, $\dot{v}$, and $\dot{w}$ denote fluid velocity components in x, y, and z directions. The following two assumptions are made in deriving the equations:

(1) All fluid particles in the element shown in Figures A.4 and A.5 travel with uniform $\dot{u}$.

(2) All fluid particles in the same element travel with uniform $\dot{v}$.
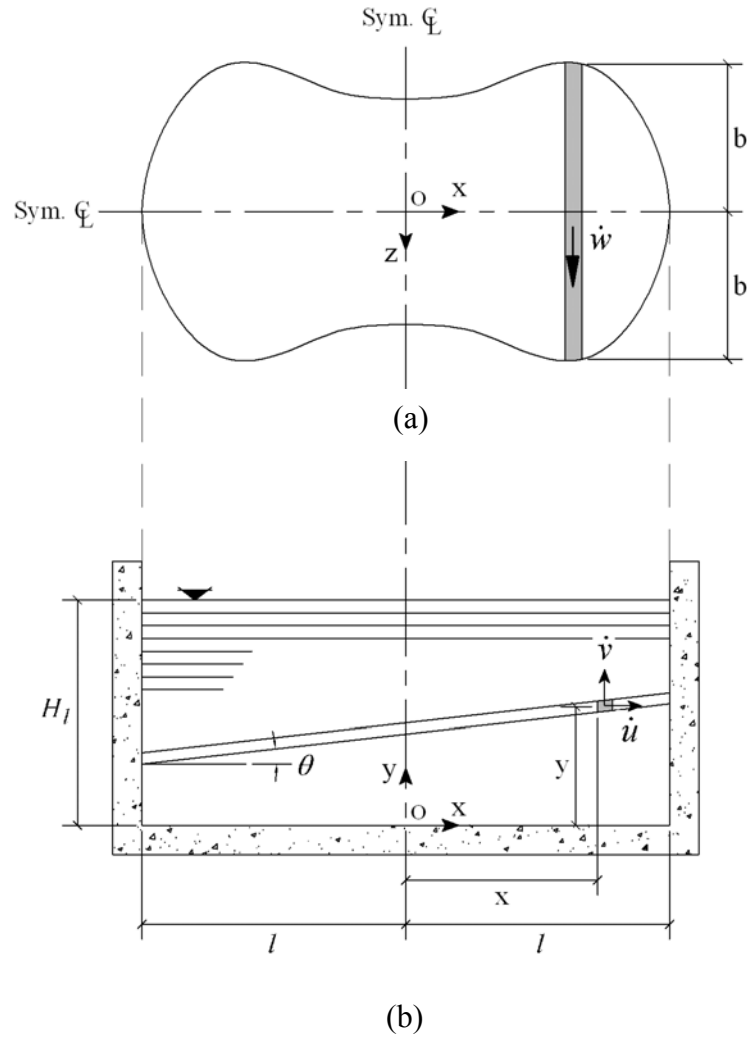
Figure A.4 Generalized symmetrical tank model (for cylindrical tanks $l = R$);

(a) tank plan, (b) tank section

Applying the mass balance criterion on the fluid element shown in Figure A.5 results in the following equation:

$$-2\frac{\partial}{\partial x}(\dot{u}b)dxdy - 2b\frac{\partial \dot{v}}{\partial y}dxdy = 0 \qquad \text{or} \qquad (A\text{-}13)$$

$$\frac{\partial}{\partial x}(\dot{u}b) = -b\frac{\partial\dot{v}}{\partial y}$$

Assumption (2) described above will lead to the following equation:

$$\dot{v} = x\dot{\theta} \qquad\qquad\qquad\qquad\qquad\qquad\qquad\qquad (A\text{-}14)$$

where, $\dot{\theta}$ is the derivative of angle of oscillation (θ).

Eq. A-14 is valid only if θ is small enough. The equation of continuity can be obtained by applying the mass balance criterion to a differential element having dimensions dx, dy, and dz, hence:

$$-\frac{\partial\dot{u}}{\partial x}dxdydz - \frac{\partial\dot{v}}{\partial y}dxdydz - \frac{\partial\dot{w}}{\partial z}dxdydz = 0 \qquad \text{or} \qquad\qquad (A\text{-}15)$$

$$\frac{\partial\dot{w}}{\partial z} = -(\frac{\partial\dot{u}}{\partial x} + \frac{\partial\dot{v}}{\partial y})$$
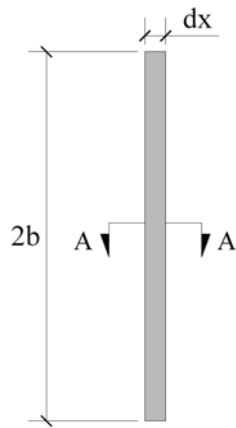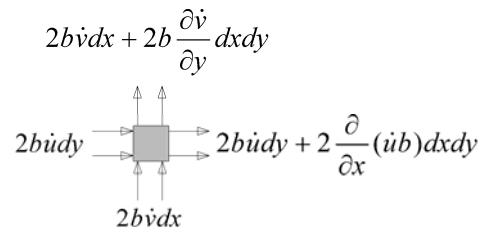
(a)   (b)

Figure A.5 Fluid element free body diagram; (a) Plan, (b) Section A-A

It is important to note that θ is a function of y and t but not of x. As a result, at a particular time, the membrane rotation is only a function of its vertical location. The following boundary conditions exist for the considered model:

$$\dot{u} = 0 \text{ at } x = \pm l \tag{A-16}$$

$$\dot{w} = 0 \text{ at } z = 0 \tag{A-17}$$

$$\theta = 0 \text{ at } y = 0 \tag{A-18}$$

$$\theta = \theta_H \text{ at } y = H_l \tag{A-19}$$

Similar to the procedure explained in the previous section, the appropriate equations of motion can be determined for the tank under consideration. Substituting the obtained variables into appropriate equations and taking the required integrations, the following equations for velocity components $\dot{u}$ and $\dot{w}$ are resulted:

$$\dot{u} = -\frac{1}{b}\frac{\partial \dot{\theta}}{\partial y}\int_{-l}^{x} b(\bar{x})\bar{x}d\bar{x} \tag{A-20}$$

$$\dot{w} = -z\frac{b'}{b^2}\frac{\partial \dot{\theta}}{\partial y}\int_{-l}^{x} b(\bar{x})\bar{x}d\bar{x} \tag{A-21}$$

where, $b' = db/dx$.

In the next step, the total kinetic energy and potential energy are determined and used in Hamilton's principle. The total kinetic energy is defined as the integral over the volume of the kinetic energy of the fluid elements. The potential energy is calculated by summing the energy contributions from each fluid element located in the disturbed surface due to its average displacement from the equilibrium condition. Applying the Hamilton's principle and taking the required integrations and derivatives, the following equations are derived:

$$\theta = \theta_{Hm}\frac{\sinh\sqrt{\frac{I}{K}}y}{\sinh\sqrt{\frac{I}{K}}H_l}\sin \omega t \tag{A-22}$$

in which, θ_{Hm} is the maximum angular amplitude of fluid motion at the free surface and is defined in the flowing equation:

$$\theta_H = \theta_{Hm} \sin \omega t \tag{A-23}$$

Variables I and K are defined as follows:

$$I = \int_{-l}^{l} \int_{-b}^{b} x^2 \, dxdz \tag{A-24}$$

$$K = 2 \int_{-l}^{l} \frac{1}{b} \left[\int_{-l}^{x} b(\bar{x}) \bar{x} d\bar{x} \right]^2 (1 + \frac{b'^2}{3}) dx \tag{A-25}$$

ω is the natural frequency of the fundamental mode of free surface vibration and is defined as follows:

$$\omega^2 = g \sqrt{\frac{I}{K}} \tanh \sqrt{\frac{I}{K}} H_l \tag{A-26}$$

Neglecting the higher order terms, the equations of motion can be written as:

$$\frac{\partial p}{\partial x} = -\rho_l \ddot{u} \qquad \text{and} \tag{A-27}$$

$$\frac{\partial p}{\partial z} = -\rho_l \ddot{w} \tag{A-28}$$

where, p represents the hydrodynamic convective pressure. It is worth noting that in deriving the fluid pressure formulations, only the fluid motion along the x direction is considered, even though the membranes also experience accelerations along the vertical direction. Using Eqs. A-20 and A-21 in Eqs. A-27 and A-28, the pressure differential can be written as:

$$dp = -\rho_l \ddot{u} dx = \rho_l \frac{\partial \ddot{\theta}}{\partial y} \frac{B}{b} dx \tag{A-29}$$

where,

$$B = \int_{-l}^{x} b(\bar{x})\bar{x}d\bar{x} \tag{A-30}$$

Integrating Eq. A-29, with the condition that $p(0, y, 0) = 0$, because of symmetry, we have:

$$p = \rho_l \frac{\partial \ddot{\theta}}{\partial y} \left[\int_0^x \frac{B(\bar{x})}{b(\bar{x})} d\bar{x} \right] \tag{A-31}$$

In the above equation, p is the dynamic convective pressure. Having obtained pressure, one can determine the resulting forces and moments on the wall and the floor of the tank simply. The obtained equations can then be applied to any container of specified shape having two-fold symmetry such as rectangular and cylindrical tanks.

A.1.3 Impulsive and convective pressures in cylindrical tanks

In this section, the specific case of a circular cylindrical tank is treated in detail and important formulations are presented. A typical cylindrical tank with the radius of R is shown in Figure A.6. The tank is considered to be subjected to the horizontal acceleration $\ddot{u}_0$ along the x direction. In cylindrical tanks, each slice of fluid domain may be assumed as if it were a narrow rectangular tank, and as a result, the equations corresponding to the rectangular tanks can be applied to each slice. Therefore, the hydrodynamic impulsive pressure (p) exerted on the wall of a cylindrical tank can be obtained from the following equation:

$$p = -\rho_l \ddot{u}_0 H_l \left[\frac{y}{H_l} - \frac{1}{2} (\frac{y}{H_l})^2 \right] \sqrt{3} \tanh(\sqrt{3} \frac{R}{H_l} \cos\phi) \tag{A-32}$$

In order to further simplify the preceding expression, the following modification to Eq. A-32 may be suggested:

$$p = -\rho_l \ddot{u}_0 H_l \left[\frac{y}{H_l} - \frac{1}{2} (\frac{y}{H_l})^2 \right] \sqrt{3} \cos\phi \tanh(\sqrt{3} \frac{R}{H_l}) \tag{A-33}$$

Eq. A-33 gives very accurate estimations when $\dfrac{R}{H_l}$ is small but may overestimate the

impulsive pressure values when $\dfrac{R}{H_l}$ is not small enough. Using this equation, the resultant total

impulsive force exerted on the wall is:

$$P = \int_0^{H_l} \int_0^{2\pi} pR\cos\phi \, d\phi \, dy = -\rho_l \ddot{u}_0 \pi R^2 H_l \frac{\tanh(\sqrt{3}\,\dfrac{R}{H_l})}{(\sqrt{3}\,\dfrac{R}{H_l})} \tag{A-34}$$

(a)   (b)
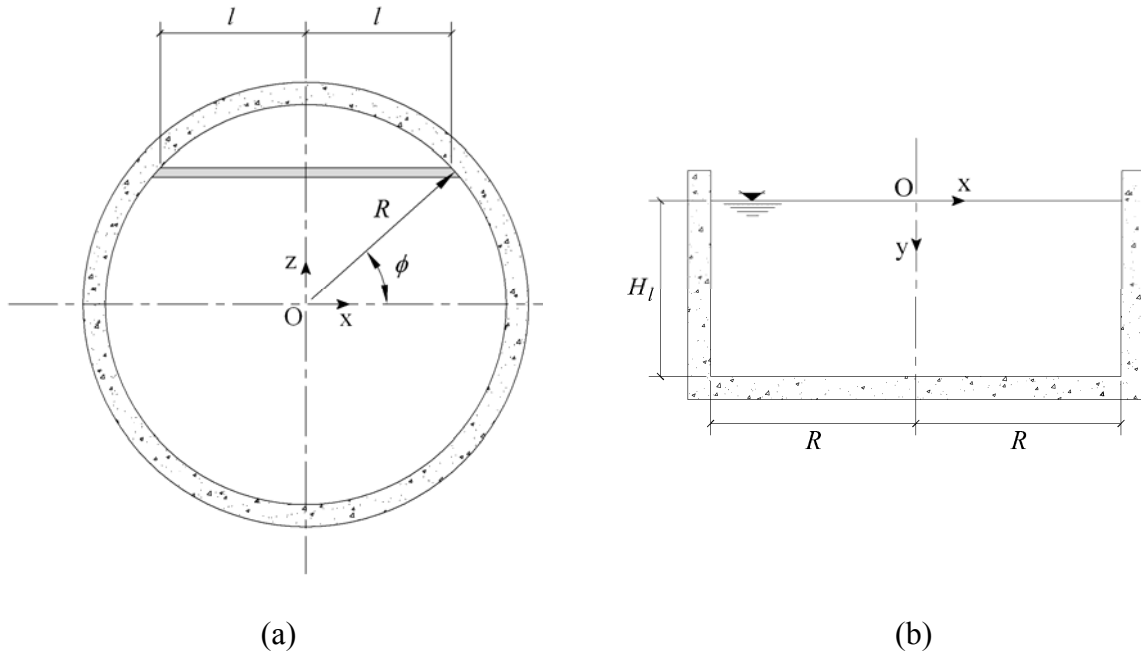
Figure A.6 Typical cylindrical tank; (a) tank plan, (b) tank section

It can be seen that the overall effect of the impulsive fluid on the walls of the tank is the

same as if an equivalent lumped mass, M_i were rigidly attached to the walls at an equivalent

height, h_i above the base. The magnitude and location of M_i is determined as follows:

$$M_i = -\frac{P}{\ddot{u}_0} = \rho_l \pi R^2 H_l \frac{\tanh(\sqrt{3}\,\frac{R}{H_l})}{(\sqrt{3}\,\frac{R}{H_l})} = M \frac{\tanh(\sqrt{3}\,\frac{R}{H_l})}{\sqrt{3}\,\frac{R}{H_l}} \tag{A-35}$$

where, M is the total mass of fluid.

In order to produce a moment equal to that exerted by the impulsive pressure on the wall, the impulsive mass M_i should be located at a height $h_i = \frac{3}{8} H_l$ above the base of the tank (see Figure A.7). This height, h_i does not take into account the effect of fluid pressure exerted on the tank floor.

Regarding the oscillation of the fluid free surface in the fundamental mode (convective response), the following expressions for the angle of oscillation (θ) and natural frequency of vibration (ω) are obtained in cylindrical tanks:

$$\theta = \theta_{Hm} \frac{\sinh\sqrt{\frac{27}{8}\frac{y}{R}}}{\sinh\sqrt{\frac{27}{8}\frac{H_l}{R}}} \sin \omega t \tag{A-36}$$

$$\omega^2 = \frac{g}{R}\sqrt{\frac{27}{8}} \tanh\sqrt{\frac{27}{8}\frac{H_l}{R}} \tag{A-37}$$

The hydrodynamic convective pressure on the wall of a cylindrical tank is obtained by the following equation:

$$p = \sqrt{\frac{3}{8}}\rho_l R^2 \theta_{Hm}(1-\frac{1}{3}\cos^2\phi)\cos\phi \frac{\cosh\sqrt{\frac{27}{8}\frac{y}{R}}}{\sinh\sqrt{\frac{27}{8}\frac{H_l}{R}}} \omega^2 \sin \omega t \tag{A-38}$$

As a result, the total convective force exerted on the wall is:

$$P = \int_0^{H_l} \int_0^{2\pi} pR\cos\phi\, d\phi\, dy = \frac{1}{4}\pi\rho_l R^4 \theta_{Hm}\omega^2 \sin \omega t = M_c A_c \omega^2 \sin \omega t \tag{A-39}$$

As shown in Eq. A-39, the force P should be equal to that produced by an equivalent convective mass M_c oscillating in horizontal direction with the motion defined as:

$$x_c = A_c \sin \omega t \qquad \text{(A-40)}$$

Solving the relevant equations, one can determine A_c and M_c as:

$$A_c = \frac{H_l \theta_{Hm}}{\sqrt{\frac{27}{8} \frac{H_l}{R}} \tanh \sqrt{\frac{27}{8} \frac{H_l}{R}}} \qquad \text{(A-41)}$$

$$M_c = 0.46 \frac{MR}{H_l} \tanh \sqrt{\frac{27}{8} \frac{H_l}{R}} \qquad \text{(A-42)}$$

where, M is the total mass of fluid.
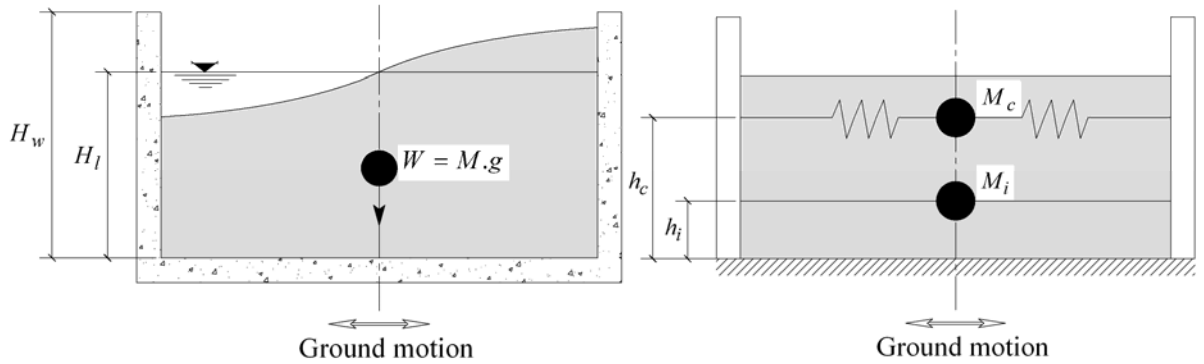
Figure A.7 Original tank and its equivalent mechanical model (Housner's model)

The equivalent elevation of M_c above the base may be determined by equating the moment exerted on the wall due to convective pressure and that produced by the equivalent mass M_c. As a result

$$h_c = H_l (1 - \frac{1}{\sqrt{\frac{27}{8} \frac{H_l}{R}} \tanh \sqrt{\frac{27}{8} \frac{H_l}{R}}} + \frac{1}{\sqrt{\frac{27}{8} \frac{H_l}{R}} \sinh \sqrt{\frac{27}{8} \frac{H_l}{R}}}) \qquad \text{(A-43)}$$

It should be noted that the above equation does not take into account the effect of fluid pressure on the tank floor. The resulting two-mass equivalent mechanical model taking into consideration the effects of both impulsive and convective fluid components is shown in Figure A.7. This model can only consider a slosh wave with one peak and one valley. This sloshing mode represents the fundamental anti-symmetric wave having the lowest natural frequency. Other sloshing modes with two or more peaks and valleys having higher natural frequencies may also be developed as a result of seismic excitation. The effect of these higher sloshing modes can be included by incorporating additional sprung masses corresponding to the higher order sloshing waves into the model. The equivalent masses corresponding to these higher order sloshing modes are very small compared to that of fundamental mode and therefore their dynamic effect is usually neglected. As mentioned before, most of the current codes and standards including ACI 350.3-06 have employed the Housner's mechanical model with some modifications for estimating the hydrodynamic forces in liquid containers.

APPENDIX B

TEXT COMMAND FILES OF THE TANK'S PARAMETRIC MODEL

AND THE POST-PROCESSOR ALGORITHMS

B.1 Input file for the tank's parametric model

The parameters defined for the tank's parametric model are indicated in Figure B.1. Parameters "ntop", "n3", "nc", and "nshaft" represent the number of mesh divisions to be set on different parts of the tank-pedestal system as shown in Figure B.1. Not included in the figure, parameter "nr" denotes the number of tangential mesh divisions on one-quarter of the tank's circumference. Parameter "mfloor" represents the equivalent mass of the platforms inside the shaft with their full live load. This mass is applied as a distributed mass at a specific height above the base corresponding to the center of gravity of the platforms. An equivalent distributed mass attributed to other structural components not included in the model such as roof, access tube, and other tank's accessories is applied at the ring beam level, "mring". Other parameters are defined as follows:

rt : Radius of the cylindrical steel shell

Rroot : Radius of the supporting shaft

htop : Free board (distance between the water free surface and the roof)

h3 : Height of water in the cylindrical portion of the tank

hc : Height of the conical portion of the tank

hshaft : Height of the supporting shaft

tcyl : Average thickness of the cylindrical portion of the tank

tcon : Average thickness of the conical portion of the tank

tfloor : Thickness of the tank's floor

tshaft : Thickness of the shaft wall

teta : Cone angle
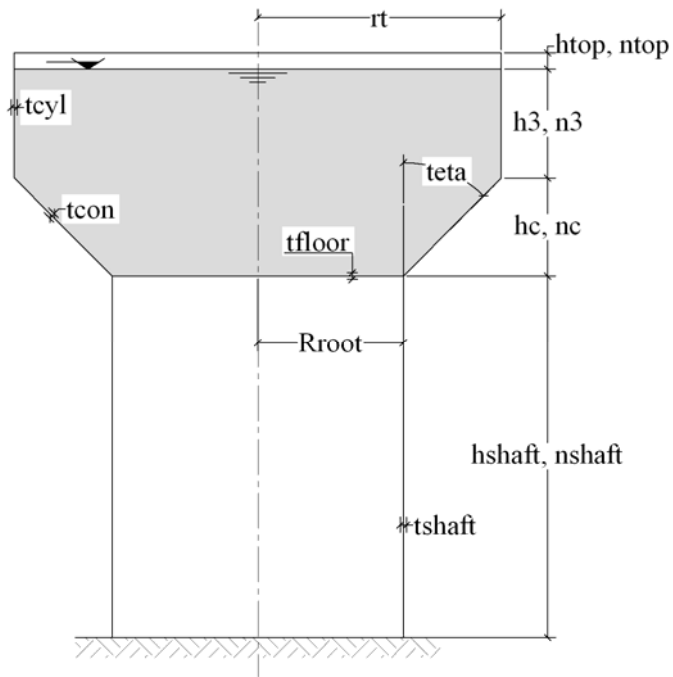
Figure B.1 Parameters defined for the tank's parametric model

The text command file for the tank's parametric model using the parameters defined in Figure B.1 is given below:

```
/BATCH
! /COM,ANSYS RELEASE 11.0SP1 UP20070830       July 2009
!/CWD,'C:\Project Section\Elevated and ground-supported cylindrical
tanks'

! /GRA,POWER
! /GST,ON
! /PLO,INFO,3
! /GRO,CURL,ON
! /CPLANE,1
WPSTYLE,,,,,,,O

*SET,h3,6.85
*SET,hc,4.795
```

```
*SET, rt, 10. 6175
*SET, rroot, 5. 8225
*SET, hshaft, 15. 8
*SET, tcyl, 0. 0088307
*SET, tcon, 0. 024511
*SET, htop, 0. 5
*SET, mfloor, 12760
*SET, mring, 7818
*SET, tfloor, 0. 3302
*SET, tshaft, 0. 381

!teta=(atan((rt-rroot)/hc))*180/3. 1415
*SET, teta, (atan((rt-rroot)/hc))*180/3. 1415

*SET, ntop, 2
*SET, n3, 14
*SET, nc, 14
*SET, nshaft, 13
*SET, nr, 14
*SET, MINFLOOR ,  -h3-hc-0. 385*hshaft-0. 5*hshaft/nshaft
*SET, MAXFLOOR ,  -h3-hc-0. 385*hshaft+0. 5*hshaft/nshaft
*SET, massfloor, 56*1270
*SET, massring, 56*7818

!*********************Element type
ET, 1, FLUID80
KEYOPT, 1, 2, 1
ET, 2, MASS21
KEYOPT, 2, 1, 0
KEYOPT, 2, 2, 0
KEYOPT, 2, 3, 0
ET, 3, SHELL63
KEYOPT, 3, 1, 0
KEYOPT, 3, 2, 0
KEYOPT, 3, 3, 0
KEYOPT, 3, 5, 0
KEYOPT, 3, 6, 0
KEYOPT, 3, 7, 0
KEYOPT, 3, 8, 0
KEYOPT, 3, 9, 0
KEYOPT, 3, 11, 0

!***************Material  Properties
MPTEMP, , , , , , , ,
MPTEMP, 1, 0
MPDATA, DENS, 1, , 1000
MPTEMP, , , , , , , ,
MPTEMP, 1, 0
MPDATA, EX, 1, , 2. 1e9
MPDATA, PRXY, 1, ,
MPTEMP, , , , , , , ,
MPTEMP, 1, 0
MPDATA, DENS, 2, , 7898
MPTEMP, , , , , , , ,
MPTEMP, 1, 0
MPDATA, EX, 2, , 2e11
MPDATA, PRXY, 2, , 0. 3
MPTEMP, , , , , , , ,
```

```
MPTEMP, 1, 0
MPDATA, DENS, 3, , 2400
MPTEMP, , , , , , ,
MPTEMP, 1, 0
MPDATA, EX, 3, , 2.4856e10
MPDATA, PRXY, 3, , 0.16

!*************************** Real  Constants
R, 1, tcon, , , , , ,
RMORE, , , ,
RMORE
RMORE, ,
R, 2, tcyl, , , , , ,
RMORE, , , ,
RMORE
RMORE, ,
R, 3, tfloor, , , , , ,
RMORE, , , ,
RMORE
RMORE, ,
R, 4, t, , , , , ,
RMORE, , , ,
RMORE
RMORE, ,
R, 5, mring, mring, mring, , , ,
R, 6, mfloor, mfloor, mfloor, , , ,
R, 4, , tfloor, 0, 0, 0, 0,
RMORE, 0, 0, 0,
RMORE
RMORE, 0,
R, 4, tfloor, 0, 0, 0, 0, 0,
RMORE, 0, 0, 0,
RMORE
RMORE, 0,
/PREP7
CSYS, 1
DSYS, 1
K, 1, rroot, 0, -h3-hc-hshaft,
K, 2, rroot, 0, -h3-hc,
LSTR,           1,           2
K, 3, 0, 0, -h3-hc,
K, 4, 0, 0, 0,
LSTR,           3,           4
FLST, 2, 1, 4, ORDE, 1
FITEM, 2, 1
FLST, 8, 2, 3
FITEM, 8, 3
FITEM, 8, 4
AROTAT, P51X, , , , , , P51X, , 360, 4,
K, 11, rt, 0, -h3,
LSTR,           2,          11
FLST, 2, 1, 4, ORDE, 1
FITEM, 2, 14
FLST, 8, 2, 3
FITEM, 8, 3
FITEM, 8, 4
AROTAT, P51X, , , , , , P51X, , 360, 4,
K, 18, rt, 0, 0,
```

296

```
LSTR,          11,          18
FLST, 2, 1, 4, ORDE, 1
FITEM, 2, 26
FLST, 8, 2, 3
FITEM, 8, 4
FITEM, 8, 3
AROTAT, P51X,  ,  ,  ,  ,  , P51X,  , 360, 4,
K, 25, rt, 0, htop,
LSTR,          18,          25
FLST, 2, 1, 4, ORDE, 1
FITEM, 2, 38
FLST, 8, 2, 3
FITEM, 8, 3
FITEM, 8, 4
AROTAT, P51X,  ,  ,  ,  , P51X,  , 360, 4,
LSTR,           3,           2
FLST, 2, 1, 4, ORDE, 1
FITEM, 2, 50
FLST, 8, 2, 3
FITEM, 8, 3
FITEM, 8, 4
AROTAT, P51X,  ,  ,  ,  , P51X,  , 360, 4,
WPCSYS, -1
CONE, rroot, rt, -h3-hc, -h3, 0, 360,
CONE, rt, rt, 0, -h3, 0, 360,
DSYS, 0
KWPLAN, -1,          15,          29,          18
FLST, 2, 2, 6, ORDE, 2
FITEM, 2, 1
FITEM, 2, -2
VSBW, P51X
KWPLAN, -1,          13,          24,          31
FLST, 2, 4, 6, ORDE, 2
FITEM, 2, 3
FITEM, 2, -6
VSBW, P51X
WPCSYS, -1
FLST, 5, 8, 6, ORDE, 4
FITEM, 5, 1
FITEM, 5, -2
FITEM, 5, 7
FITEM, 5, -12
VSEL, S,  ,  , P51X
ASLV, S
LSLA, S
KSLL, S
NUMMRG, KP,  ,  ,  , LOW
ALLSEL, ALL
ASLV, U
LSLA, S
KSLL, S
NUMMRG, KP,  ,  ,  , LOW
ALLSEL, ALL
ASLV, U
FLST, 5, 4, 5, ORDE, 2
FITEM, 5, 1
FITEM, 5, -4
CM, _Y, AREA
```

```
ASEL, , , ,P51X
CM,_Y1,AREA
CMSEL,S,_Y
FLST,5,4,5,ORDE,2
FITEM,5,1
FITEM,5,-4
CM,_Y,AREA
ASEL, , , ,P51X
CM,_Y1,AREA
CMSEL,S,_Y
R,4,tshaft,0,0,0,0,0,
RMORE,0,0,0,
RMORE
RMORE,0,
FLST,5,4,5,ORDE,2
FITEM,5,1
FITEM,5,-4
CM,_Y,AREA
ASEL, , , ,P51X
CM,_Y1,AREA
CMSEL,S,_Y
CMSEL,S,_Y1
AATT,            3,            4,     3,            0,
CMSEL,S,_Y
CMDELE,_Y
CMDELE,_Y1
FLST,5,4,5,ORDE,2
FITEM,5,5
FITEM,5,-8
CM,_Y,AREA
ASEL, , , ,P51X
CM,_Y1,AREA
CMSEL,S,_Y
CMSEL,S,_Y1
AATT,            2,            1,     3,            0,
CMSEL,S,_Y
CMDELE,_Y
CMDELE,_Y1
FLST,5,8,5,ORDE,2
FITEM,5,9
FITEM,5,-16
CM,_Y,AREA
ASEL, , , ,P51X
CM,_Y1,AREA
CMSEL,S,_Y
CMSEL,S,_Y1
AATT,            2,            2,     3,            0,
CMSEL,S,_Y
CMDELE,_Y
CMDELE,_Y1
LSLA,S
FLST,5,4,4,ORDE,3
FITEM,5,1
FITEM,5,3
FITEM,5,-5
CM,_Y,LINE
LSEL, , , ,P51X
CM,_Y1,LINE
```

```
CMSEL,,_Y

!***********************Mesh divisions
LESIZE,_Y1, , ,nshaft, , , , ,0
FLST,5,4,4,ORDE,2
FITEM,5,14
FITEM,5,-17
CM,_Y,LINE
LSEL, , , ,P51X
CM,_Y1,LINE
CMSEL,,_Y
LESIZE,_Y1, , ,nc, , , , ,0
FLST,5,4,4,ORDE,2
FITEM,5,26
FITEM,5,-29
CM,_Y,LINE
LSEL, , , ,P51X
CM,_Y1,LINE
CMSEL,,_Y
LESIZE,_Y1, , ,n3, , , , ,0
FLST,5,4,4,ORDE,2
FITEM,5,38
FITEM,5,-41
CM,_Y,LINE
LSEL, , , ,P51X
CM,_Y1,LINE
CMSEL,,_Y
LESIZE,_Y1, , ,ntop, , , , ,0
FLST,5,20,4,ORDE,14
CM,_Y,LINE
LSEL, , , ,P51X
CM,_Y1,LINE
CMSEL,,_Y
LESIZE,_Y1, , ,nr, , , , ,0
ASLV,U
FLST,5,4,5,ORDE,2
FITEM,5,17
FITEM,5,-20
CM,_Y,AREA
ASEL, , , ,P51X
CM,_Y1,AREA
CMSEL,S,_Y
CMSEL,S,_Y1
AATT,            3,            3,    3,            0,
CMSEL,S,_Y
CMDELE,_Y
CMDELE,_Y1
MSHAPE,0,2D
MSHKEY,1
FLST,5,20,5,ORDE,2
FITEM,5,1
FITEM,5,-20
CM,_Y,AREA
ASEL, , , ,P51X
CM,_Y1,AREA
CHKMSH,'AREA'
CMSEL,S,_Y
AMESH,_Y1
```

```
CMDELE, _Y
CMDELE, _Y1
CMDELE, _Y2
/UI, MESH, OFF
NUMMRG, NODE,  ,  ,  , LOW
ALLSEL, ALL
CSYS, 1
ALLSEL, ALL
CSYS, 1
NSEL, S, LOC, Z, -h3-hc
NSEL, R, LOC, X, rroot
/GO
KNODE, 0, all
ASLV, U
LSLA, S
KSLL, S
KSLN, A
ALLSEL, ALL
KSLN, S
ALLSEL, ALL
ASLV, U
LSLA, S
KSLL, S
FLST, 5, 16, 3, ORDE, 16
KSEL, U,  ,  , P51X
KSLN, A
ALLSEL, ALL
ASLV, S
LSLA, S
KSLL, U
KSLN, U
ALLSEL, ALL
ASLV, S
LSLA, S
KSLL, U
NUMMRG, KP,  ,  ,  , LOW
ALLSEL, ALL
NSEL, S, LOC, Z, minfloor, maxfloor
KNODE, 0, all
ALLSEL, ALL
ASLV, U
NSEL, ALL
ALLSEL, ALL
ASLV, S
LSLA, S
KSLL, U
KSEL, R, LOC, Z, -h3-hc
KSEL, R, LOC, X, rroot
FLST, 5, 80, 3, ORDE, 22
CM, _Y, KP
KSEL,  ,  ,  , P51X
CM, _Y1, KP
CMSEL, S, _Y
CMSEL, S, _Y1
KATT,            1,          5,     2,            0
CMSEL, S, _Y
CMDELE, _Y
CMDELE, _Y1
```

```
FLST, 2, 80, 3, ORDE, 22
KMESH, all
ALLSEL, ALL
ESEL, S, TYPE, , 2
ALLSEL, ALL
KSEL, S, LOC, Z, minfloor, maxfloor
FLST, 5, 80, 3, ORDE, 6
CM, _Y, KP
KSEL,    ,   ,   , P51X
CM, _Y1, KP
CMSEL, S, _Y
CMSEL, S, _Y1
KATT,            1,           6,      2,             0
CMSEL, S, _Y
CMDELE, _Y
CMDELE, _Y1
FLST, 2, 80, 3, ORDE, 6
KMESH, all
ALLSEL, ALL
NUMMRG, NODE,    ,   ,   , LOW
/UI, MESH, OFF
ASLV, S
LSLA, S
FLST, 5, 12, 4, ORDE, 4
CM, _Y, LINE
LSEL,    ,   ,   , P51X
CM, _Y1, LINE
CMSEL, , _Y
LESIZE, _Y1,   ,   , nr,   ,   ,   , , 0
FLST, 5, 4, 4, ORDE, 4
CM, _Y, LINE
LSEL,    ,   ,   , P51X
CM, _Y1, LINE
CMSEL, , _Y
LESIZE, _Y1,   ,   , n3,   ,   ,   , , 0
FLST, 5, 3, 4, ORDE, 3
CM, _Y, LINE
LSEL,    ,   ,   , P51X
CM, _Y1, LINE
CMSEL, , _Y
LESIZE, _Y1,   ,   , n3,   ,   ,   , , 0
FLST, 5, 5, 4, ORDE, 5
CM, _Y, LINE
LSEL,    ,   ,   , P51X
CM, _Y1, LINE
CMSEL, , _Y
LESIZE, _Y1,   ,   , nc,   ,   ,   , , 0
MSHAPE, 0, 3D
FLST, 5, 8, 6, ORDE, 4
CM, _Y, VOLU
VSEL,    ,   ,   , P51X
CM, _Y1, VOLU
CHKMSH, 'VOLU'
CMSEL, S, _Y
VMESH, _Y1
CMDELE, _Y
CMDELE, _Y1
CMDELE, _Y2
```

301

```
/UI, MESH, OFF
ACEL, 0, 0, 9. 807,
LSEL, S, LOC, Z, -hc-h3-hshaft
NSLL, S, 1
FLST, 2, 80, 1, ORDE, 8
/GO
D, all, , , , , , UX, UY, UZ, , ,
ALLSEL, ALL
CSYS, 1
FLST, 2, 45673, 1, ORDE, 4
NROTAT, all
NSEL, S, LOC, Z, 0, -h3
CPINTF, UX, 0. 0001,
NSEL, R, LOC, Z, -h3
CPINTF, UZ, 0. 0001,
ALLSEL, ALL
NSEL, S, LOC, Z, -h3-hc, -h3-0. 05
NSEL, S, LOC, X, rroot, rt
ALLSEL, ALL
NSEL, S, LOC, Z, -h3-hc, -h3-0. 05
NSEL, R, LOC, X, rroot, rt
CSYS, 1
FLST, 2, 5660, 1, ORDE, 971
NROTAT, all
nmodif, all, , , , , , , teta
CPINTF, UX, 0. 0001,
ALLSEL, ALL
NSEL, S, LOC, Z, -h3-hc
CPINTF, UZ, 0. 0001,
ALLSEL, ALL
ESEL, S, TYPE, , 1
NSLE, S
NUMMRG, NODE, , , , LOW
ALLSEL, ALL
LSEL, S, LOC, Z, -hc-h3-hshaft
NSLL, S, 1
/GO
D, all, , , , , , UX, UY, UZ, , ,
ALLSEL, ALL
WPSTYLE, , , , , , , , 0
NSEL, S, LOC, Z, -h3-hc
NSEL, R, LOC, X, rroot
CSYS, 1
FLST, 2, 112, 1, ORDE, 21
NROTAT, all
ALLSEL, ALL
```

B.2 Text command file of the post-processor "POST-CYL"

The text command file of the post-processor "POST-CYL" is given below:

```
!/POST-PROCESSOR "POST-CYL"
*DIM, EPRESSURE, ARRAY, n3, 1
*Do, k, 1, n3, 1
ESLV, S
NSEL, S, LOC, Z, 0-(k-1)*h3/n3
NSEL, R, LOC, X, rt
ESLN, R
NSEL, S, LOC, Z, 0-(k-1-1)*h3/n3
ESLN, U
/POST1
PLESOL,  SMISC, 1,  0, 1.0
*GET, EPRESSURE(k), PLNSOL, 0, MAX
ALLSEL, ALL
*ENDDO
Finish
*CFOPEN, PSCyl
*VWRITE, EPRESSURE(1)
(F15.4)
```

B.3 Text command file of the post-processor "POST-CON"

The text command file of the post-processor "POST-CON" is given below:

```
!/POST-PROCESSOR "POST-CON"
*DIM, EPRESSURE, ARRAY, nc, 1
*Do, k, 1, nc, 1
ESLV, S
NSEL, S, LOC, Z, -h3-k*hc/nc
NSEL, R, LOC, X, ((rt-rroot)*(hc-k*hc/nc)/hc)+rroot
ESLN, R
NSEL, S, LOC, Z, -h3-(k+1)*hc/nc
ESLN, U
ESEL, U, TYPE, , 3
```

```
/POST1
PLESOL, SMISC,1, 0,1.0
*GET,EPRESSURE(k),PLNSOL,0,MAX
ALLSEL,ALL
*ENDDO
Finish
*CFOPEN,PScone
*VWRITE,EPRESSURE(1)
(F15.4)
```

B.4 Text command file of the post-processor "POST-FLOOR"

The text command file of the post-processor "POST-FLOOR" is given below:

```
!/POST-PROCESSOR "POST-FLOOR"
*DIM,EPRESSURE,ARRAY,nr,1
*Do,k,1,nr,1
ESLV,S
NSEL,S,LOC,Z,-h3-hc
NSEL,R,LOC,X,rroot-(k-1)*rroot/nr
ESLN,R
NSEL,R,LOC,X,rroot-(k-2)*rroot/nr
ESLN,U
ESEL,U,TYPE,,3
/POST1
PLESOL, SMISC,1, 0,1.0
*GET,EPRESSURE(k),PLNSOL,0,MAX
ALLSEL,ALL
*ENDDO
Finish
*CFOPEN,PSfloor
*VWRITE,EPRESSURE(1)
(F15.4)
```

APPENDIX C

RESULTS OF THE PARAMETRIC STUDY ON LIQUID-FILLED

CONICAL ELEVATED TANKS

C.1 Hydrodynamic pressure distribution graphs

The normalized convective and impulsive pressure graphs obtained through the parametric study corresponding to the three different ranges of shaft stiffness considered are given in Figures C.1 through C.26.
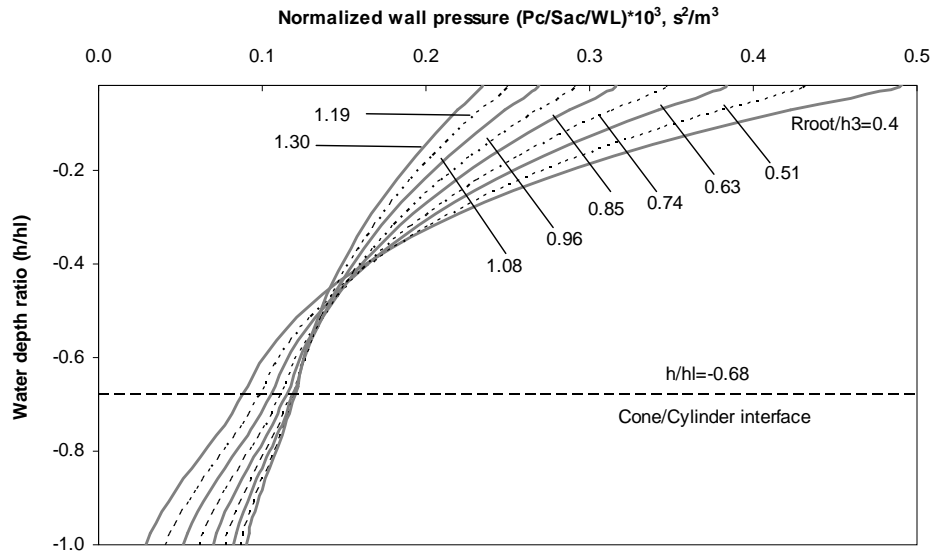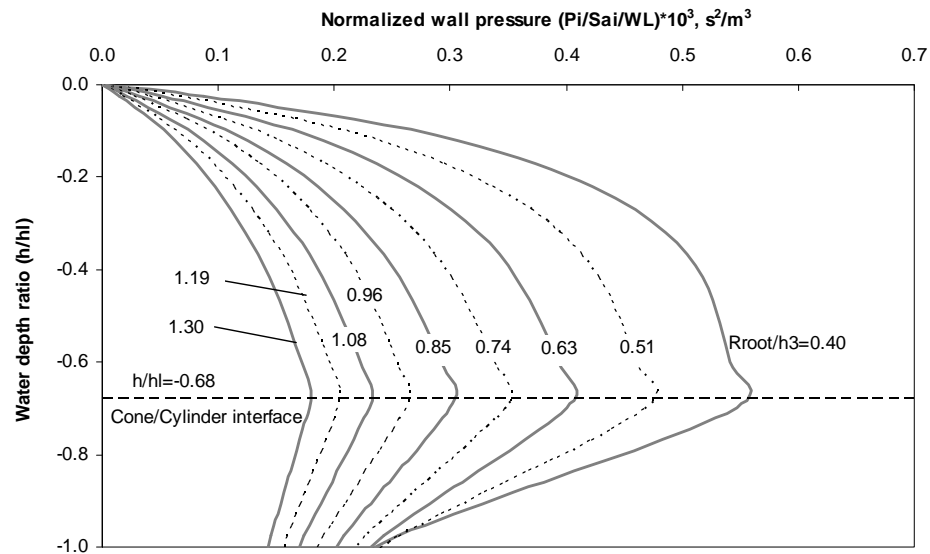
Figure C.1 Pressure distribution over the tank wall for Ks= 4.5E9 N/m and hc/h3=0.475;

(a) Convective, (b) Impulsive
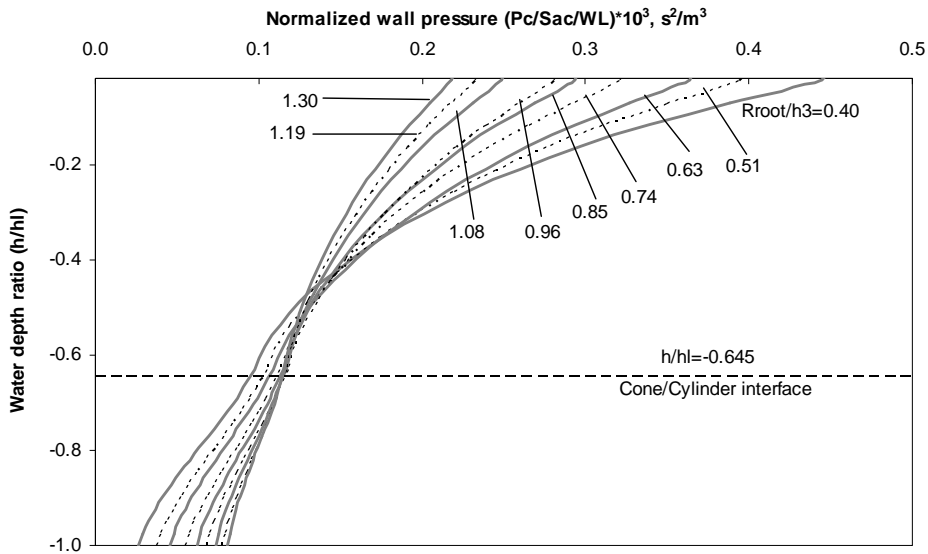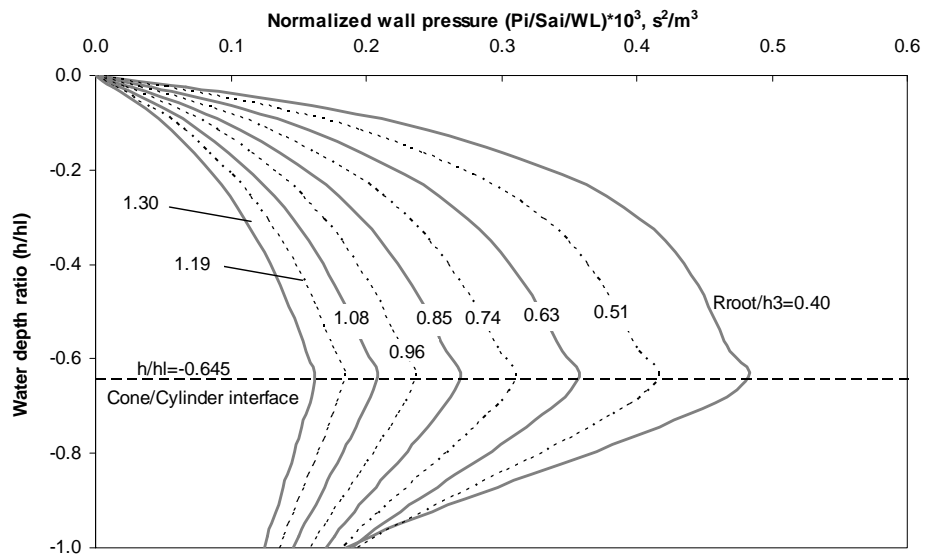
Figure C.2 Pressure distribution over the tank wall for Ks= 4.5E9 N/m and hc/h3=0.55;

(a) Convective, (b) Impulsive
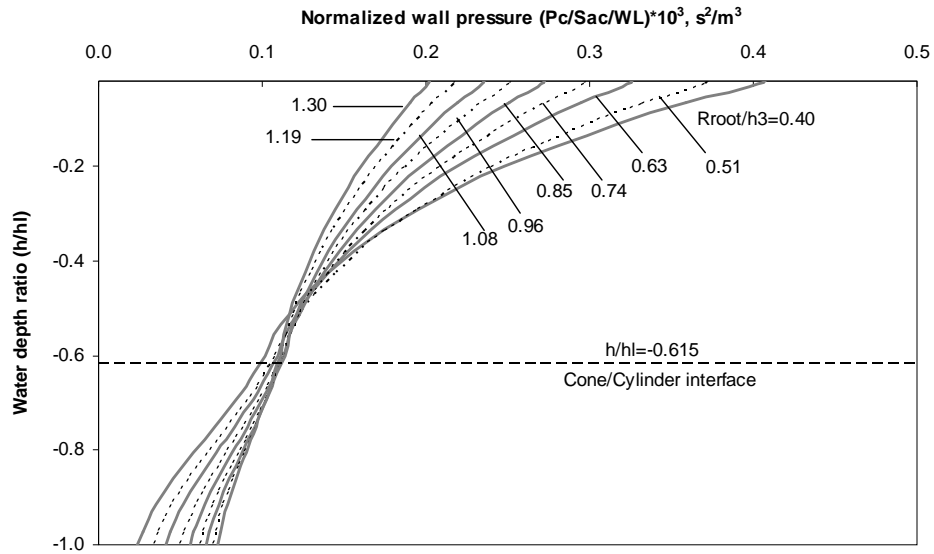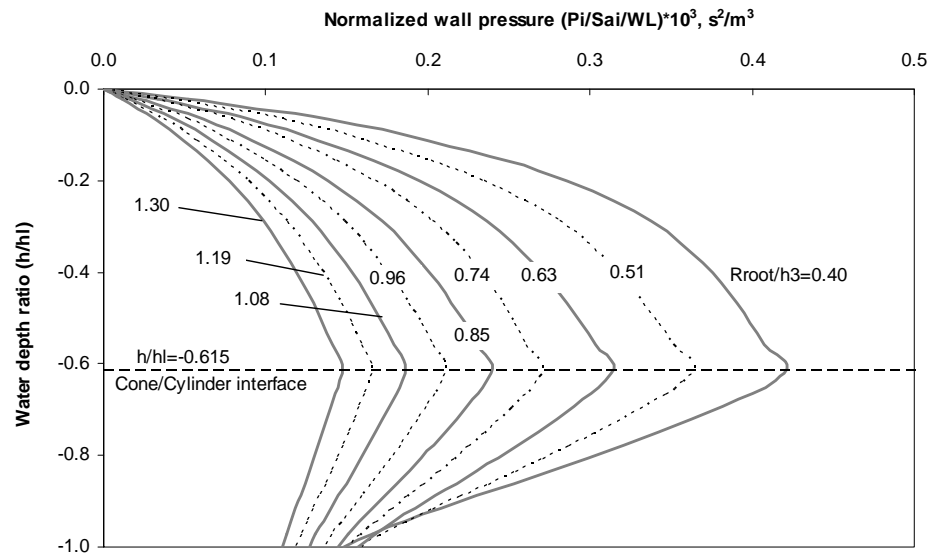
Figure C.3 Pressure distribution over the tank wall for Ks= 4.5E9 N/m and hc/h3=0.625;
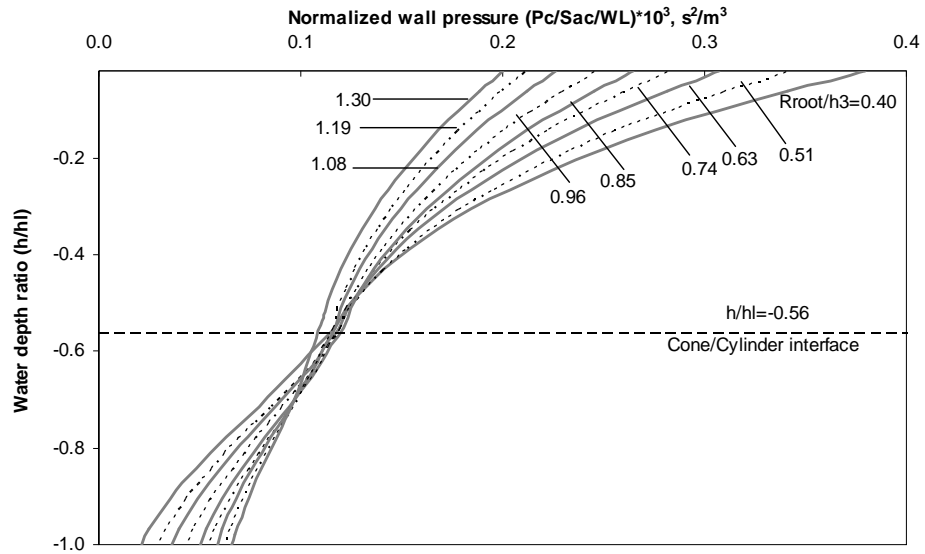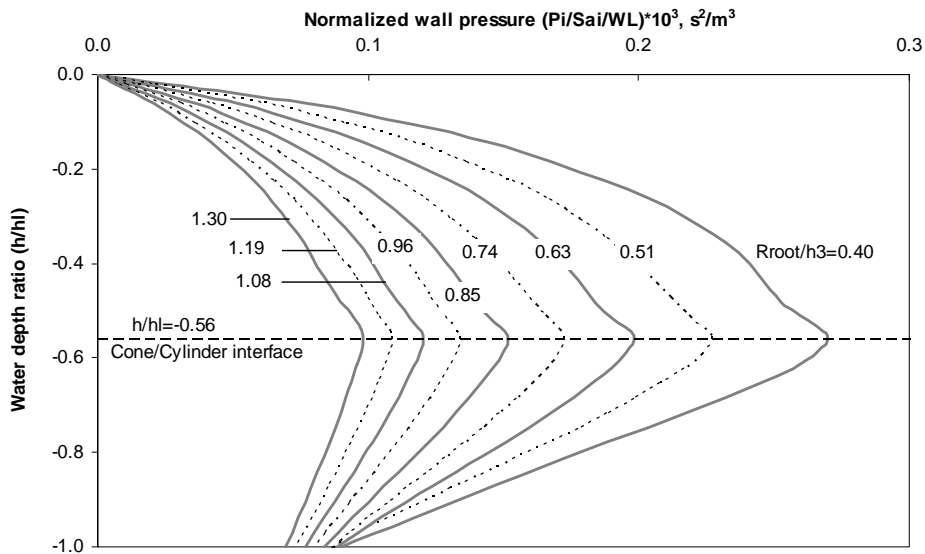
(a) Convective, (b) Impulsive

Normalized wall pressure (Pc/Sac/WL)*10³, s²/m³

(a)

Normalized wall pressure (Pi/Sai/WL)*10³, s²/m³
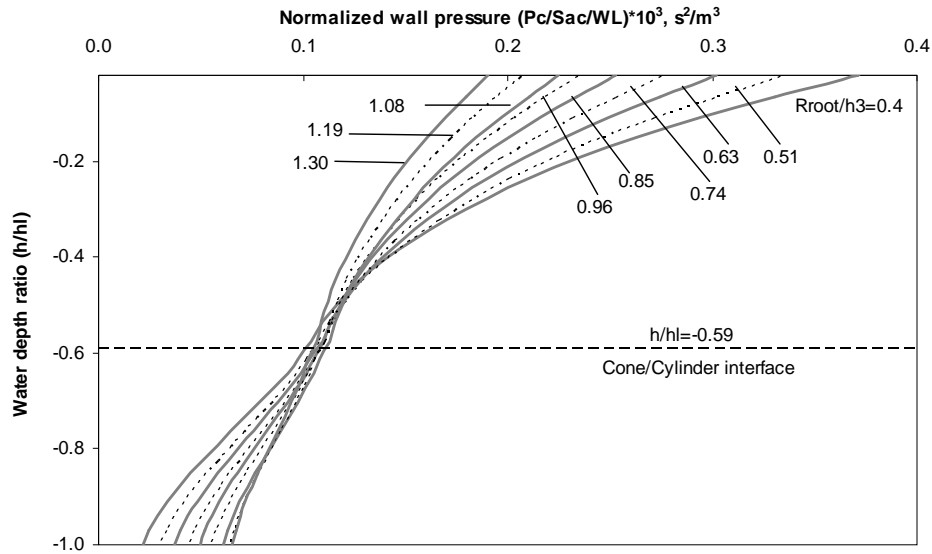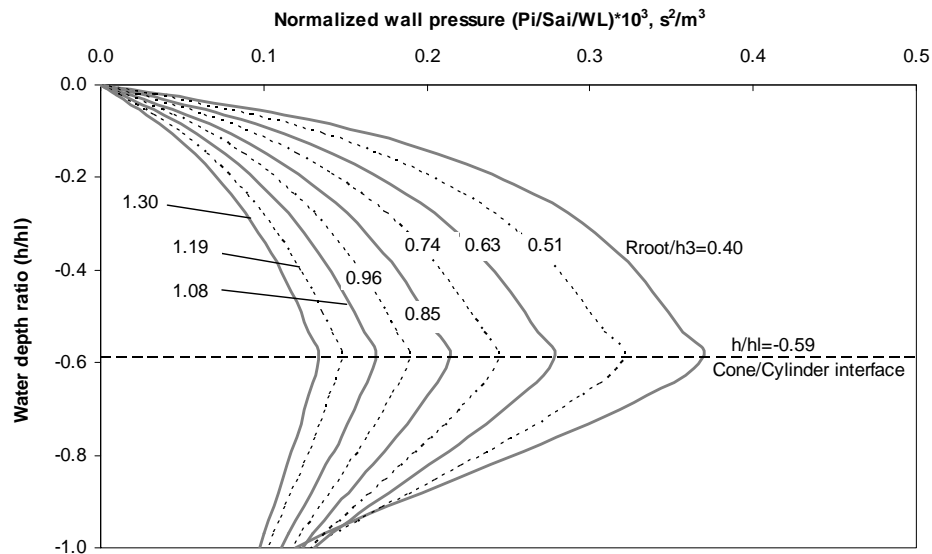
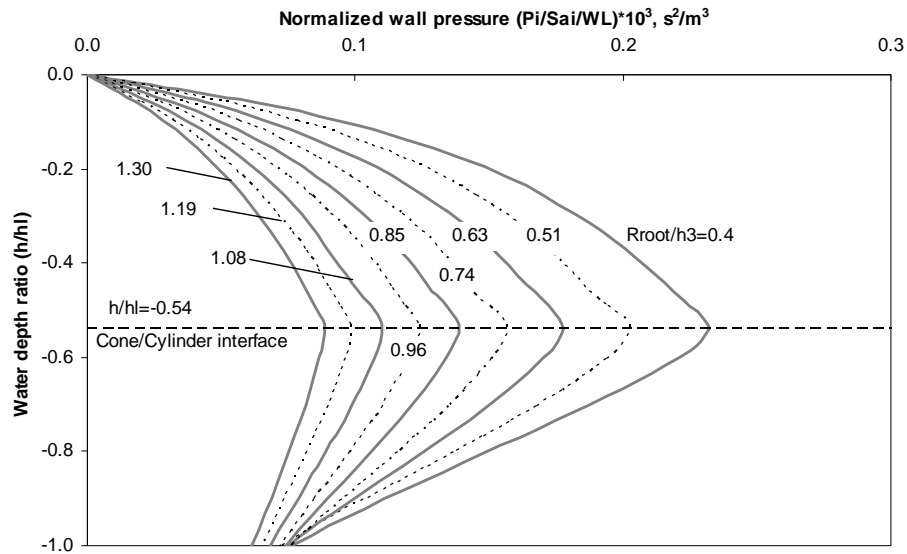(b)

Figure C.4 Pressure distribution over the tank wall for Ks= 4.5E9 N/m and hc/h3=0.7;

(a) Convective, (b) Impulsive
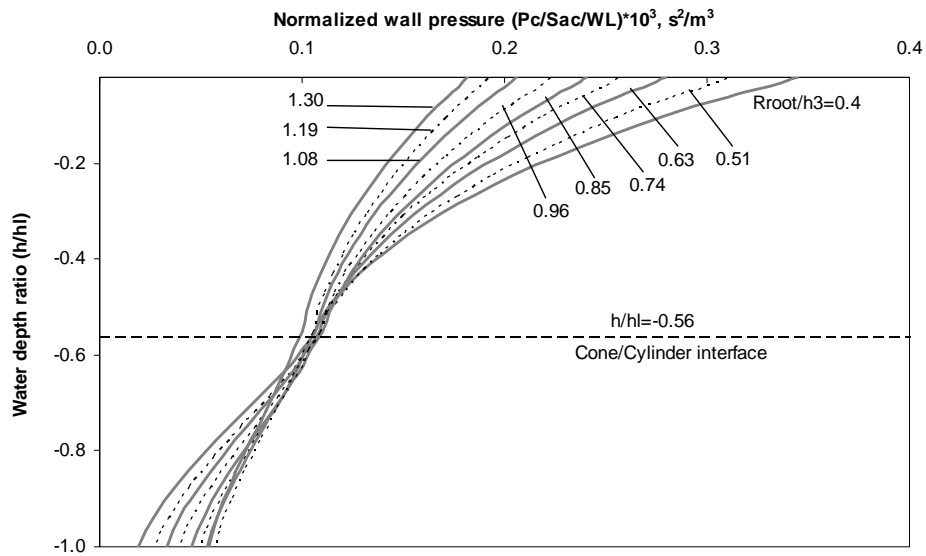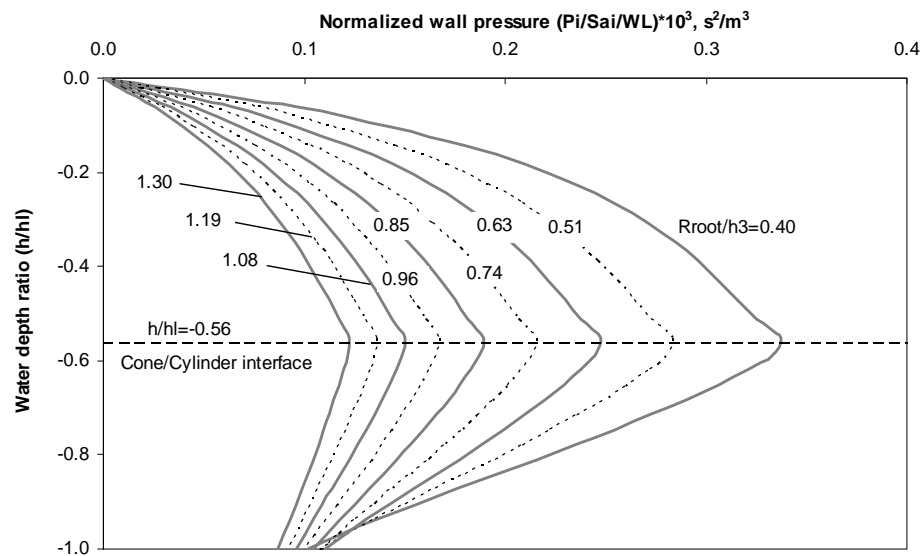
Figure C.5 Pressure distribution over the tank wall for Ks= 4.5E9 N/m and hc/h3=0.775;

(a) Convective, (b) Impulsive
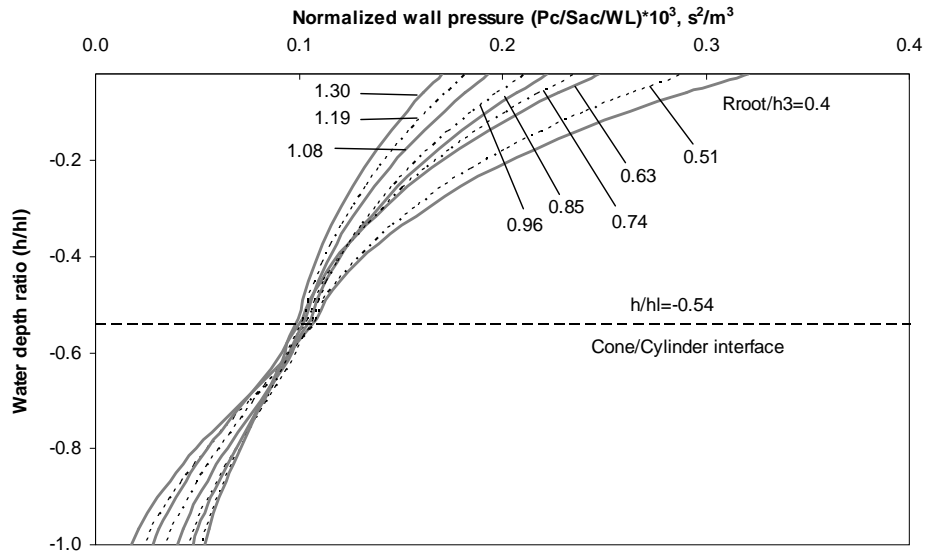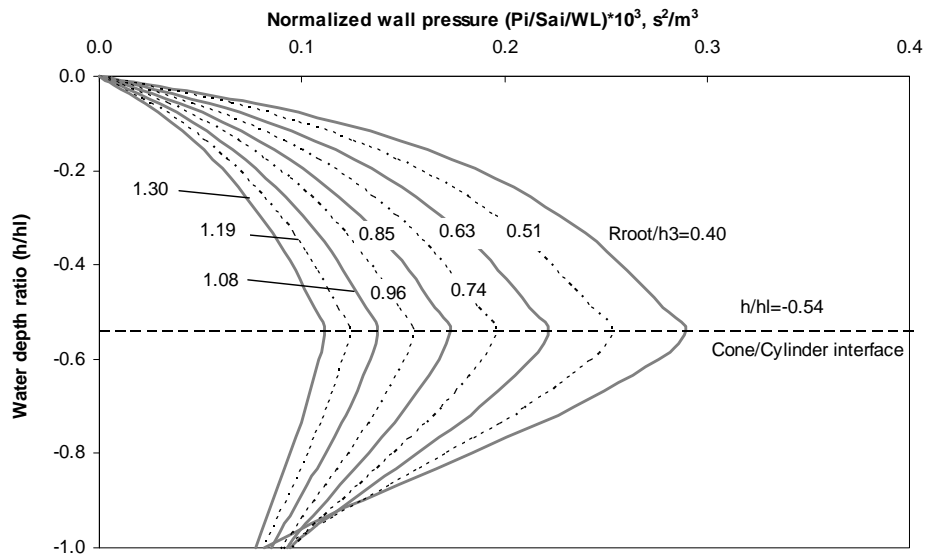
Figure C.6 Pressure distribution over the tank wall for Ks= 4.5E9 N/m and hc/h3=0.85 ;
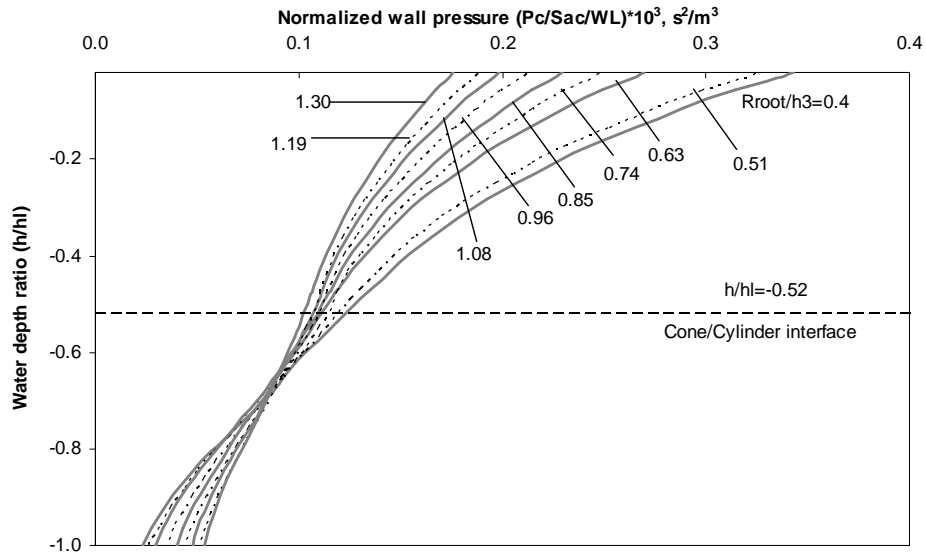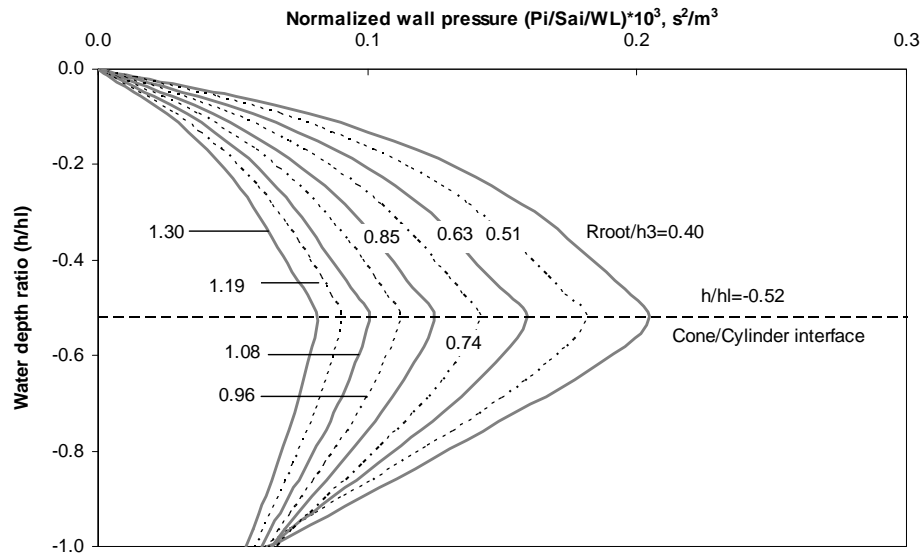
(a) Convective, (b) Impulsive
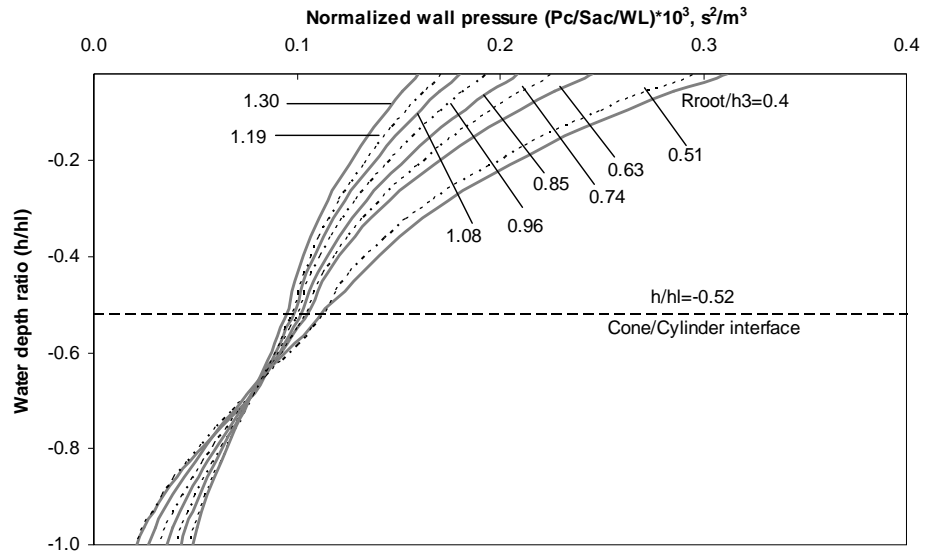
(a)
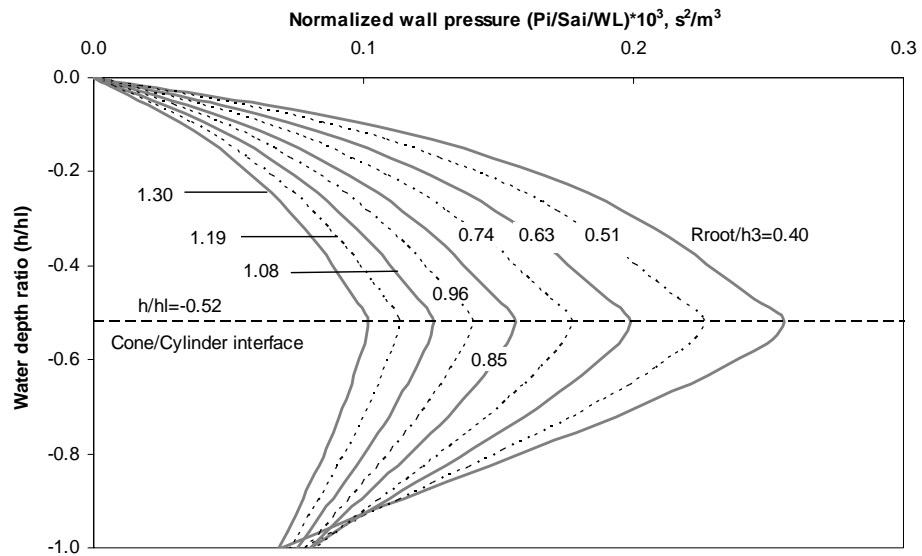
(b)

Figure C.7 Pressure distribution over the tank wall for Ks= 4.5E9 N/m and hc/h3=0.925 ;

(a) Convective, (b) Impulsive
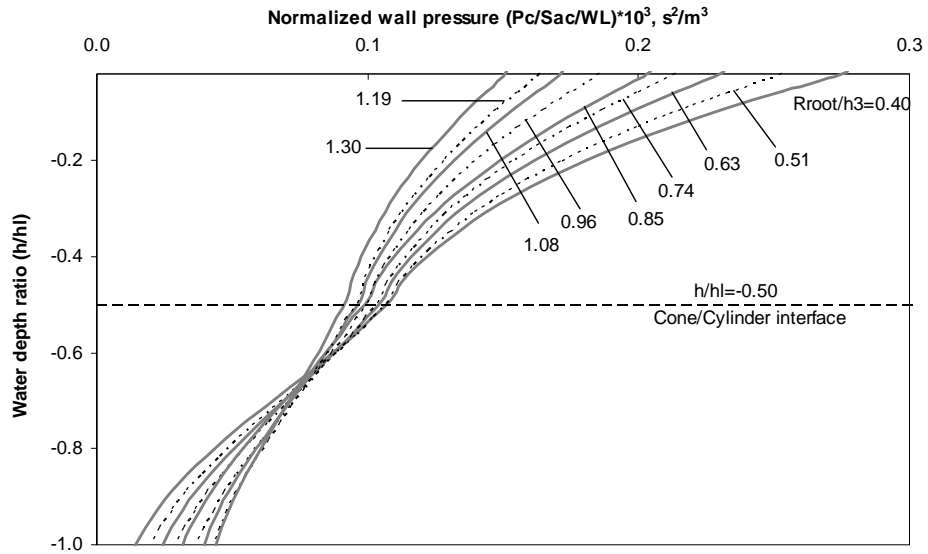
(a)
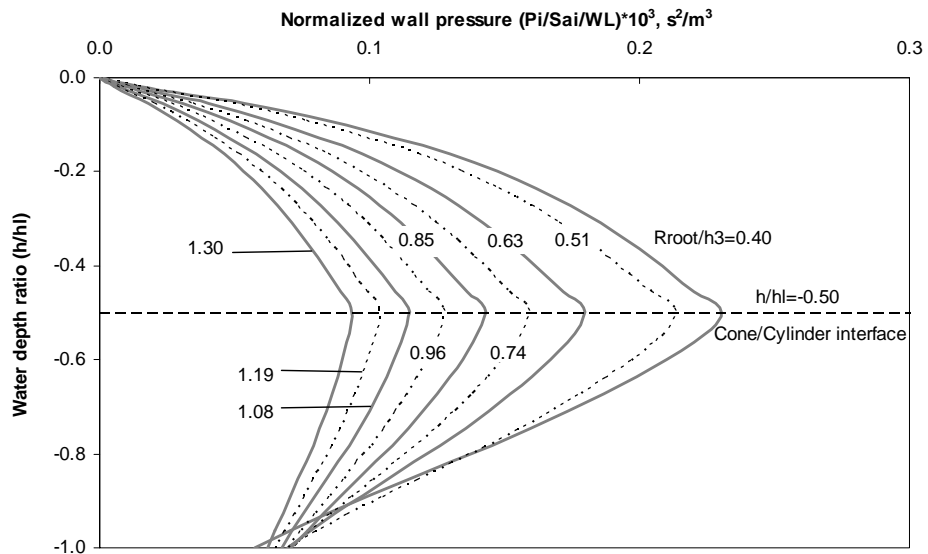
(b)

Figure C.8 Pressure distribution over the tank wall for Ks= 4.5E9 N/m and hc/h3=1.00 ;

(a) Convective, (b) Impulsive
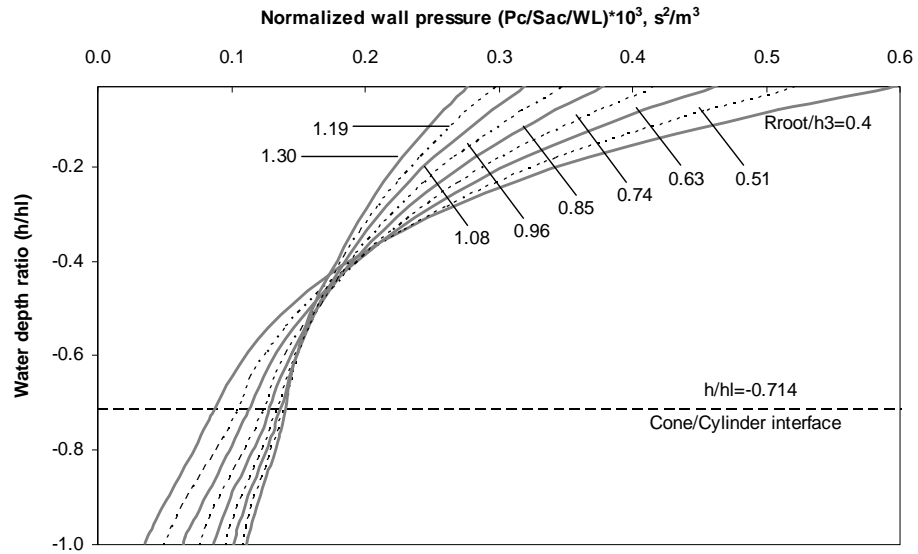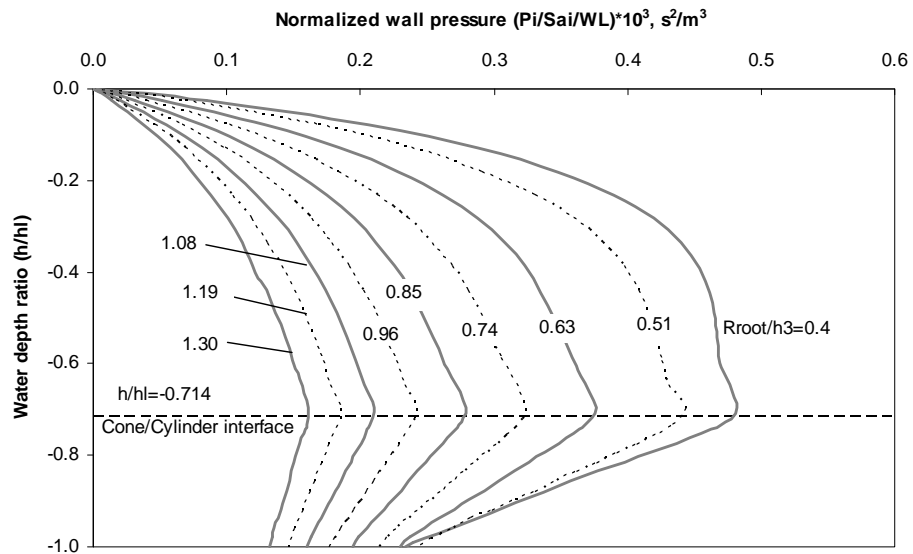
Figure C.9 Pressure distribution over the tank wall for Ks= 1.3E8 N/m and hc/h3=0.4 ;

(a) Convective, (b) Impulsive

314
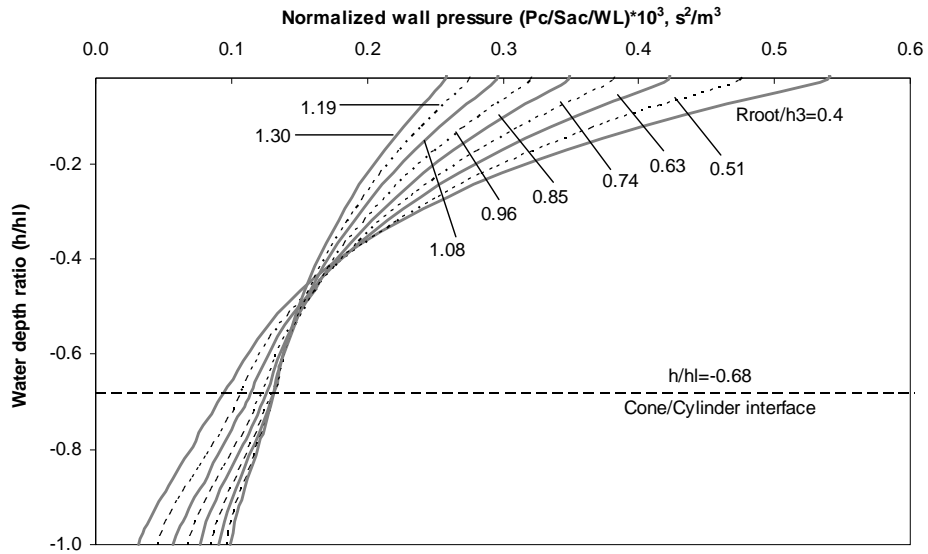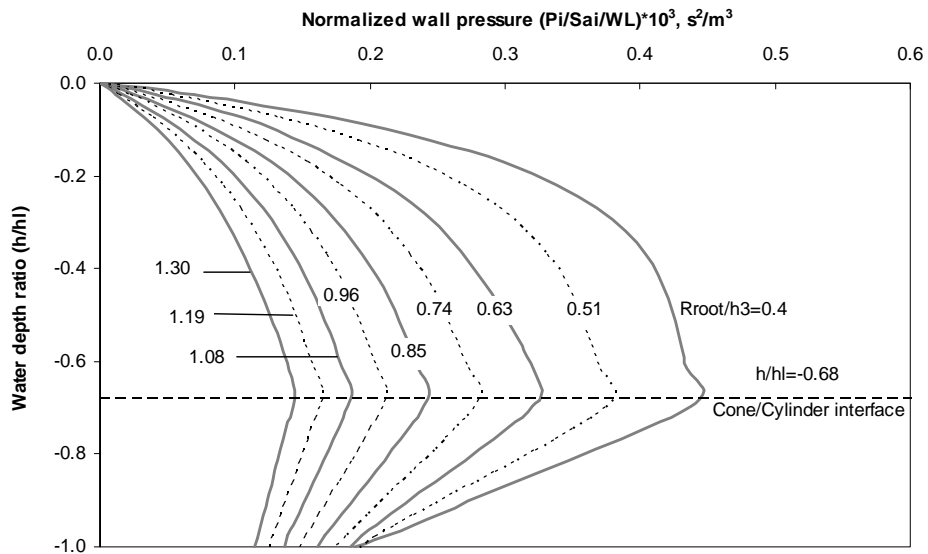
Figure C.10 Pressure distribution over the tank wall for Ks= 1.3E8 N/m and hc/h3=0.475 ;

(a) Convective, (b) Impulsive
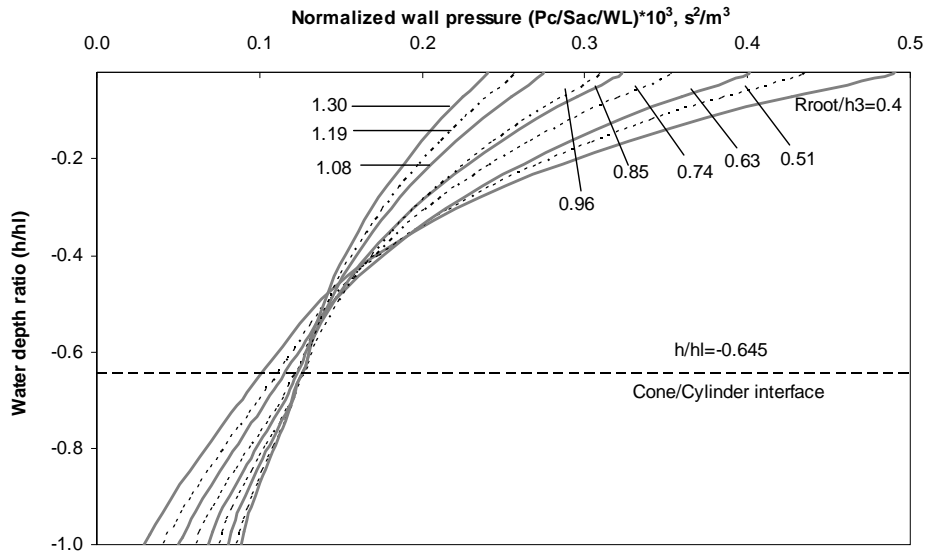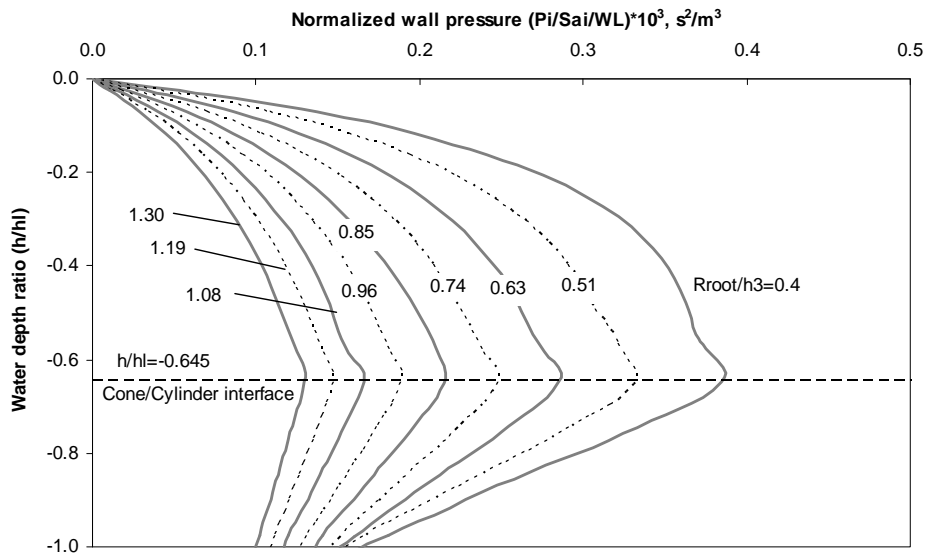
Figure C.11 Pressure distribution over the tank wall for Ks= 1.3E8 N/m and hc/h3=0.55 ;
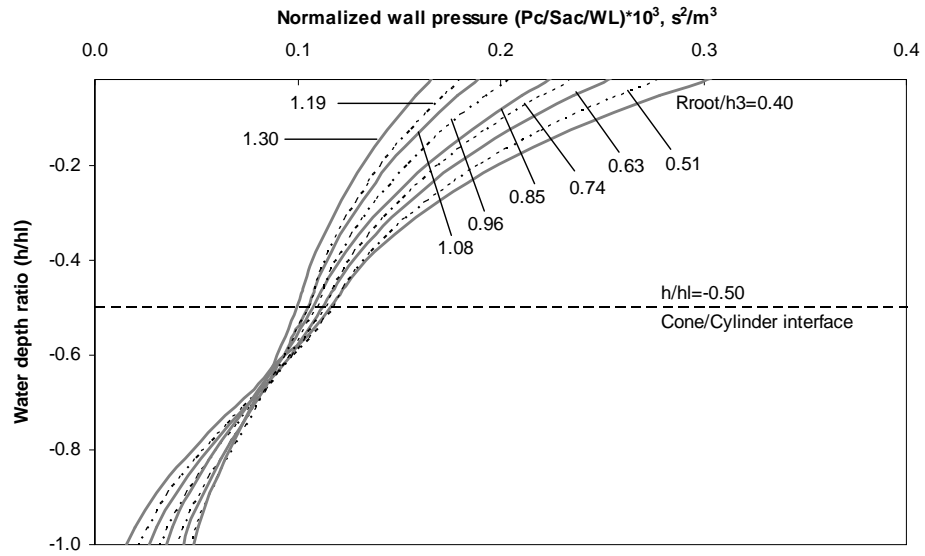
(a) Convective, (b) Impulsive
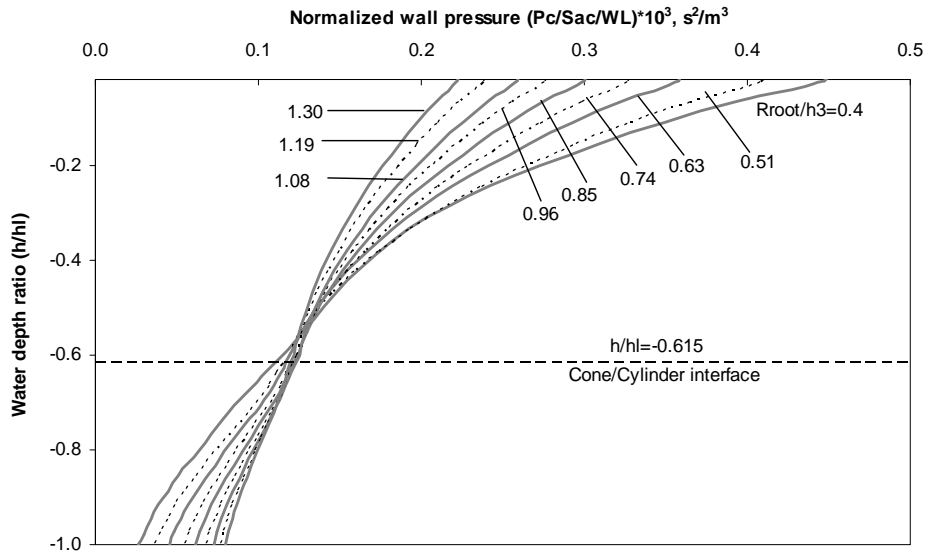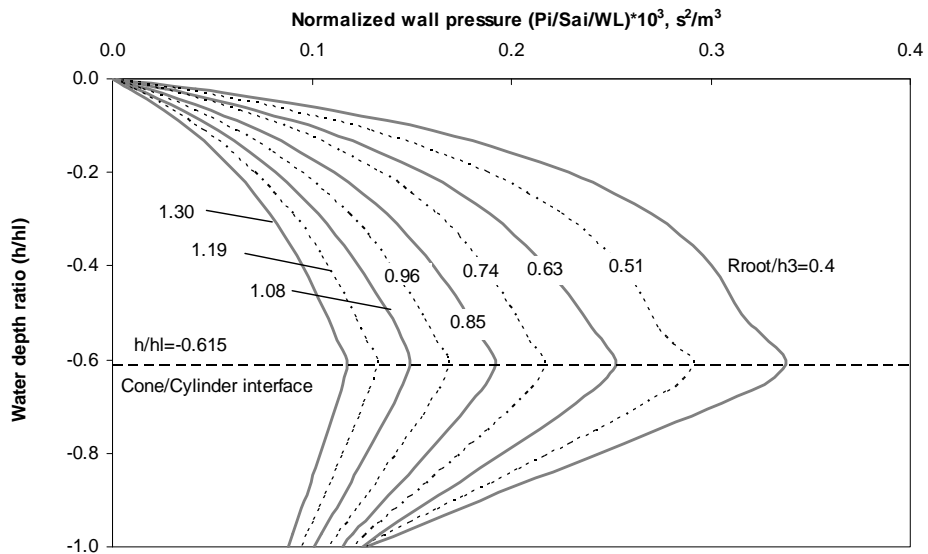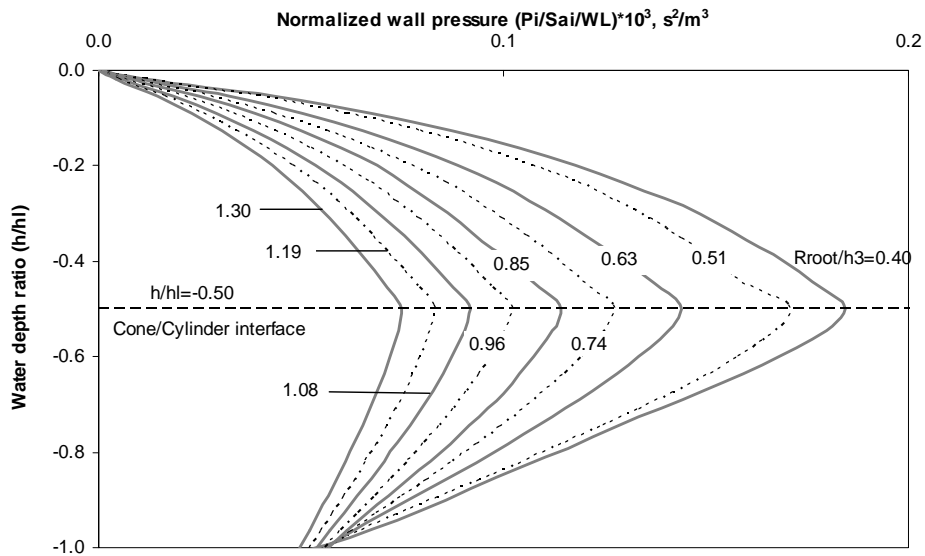
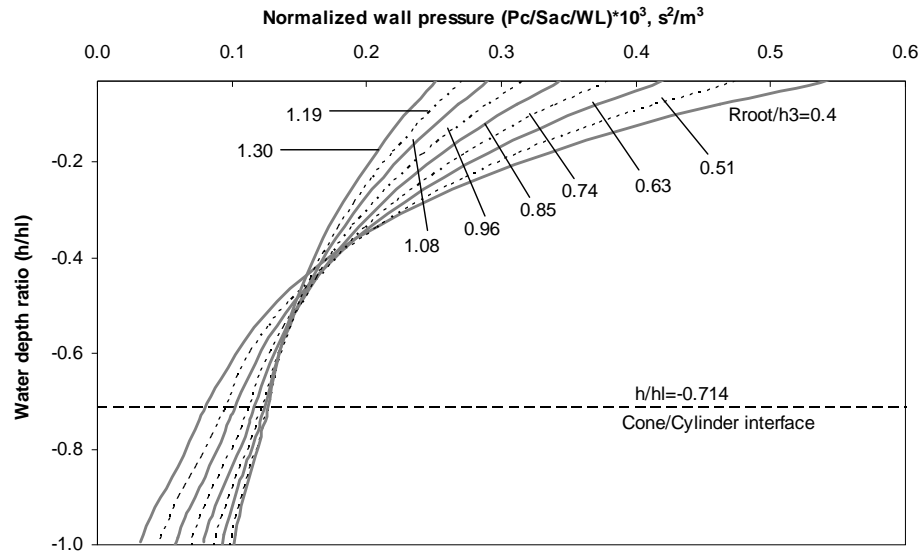Figure C.12 Pressure distribution over the tank wall for Ks= 1.3E8 N/m and hc/h3=0.625 ;

(a) Convective, (b) Impulsive
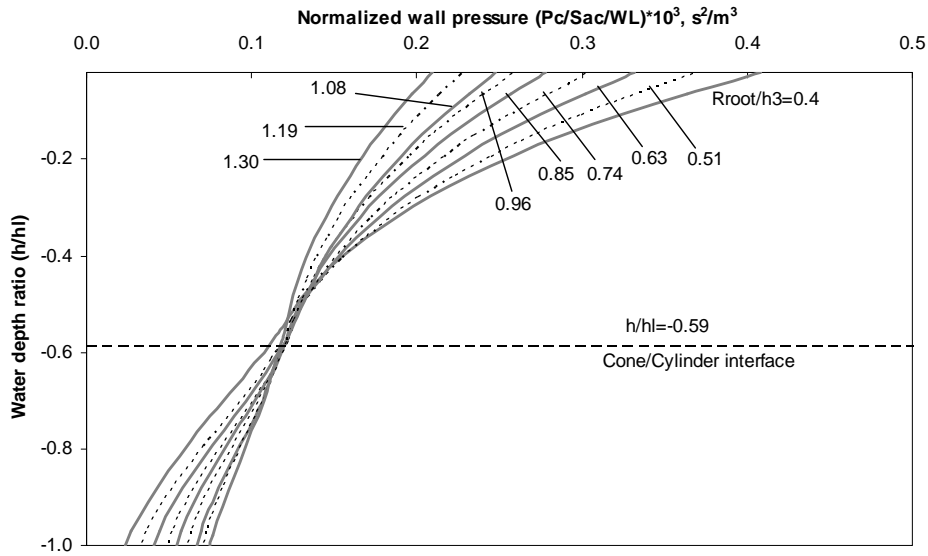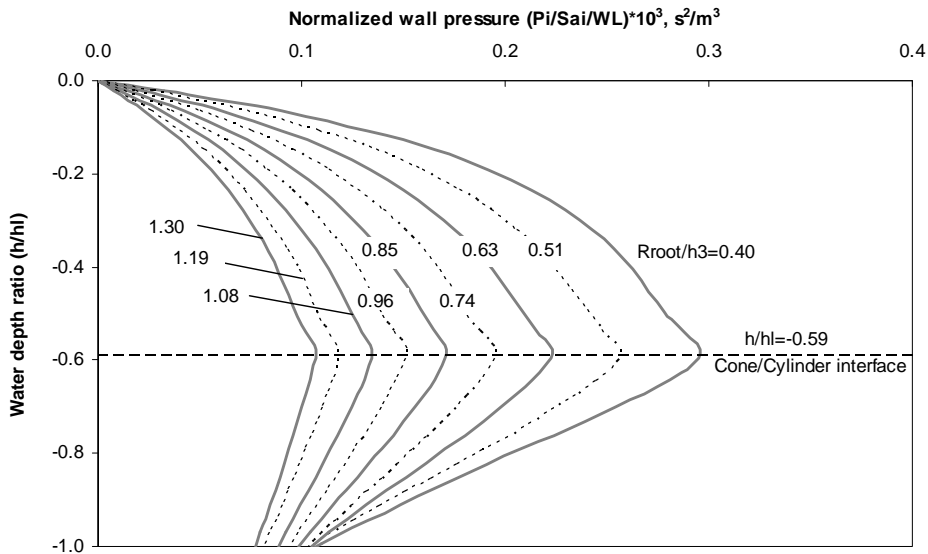
Figure C.13 Pressure distribution over the tank wall for Ks= 1.3E8 N/m and hc/h3=0.7 ;

(a) Convective, (b) Impulsive

Normalized wall pressure (Pc/Sac/WL)*10³, s²/m³

(a)

Normalized wall pressure (Pi/Sai/WL)*10³, s²/m³

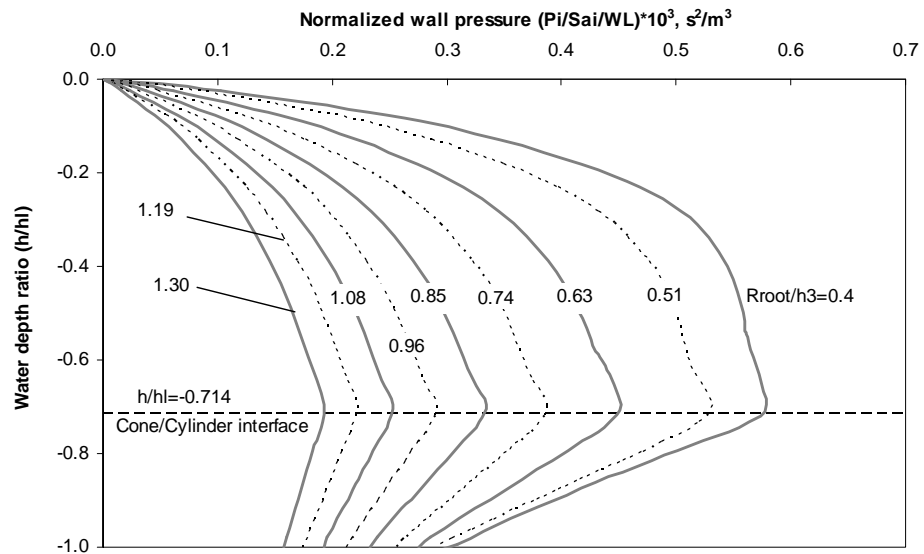(b)

Figure C.14 Pressure distribution over the tank wall for Ks= 1.3E8 N/m and hc/h3=0.775 ;

(a) Convective, (b) Impulsive
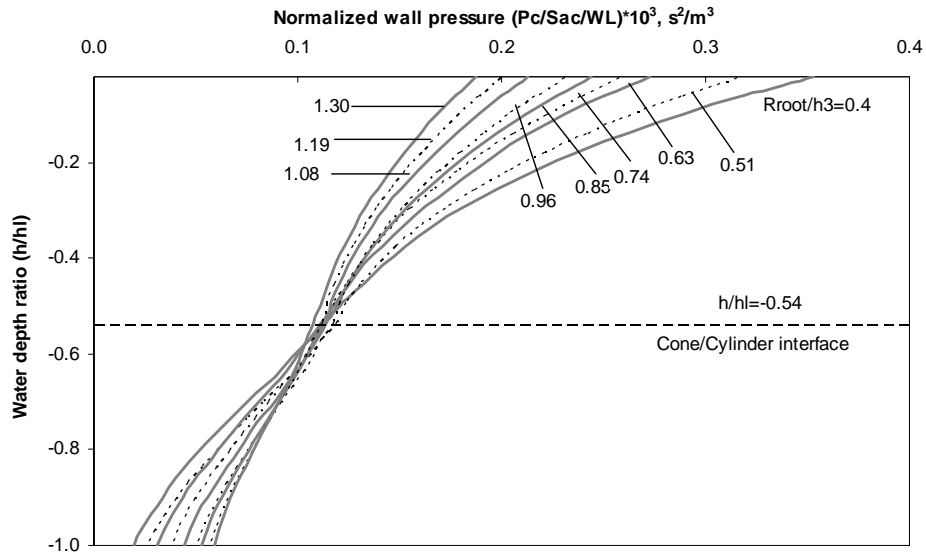
Figure C.15 Pressure distribution over the tank wall for Ks= 1.3E8 N/m and hc/h3=0.85 ;
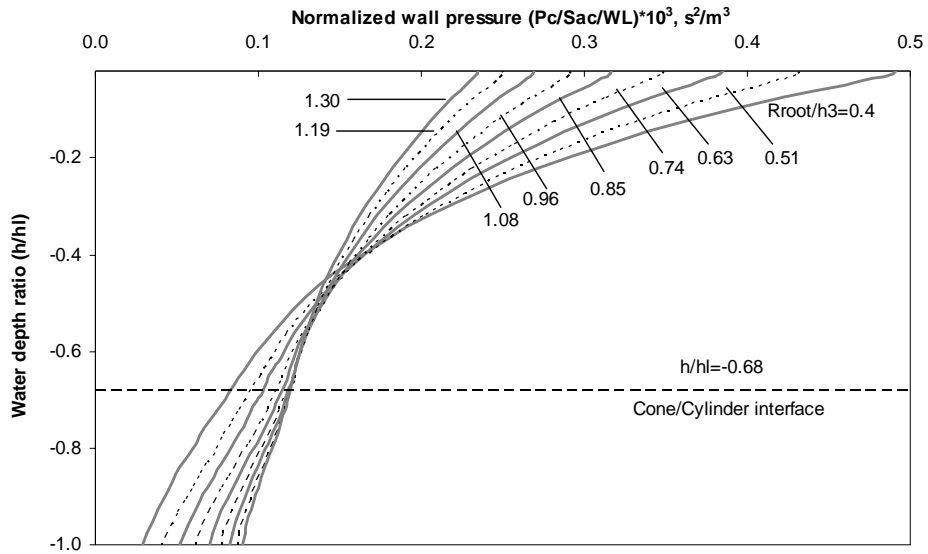
(a) Convective, (b) Impulsive

Figure C.16 Pressure distribution over the tank wall for Ks= 1.3E8 N/m and hc/h3=0.925 ;

(a) Convective, (b) Impulsive

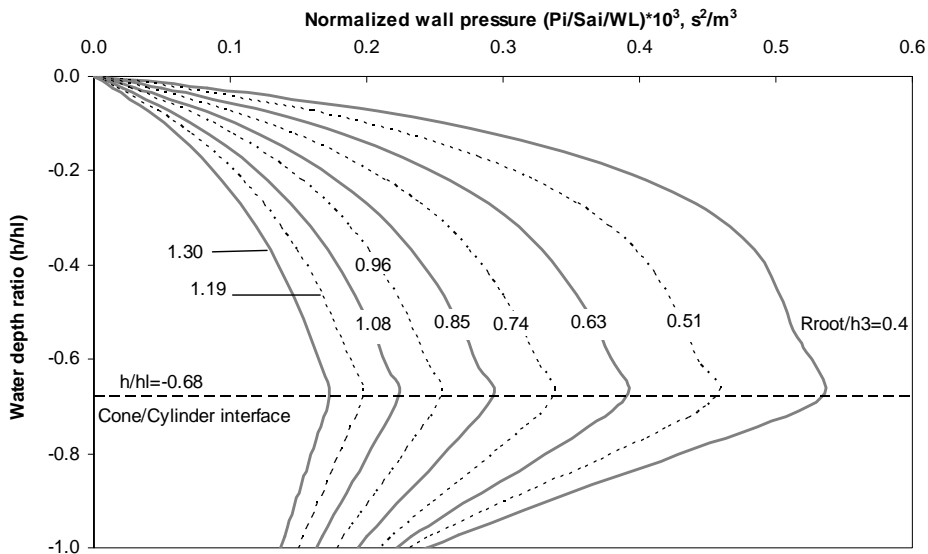Figure C.17 Pressure distribution over the tank wall for Ks= 1.3E8 N/m and hc/h3=1.00 ;

(a) Convective, (b) Impulsive

Figure C.18 Pressure distribution over the tank wall for Ks= 1.4E10 N/m and hc/h3=0.4 ;
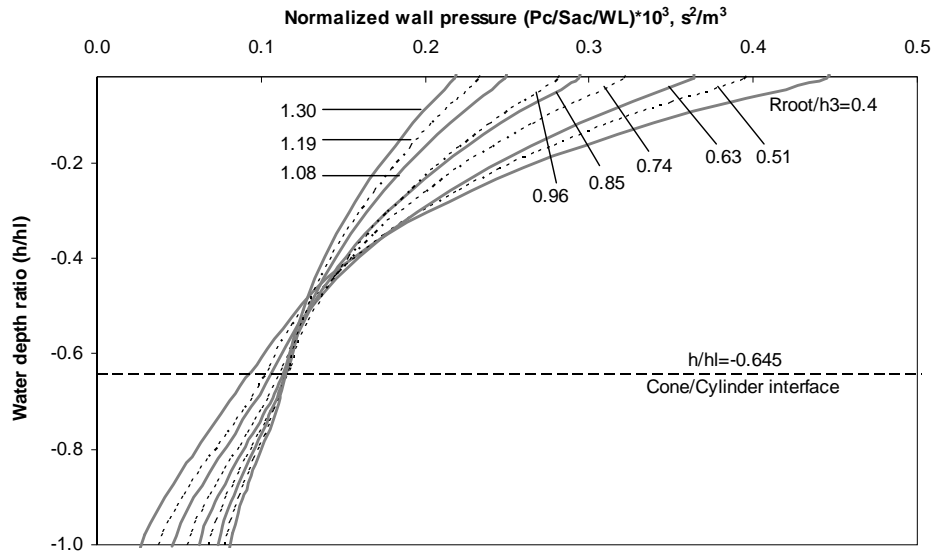
(a) Convective, (b) Impulsive

Figure C.19 Pressure distribution over the tank wall for Ks= 1.4E10 N/m and hc/h3=0.475 ;

(a) Convective, (b) Impulsive

324
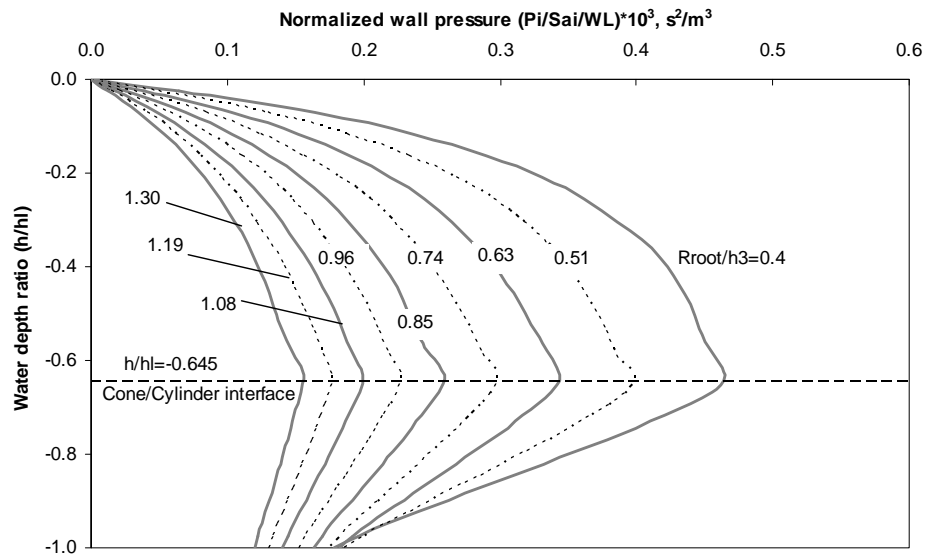
Figure C.20 Pressure distribution over the tank wall for Ks= 1.4E10 N/m and hc/h3=0.55 ;

(a) Convective, (b) Impulsive

(a)

(b)

Figure C.21 Pressure distribution over the tank wall for Ks= 1.4E10 N/m and hc/h3=0.625;

(a) Convective, (b) Impulsive

326
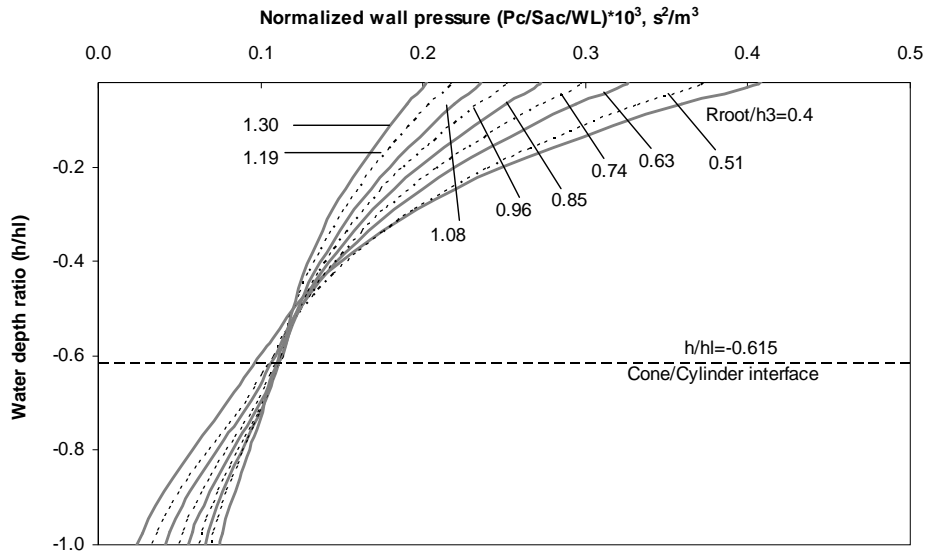
Figure C.22 Pressure distribution over the tank wall for Ks= 1.4E10 N/m and hc/h3=0.7 ;

(a) Convective, (b) Impulsive

Figure C.23 Pressure distribution over the tank wall for Ks= 1.4E10 N/m and hc/h3=0.775 ;
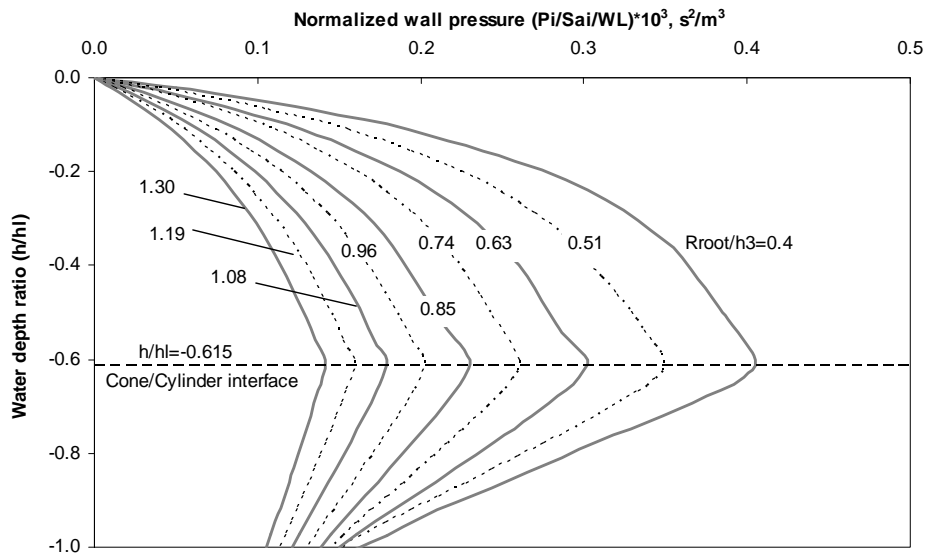
(a) Convective, (b) Impulsive

Figure C.24 Pressure distribution over the tank wall for Ks= 1.4E10 N/m and hc/h3=0.85 ;

(a) Convective, (b) Impulsive

(a)

(b)

Figure C.25 Pressure distribution over the tank wall for Ks= 1.4E10 N/m and hc/h3=0.925 ;

(a) Convective, (b) Impulsive

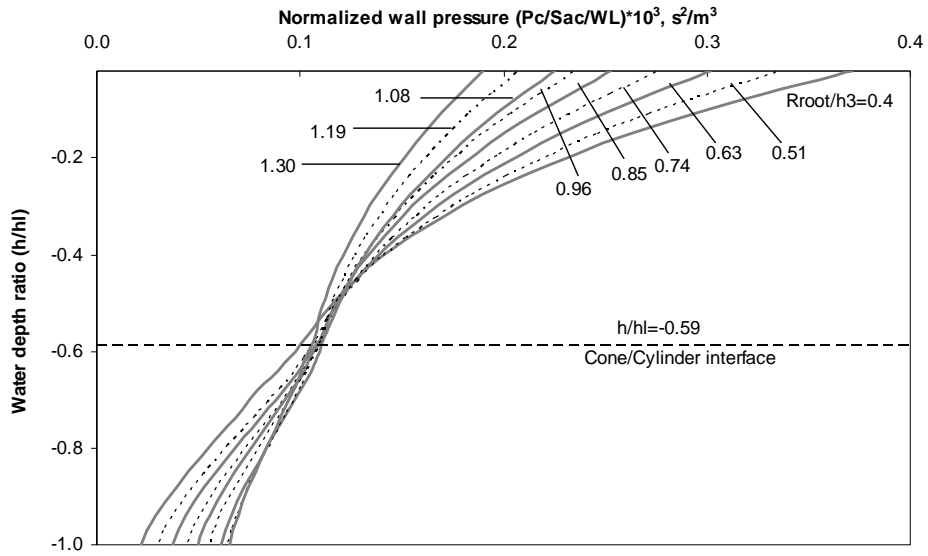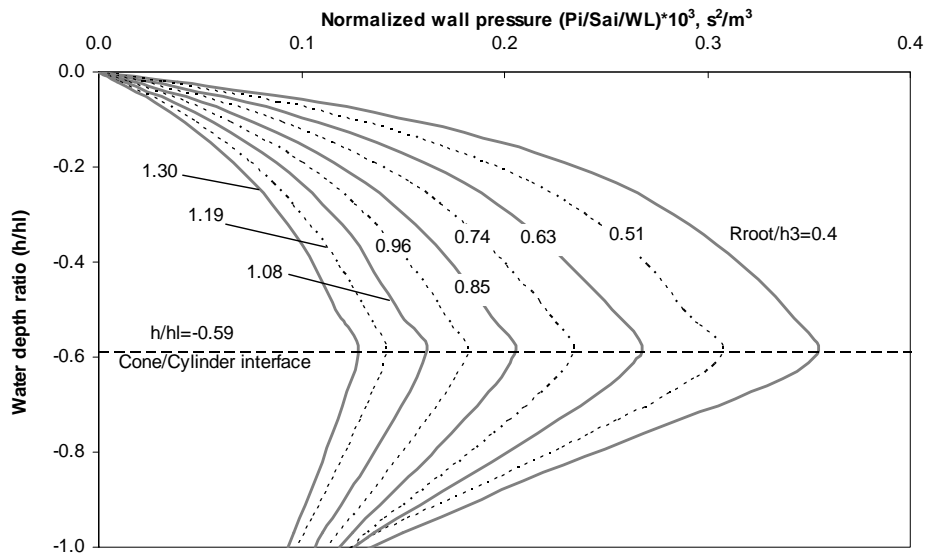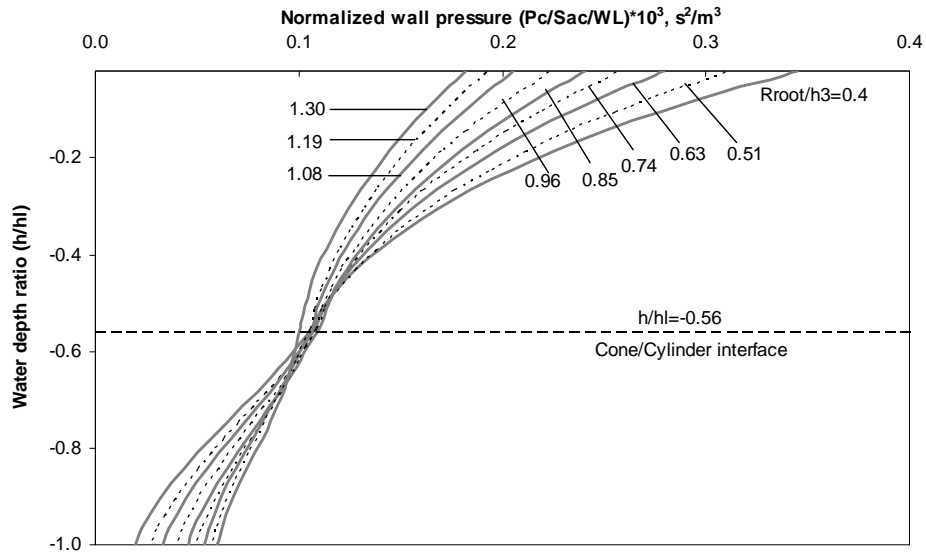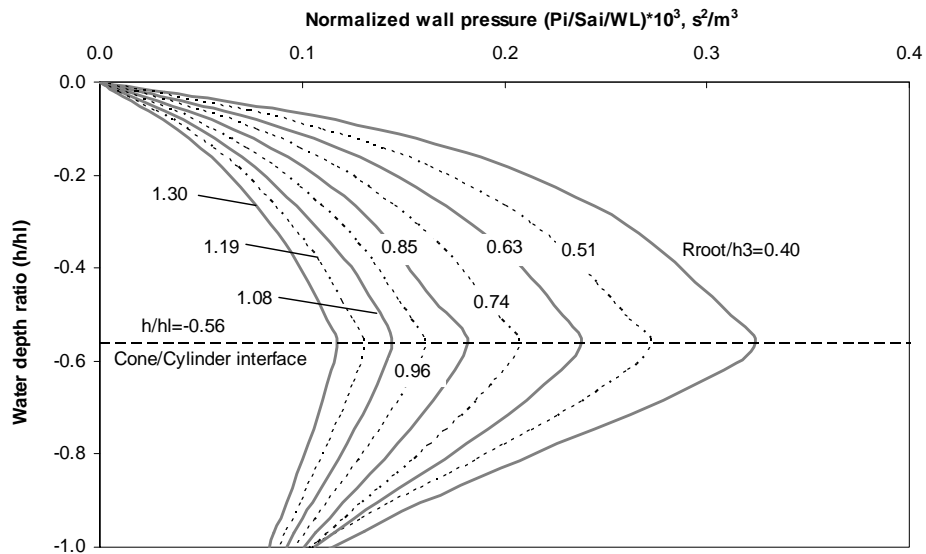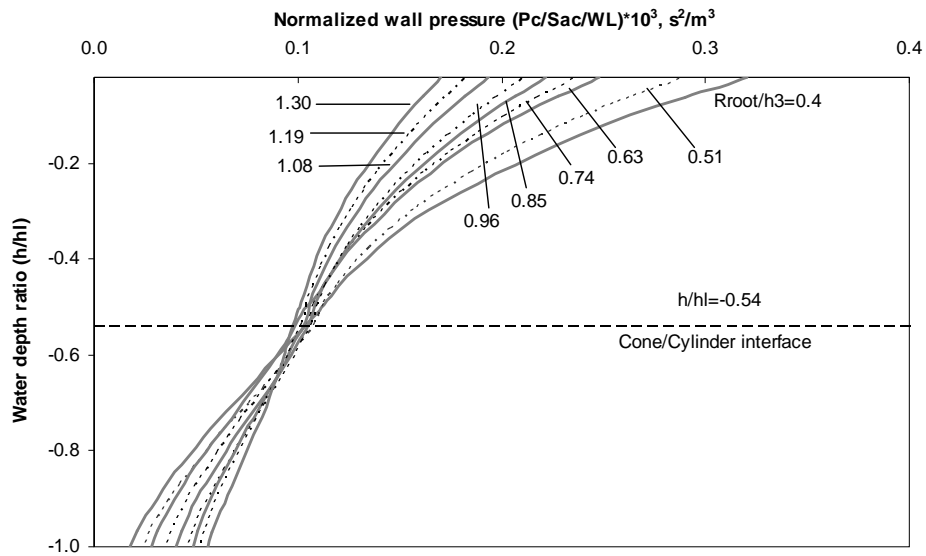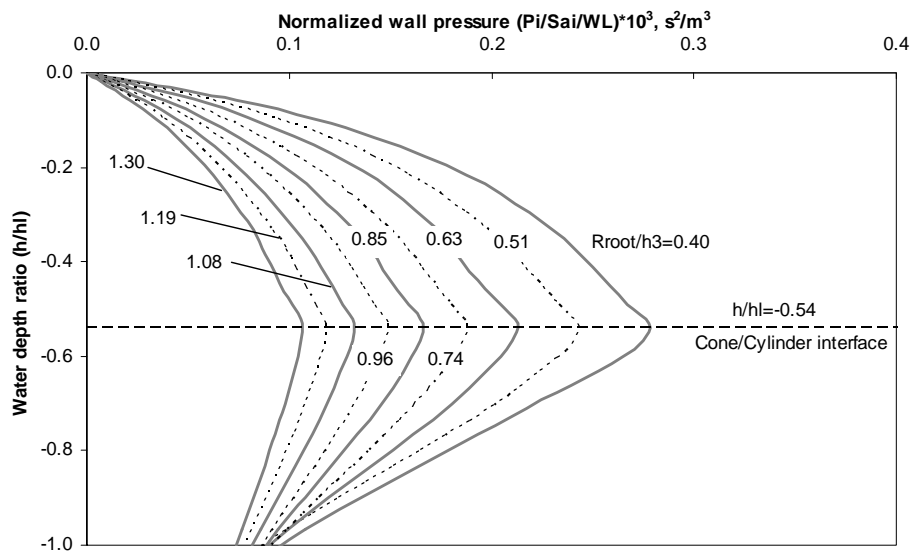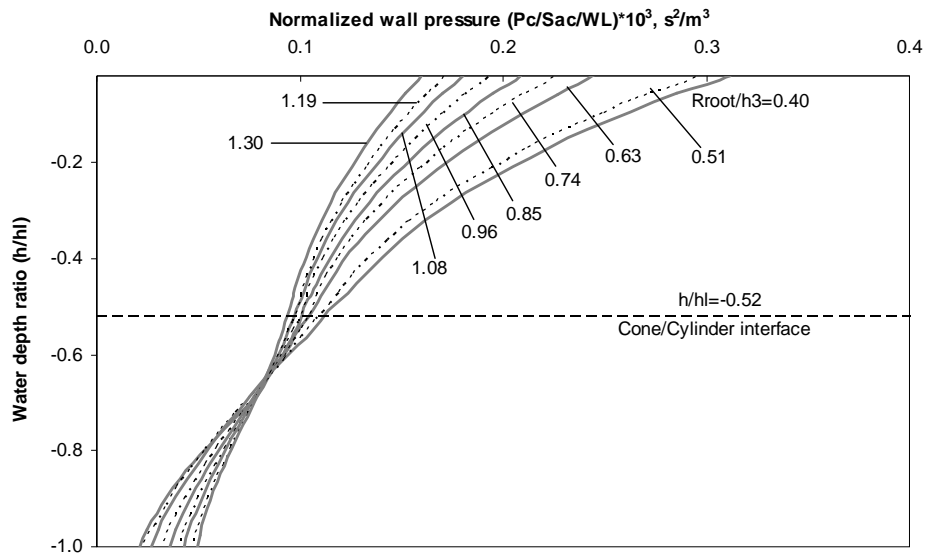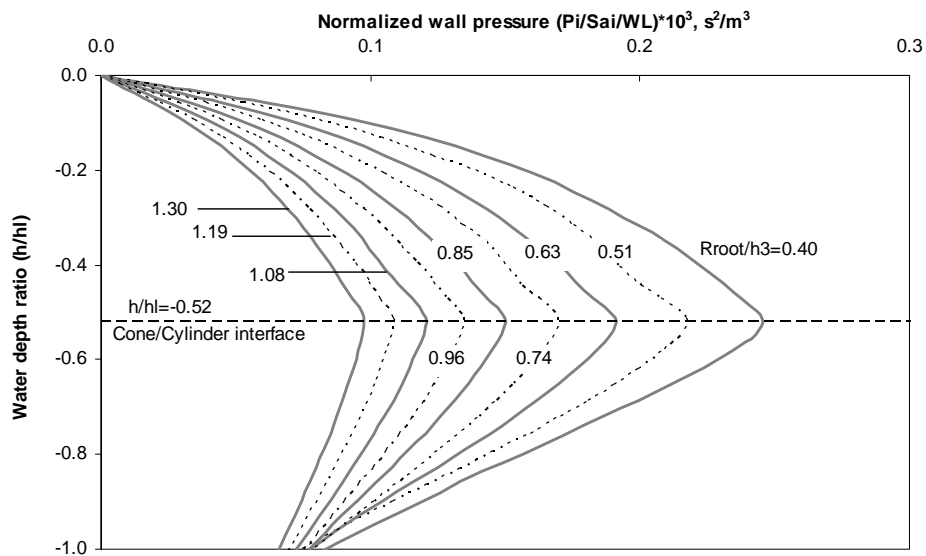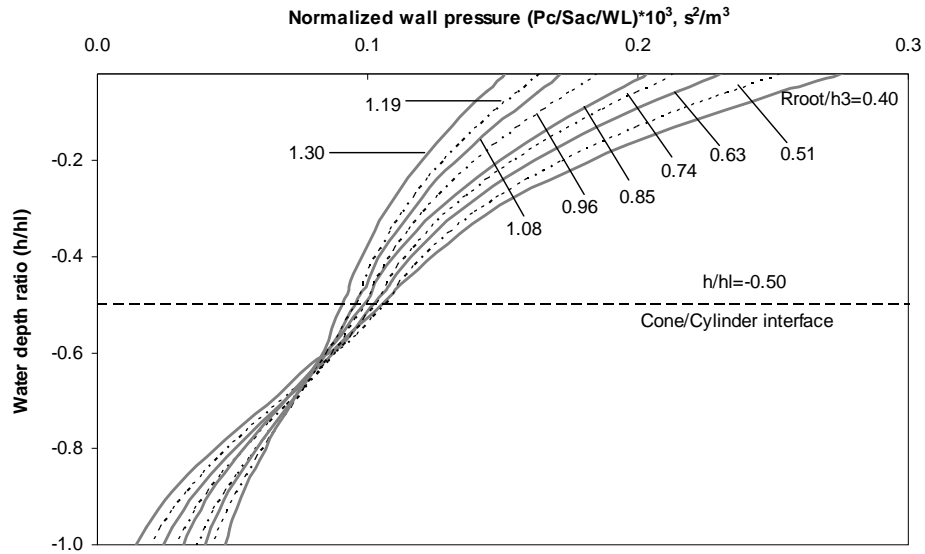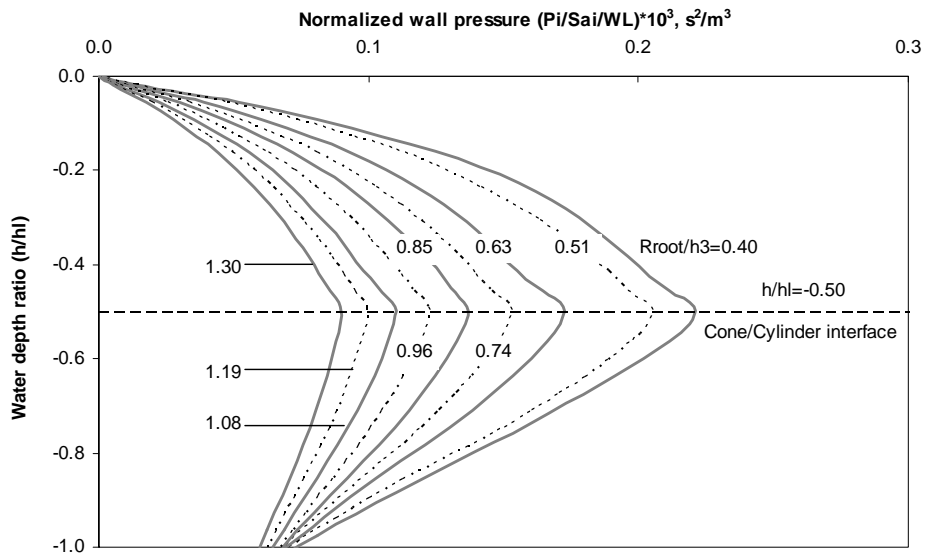Figure C.26 Pressure distribution over the tank wall for Ks= 1.4E10 N/m and hc/h3=1.00 ;

(a) Convective, (b) Impulsive

331

REFERENCES

Abromowitz, M., and Stegun, T.A., 1972, "Handbook of mathematical functions with formulas, graphs and mathematical tables", 10. Applied mathematics series, 55. Washington: National Bureau of Standards.

ACI Committee 350-01, 2001, "Code requirements for environmental engineering concrete structures (ACI 350-01) and commentary (ACI 350R-01)", American Concrete Institute, Farmington Hills, MI, U.S.A.

ACI Committee 350.3-06, 2006, "Seismic design of liquid-containing concrete structures (ACI 350.3-06) and commentary (ACI 350.3R-06)", American Concrete Institute, Farmington Hills, MI, U.S.A.

ACI Committee 371, 2008, "Guide for the analysis, design and construction of elevated concrete and composite steel-concrete water storage tanks (ACI 371R-08)", American Concrete Institute, Farmington Hills, MI, U.S.A.

Anshel, J.S., 1999, "Kobe earthquake of January 17, 1995. Lifeline performance. 1995", ASCE Publication.

Aoyagi, M., and Shiomi, 1985, "Studies on menshin structures", Report of Central Research Institute of Electric Power Industry, 385010.

American Petroleum Institute, API 620, 1998, "Design and construction of large, welded, low-pressure storage tanks", American Petroleum Institute Standard, Washington D.C., U.S.A.

American Petroleum Institute, API 650, 1998, "Welded steel tanks for oil storage", American Petroleum Institute Standard, Washington D.C., U.S.A.

Arias, A., 1970, "A measure of earthquake intensity", Seismic Design for Nuclear Power Plants, MIT Press, Cambridge.

American Society of Civil Engineers (ASCE), 1980, "Structural analysis and design of nuclear plant facilities", ASCE Manuals and Reports on Engineering Practice No. 58, New York, New York.

American Society of Civil Engineers (ASCE), 1998, "Seismic analysis of safety-related nuclear structures and commentary", ASCE 4-98, Reston, VA.

American Society of Civil Engineers (ASCE), Structural Engineering Institute, 2006, "Minimum design loads for buildings and other structures", ASCE/SEI 7-05, Reston, VA.

American Society of Civil Engineers (ASCE), Structural Engineering Institute, 2010, "Minimum design loads for buildings and other structures", ASCE/SEI 7-10, Reston, VA.

American Water Works Association (AWWA), 1984 and 2005, "Welded steel tanks for water storage", AWWA D100, CO.

American Water Works Association (AWWA), 1995, "Wire and strand-wounded circular prestressed concrete water tanks", AWWA D110, Denver, CO.

American Water Works Association (AWWA), 1995, "Circular prestressed concrete water tanks with circumferential tendons", AWWA D115, Denver, CO.

Balendra, T., Ang, K.K., Paramasivan, P., and Lee, S.L., 1982, "Seismic design of flexible cylindrical liquid storage tanks", Earthquake Engineering and Structural Dynamics, 10, 477-496.

Barton, D.C., and Parker, J.V., 1987, "Finite element analysis of the seismic response of anchored and unanchored liquid storage tanks", Earthquake Engineering and Structural Dynamics, 15, 299-322.

Blakeley, R.W.G., Cormack, L.G., and Stockwell, M.J., 1980, "Mechanical energy dissipation devices", Bull. N. Z. Natl. Soc. Earthquake Eng., 13, 264 – 268.

Bleiman, D., and Kim, S., 1993, "Base isolation of high volume elevated water tanks", Proc., Seminar on Seismic Isolation, Passive Energy Dissipation and Active Control, ATC 17-1, Applied Technology Council, Redwood City, Calif.

Bo, L., and Jia-xiang, T., 1994, "Vibration studies of base-isolated liquid storage tanks", Comp. and Struct., 52(5), 1051-1059.

BS 8007, 1987, "Code of practice for design of concrete structures for retaining aqueous liquids", British Standard Institution.

Chalhoub, M.S., and Kelly, J.M., 1990, "Shake table test of cylindrical water tanks in base-isolated structures", J. Engrg. Mech., ASCE, 116(7), 1451-1472.

Chandrasekaran, A.R., and Krishna, 1965, "Water towers in seismic zones", 1965 Proceedings of the Third World Conference on Earthquake Engineering, New Zealand, IV, 161-171.

Chen, J.Z., and Kianoush, M.R., 2005, "Seismic response of concrete rectangular tanks for liquid containing structures", Canadian Journal of Civil Engineering, 32, 739-752.

Chopra, A.K., 2000, "Dynamics of structures: theory and applications to earthquake engineering", 2nd edition, Prentice-Hall.

Clough, R.W., and Clough, D.P., 1977, "Seismic response of flexible cylindrical tanks", Paper K 5/1 Trans. 4th International Conference on Structural Mechanics in Reactor Technology, San Francisco, CA.

Clough, R.W., Niwa, A., and Clough, D.P., 1979, "Experimental seismic study of cylindrical tanks", Journal of the Structural Division, ASCE, Vol. 105, No. 12, pp. 2565-2590.

Dogangun, A., Durmus, A., and Ayvaz, Y., 1997, "Earthquake analysis of flexible rectangular tanks using the Lagrangian fluid finite element", Euro. J. Mech.-A/Solids, 16: 165-182.

Dogangun, A., and Livaoglu, R., 2004, "Hydrodynamic pressures acting on the walls of rectangular fluid containers", Structural Engineering and Mechanics, 17 (2), 203-214.

Dutta, S.C., Dutta, S., and Roy, R., 2009, "Dynamic behavior of R/C elevated tanks with soil-structure interaction", Journal of Engineering Structures, 31, 2617-2629.

European Committee for Standardization (ECS), 1998 and 2006, "Design provisions for earthquake resistance of structures, Part 1– General rules and Part 4 – Silos, tanks and pipelines", Eurocode 8, Brussels, Belgium.

Edwards, N., 1969, "A procedure for the dynamic analysis of thin walled cylindrical liquid storage tanks", Ph.D. Thesis, University of Michigan, Ann Arbor, MI.

El Damatty, A.A., Mirza, F.A., and Korol, R.M., 1997A, "Stability of imperfect steel conical tanks under hydrostatic loading", J. Struct. Engng., ASCE, 123, 703-712.

El Damatty, A.A., Korol, R.M., and Mirza, F.A., 1997B, "Stability of elevated liquid-filled conical tanks under seismic loading, Part I—Theory", Earthquake Eng. Struct. Dyn., 26, 1191–1208.

El Damatty, A.A., Korol, R.M., and Mirza, F.A., 1997C, "Stability of elevated liquid-filled conical tanks under seismic loading, Part II —Applications", Earthquake Eng. Struct. Dyn., 26, 1209–1229.

El Damatty, A.A., Korol, R.M., and Tang, L.M., 2000, "The sloshing response of conical tanks", Proceedings of World Conference on Earthquake Engineering, Paper No. 966, Topic No. 7, New Zealand.

El Damatty, A.A., Saafan, M.S., and Sweedan, A.M.I., 2005, "Experimental study conducted on a liquid-filled combined conical tank model", Journal of Thin Walled Structures, 43, 1398–417.

Epstein, H.I., 1976, "Seismic design of liquid storage tanks", Journal of the Structural Division, 102 (9): 1659-1673.

Fischer, F.D., 1979, "Dynamic fluid effects in liquid-filled flexible cylindrical tanks", Earthquake Engng. Struct. Dyn., 7, 587-601.

Flugge, W., 1960, "Stress in shells", Springer-Verlag, Berlin.

Fox, D.W., and Kuttler, J.R., 1983, "Sloshing frequencies", Journal of Applied Mathematics and Physics, 34, 668-696.

Garcia, S.M., 1969, "Earthquake response analysis and seismic design of cylindrical tanks", Proceedings of the Fourth World Conference on Earthquake Engineering, Santiago, B-4, 169-182.

Ghaemmaghami, A.R., Moslemi, M., and Kianoush, M.R., 2010, "Dynamic behaviour of concrete liquid tanks under horizontal and vertical ground motions using finite element method", 9th US National and 10th Canadian Conf. on Earthquake Eng., Toronto, Canada.

Gupta, R.K., 1995, "Free vibrations of partially filled cylindrical tanks", Journal of Engineering Structures, 17(3), 221-230.

Haroun, M.A., 1980, "Dynamic analyses of liquid storage tanks", EERL, Report No. 80-04, Earthquake Engineering Research Laboratory Report, California Institute of Technology, Pasadenas, CA.

Haroun, M.A., 1983, "Vibration studies and tests of liquid storage tanks", Earthquake Engng. Struct. Dyn., 11, 190-206.

Haroun, M.A., 1984, "Stress analysis of rectangular walls under seismically induced hydrodynamic loads", Bulletin of the Seismological Society of America, 74(3), 1031-1041.

Haroun, M.A., and Ellaithy, H.M., 1985, "Seismically induced fluid forces on elevated tanks", J. Tech. Topics Civil Eng., 1, 1-15.

Haroun, M.A., and Housner, G.W., 1981A, "Seismic design of liquid storage tanks", Journal of the Technical Councils of ASCE, 107, 191- 207.

Haroun, M.A., and Housner, G.W., 1981B, "Earthquake response of deformable liquid storage tanks", Journal of Applied Mechanics, ASME, 48, 411-418.

Haroun, M.A., and Tayel, M.A., 1985, "Response of tanks to vertical seismic excitations", Earthquake Engng. Struct. Dyn., 13, 583-595.

Hazardous Material Technology Standards Committee: Fire Defense Agency, 1979, "Report on causes of damage to petroleum tanks in Sendai Refinery of Tohoku Petroleum Company during the 1978 earthquake of Miyagi prefecture".

Housner, G.W., 1952, "Spectrum intensities of strong motion earthquakes", Proc. of Symposium on Earthquake and Blunt Effects on Structures, Earthquake Engineering Research Institute.

Housner, G.W., 1957, "Dynamic pressures on accelerated fluid containers", Bulletin of the Seismological Society of America 47(1), 15-37.

Housner, G.W., 1963, "The dynamic behavior of water tanks", Bulletin of the Seismological Society of America 53(2), 381-389.

Housner, G.W., 1975, "Measures of severity of earthquake ground shaking", Proceedings of the U.S. National Conference on Earthquake Engineering, EERI, Ann Arbor, MI.

Hunt, B., and Priestley, N., 1978, "Seismic water waves in a storage tank", Bulletin of the Seismological Society of America, 68(2), 487-499.

IBC., 2011, "International Building Code", International Code Council, Inc., USA: ICC.

Ibrahim, R.A., 2005, "Liquid sloshing dynamics", Cambridge University Press.

Ifrim, M., and Bratu, C., 1969, "The effect of seismic action on the dynamic behavior of elevated water tanks", Proceedings of the Fourth World Conference on Earthquake Engineering, Santiago, B-4, 127-142.

Jacobsen, L.S., 1949, "Impulsive hydrodynamics of fluid inside a cylindrical tank and of fluid surrounding a cylindrical pier", Bulletin of the Seismological Society of America, Vol. 39, No. 3, pp. 189-203.

Jacobsen, L.S., and Ayre, R.S., 1951, "Hydrodynamic experiments with rigid cylindrical tanks subjected to transient motions", Bulletin of the Seismological Society of America, 41(4), 313-346.

Jadhav, M.B., and Jangid, R.S., 2004, "Response of base-isolated liquid storage tanks", Shock and Vibration, 11, 33-45.

Jadhav, M.B., and Jangid, R.S., 2006, "Response of base-isolated liquid storage tanks to near-fault motions", Structural Engineering and Mechanics, 23, 615-634.

Jennings, P.C., 1971, "Engineering features of the San Fernando earthquake of February 9, 1971. Technical Report", CaltechEERL: 1971.EERL-71-02, California Institute of Technology.

Joshi, S.P., 2000, "Equivalent mechanical model for horizontal vibration of rigid Intze tanks", ISET Journal of Earthquake Technology, 37, 39-47.

Kianoush, M.R., and Chen, J.Z., 2006, "Effect of vertical acceleration on response of concrete rectangular liquid storage tanks", Engineering Structures, 28(5), 704-715.

Kianoush, M.R., Mirzabozorg, H., and Ghaemian, M., 2006, "Dynamic analysis of rectangular liquid containers in three-dimensional space", Canadian Journal of Civil Engineering, 33, 501-507.

Kim, J.K., Koh, H.M., and Kwahk, I.J., 1996, "Dynamic response of rectangular flexible fluid containers", ASCE Journal of Engineering Mechanics, 122(9), 807-817.

Kim, N.S., and Lee, D.G., 1995, "Pseudo-dynamic test for evaluation of seismic performance of base-isolated liquid storage tanks", Engineering Structures, 17(3), 198-208.

King, P.G., 1980, "Mechanical energy dissipation for seismic structures", Report 228, Department of Civil Engineering, University of Auckland, Auckland.

Koh, H.M., Kim, J.K., and Park, J.H., 1998, "Fluid–structure interaction analysis of 3D rectangular tanks by a variationally coupled BEM–FEM and comparison with test results", Earthquake Engng. Struct. Dyn., 27, 109–124.

Kono, 1980, "Facts about failures and instability of plant structure (mainly for flat bottom cylindrical storage tanks)", Preprint, the 31st Nat. Cong. of Theoretical & Applied Mechanics, pp. 7-12.

Kumieda, 1976, "Vibration suppression institute of Japan and menshin design of structures", Jour. JSME, 79 (689), 360-365.

Lee, D.M., and Medland, I.C., 1981, "Base isolation systems for earthquake protection of multi-storey shear structures", Earthquake Eng. Struct. Dyn., 7, 555-568.

Lund, L.V., 1996, "Lifeline utilities performance in the 17 January 1994 Northridge, California earthquake", Bulletin of the Seismological Society of America, Vol. 86, No. 1B.

Malhotra, P.K., 1995, "Base uplifting analysis of flexibly supported liquid-storage tanks", Journal of Earthquake Engineering and Structural Dynamics, Vol. 24, No. 12, pp. 1591–1607.

Malhotra, P.K., 1997A, "Seismic response of soil-supported unanchored liquid-storage tanks", Journal of Structural Engineering, ASCE, New York, Vol. 123, No. 4, pp. 440–450.

Malhotra, P.K., 1997B, "Method for seismic base isolation of liquid storage tanks", J. Struct. Engrg., ASCE, 123(1), 113-116.

Malhotra, P.K., 1997C, "New method for seismic isolation of liquid storage tanks", Journal of Earthquake Engineering and Structural Dynamics, 26, 839-847.

Malhotra, P.K., 1998, "Seismic strengthening of liquid storage tanks with energy-dissipating anchors", J. Struct. Engrg., ASCE, 124(4), 405-414.

Malhotra, P.K., 2000, "Practical nonlinear seismic analysis of tanks", Earthquake Spectra, 16(2), 473-492.

Malhotra, P.K., Wenk, T., and Wieland, M., 2000, "Simple procedure for seismic analysis of liquid-storage tanks", Structural Engineering International, International Association for Bridge and Structural Engineering (IABSE), Zurich, Switzerland, 10(3), pp. 197-201.

Manos, G.C., and Clough, R.W., 1985, "Tank damage during the May 1983 Coalinga earthquake", Journal of Earthquake Engineering & Structural Dynamics, 13(4), 449-466.

Meggett, L.M., 1978, "Analysis and design of a base-isolated reinforced concrete frame building", Bull. N. Z. Natl. Soc. Earthquake Eng., 11, 245-254.

Minowa, C., 1980, "Dynamic analysis for rectangular water tanks", Recent Advances in Lifeline Earthquake Engineering in Japan, 135-142.

Minowa, C., 1984, "Experimental studies of seismic properties of various type water tanks", Proceedings of Eighth WCEE, San Francisco, 945-952.

Mirzabozorg, H., Khaloo, A.R., and Ghaemian, M., 2003, "Staggered solution scheme for three dimensional analysis of dam reservoir interaction", Dam Engineering, 14(3), 147-179.

MITI, 1980, "Technical standards for structures for nuclear power plant equipment", MITI Notification No. 501.

Moslemi, M., Kianoush, M.R., and Pogorzelski, W., 2011, "Seismic response of liquid-filled elevated tanks", Journal of Engineering Structures, 33(6), 2074-2084.

Niigata Nippo Co., 1964, "Records of Niigata earthquake".

NZS 3106, 1986 and 2010, "Code of practice for concrete structures for the storage of liquids", Standards Association of New Zealand, Wellington.

Ogden, R.W., 1984, "Nonlinear Elastic Deformations", Dover Publications, Inc.

Ogden, R.W., 1986, "Recent advances in the phenomenological theory of rubber elasticity", J. Rubber Chem. Technol., 59, 361-383.

Park, J.H., Koh, H.M., and Kim, J., 1992, "Liquid–structure interaction analysis by coupled boundary element – finite element method in time domain", Proceedings of the 7th International Conference on Boundary Element Technology, Albuquerque, New Mexico, Edited by Brebbia, C.A., and Ingber, M.S., Computational Mechanics Publication BE-TECH/92, Southampton, UK., pp. 89–92.

Rai, D.C., 2002, "Elevated tanks", Earthquake Spectra – 2001 Bhuj India Earthquake Reconnaissance Report, (ed. Jain, Lettis, Bardet, and Murty), EERI., Supplement A to Vol. 18, 279-295.

Rai, D.C., Narayan, J.P., Pankaj, and Kumar, A., 1997, "Jabalpur earthquake of May 22, 1997: Reconnaissance Report", Department of Earthquake Engineering, University of Roorkee, India.

Rinne, J.E., 1967, "Oil storage tanks", The Prince William Sound, Alaska Earthquake of 1964 and Aftershocks, Vol II, Part A, U.S. Coast and Geodetic Survey, Washington D.C., 245-252.

Robinson, W.H., 1982, "Lead-rubber hysteretic bearings suitable for protecting structures during earthquakes", Earthquake Engrg. and Struct. Dyn., 10, 593-604.

Robinson, W.H., and Tucker, A.G., 1981, "Test results for lead-rubber bearings for Wm. Clayton building, Toe Toe bridge and Waiotukupuna bridge", Bulletin of the New Zealand National Society for Earthquake Engineering, 14(1), 21-33.

Sezen, H., and Whittaker, A.S., 2006, "Seismic performance of industrial facilities affected by the 1999 Turkey earthquake", ASCE Journal of Performance of Constructed Facilities, 20(1), 28-36.

Shekari, M.R., Khaji, N., and Ahmadi, M.T., 2009, "A coupled BE-FE study for evaluation of seismically isolated cylindrical liquid storage tanks considering fluid-structure interaction", Journal of Fluids and Structures, 25, 567-585.

Shenton III, H.W., and Hampton, F.P., 1999, "Seismic response of isolated elevated water tanks", ASCE Journal of Structural Engineering, 125(9), 965-976.

Shepherd, R., 1972, "Two mass representation of a water tower structure", Journal of Sound and Vibration, Vol. 24.

Shibata, 1974, "Report of earthquake damages in overseas industrial facilities – Spherical tank and cylindrical tank", Seisan Kenkyu, 26(7), 259-264.

Shirmali, M.K., and Jangid, R.S., 2003, "The seismic response of elevated liquid storage tanks isolated by lead-rubber bearings", Bulletin of the New Zealand Society of Earthquake Engineering, pp. 141-164.

Simo, J.C., and Hughes, T.J.R., 1997, "Computational inelasticity", Springer-Verlag.

Sonobe, Y., and Nishikawa, T., 1969, "Study on the earthquake proof design of elevated water tanks", Proceedings of the Fourth World Conference on Earthquake Engineering, B-4, Santiago, Chile, pp. 11-24.

Sweedan, A.M.I., 2009, "Equivalent mechanical model for seismic forces in combined tanks subjected to vertical earthquake excitation", Journal of Thin Walled Structures, 47, 942–952.

Sweedan, A.M.I., and El Damatty, A.A., 2002, "Experimental identification of the vibration modes of liquid-filled conical tanks and validation of a numerical model", Earthq. Eng. Struct. Dyn., 32(9), 1407-1430.

Sweedan, A.M.I., and El Damatty, A.A., 2005, "Equivalent models of pure conical tanks under vertical ground excitation", Journal of Structural Engineering, ASCE, 131(5), 725-733.

Tamiah, B.K., and Rajata Mohana Gupta, D.S., 1966, "Factors effecting seismic design of water towers", Proceedings of the American Society of Civil Engineers, ST4, 13-30.

Tokuda, N., Sakurai, T., and Teraoku, T., 1995, "Sloshing analysis method using existing FEM structural analysis code", ASME J. Pres. Ves. Techn., 117, 268-272.

Treloar, L.R.G., 1944, "Stress-strain data for vulcanized rubber under various types of deformations", Trans. Faraday Soc., 40, 59-70.

Treloar, L.R.G., 1975, "The physics of rubber elasticity", Oxford, Clarendon Press.

Trifunac, M.D., and Brady, A.G., 1975, "A study on the duration of strong earthquake ground motion", Bulletin of the Seismological Society of America, 65(3), 581-626.

Vandepitte, D., Rathe, J., Verhegghe, B., Paridaens, R., and Verschaeve, C., 1982, "Experimental investigation of hydrostatically loaded conical shells and practical evaluation of the buckling load", Buckling of Shells, ed. Ramm, E., Proc. State-of the-Art Colloquium, Universitat Stuttgart, Germany, pp. 375-399.

Veletsos, A.S., 1974, "Seismic effects in flexible liquid storage tanks", Proc. 5th World Conf. Earthquake Eng., Rome, Italy, 1, 630-639.

Veletsos, A.S., 1984, "Seismic response and design of liquid storage tanks", American Society of Civil Engineers (ASCE), New York, Guidelines for the Seismic Design of Oil and Gas Pipeline Systems.

Veletsos, A.S., and Kumar, A., 1984, "Dynamic response of vertically excited liquid storage tanks", Proceedings of the Eighth World Conference on Earthquake Engineering, Vol. I, California, USA, pp. 453-459.

Veletsos, S.A., and Shivakumar, P., 1997, "Dynamic response of tanks containing liquids or solids", Computer Analysis and Design of Earthquake-Resistant Structures, Earthquake Engineering Series V.3, Beskos, D.E., and Anagnostopoulos, S.A., eds., Computational Mechanics Publications, Billerica, Mass., 936 pp.

Veletsos, A.S., and Tang, Y., 1986, "Dynamics of vertically excited liquid storage tanks", ASCE Journal of Structural Engineering, 112(6), 1228-1246.

Veletsos, A.S., and Tang, Y., 1990, "Soil-structure interaction effects for laterally excited liquid-storage tanks", Journal of Earthquake Engineering and Structural Dynamics, Vol. 19, No. 4, pp. 473-496.

Veletsos, A.S., and Yang, J.Y., 1977, "Earthquake response of liquid storage thanks", Proc. 2nd Adv. Civil. Eng. through Eng. Mech. Conf., ASCE, North Carolina, 1-24.

Virella, J.C., Godoy, L.A., and Suarez, L.E., 2006, "Fundamental modes of tank-liquid systems under horizontal motions", Journal of Engineering Structures, 28, 1450-1461.

Yang, J.Y., 1976, "Dynamic behavior of fluid tank system", Ph.D. Thesis, Civil Engineering, Rice University, Houston, Tex.